Photonic and plasmonic structures for enhancing efficiency of thin film silicon solar cells

by

Sambit Pattnaik

A dissertation submitted to the graduate faculty in partial fulfillment of the requirements for the degree of

DOCTOR OF PHILOSOPHY

Major: Electrical Engineering

Program of Study Committee:

Vikram Dalal, Co-major Professor

Rana Biswas, Co-major Professor

Ruth Shinar

Sumit Chaudhary

Mani Mina

Iowa State University

Ames, Iowa

2012

Table of Contents

List of Figures

List of Tables

Acknowledgements

I wish to express my deep gratitude and sincere thanks to my supervisors Dr. Vikram Dalal and Dr. Rana Biswas for their expert guidance, support and encouragement throughout the present research. I would also like to thank Dr. Ruth Shinar for her helpful discussions and collaboration in the inorganic-organic project. I also appreciate Dr. Sumit Chaudhary and Dr. Mani Mina for their contributions and efforts serving as my committee members.

I also thank all members of the Microelectronic Research Center starting with Max Noack who helped us maintain most of our equipment and set-up many of our experiments. I would like to especially thank Kequin Han and Dr. Nayan Chakravarty for providing a helping hand during fabrication of devices and Dr. Ashutosh Shyam for relieving us by working in the evenings. I would also like to also thank Siva, Shantan, Joydeep, Ron, Brian, Bob, Randy, Brian (Lewis), Ben (Pierce), Ben (Curtin), Spencer, Wai and other members of the MRC team for their continuous help including Teng who helped me by fabricating organic solar cells. I also acknowledge the help of our administrative team Nancy, Pam and Sunny over the years.

I am grateful to Light wave Power for providing us with nano imprinted substrates and NSF for funding the project.

I am thankful to Rocky, Reddy, Siva-munni, Bharat, Alekhya, Prasad, Kiran , Kirthi, Vishwa-Vani , Rokkam , Diwadkar and all my other friends in Ames for their support and companionship and wish them all success in their life.

Last, but not the least, it is the moral support, motivation and encouragement from my parents and the affection of my family that made it possible to reach this stage in my life.

Abstract

Crystalline silicon solar cells use high cost processing techniques as well as thick materials that are ~ 200μm thick to convert solar energy into electricity. From a cost viewpoint, it is highly advantageous to use thin film solar cells which are generally made in the range of 0.1-3μm in thickness. Due to this low thickness, the quantity of material is greatly reduced and so is the number and complexity of steps involved to complete a device, thereby allowing a continuous processing capability improving the throughput and hence greatly decreasing the cost. This also leads to faster payback time for the end user of the photovoltaic panel. In addition, due to the low thickness and the possibility of deposition on flexible foils, the photovoltaic (PV) modules can be flexible. Such flexible PV modules are well suited for building-integrated applications and for portable, foldable, PV power products.

For economical applications of solar cells, high efficiency is an important consideration. Since Si is an indirect bandgap material, a thin film of Si needs efficient light trapping to achieve high optical absorption. The previous work in this field has been mostly based on randomly textured back reflectors. In this work, we have used a novel approach, a periodic photonic and plasmonic structure, to optimize current density of the devices by absorbing longer wavelengths without hampering other properties. The two dimensional diffraction effect generated by a periodic structure with the plasmonic light concentration achieved by silver cones to efficiently propagate light in the plane at the back surface of a solar cell, achieves a significant increase in optical absorption. Using such structures, we achieved a 50%+ increase in short circuit current in a nano-crystalline (nc-Si) solar cell relative to stainless steel. In addition to nc-Si solar cells on stainless steel, we have also used the periodic photonic structure to enhance optical absorption in amorphous cells and tandem junction amorphous/nano-crystalline cells. These structures have been fabricated on flexible plastic substrates.

We will describe the use of periodic structures to achieve increased light absorption and enhanced photocurrents in thin film solar cells, and also compare them systematically with other textured substrates. We discuss the various technological aspects and obstacles faced before successful fabrication of such structure, and during the fabrication of solar cells on these structures. The ideas of periodic texturing and random texturing will be compared and an implementation of them together will be discussed.

Introduction

1.1 Motivation

Our society has been continually consuming resources at a rapidly increasing rate. The increasing consuming capacity has filled in the necessity to produce not only more energy, but also more effectively to fill in the gap. In history, one very good example would be the Industrial revolution which made possible the advent of many types of machinery that we take for granted today, leading to more modernized societies. The growth has continued; technologies have advanced, so has our capability to make better and more machines. This has also lead to an ever-growing requirement of more energy to sustain this modern society. This is where the requirement of various sources of energy emerge which include non-renewable sources such as fossil fuel based from oil, coal or natural gas and nuclear and the renewable sources such as solar, wind, hydro-electric, geothermal and biomass based.

Since we have mentioned two types of energy, there also comes the issue of consumption of resources wherein the non-renewable sources are getting consumed at an alarming rate which leads to the question till when would they last. It is also the nature of these non-renewable sources to be pollutant to the environment causing global warming which threatens our future on this planet. Nuclear has always had safety issues attached to it lately proven by the unfortunate events during the tsunami in Japan in March 2011. In addition oil has also seen it's own share of unfortunate events which has led to polluting the environment, for eg: the BP oil spill in 2010 or the coal ash spill in Tennessee in 2008. These environmental factors also have led to question of sustenance, where we not only produce enough energy for the present but also safeguard the interests of the future generations. Due to all these factors there has been increasing interest in renewable energy sources.

Among renewable energy sources, one of the most important ones is solar energy, where the energy from the sun is absorbed by solar absorber layer and converted to electricity. The sun continually provides huge energy flux towards the Earth and about 70% of which reaches the Earth's surface (1040 W/m^2). In factual terms the sun provides double the energy in a year than all the non-renewable sources together. The planet already converts a lot of energy from

the sun 3000 Exa-Joule through photosynthesis, which can be later on be used as biomass. But that is still a miniscule amount compared to the energy that is received by the Earth from the Sun.

Currently the solar energy industry is dominated by crystalline silicon solar cells. The most promising and most studied solar device that has been studied is the crystalline silicon solar cell, which is composed of mono-crystalline or polycrystalline silicon synthesized from rigid modules. The cost of silicon in pure form still remains costly due to the processing involved, not just that the post processing to make a solar cell is also high.

Crystalline silicon uses a high cost of the silicon feedstock through material which may be > 250µm, whereas thin film solar cells are generally made in the range of 0.1-3µm in thickness. Due to this low thickness of material, the quantity of material is greatly reduced, and so is the number and complexity of steps involved to complete a device, thereby allowing a continuous processing capability improving the throughput and hence decreasing cost greatly. This also leads to faster payback time for the consumers. In addition, due to the low thickness a possibility of flexible modules come in, which allows for portable use and more robust use as in building integrated products which could also incorporate some aesthetic applications.

The main goal of improving a solar cell is to improve the power conversion efficiency. Silicon is a material with an indirect bandgap as well as long absorption length which make it harder to absorb long wavelength photons in the red and infra-red regions of the spectrum. But increasing the thickness of the device means more material or higher cost, and in the case of thin film devices which need built-in electric field assist thicker materials could be detrimental. So, there has been considerable research in the area of developing light trapping structures for thin film solar cells. Most of these light trapping structures have been based on randomly textured back reflectors. In this work we have tried to optimize periodically designed back reflectors for use in the solar cells to improve current density of the devices by absorbing longer wavelengths.

Thin film solar cell require a backing material as in a substrate on which they can be grown and if we can use a cheap substrate that is abundantly available it would lower the production costs. The use of plastic materials which are abundantly available and easily processed, provides the added advantage of being light weight and flexible, making them easily installable as well as

the ability to be integrated with other products for smarter applications. This work deals with growth of thin film silicon solar cells on periodic light trapping structures on flexible substrates.

1.2 Fundamentals of Solar cell

A solar cell is an electrical device that converts energy from the sunlight to provide electricity. This effect is also known as photovoltaic effect which is the creation of voltage or current on exposure to light. Therefore solar cells are also called photovoltaic cells. Sun light contains streams of photons and these photons when incident on a semiconducting material may be absorbed, reflected or passes through. The part of the sunlight that is not reflected can excite an electron from the valence to conduction band such that it can result in producing electricity when attached to load as shown in Figure 1.1. As the semiconductor absorbs the light intrinsic carriers are excited and an internal field in the material helps electron to move towards the n-type semiconductor and holes towards the p-type semiconductor. When a load is connected the carriers flow out of the cell, leading to production of electricity. An array of this type of solar cell can be connected together to provide power for the required usage.

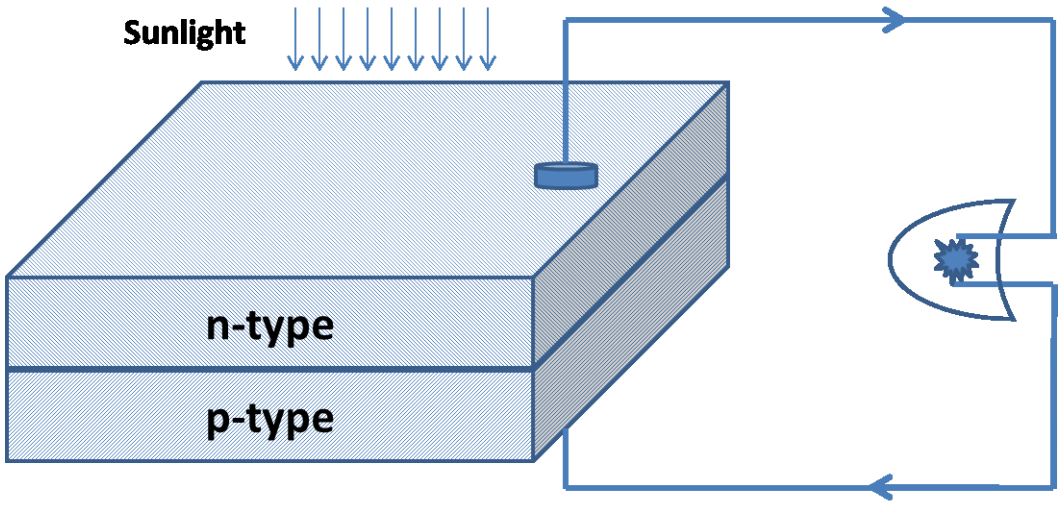

Figure 1.1: Schematic diagram of a solar cell

1.3 Materials for solar cells

There are a lot of materials that have been used for solar cells and they are based on the various factors namely

1. *Absorption coefficient:* It is the ability of a material to absorb at a particular wavelength; a good material should have high absorption capability over a wide range of wavelengths.
2. *Bandgap:* It is a very important property as it is the minimum energy required to excite an electron from the valence band to the conduction band, can also be defined as minimum energy required to move an electron from a bound to mobile state. The band gap is very important as all energies below the bandgap are not absorbed. The energy of photo-excited electrons above the bandgap is lost as heat. A preferable bandgap for a single layer solar cell is defined by conversion efficiency which was described by the Shockley Queisser limit [1], with the highest conversion for Gallium Arsenide which has a bandgap of 1.424eV. But, there exists ways to overcome the Shockley Queisser limit which will be discussed later.
3. *Cost of Materials:* This is an obvious factor in any manufacturing unit. It is not only dependent on how abundant the material is, but on other factors. The purity of material also plays a role in the performance of a solar cell, as the semiconducting layers also have to carry free carriers across them to be used for electricity whereas impurities tend to hamper the transport. Similarly crystallinity also starts to play a role then as carriers have to then move through a non-uniform area.
4. *Process ability:* Manufacturing the solar cell plays an important role in its final cost. Simple production methods are preferred to complex ones, as well as the reproducibility in large area/volume is also a requirement for low cost production.

1.3.1 Silicon based Materials

1.3.1.1 Crystalline silicon

The Solar industry is dominated by crystalline silicon, which is the more pure form of silicon. Silicon is widely available on the earth's crust and is widely used by the microelectronics industry. The purification of silicon starts with the reduction of sand/silica with a source of carbon (charcoal/coal) at high temperatures of 1500-2000^{o}C in an arc furnace. Further purification is also done to remove impurities, where the microelectronics industry uses very good quality or highly pure silicon which also drives up the cost of the feedstock material. Solar grade silicon can tolerate a little higher impurity levels and to decrease costs of production. A

standard method of refining is the Czokralski process where a seed crystal is used to pull silicon of desired orientation from a bath of molten silicon. There also exist other methods of refining silicon which are not discussed here. The solar industry uses a balance of economics, where mono-crystalline silicon is used for high efficiency at a higher cost, whereas poly-crystalline silicon is also used with relatively lower efficiency but gain in the cost of the feedstock material. The recent trends have turned towards lower thickness of high purity silicon to reduce costs, without losing more material during the process of slicing wafers.

1.3.1.2 Amorphous Silicon (a-Si)

Amorphous silicon is a widely studied material. It has a high absorption coefficient, but due to the disordered nature it was not used as a photovoltaic material as it contained many dangling bonds which acted as recombination centers. It was not until Chittick et. al. used hydrogen to passivate the bonds to make a more stable material with less defects that it was seriously considered as a photovoltaic material [2]. Another important improvement was that a-Si:H could be deposited through CVD methods by using different gas precursors which could be doped to form the n+ and p+ regions. Amorphous silicon based alloys can also be produced by alloying with carbon for higher bandgap, and germanium for lower bandgap.

1.3.1.3 Nano crystalline Silicon (nc-Si)

This is a material formed from small scale ordered silicon or as the name suggests it contains nano-crystallites of silicon in an a-Si:H matrix. It was initially believed to be a very poor material for solar cells. But the material was further developed by A. Shah et. al. [3] of IMT Neutchatel to give rise to a material which behaved closer to c-Si than a-Si.

1.3.2 Polycrystalline thin materials

There are other thin film materials also which show capability to absorb solar energy for production of electricity. Figure 1.2 shows the absorption coefficient where two more prospective thin film photovoltaic materials are shown

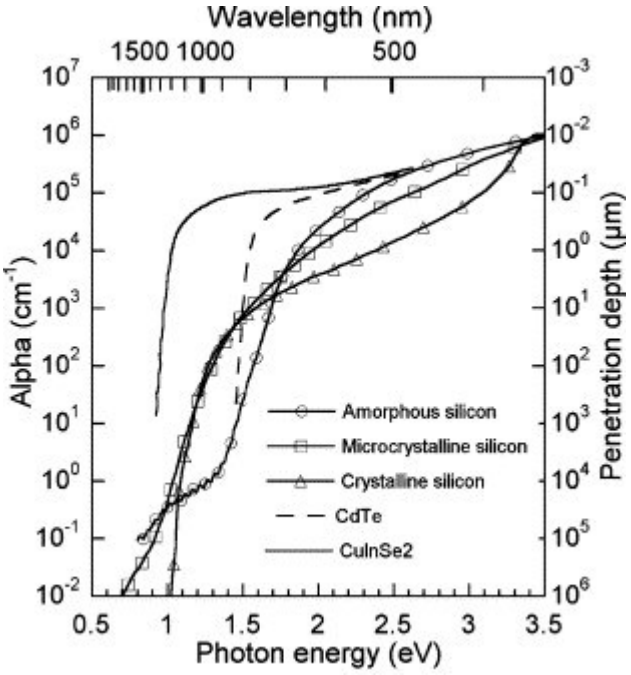

Figure 1.2: Absorption coefficient of thin film photovoltaic materials[4]

1.3.2.1 CIS or CIGS

CIS/CIGS is a solid solution of Copper Indium gallium Selenide and is a direct bandgap semiconductor which has very high absorption coefficient as seen in Figure 1.2. It is generally fabricated on glass substrates and as it uses a solid solution the processing window is narrow since it involves four elements. There also has been a lot of discussion for replacing costly material like indium and gallium which not only increase production costs, but also in case of indium there are other competing industries which would lead to a lack of material for large scale production. There has been research to replace Indium by zinc and gallium by tin respectively. Although CZTS uses non-toxic and earth abundant material, it is still being researched and only small scale production, and more work is required for commercialization.

1.3.2.2 CdTe

Cadmium telluride has grown at an exceptional rate is the last few years due to it's cheaper production costs. The major growth has come from First Solar and GE has also shown interest in manufacturing CdTe solar cells. Although there is a low cost, it does suffer from the use of cadmium which is a toxic material which may cause an issue during disposal. The disadvantage are that Cadmium is a heavy metal and Tellurium is not a widely abundant material. The major

problem in the application of CdTe cells have been forming the ohmic contact where Cu_2S was applied for a long time. But Cu_2S also suffers from stability issues.

1.3.3 Single crystal solar cells

In single crystal solar cells, the most widely used solar cell is based out of gallium arsenide. As it is a direct bandgap material, efficiencies very close to their theoretical limit can be realized according to various predictions [5, 6]. In practice an efficiency of 28.8% has already been achieved by Alta devices [7]. These solar cells are also in use with multi-junction solar cells which are complicated as materials of different band gaps have to be made with each of the layers giving equal currents. They are able to demonstrate efficiency in excess of 40% [7]. However the cost of manufacturing is very high and additionally the sun does provide a constant energy flux through the day, so they are more functional for space application where the cost would not be a major factor.

1.3.4 New Technology materials

Organic semiconductors are light and flexible, employing simple processing techniques. Since they are made out of simple carbon and hydrogen the idea is to tailor properties as required by adding side chains or ligands. There are some obstacles also especially dealing with it's reliability or long term stability and the effect of environmental factors on it. Nevertheless, a lot of work is going on developing new materials for polymer solar cells, small molecule based solar cells and dye sensitized solar cells [8-10].

There are also other groups looking at very cheap materials which are widely available to fill in as solar cells. There is research into pyrites which are cheap and abundantly available, and can be used for solar applications for large scale deployment [11-13].

Review of Literature

Although the photovoltaic effect was discovered in the early 20th century, it was not until the 1950's that major work started on PV technologies. PV technologies focused not just the work on crystalline silicon p-n junctions, but also the development of amorphous silicon (a-Si) as a PV material. The early studies on a-Si involved mostly growth of a-Si by evaporation and sputtering techniques which resulted in very pure quality material. Although it had good absorption properties, it also had a very high defect density due to its disordered nature leading to high recombination and poor conversion of light to current and hence did not lead to good solar cells, which required carriers to be collected after being excited by absorbed photons.

2.1 Hydrogenated amorphous Silicon (a-Si:H)

Hydrogenated amorphous silicon (a-Si:H) generated many applications to the study of disordered materials where the electronic defects could now be passivated with hydrogen which resulted in material with much better electrical properties. Today, all electronic grade amorphous silicon is an alloy of silicon and hydrogen. The initial experiments also involved the breaking down of silane at high temperatures [2] and even today silane is the main precursor gas used for deposition of a-Si:H. One of the most important discoveries in this area was the ability to dope a-Si:H to either n-type or p-type by adding phosphine or diborane respectively to the gas mixture of the plasma discharge used for depositing a-Si:H [2, 14]. This ability to dope a-Si in a glow discharge enabled device fabrication and initiated a lot of interest in further development of the material for fabricating thin film transistors, solar cells etc.

2.1.1 Atomic Structure

It is very important that we distinguish a-Si:H from c-Si which exhibit similar properties when measured optically, but does not have the same performance in a device. This distinction can be explained by looking closely at the atomic structure. As shown in Figure 2.1 c-Si has long range order, where every silicon atom is covalently bonded to four neighboring atoms. This makes the entire set of bonds equal in length and energy, all bond angles are same.

Unlike c-Si, a-Si:H has a random network, with similar short range order as the crystal i.e. most silicons are covalently bonded with four neighbors (saturated). This short range order is what makes a-Si:H have properties similar to c-Si. Although, the bond lengths and bond energies

deviate from that of c-Si, a distribution of bond angles exists with multiple local atomistic geometries. In the absence of hydrogen there are a lot of voids or dangling bonds or unsaturated bonds which leads a large number of electronics defects which cannot lead to effective devices. A dangling bond is when the silicon has 3 or lower neighbors and cannot covalently share its four electrons and is left with one or more unpaired electrons. Hydrogenation is the process of using the single electron of hydrogen to form a bond with the unpaired electron; this method is called hydrogen passivation.

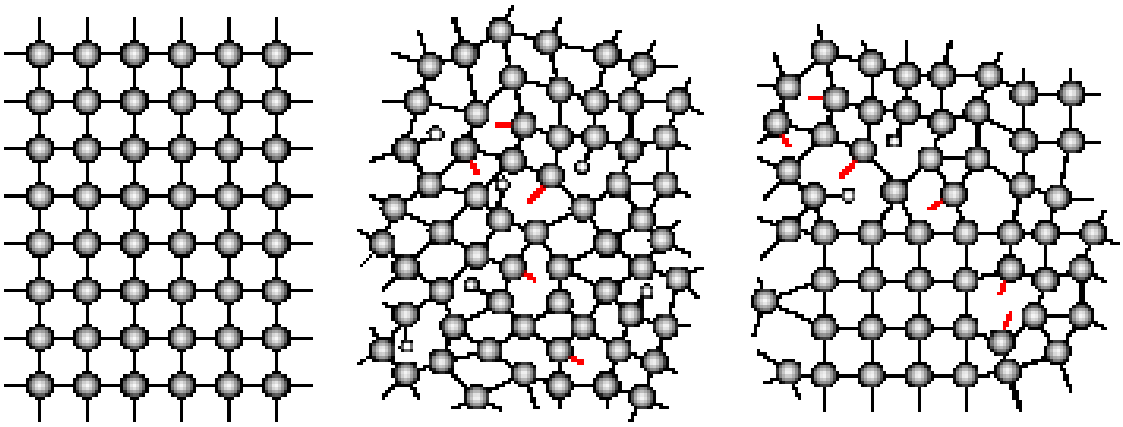

Figure 2.1: Atomic structure of silicon lattices (Left) c-Si (middle) a-Si:H and (right) nc-Si:H [15]

The density of states for c-Si and a-Si:H vary significantly due to presence of point defects or dangling bonds. Due to the presence of dangling bonds, a range of defects are present throughout the forbidden electronic energy gap state unlike c-Si whose energy gap state has no available states ideally in the bandgap region. A representative figure of the band diagram is shown in Figure 2.2 which shows that there are tail states and an mid gap defect states in a-Si:H. The tail states play a critical role in the performance of the solar cell and it is described by the Urbach energy which gives a width of the tail states. The concept of bandgap deviates from the classical model for a-Si:H where so many states are available in the bandgap and hence the term mobility gap is used to define band gap in a-Si:H. The typical value of mobility gap in a-Si:H is ~1.8eV which is larger than various optical gaps, other definitions of bandgap called Tauc's gap also exists and will be mentioned later.

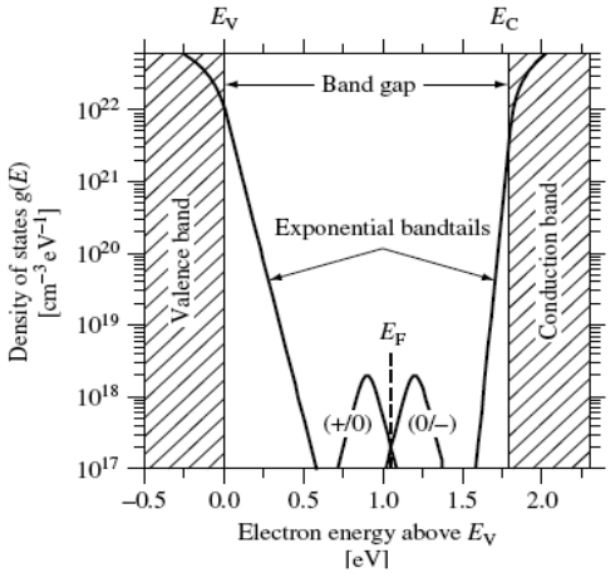

Figure 2.2: Density of state diagram for c-Si and a-Si [16]

It is especially important to talk about the optical properties of a-Si:H when discussing the application for solar cells. The optical properties make a-Si:H a very good material for application as a solar cell as seen in Figure 2.3. Amorphous silicon has a higher bandgap than c-Si but at higher energy it has a higher absorption coefficient which is attributed to the disordered network making it behave as a direct bandgap semiconductor, and absorbing photons more effectively.

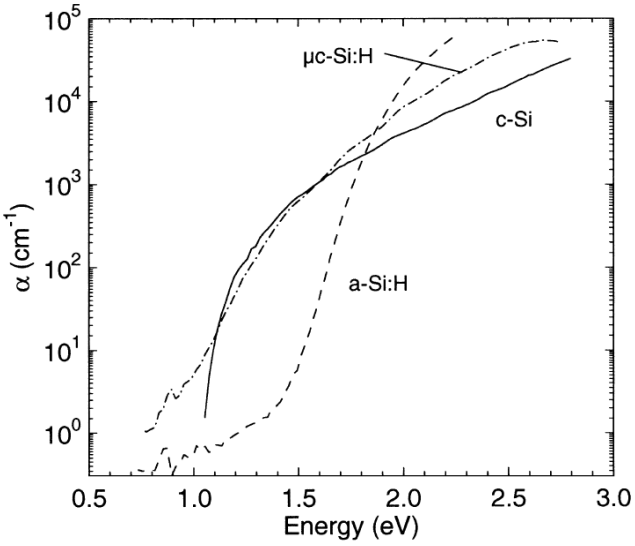

Figure 2.3: Absorption coefficient of silicon (a-Si:H, c-Si and μc-Si)[17]

2.1.2 Doping and Alloying

Doping played a very important role in the development of a-Si:H as a material for electronic devices as it was believed that due to high defect densities in a-Si, it could not be doped. The calculated mid-gap defect density was ~10^{21}/cm^3 for un-hydrogenated a-Si, which was decreased by hydrogen passivation to ~10^{15}-10^{16}/cm^3. This a-Si:H could be doped, but it took almost 10 years for a systematic study by Spear and LeComber [14] to show that it was possible to dope amorphous silicon by additional diborane and phosphine to their glow discharge deposition method. In the same paper [14], they also showed that it was possible to change the conductivity by a factor of 10^8 ,as well as to change the activation energy. This method has been effectively applied today by using different precursor gases especially in PECVD to change properties of films. Doping in a-Si:H is explained by Street et. al [18] by the model named as auto-compensation model. It is important to note also that when we increase doping in a-Si:H, the Fermi energy shifts close to the band tail states, so ionized doping atoms are compensated by space charge in the tail states so the Fermi energy would never move very close to the band edges.

Another important advantage is that the bandgap of a-Si:H can be varied by alloying it with other miscible elements like germanium and carbon. Germane (GeH_4) and methane (CH_4) are the precursor gases used in the plasma CVD process to deposit alloyed a-Si,Ge:H or a-Si,C:H. The first successful alloying is actually hydrogenation which effectively creates bandgaps from ~1.5eV to 2eV. But by adding miscible elements such as germanium to lower the bandgap and increase absorption coefficient due to additional germanium allows to make materials which are applicable in tandem junction solar cells (discussed later). The addition of carbon helps to increase bandgap and can be used as the top cell for a tandem junction cell. There has been a lot of very recent development of doping oxygen to make a wide bandgap a-SiO:H alloy which can be doped both n-type and p-type and have been used to replace the n+ or p+ layers respectively which prove to be efficient due to their higher bandgap [19-23].

2.1.3 Device structure

In c-Si the solar cell design is basically a wide p-n junction. However, a-Si:H cannot function in the same manner. Firstly, the diffusion length of carriers is very small in a-Si:H compared to c-Si, instead a modified structure of p-i-n or n-i-p is used where the ‘n’ and ‘p’ stand for n-type and

p-type doped layers and 'i' stands for intrinsic or undoped layer. Since diffusion is limited, the carrier collection is heavily dependent on the built-in electric field created by the difference between the Fermi levels of the p-type and the n-type layer. The carrier collection of a solar cell is therefore dependent on the electric field and hence the thickness of absorbing intrinsic layer has to be designed carefully to have enough electric field for good carrier collection.

An important factor affecting a-Si:H solar cells is the light induced degradation also known as the Staebler Wronki effect [24]. The loss in efficiency due to this long term effect due to light exposure which can partly be reversed by annealing at ~180-200^{o}C has been studied widely, although the exact nature of defects is still being studied and predicted [25-30]. Unfortunately, there has been no known way to completely eliminate light induced degradation, but there have been efforts to improve the cell quality by different methods such as chemical annealing [31-33] to improve the quality of the intrinsic layer, using thinner intrinsic layer with effective light trapping methods [34-38] and introducing materials like Nano crystalline Silicon (nc-Si) which are stable to light exposure.

2.2 Nanocrystalline Silicon (nc-Si:H)

Nanocrystalline Silicon (nc-Si:H) also called microcrystalline silicon (μc-Si), is a material in between the ordered c-Si and the random network a-Si:H. It contains crystallites of nanometer size (10-75nm) in a matrix of a-Si:H. The first development was described by S. Veprek and Mareek in 1968, other groups [39-42] followed through to develop it in PECVD deposition not only for solar cells but also for thin film transistors. But, these materials were of poor quality due to unintentional doping due to the incorporation of oxygen during film growth, as well as the deposition process was slow. Significant development came through with the work done at IMT Neuchatel [43, 44] to achieve conversion efficiency of 7.7% in a nc-Si:H solar cell [45].

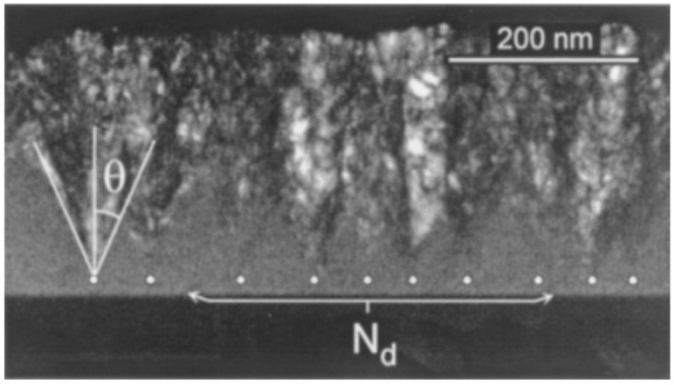

Figure 2.4: TEM image of growth of nc-Si:H showing conical growth [46]

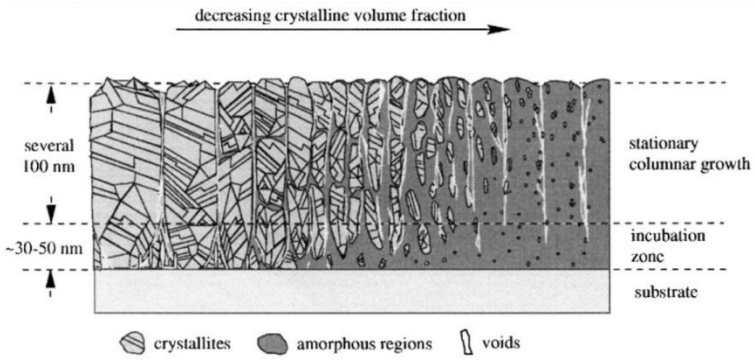

Figure 2.5: Schematic diagram showing the change in microstructural characteristics of nc-Si:H with crystallinity[17]

2.2.1 Growth Mechanisms

The growth mechanism in nc-Si:H silicon is a highly researched area and there are different methods followed by different groups. The primary difference from a-Si:H growth is the use of higher power and a high hydrogen dilution. It is important to mention here that dilution signifies the ratio of hydrogen flow rate to silane flow rate in this work, but other groups do have different methods of explaining dilution ratios. Although all the groups grow nc-Si:H consisting of an a-Si:H tissue, otherwise known as a incubating layer that provides sites for nucleation of crystallites for nc-Si:H growth (Figure 2.4) where the nc-Si:H growth is shown from the nucleation sites. The phenomenon of nucleation and the different parameters that affect it have been studied widely. It has been widely accepted by various groups that nc-Si:H growth takes

place by first nucleation and then growth in conical fashion [46-49]and then columnar growth takes place as shown in Figure 2.5.

There have been various models proposed for the growth of nc-Si:H. The *Surface diffusion* model proposed by Matsuda et. al. suggests that hydrogen plays a crucial role in nucleation of crystallites by providing local heating. SiH_3 radicals diffuse on the film and are adsorbed at theses preferential sites generated by local heating and then crystal growth continues through epitaxial growth [50]. The model suggests that the growth mainly depends on the substrate temperature, number of ions impinging and number of dangling bonds. While Dalal et. al. propose that Si-H bond energy ~3eV is hard to break [51]. Robertson et. al. also propose that excess hydrogen can be removed by formation of hydrogen complex . The *Etching model* proposed by C.C.Tsai et. al. which proposed that hydrogen atoms can break weak Si-Si bond to leave behind a more ordered structure where more layers can be added [52]. *Chemical anneal or layer by layer model* suggests that hydrogen in the bulk helps to break weaker bonds such that stronger bonds can be formed. There has been research in this area by various groups for stabilization of a-Si:H cells[32, 53-56].

Nc-Si:H has crystallites of size ranging from 10-75nm with the boundaries formed by a-Si:H and hydrogen mostly as shown in Figure 2.6(c). Therefore, the atomic structure is intermediate between c-Si and a-Si:H (see Figure 2.6(b)) where the crystallites represents the atomic structure of c-Si but the tissue is same as a-Si:H. The grain boundaries are rich in hydrogen content, shown by simulations done by Pan et. al. where they carry out molecular dynamic simulations [57]. A model developed by Kocka et. al. for the growth of nc-Si:H is shown here where they explain that after nucleating nc-Si grains, many small crystallites grow together in conical fashion and as thicker material is grown, the two cones eventually collide [49]. Smaller cones of crystallites have much lower defect density and therefore do not present a barrier for band like transport whereas when larger cones collide they form large grain boundaries. In addition, these grain boundaries are also potential sites for oxygen, carbon, nitrogen and even hydrogen to be trapped in during the growth process. These impurities can later segregate at the grain boundaries and have a different mobility gap or act as recombination centers.

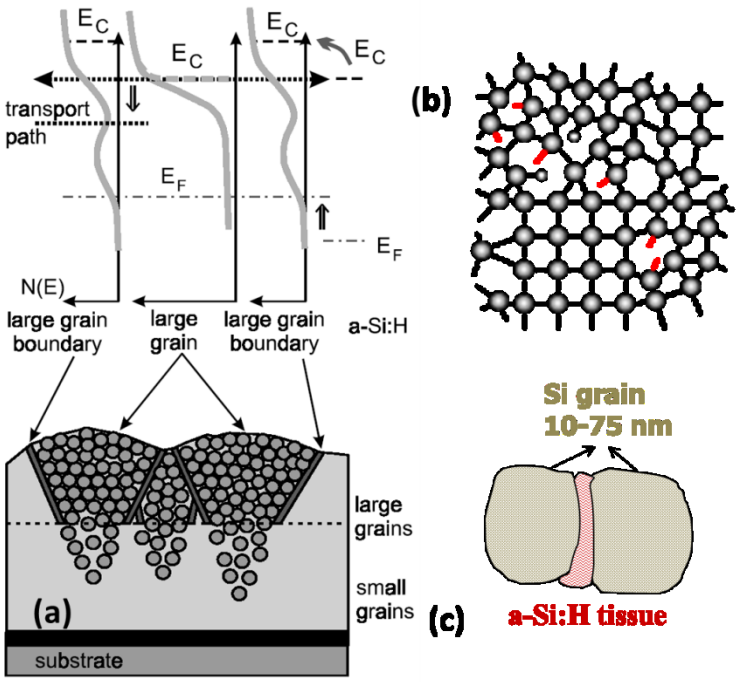

Figure 2.6: (a) Density of states for nc-Si:H[49] ,(b) Schematic of atomic structure of nc-Si:H and (c) Representation of crystallites in a-Si:H matrix for nc-Si:H

2.2.2 Design of Solar cells

The solar cell design is dependent on the fact that growth starts with nucleation but continues to grow in columnar manner and may lead to a very crystalline film as we proceed. Various approaches have been used by different groups to overcome the increasing crystallinity during growth. When we grow a film with the same power and gases as the film grows thicker the crystallinity also increases and the micro crystallites size increases with the defect density, so it is necessary to control the formation of such large crystallite and keep the defect density low.

The *Hydrogen dilution profile* is used by many groups [58-60] to control the crystallinity as the film is growing by decreasing the dilution as it grows to control the crystalline volume in the film. The growth of nc-Si:H films at constant dilution with other parameters kept constant is shown in Figure 2.7(b) where it has been shown that crystallinity continuously increases as thickness increases. Another important result is shown in Figure 2.7(a) which shows the Raman crystallinity (explained later) where the crystalline volume fraction is not changing with increasing thickness of the film when hydrogen dilution is employed.

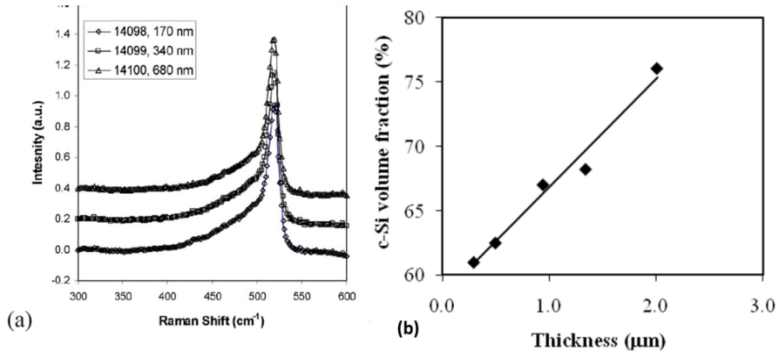

Figure 2.7: (a) Raman spectra nc-Si:H of different thickness [61] and (b) Increasing crystallinity at constant dilution [62]

The *Power profile* is based on the change of crystallinity due to power used to grow films, and has been found to be less widely used than hydrogen profile which may be due to additional factors affecting the growth when power is changed. But, recently good device quality has been shown by Han et. al.[63], who found that reduced ion bombardment helped improve their film quality. The crystallinity as well as the grain size remains in the same order when power profiling is employed is similar to that found in the hydrogen dilution case, as show in Figure 2.8.

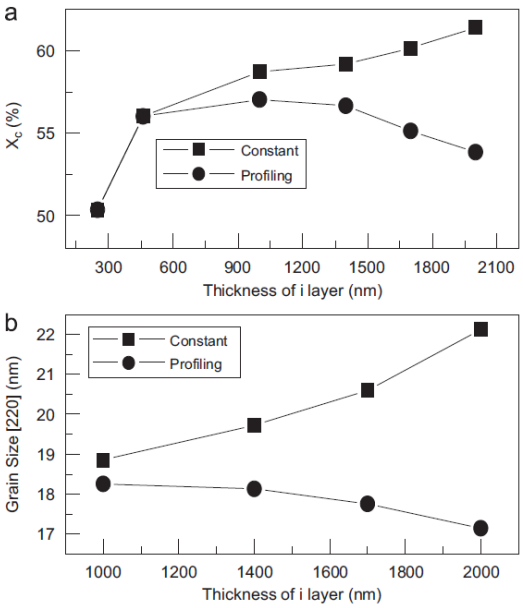

Figure 2.8: Variation of crystallinity with i-layer thickness for constant and profiling of power [63]

The *Superlattice design* is a method of nc-Si:H layer by layer groeth where the growth of nc-Si:H and a-Si:H layers are alternated. The growth of nc-Si:H layer is inhibited by a thin a-Si:H layer which helps in termination of the crystallite growth and then enables re-nucleation and growth of nc-Si:H until it is again terminated by an a-Si:H layer. This process is repeated many times to achieve desired thickness. A scheme of the design is displayed in Figure 2.9 showing the alternate layers. The thickness of both the layers plays significant role in the design and performance of the solar cell, for example thicker a-Si:H layers may provide a barrier for carrier flow and thicker nc-Si:H layers make it too crystalline. There is an in depth study of the design and fabrication of superlattice nc-Si:H solar cells in the doctoral thesis by A. Madhavan [64].

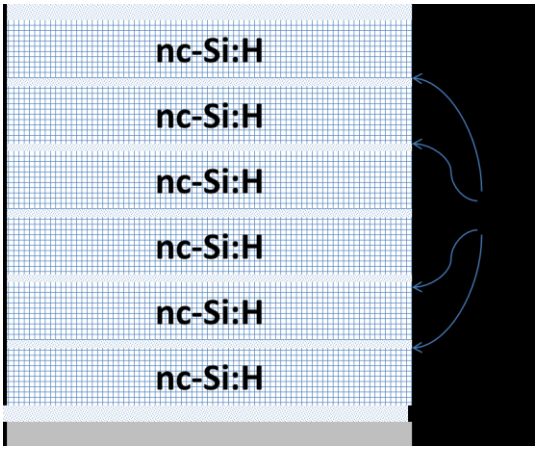

Figure 2.9: Schematic diagram of Superlattice structure

Superlattice design of fabricating devices has advantages for commercial use since the gas ratios would remain constant and the only change is the power cycling which can lead to amorphous or nanocrystalline films making the process less susceptible to processing errors. Moreover, the process windows in case of hydrogen profile devices are not that wide as shown in Figure 2.10 which makes it harder to achieve during commercial application. The thickness of the layers is controlled by changing the time of deposition of each layer and can easily be automated by using computer controls. The major advantage of cycling comes from the fact that the crystallinity remains independent of thickness as show in Figure 2.11. Further discussions have been made about the superlattice structure in latter chapters of the thesis.

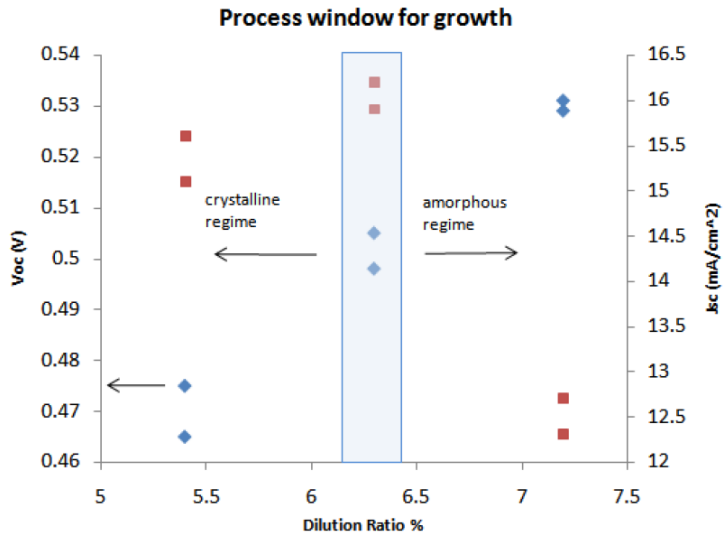

Figure 2.10: Process window for growth of hydrogen dilution profile devices [64]

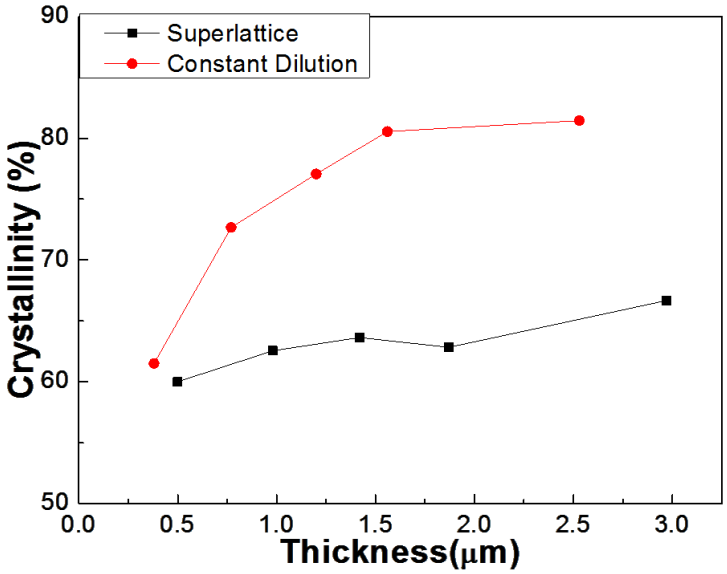

Figure 2.11: Comparison of superlattice and constant dilution nc-Si:H films [61]

2.3 Tandem cells

The concept of using multi-junction cells is to overcome the Shockley-Queisser limit, which defines the maximum theoretical efficiency for the single junction solar cells [1]. The detailed plot places silicon very close to the highest conversion efficiency of 33.7% possible. There have been various studies to cross this limit to cross this limit and one of the first thoughts is using multi junction cells which absorb light in complimentary wavelength ranges to absorb more

energy from the spectrum of sunlight. There have been calculations to verify that a maximum of ~86.8% efficiency can be achieved if infinite numbers of cells are connected in series with solar concentrator [65]. For a tandem cell with 2 bandgaps the Shockley-Queisser thermodynamic limit is 37% which moves to 42% for 3 bandgaps. A detailed investigation is shown in Figure 2.12 which suggests that the best matching cells for tandem solar cells is the micromorph solar cell in which the bottom cell of low bandgap nc-Si:H and top cell of higher bandgap a-Si:H[66]. We also show a-Si:H/a-SiGe:H/a-SiGe:H triple-junction solar cell in which gave an initial efficiency of 14.6% and stabilized efficiency of 13% [62].

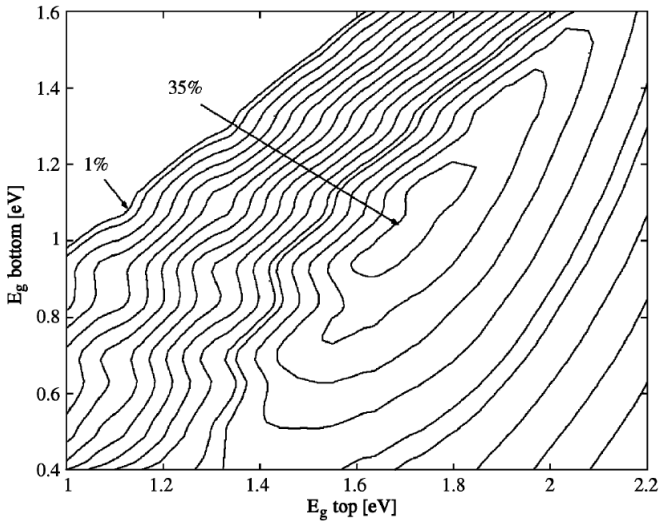

Figure 2.12: Efficiency limit for p-i-n/p-i-n tandem solar cells[66]

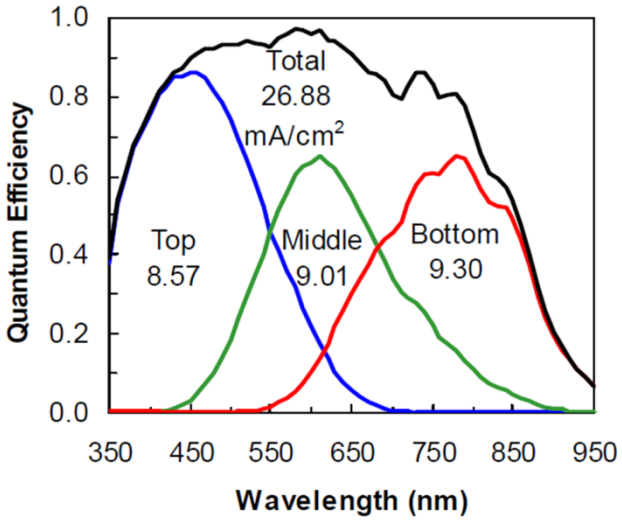

Figure 2.13: QE curves of a high efficiency a-Si:H/a-SiGe:H/a-SiGe:H triple-junction solar cell from the Unisolar group [62]

Tandem cells can consist of two or more cells connected together; however each additional cell comes with an added process complexity. For commercial purposes two or three layers are preferred. But, more complex architectures with multiple layers are also being researched especially for use in space or for concentrated photovoltaic applications where sunlight is concentrated to 10-100 times to a smaller area of the cell. They can be connected either in series or in parallel and depending on the connection, in-series the voltage gets added whereas in parallel the currents add up, and the cell is limited by the cell of lower current or lower voltage respectively. In this thesis most work carried out has been in the series connection mode where the voltages get added up and current is limited one of the cells.

2.4 Light Management

Light trapping is essential for enhancing efficiency in the solar cells. Silicon is a very good material for solar cell with high absorption coefficient, but absorption depth which is basically inversely related to the absorption coefficient does not tell same story. A better explanation for absorption depth is the distance a photon of a certain wavelength has to travel inside the material to get absorbed. In Figure 2.14 the absorption properties of silicon are shown and we see that if light passes through a standard wafer of silicon of 300µm (presently wafers for solar application are thinner) then longer wavelengths may not be absorbed at a single pass, it is difficult to absorb read and near IR wavelengths (λ> 600nm) in silicon solar cells. Making the

absorber layer thicker is not the right path as diffusion length is limiting the thickness of the cell. Also thicker devices imply higher chance of recombination and hence decrease in open circuit voltage (V_{oc}) as well as short circuit current (I_{sc}). This forces the designers to consider light management in the solar cells to make sure light can stay longer in the absorber so that it can be absorbed. There are also other loss mechanisms involved such as optical losses, recombination losses and resistance losses. Light trapping and antireflective coating are ways to reduce optical losses.

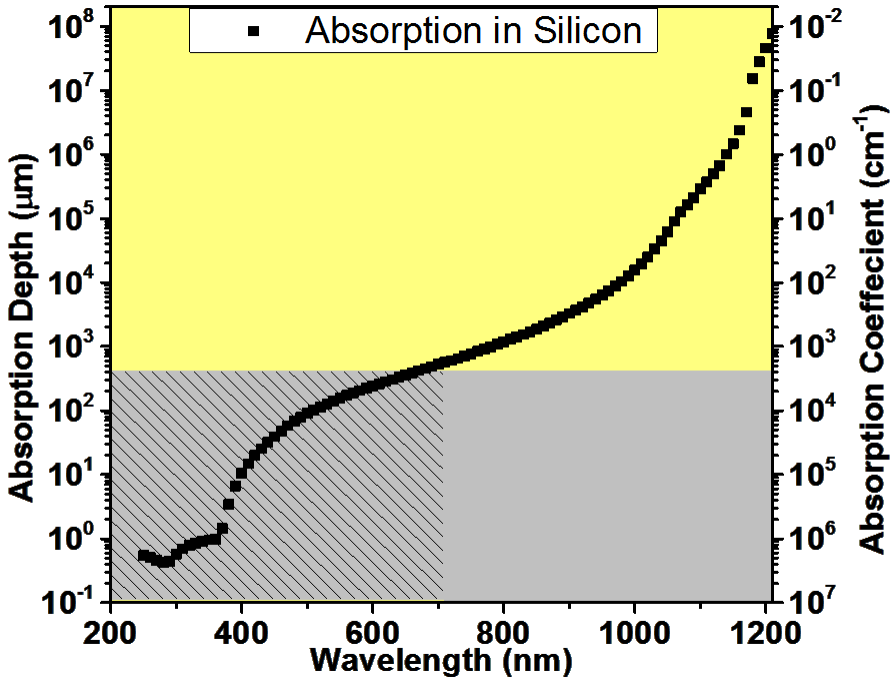

Figure 2.14: Absorption depth of silicon adopted from data by Green et. al. showing the regions where light management is required for absorption due to increases absorption depth[67]

In thin films, we work with lower quality material than c-Si, therefore the diffusion length is limited, for example: diffusion lengths of a-Si:H~20-50nm and nc-Si:H~1-5µm. The thickness of i-layer in a-Si:H is generally below 300nm. Therefore, light trapping is more important in thin films as they depend upon the electric field in the device for efficient carrier collection. So there has been various strategies to develop light trapping structures and models to enhance absorption in the absorber layer.

2.4.1 Anti-Reflective Coating (ARC)

As we had earlier explained that the light incident on the solar cell can optically be either reflected, absorbed or transmitted. Anti-reflective coatings have the primary function to minimize the reflection from the top surface, but most ARC's simulatneously work as the top contact and therefore must be conductive enough to decrease resistive losses. Although, present designs do incorporate metal busbars and fingers to decrease resistive losses, their design is important to minimize reflection and shadow effects from these metal lines [68, 69]. ARC generally consist of a thin dielectric layer, in case of thin films it is generally a transparent conducting oxide (TCO) such as Indium tin oxide(ITO) ,zinc oxide (ZnO) and tin oxide (SnO_2); more details about their fabrication and properties is given in the next chapter.

In a very simple case if we need to minimize the reflection, the idea is to choose a thickness for the TCO that has destructive interference for the light reflecting back. The calculation is done by simple ray model and there is an ideal thickness(d) for each wavelength (λ) which is one quarter the wavelength of light in the layer; d= λ/4n , where n is the refractive index of the TCO. Also, the ideal refractive index for the TCO is given by geometric mean of the materials i.e $n = \sqrt{n_1 * n_2}$ on either side of the TCO. For c-Si, there is also use of double layer of ARC to have less reflection but most thin film use a single layer of ARC to keep low cost of manufacturing. A single layer TCO is optimized for a single wavelength and not the entire solar spectrum leading to losses in other areas of the spectrum. The addition of texturing by various methods discussed later here also help in decreasing light trapping.

2.4.2 Theoretical model for light trapping

Crystalline silicon solar cells were developed more aggressively than thin films and so the initial research in light trapping methods were also developed for c-Si as the model material. Thin film silicon has used the same light concepts. The most famous work accepted for theoretical calculation of the limits of light trapping is the work done by Yablonovitch et. al. [70-72]. They adopt a statistical model where they assume that the light trapping is ideal; and there is an ideal loss less reflecting surface which reflects 100% of the light back that reaches the lossless reflector equally into all optical modes. The light rays are completely randomized by the lambertian scattering surface where all modes are equally populated within the absorber layer. The absorber layer has a refractive index (n) such that any light that comes in if scattered at an

angle more than the critical angle at the top surface, it would get reflected back into the absorber layer by total internal reflection. Therefore, the only loss for incoming light is due to any light that escapes through the escape cone when reflected at an angle less than critical angle as shown in Figure 2.15, which depends on the refractive index of the involved materials.

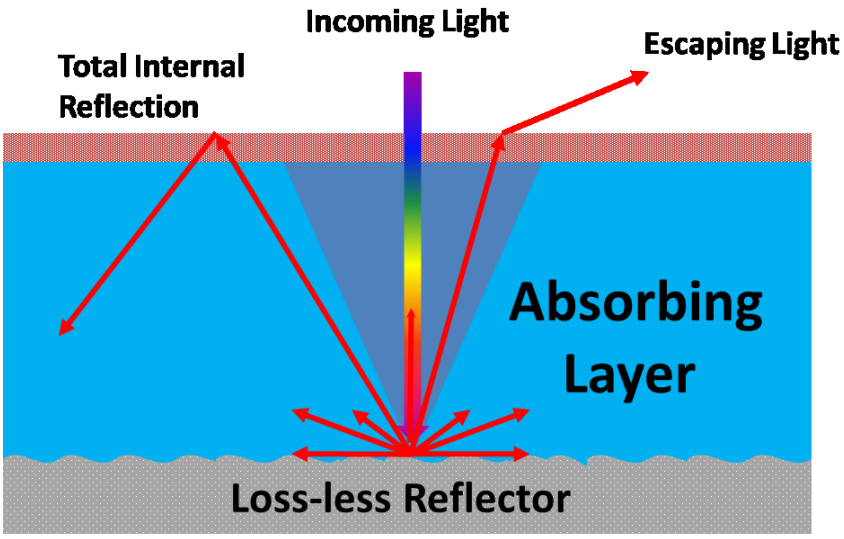

Figure 2.15: Schematic diagram for Lambertian reflector

The maximum path length of the incoming light can be enhanced by $4n^2$ times the thickness of the absorber layer (where 'n' is the refractive index of the absorber layer at each wavelength). This $4n^2$ value is also widely known as the Lambertian limit. This has been shown by the statistical approach of summing up the trapped rays in the absorber[71] or also comparing the area of the escape cone to the total surface area of the sphere for various modes in the semiconductor[73]. Finally, in case of silicon which has refractive index of ~3.5 the factor of enhancement in path length is ~50. A modified version of the model has also been reviewed by Stuart et. al. where they mention that for thin films not all the optical modes are useful, but if we took to account just the first three then about ~12-13 times path length enhancement is possible [74]. The current research by various groups is to approach or exceed the Lambertian limit of $4n^2$ [73, 75-88].

2.4.3 Random or Lambertian

The basis of light trapping is to increase the path length of light in the absorber layer. if we had a surface that was able to change the direction of the incident light; we can not only

decrease the reflection of light back (ARC) but also scatter light at different angles in to the absorber with additional help from a bottom reflecting surface to keep the light trapped inside the absorber layer by multiple reflection including TIR. The light trapping discussed here pertains to both substrate and superstrate type structure. There have been various approaches for developing these random structures and few methods have been explained here

2.4.3.1 Annealed/Hot Silver

Silver is an excellent reflector and has a property of agglomeration when thin films of Ag are heated at higher temperature, it agglomerates into islands. The basic idea is that silver has a higher affinity towards clustering than other materials and hence it tries to bond to other silver atoms close by and forms spherical shaped clusters to minimize energy, or go to its most favored state. This property of silver is used by various groups [89-92] to form what is known as annealed or agglomerated or hot silver. The process followed is to either deposit silver on a hot substrate or deposit silver and then heat at higher temperatures. It is mostly used for the substrate type configuration[93] but can also be used in other configurations which are discussed in sections 2.4.3.3.2 and notable this is an plasmonic effect discussed in section 2.4.4.2.

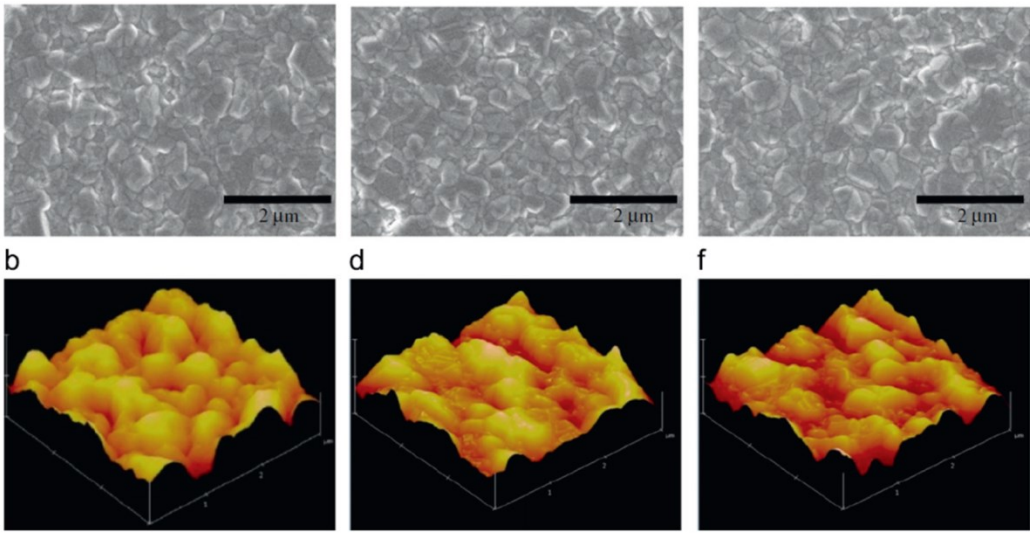

Figure 2.16: Annealing of silver at different deposition pressures with constant temperature (500^{o}C) and thickness (300nm); (b) σ_{rms}= 56.2 nm at P=1 mTorr,(d) σ_{rms} = 44.7 nm at P= 3 mTorr and (f) σ_{rms} = 42.1 nm at P=5 mTorr [91].

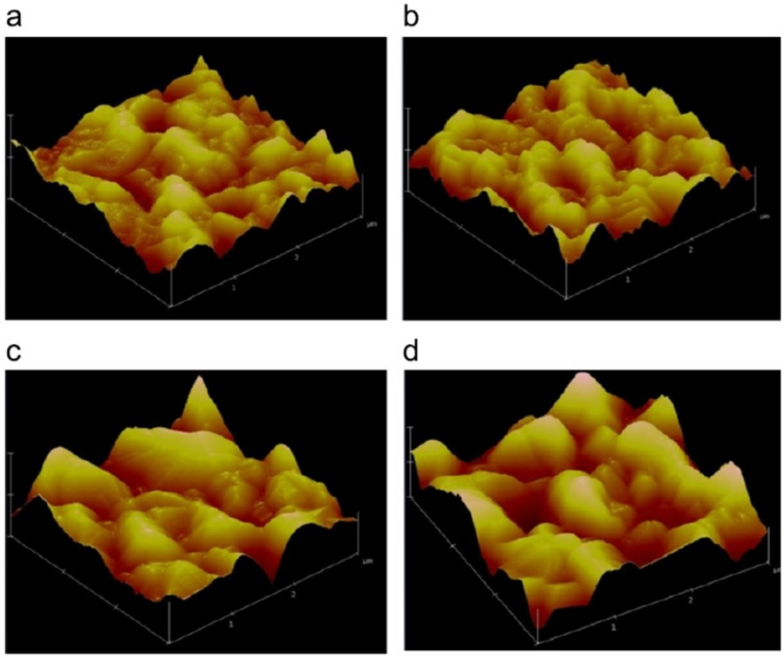

Figure 2.17: AFM images showing changes in the surface morphology and the surface roughness of the Ag films as a function of film thickness(T); (a) σ_{rms} = 48.3 nm at T= 100 nm,(b) σ_{rms} = 56.2 nm at T=300 nm,(c) σ_{rms} = 63.7 nm at T= 500 nm and (d) σ_{rms} = 88.0 nm at T=700 nm [91].

A schematic diagram of how silver agglomerates with changing pressure at constant thickness and temperature are shown in Figure 2.16 and Figure 2.17 shows the change in roughness (σ_{rms}) with thickness at constant temperature and pressure of deposition. These parameters can change the growth of silver during deposition itself. There exists another method to form these structures by first depositing it at room temperature and then annealing it at higher temperature to form roughened structures shown in later sections. In case of annealing, there is less effect at lower temperatures (~150°C) but on annealing and at higher temperatures (~400°C) the agglomeration pace picks up. The requirement (total= specular + diffused) is to have good reflection as well as good conduction (coverage all over). It is important to mention that the change of substrate has an additional effect not accounted for here.

There are various parameters that needed for fabricating the back reflector with the most important being the reflective properties. Unfortunately we also need to deal with roughness, since with increased roughness there is a chance of higher defect density which leads to poor

device quality or the lowering of V_{oc} and FF[89, 94-96]. So, an optimization is done to find the best match for higher current without decreasing the V_{oc} and FF. There have been various attempts at this work [61, 89, 97]. It must be mentioned here that silver is not used alone; it is used most generally in conjunction with ZnO as the dielectric layer on top for efficient coupling of light. ZnO also separates silicon from being in direct contact with the metal to avoid reactions and failure during use.

2.4.3.2 Etched or LPCVD ZnO

Zinc oxide (ZnO) is an important TCO which has been extensively used in both substrate and superstrate type configuration. It works as a TCO so is used for the incoming light and it can also be textured using wet chemical etch or CVD processes. There have been various studies on the use of ZnO in many different applications for multipurpose use. A lot of work has been performed to get lower absorption and higher conductivity as well as forming different structures for use for specific application also with multiple texturing on the substrate[98] as shown in Figure 2.18.

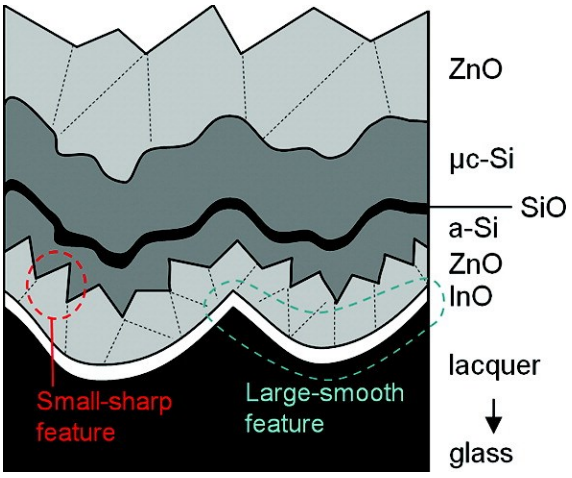

Figure 2.18: Schematic diagram of use of multiple texturing of the substrate at different stages [98]

There has been a lot of research for development of the chemistry of deposition of ZnO with additional dopants to increase conductivity, while maintaining a balance not to increase the absorption as it has been seen in case of many groups [99-101]. The most common dopant has been Aluminum, while other dopants such as gallium, boron, indium etc. have also been tried

for getting a balance between absorption and conductivity [101-105]. Figure 2.19 shows the increase of dopants affecting the carrier concentration which leads to lower resistivity when the dopant concentration is increased; on the other hand the absorption coefficient also increases due to the additional dopant atoms. Therefore, a lot of work has been done to optimize the dopant concentrations.

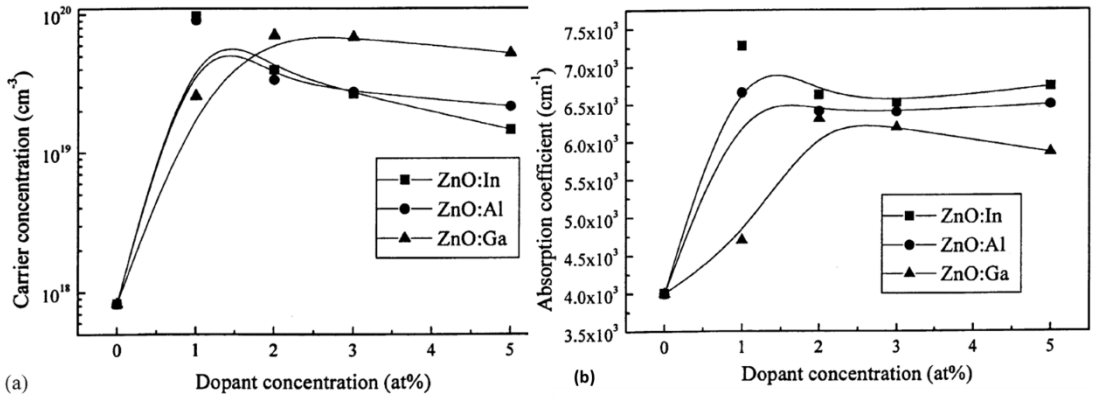

Figure 2.19: Effect of dopants on the (a) carrier concentration and hence the resistivity and (b) absorption coefficient [101]

While using magnetron sputtering on a flat surface, the properties of ZnO is also dictated by the chosen target which is predoped with a fixed amount and type of dopant. The deposited ZnO is then etched using a dilute solution of hydrochloric acid to get textures on the ZnO [89, 92, 99, 103, 104, 106-113] as shown in Figure 2.21. Another method of fabricating the textured ZnO substrates is by the use of LPCVD ZnO, which is self-texturing i.e. the as deposited films grow in pyramid shape and then can be plasma treated to make smoother surfaces or with controlled smoothnes as shown in Figure 2.22 and dopants can be added with a greater control while deposition to result in various properties [98, 100, 114-116].

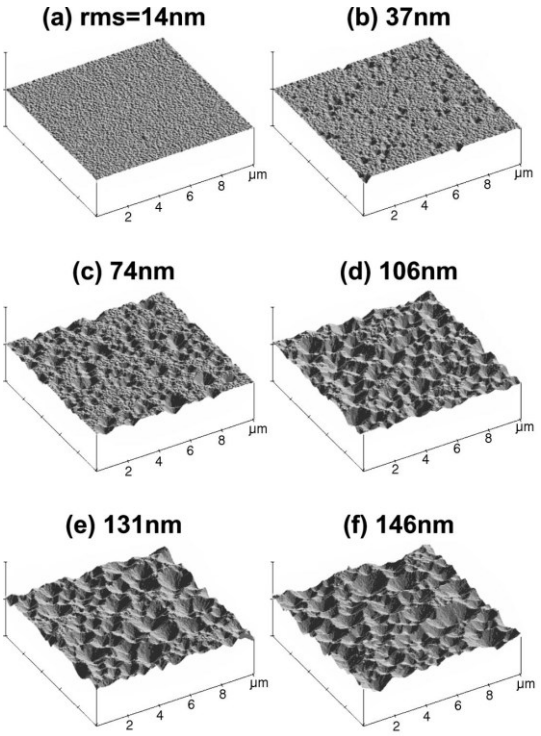

Figure 2.20: Increasing roughness of ZnO as time of etching is increased [117]

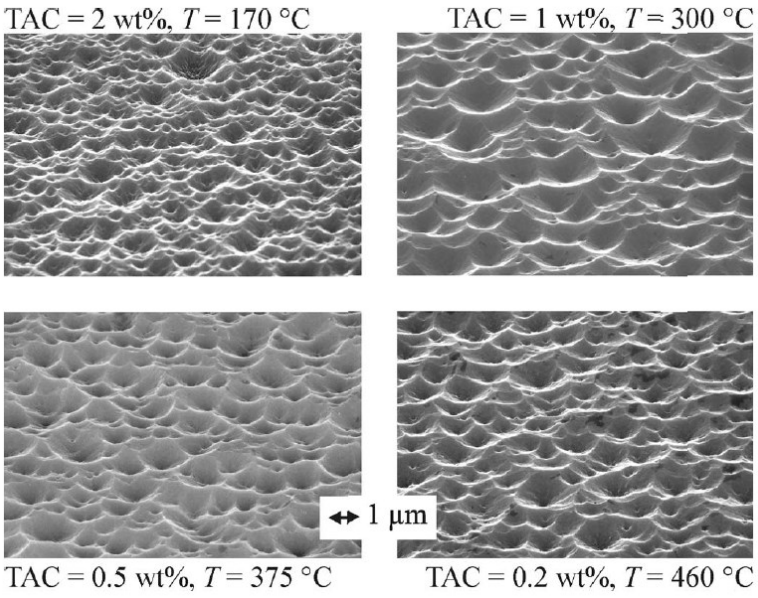

Figure 2.21: Textures of Al doped ZnO substrates by etching with HCl[99]

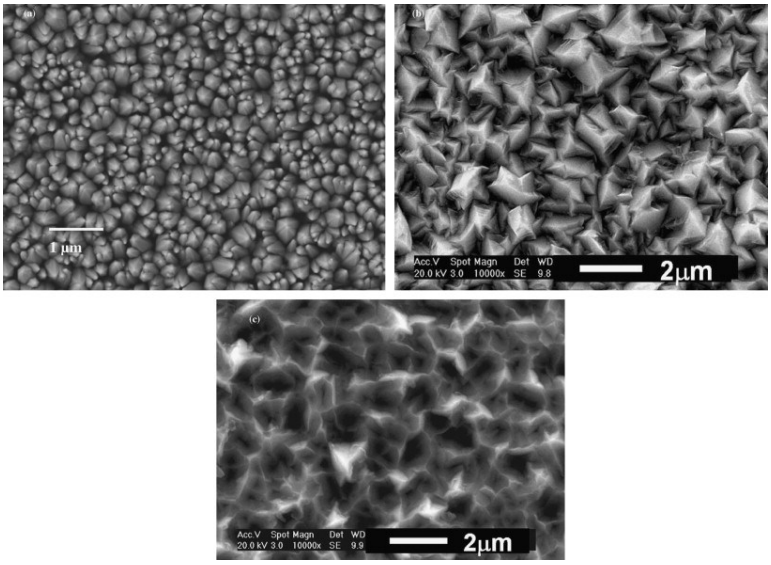

Figure 2.22: (a) SEM picture of multiple textured ZnO film. (b) SEM picture of a standard LPCVD ZnO film. (c) SEM picture of a standard treated LPCVD ZnO film[118] .

There has also been development to correlate the final roughness of the textured ZnO [89, 94, 95] to the quality of the device produced, and it has been found that high roughness is good for light trapping, but may lead to increase in defect density and in some cases even to crack formation [94, 95, 119]. The measures taken are structures without any sharp features, so a compromise has to be made with a lower light trapping for better device quality. In case of etching this has been taken care by etching less rougher structures[97] and in LPCVD ZnO a plasma treatment is used to change from V-shaped to U-shaped structures[95] which results in better quality film as shown in Figure 2.23.

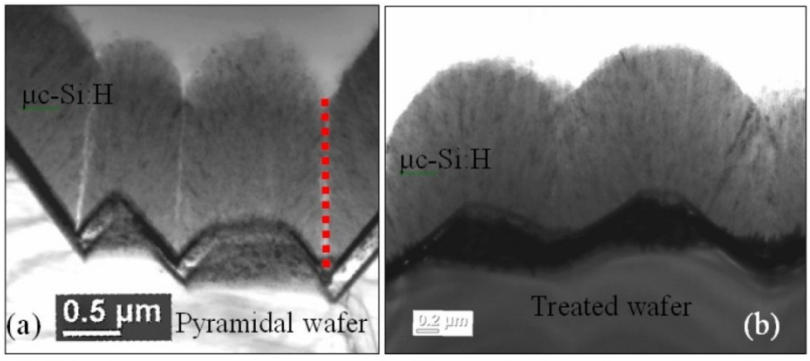

Figure 2.23: Crack formed on the V-shaped structures (left) and dense good quality film on U-shaped structures

There is also new development of transfer of the optimized textured ZnO structures to plastic substrates using nano lithography [76, 120-123]. In this scheme optimized structure is chosen and then replicated as shown in Figure 2.24 on plastic substrates.

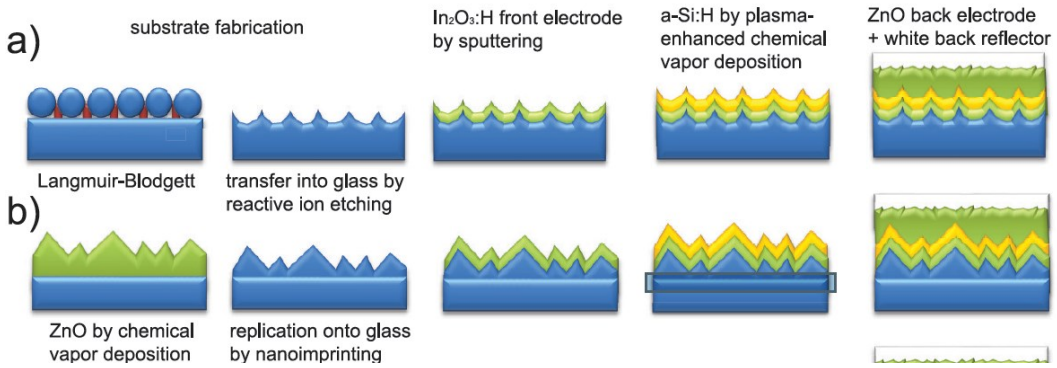

Figure 2.24: Schematic process flow of substrate and solar cell fabrication for the periodic nanocavity substrate (a), the random pyramidal texture (b), and the flat reference [76]

2.4.3.3 Other Methods

In addition, to the above two widely used light trapping structures new methods of randomly textured substrates are being developed by various groups. These methods are diverse and a few of the methods are discussed here briefly.

2.4.3.3.1 Silica Nanospheres

Silica nanospheres can be used to form a periodic self-assembled mono-layer which can be then coated with a reflecting surface which would reflect light randomly in different directions at the bottom for use in substrate type configuration. It is important to get a uniform monolayer of deposition using simple methods such as dip coating or spin coating or even costly processes as Langmuir-blodgett [124]. In Figure 2.25 a SEM image of a dip coated substrates are shown on glass and stainless steel.

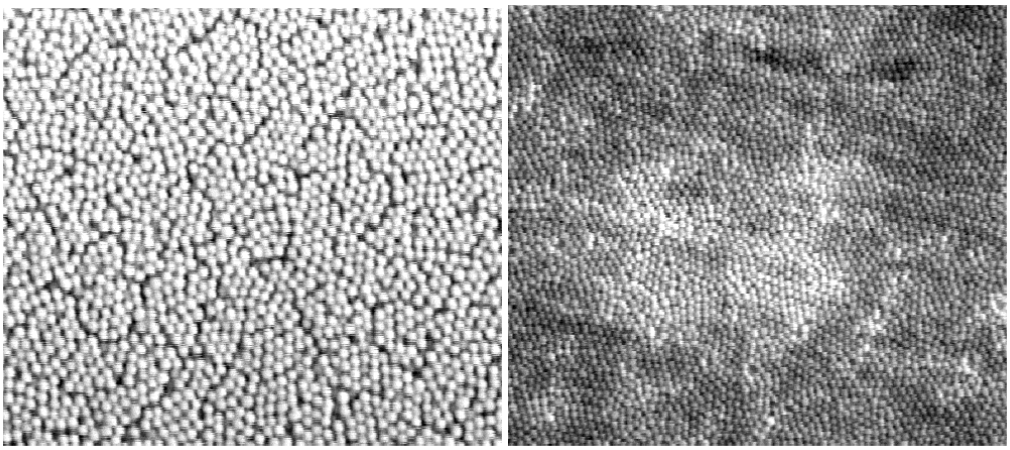

Figure 2.25: Monolayer of nano sphere particles deposited on glass (left) and stainless steel (right) with a layer of Ag deposited on top of the nano spheres [124].

2.4.3.3.2 Nanoparticles

The use of nanoparticles for light trapping is inspired from the plasmonic effect due to the light and metal interaction. Silver is generally the choice of metal here due to its low absorption in the region of interest and large scattering cross-section. It may be argued that it is similar to the concept used in annealed/hot silver but due to their small size they can create surface plasmons. A number of groups have studied this phenomenon of both theoretically and experimentally [85, 125, 126] and it is similar to concept used in Plasmonics (discussed later).

2.4.4 Periodic

The randomly oriented structures do not all have the same morphology and the experiments precede the model and the texturing is developed by a database of experimental data to guide the process of optimization. The periodic structures are defined as a single unit cell translated in various directions where the theoretical models and structure are predesigned by using various procedures to predict the light trapping effects and experiments follow. There are various groups that work in this area to develop new methods of light trapping using mostly nanostructures of different geometry at particular density to achieve higher absorption in the active layer [36, 38, 75, 76, 83, 90, 127-160]. There are various periodic structures which may be 1-D, 2-D or 3-D and they can be used for light trapping.

2.4.4.1 Photonic crystals (PC)

A photonic crystal (PC) is a periodic arrangement of a dielectric material that exhibits strong interaction with light. The development of photonic crystals is analogous to the atomic structure in crystals; instead of the working with Schrodinger equation here we deal with Maxwell equations. Therefore, if designed carefully photonic crystals can exhibit photonic band gaps i.e. electromagnetic waves cannot propagate in particular frequency range similar to the energy band gap in semiconductors where there is no available state in particular energy gap. The first proof of existence of photonic gap was shown in parallel by Sajeev John [161] and Eli Yablonovitch [70]in 1987 and in 3-d by Ho et. al. at Iowa State University in 1990 [162]. A schematic diagram showing the above is shown in Figure 2.26, where band gaps can form due to periodic arrangement of atoms and dielectric medium respectively.

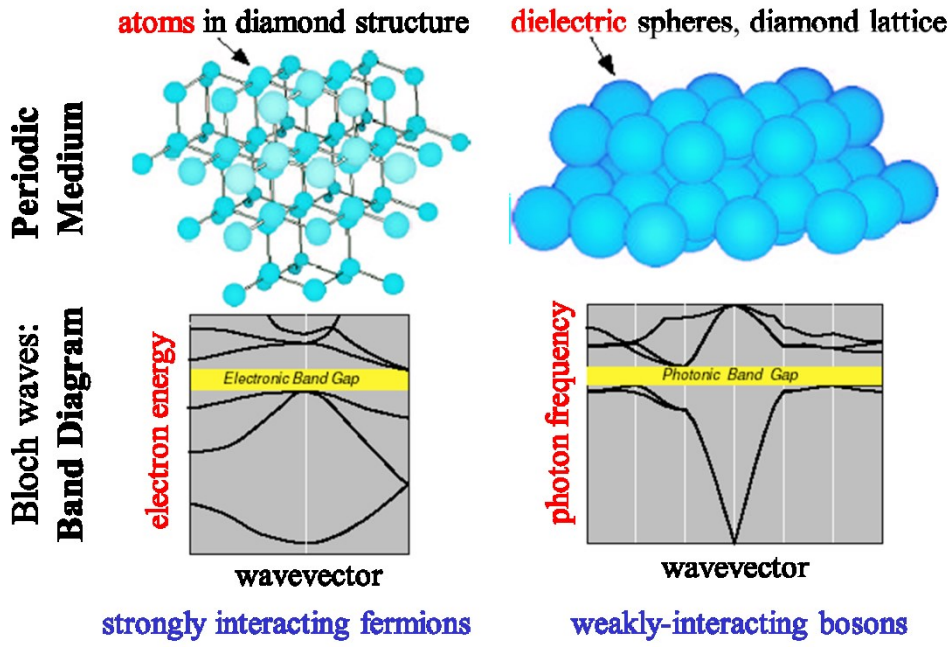

Figure 2.26: Schematic of electronic and photonic structures with bandgaps[163]

Electromagnetic radiation propagating through a dielectric medium follows a simple linear dispersion relation i.e. $\omega=ck/n$ where n is the refractive index of the dielectric medium. Now, if we have a modulation of the refractive index, through which the wave has to propagate then the simple dispersion relationship cannot explain the complete phenomenon. The design of photonic crystal is based on the four macroscopic Maxwell's equations namely

$$\nabla.\vec{B} = 0\,, \qquad \nabla \times \vec{\mathrm{E}} + \frac{\partial \vec{B}}{\partial t} = 0$$
$$\nabla.\vec{D} = \rho, \qquad \nabla \times \vec{H} - \frac{\partial \vec{D}}{\partial t} = J \qquad \text{2-1}$$

Where $\vec{E}$ and $\vec{H}$ is the electric and magnetic fields respectively and $\vec{D}$ and $\vec{B}$ are the displacement and magnetic induction fields and ρ is free charge density with J being the current density. There are some assumption made to solve the equation such as the photonic crystal is an isotropic medium, with no free charge so ρ=0 and therefore J=0 and ε(r,ω) =ε(r).

And, D(r,ω)= ε(r).E(r,ω)

The magnetic permeability is constant, So B= μ.H(r,ω)

We can rewrite Maxwell equations for each frequency,

$$\nabla.\vec{B}(r) = 0\,, \qquad \nabla \times \vec{\mathrm{E}}(\mathrm{r}) - \mathrm{j}\omega\vec{B}(r) = 0$$
$$\nabla.\vec{D}(r) = 0, \qquad \nabla \times \vec{H}(r) + j\omega\vec{D}(r) = 0 \qquad \textbf{2-2}$$

Using the above equations with c= 1/εμ, we get to

$$\nabla \times \left[\frac{1}{\varepsilon(r)}\nabla \times H(r)\right] = \left(\frac{\omega}{c}\right)^2 H(r) \qquad \text{2-3}$$

Now, Equation 2-3 is essentially an eigen value problem with an eigen value of $(\omega/c)^2$ and the operator θ

$$\theta = \nabla \times \left(\frac{1}{\varepsilon(r)}\nabla \times\right) \qquad \text{2-4}$$

These equations are then solved computationally, we use scattering matrix method to solve these quations. Another thing to note is that equation 2-3 is scalable i.e if we scale the structure by a factor s, then both frequency and field profile is scaled by the same factor. This is important in case of photonic crystal as different wavelengths can be controlled by the feature size on the PC. If we scale $\varepsilon^{I}(r) = \varepsilon(r/s)$ then equation 2-3 becomes provided that E is frequency dependent

$$\nabla \times \left[\frac{1}{\varepsilon^I(r^I)}\nabla^I \times H^I(r^I/s)\right] = \left(\frac{\omega}{cs}\right)^2 H(r^I/s) \qquad \text{2-5}$$

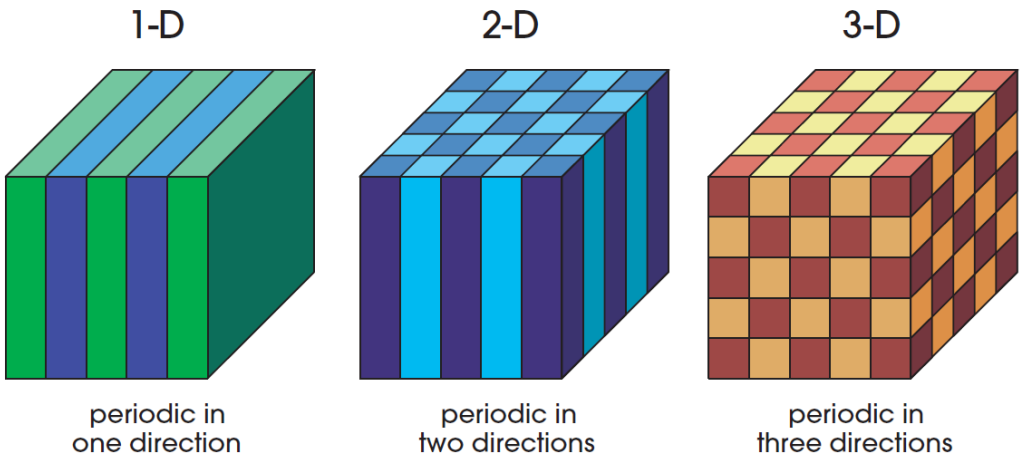

Figure 2.27: Schematic diagram of photonic crystals in 1-D, 2-D and 3-D[163]

There are certain requirements for building a photonic crystal which have been discussed in brief and summarized here

- Dimensionality: 1-D, 2-D or 3-D (shown in Figure 2.27)
- Symmetry: Similar to atomic crystals, photonic structures are also built by translation of unit cell in different directions depending upon its dimensionality. The pitch defines the distance between each repeating structure.
- Refractive index contrast: the basis of photonic crystal depends on the periodic modulation of the refractive index change. Figure 2.27 shows the changing refractive index for different dimensions of photonic crystal.
- Scalability: Since the fundamental equations are free from fundamental length scales we can use the same result of the equations to different length scales

2.4.4.1.1 Bragg Reflector

The Bragg reflector is simplest form of a 1-D structure which uses the same concept as photonic crystal by using multiple layers of dielectric materials of different refractive index to cause constructive interference at each layer to maximize reflection. It has been used as a waveguide in optical fibers; they form an important component for laser. A 1-D photonic crystal is widely known as Distributed Bragg Reflector (DBR), it has been shown before that when they are solved they lead to formation of photonic bandgap[163]. The thickness of each layer is a quarter wavelength of light in that medium and sufficient refractive index contrast is needed.

Reflectivity can be increased by increasing the number of dielectric layers or also by increasing the contrast between refractive index.

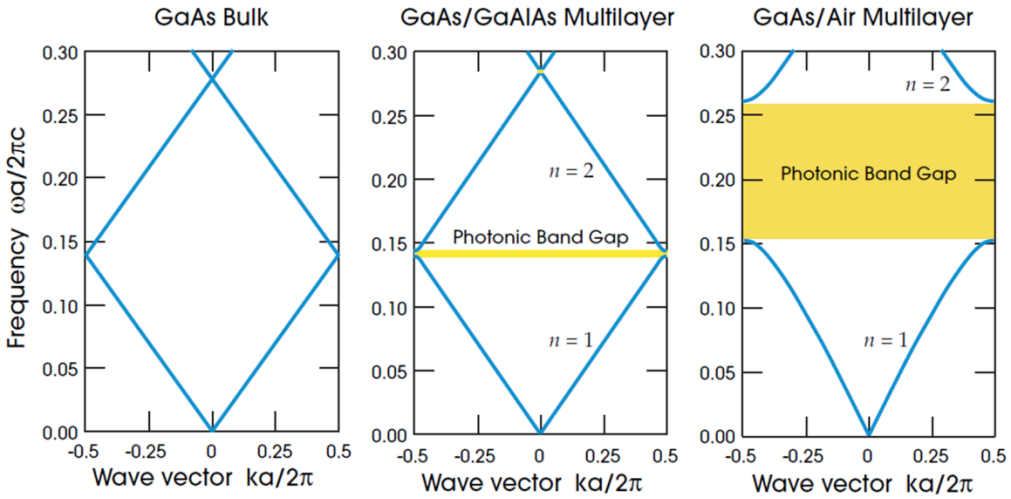

Figure 2.28: Photonic band structure for 1-D photonic crystal as shown in Figure 2.27 (left) Constant ε=13 (middle) Multilayer with ε=13 and 12 (Right) Multi-layer with ε=13 and 1 [163].

2.4.4.1.2 2-D Photonic slab

These types of photonic crystals have been extensively used due for light management in solar cells by various groups [75, 76, 83, 136, 137, 140-143, 153, 164-168] and less complex fabrication method compared to 3-D photonic structures. They generally consist of a 2-D periodic variation of dielectric index materials with particular geometry such as a hole, cone, pyramid, cylinder etc. in a lattice such as triangle, square or hexagonal. In a solar cell it acts as a diffraction grating, in c-Si SiO_2 has been used as the dielectric to provide refractive index modulation. In Figure 2.29 the TE and TM modes have been shown for a 2-D photonic crystal.

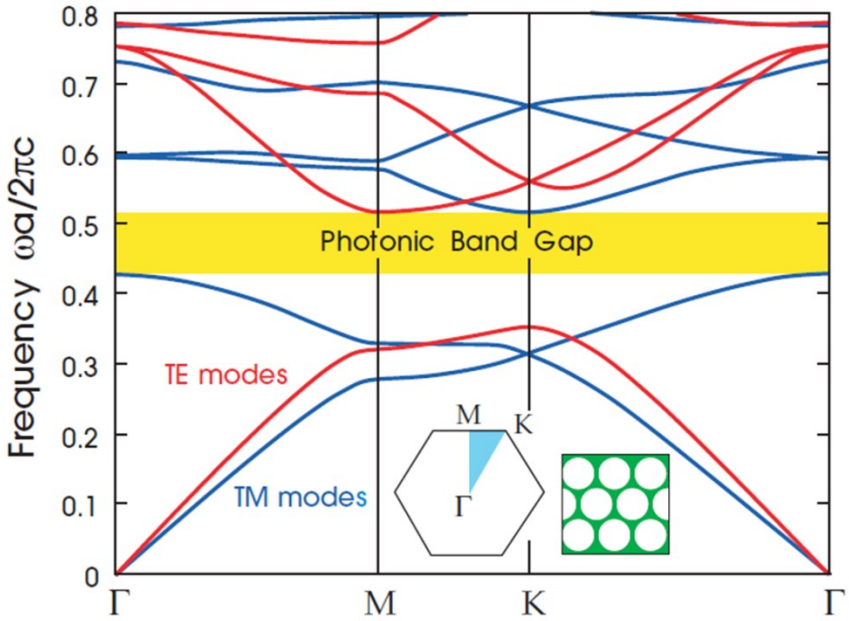

Figure 2.29: Photonic band structure for the modes of a triangular array of air columns in dielectric substrate (ε=13). (Blue: TM bands and Red: TE bands)[163]

2.4.4.1.3 3-D Photonic crystal

In theory, the 3-D crystal can be made from arrays of structure like spheres or tubes. One of the first photonic bandgap structures was found by Ho et. al. with a diamond lattice of spheres [162]. A simple thought would be putting two 2-D photonic crystals together to get a 3-D structure, but in practice it is not easy. There has also been less development due to the intricate details required for fabricating these structures making it hard for commercial application. In recent times 3-D structures have been realized in practice like Yablonovite which is made by drilling holes along three lattice vectors of FCC crystal [169], the wood pile structure is a stack of dielectrics arranged in orthogonal orientation [170] and invers opals which is one structure that has been put into application as the intermediate reflector for tandem junction solar cell [171].

2.4.4.1.4 Computational method (Scattering Matrix Method)

There are many methods for solving the Maxwell equations as mentioned in previous sections. The work done in this thesis is based on the results from scattering matrix method which is discussed by Biswas et. al.[172]. This method is an extension from the well-known transfer matrix method where the structure is divided into many layers as shown in Figure 2.30

and the coefficient of incident, reflected and transmitted fields are calculated. A small slice can be depicted for the shown slab to solve by scattering matrix

$$\begin{pmatrix} \delta_i^+ \\ \delta_{i-1}^- \end{pmatrix} = s^i \begin{pmatrix} \delta_{i-1}^+ \\ \delta_i^- \end{pmatrix} \qquad \textbf{2-6}$$

Using this scattering matrix, and an algorithm to connect all the slices together to form a total matrix we can solve the problem faster. Furthermore, the dielectric material used only varies in x and y-direction and each slice is homogeneous in the z-direction. The Maxwell equation is then integrated with the correct boundary conditions to obtain scattering matrices for each layer in the structure.

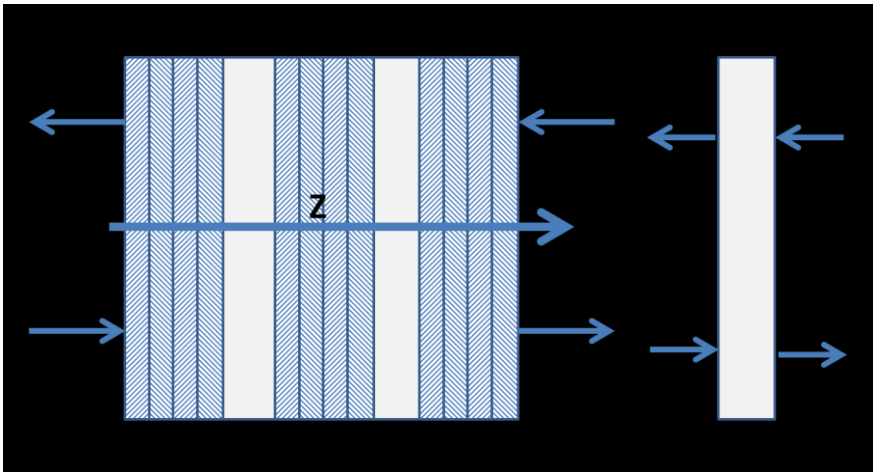

Figure 2.30: Method of slicing each slab into number of slices

Using the condition (A = 1 – R –T) where R and T are the total reflection and total transmission respectively for each wavelength we can find the absorption for each wavelength [173] this helps to calculate the weighted absorption

$$\langle A_w \rangle = \int_{\lambda_1}^{\lambda_2} A(\lambda) \frac{dI}{d\lambda} d\lambda \qquad \textbf{2-7}$$

$$J_{sc} = \frac{e}{hc} \int_{\lambda_1}^{\lambda_2} \lambda A(\lambda) \frac{dI}{d\lambda} d\lambda \qquad \textbf{2-8}$$

And the current density (J_{sc}) can also be predicted.

2.4.4.1.5 Solar cell application

PCs have been applied to solar cell light management scheme by various groups by extending the same concept of interference that is used for determining the requirement for an antireflective coating in section 2.4.1. The additional feature is to have a periodic structure which would lead to diffracting the light into different wave guiding modes. The design of the periodic structure would determine if the wave guiding mode would be effective in absorption or may lie in wavelength range the absorber layer does not absorb. The effective way to carry out this calculation is to look at the active modes in the wavelength range (>600nm). This is chosen because the first pass should be able to absorb wavelengths below 600nm for thin film silicon. The design in now an open question and many groups have tried to design different periodic structures for using this phenomenon.

There have been a lot of theoretical studies for improving the efficiency of solar cells using the PCs with an approach similar to that mentioned above. One of the first approaches was by Zeng et. al. for c-Si solar cells using 1-D PC for current enhancement in c-Si solar cell and show a enhancement up to 135 times between 1000-1200nm [168]. Bermel et. al. compare the use of different dimension of PC on a 2μm thin film of c-Si where they get a 24% , 26.3% and 31.3% enhancement by using 1-D grating, triangular lattice photonic crystal holes of air and using both over a 6 bilayer DBR [166, 167]. Mallick et. al. also simulated periodic PC structures with two layers of holes to get an absorption enhancement close to 2.5 times [153].

PCs have also been studied for thin film silicon solar cells recently for enhancing absorption. Biswas group designed a PC back reflector for a-Si:H solar cells where they compare their results with the classical $4n^2$ limit. The design considers a 2-D photonic crystal with tapered cones in a triangular lattice to improve the efficiency of the solar cell, [135, 139, 140, 142, 143]. The experimental proof of the concept of hole array has been shown by Curtin et. al. showing the improvement in the current density [139] and for tapered cones too which have been discussed later in this work. Gomard et. al. have also designed using rigorous coupled wave analysis method for simulation and then fabricated a-Si:H cells with 2-D PCs where they show that up to 28% on 100nm a-Si:H [174]and 40% increase in absorption can be obtained by employing their suggested structure [174, 175] where they pattern the a-Si:H itself to be part of the PC. There

have been efforts to use to replace the intermediate reflector using photonic crystal discussed in section 2.4.5.1.

2.4.4.2 Plasmonics

Surface plasmons are the result of electromagnetic radiation interacting with a metal surface resulting in oscillations of electron on the surface of a metal. In recent years this phenomenon has been researched for various applications such as waveguides, lasers, light emitting diodes and many others. We look at the possibility of it being used for enhancing light trapping in thin film solar cells. An important point to note here is that although we discuss plasmonic interaction in the periodic section it is applicable to both periodic structures and non-periodic ones, for example annealed/hot silver discussed in section 2.4.3.1 also has plasmonic interaction, but these localized plasmons may be lossy in nature.

A very good review of enhancing solar cell efficiency through plasmonic interaction is given by Atwater et. al.[85] where they explain the three methods how plasmonic interaction can be used favorably in a thin film solar cell for light trapping. Figure 2.31 shows three different ways that plasmonic effect can be favorable used starting with the particles on top where light can get scattered at different angles to increase the path length in the absorber layer[176, 177] as shown in Figure 2.31(a). In addition there have been reports that there would be strong constructive interference between scattered and transmitted light above surface plasmon resonance wavelength but also destructive below the plasmon resonance wavelength [178]. There has to be a balance here for the size and coverage of particles to avoid destructive interference causing reflection. The next method is to incorporate nanoparticles in the absorber to get localized plasmonic enhancement by increasing the optical absorption especially close to the metal surface plasmons which create increase light intensity and therefore an increase in optical absorption as shown in Figure 2.31(b), while this method would lead to localized plasma it is more difficult in processing without avoiding defects due to metal incorporation. Figure 2.31(c) shows use of metal structure at the back where if periodic structures exist there can be photonic wave guiding modes or even surface plasmon polariton (SPP) modes can be formed which would propagate parallel to the surface of the metal and there would be a decaying field into the semiconductor [83, 90, 134, 179].

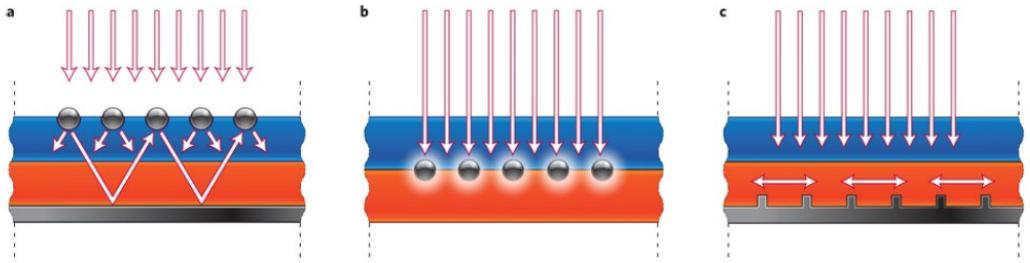

Figure 2.31: (a) Light trapping by nanoparticles from metal nanoparticles on the top surface of the solar cell (b) Light absorption enhancement in the semiconductor by embedded nanoparticles (c) Light trapping by coupling to guided modes of the solar cell from nano patterned metallic back contacts [85]

There has been a lot of work to analyze the effect of plasmonic interaction in solar cells not only in thin film solar cells[177, 180-184], but also in organic based solar cells, dye sensitized solar cells[185-190], and also crystalline solar cells[191]. In the above section the methods of how light trapping could work in a solar cell was discussed, in addition there are more factors that play a role in effective plasmonic light trapping. The shape and size of the particle from which light scatters is also very important; Chen et. al. show that particles of 200nm give them the best enhancement in J_{sc} in comparison to smaller particles[125] which has also been confirmed from other groups[134, 179, 192] that larger particles are more effective for scattering light in wider distribution angles which enhances broadband absorption. While there is also an effective size as larger particles do not have the same enhancements which may be due to multiple excitation modes with smaller scattering properties. The effect of shape of the particle is also important which is shown in Figure 2.32 showing the fraction of light scattered into the substrate for different Ag particles on a 10 nm thick SiO_2 on Si showing performance of different geometry for plasmonic enhancement. The choice of metal is predominantly silver due to low absorption loss.

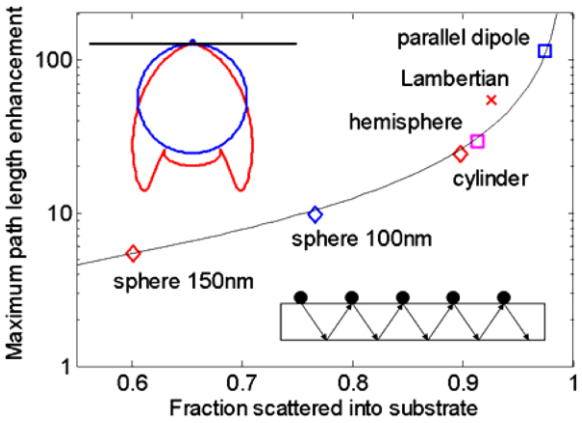

Figure 2.32: Effect of shape for light scattering into substrates[84]

These plasmonic structures however are better used with a dielectric layer as the plasmonic resonance of Ag is ~350nm in air which can be shifted towards the red/infra-red in material whose dielectric constant is higher than air as shown in Figure 2.33. There is a strong field enhancement around the metal which could lead to increased absorption in the semiconductor close by and it is more effective in small metal particles (<20nm). Unfortunately using this method in thin film silicon solar cells leads to many defects and hence high recombination so has not resulted in much use. This method has gained some importance in organic and dye sensitized solar cells.

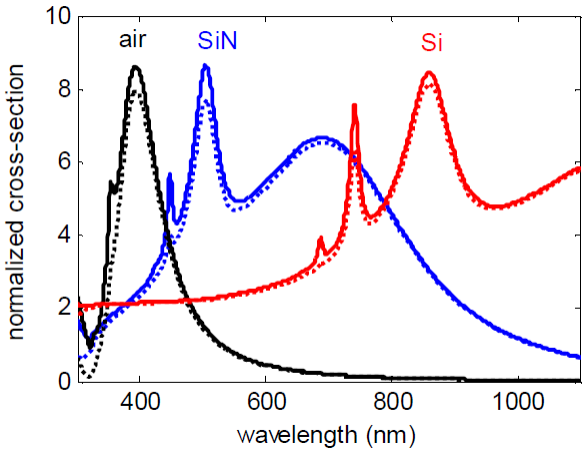

Figure 2.33: Extinction (solid lines) and scattering (dashed lines) cross-sections for 100-nm diameter Ag spheres embedded in air (black), Si3N4 (n=2, blue) and Si (red), normalized by the projected area of the sphere. [192]

Surface plasmon polaritons (SPP) can be formed when the metal is used as the bottom of the cell where the wave propagates parallel to the surface. SPPs can efficiently trap and then guide light into the absorber layer. This is possible when we use a periodic structure as shown in Figure 2.31(c) and then the geometrical shaped metal layer can be used to couple the incident light to propagate plasmonic modes or photonic wave guiding modes. The geometry of the structure plays an important role to provide good coupling in the metal-dielectric interface where the dielectric plays a role to keep the metal in indirect contact with the semiconductor such that there is no defect formation due to direct contact of metal-semiconductor. The dielectric also has higher dielectric constant makes more modes available to couple for enhancing light trapping. Both photonic and plasmonic modes are available while the photonic enhancement may be greater due to lower losses as shown by Figure 2.34 where the silver ridge is 50nm and the silicon thickness is 200nm [134].

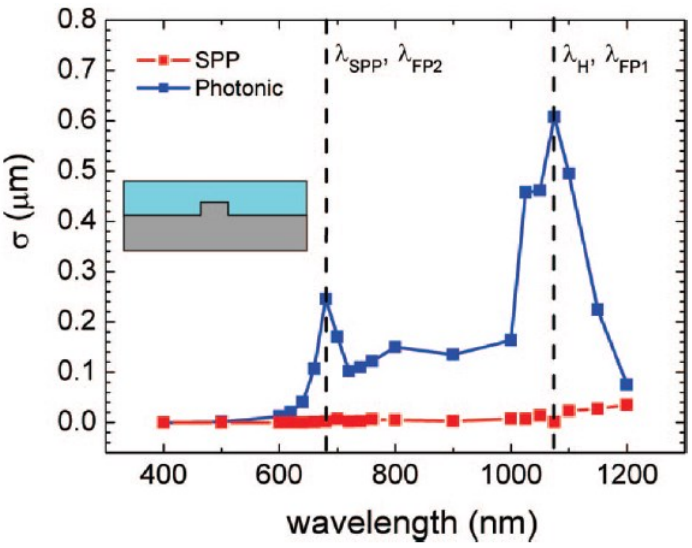

Figure 2.34: Incoupling cross-section for SPP and photonic modes for a 200nm thick Si with 50nm Ag ridges[134]

There is considerable research in this area trying to understand the phenomenon and trying to predict the enhancement by trying different structures (shape, size and geometry) both computationally and experimentally

2.4.4.2.1 Solar Cell Application

There has been a lot of research into this area and the theoretical aspects discussed above have been applied to improve cell efficiency and mostly all efforts have been to increase the current density in solar cells. We are discussing few of these developments around the work in thin film silicon solar cells, whereas plasmonic effects are widely used for organic solar cells as well.

Ferry et. al. used plasmonics to improve the efficiency of thin a-Si:H solar cells. They define the theory based on simulations where they suggest that higher absorption can be achieved by coupling the SPPs to photonic modes [128, 134]. They also perform simulation to predict structures (geometries) as well as dimensions (pitch and packing fraction) effects on the absorption [130, 131]. They also show current enhancement due to a hole array compared to flat substrates, and fabricate cells on a substrate with many different structures(varying pitch and diameter) as shown in Figure 2.35 which allowed an effective comparison between various structures [38, 132, 133].

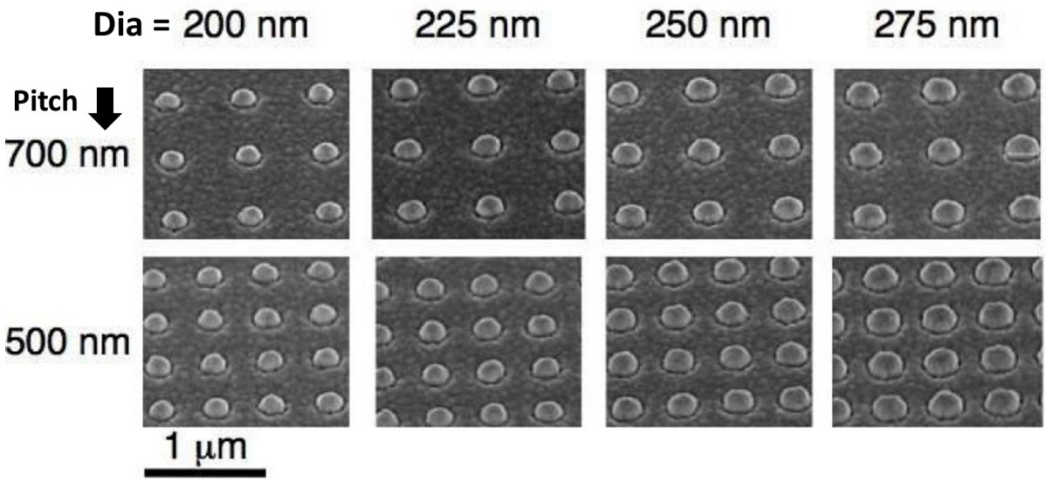

Figure 2.35: SEM images of square periodic arrays with varying pitch and diameter [132]

Haug et. al. analyze the modes that are available for effective absorption in periodic structures and then compare it to randomly textured substrates produced by LPCVD of ZnO. They also show that having the ZnO layer between the a-Si:H layer and silver may decrease the effects from plasmonic enhancement [182]. In a latter paper [181] they discuss that the ZnO layer is effective in converting SPP modes into regular wave guided mode which helps in

increasing the absorption and decreases the parasitic absorption by the metal as predicted by Springer et. al. [117]

Biswas group simulate structures which combine both photonic and plasmonic structures and they predict that it can lead to enhancement over the $4n^2$ limit also [75, 83, 90, 136, 193]. These devices and their experimental results have been discussed later in the thesis.

2.4.4.3 Other Niche Approaches

The research in the area of light trapping has taken inspiration from many areas and we mention a few of these approaches in this section.

The growth of nanowires have been useful for making many new type of devices and can also be useful in light trapping or coming up with novel structures for growing solar cell itself [37, 80, 194-200]. A method of fabricating and even measuring solar cell characteristics of a single nanowire has been shown by Kelzenberg et. al. where they fabricate nanowires (radial p-n junction) and show methods for measuring fundamental properties of the nanowire useful for photovoltaic application. They also suggest that a 5% packing fraction would be enough to get similar absorption as the Lambertian limit [198, 201, 202] In addition, nano wires can lead to very good light trapping as these structures can mimic photonic structures grown vertically and have very high enhancement in the light path length [80, 197]. Naughton et. al. also showed nano-coax cells made by etching c-Si where they could get an efficiency of 8.4% with a 90nm i-layer[199] and Kuang et. al. showed that they could get 3.4% efficiency from 25nm thick i-layer on a substrate which had nano rods formed by growing ZnO rods in an aqueous solution after it was nucleated by sputter deposition [37]. Vanecek et. al. came up with a 3-D structure inspired from Swiss cheese (Figure 2.36(e)) which is fabricated by UV-lithography and reactive ion etching and this structure results in giving a cell efficiency of 10.3% for a micromorph tandem cell [200]. Another interesting approach is the formation of black Silicon which is needle shaped structures of silicon having very high absorption up to 98% and very low reflectivity. They provide excellent material for absorption; they have been based on two structures namely the random nano porous structures [203] or periodic structures inspired by a moth-eye [204].

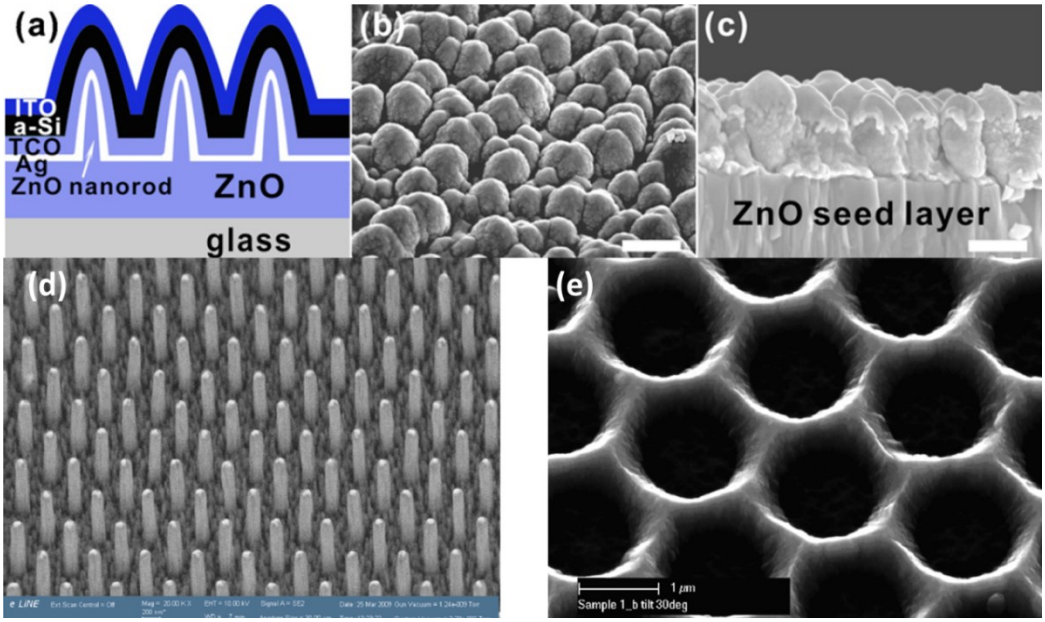

Figure 2.36: ZnO nanorod/a-Si:H cell (a) Schematic with SEM images from (b) top and (c) cross-section [37] and SEM images of (d) ZnO nano columns and (e) Swiss cheese design [200]

In the superstrate configuration, glass remains the primary substrate and as light comes in it can be scattered in various directions as discussed for ZnO case in section 2.4.3.2. But, if we could texture the glass itself then a flat TCO can be deposited onto it or even multiple texturing can be applied in the same theme as show in Figure 2.18. A widely used standard for comparing light trapping structures formed by the Asahi Glass company which is commonly known as Asahi glass, produced commercially for solar application.

There have been other research groups also pursuing this effort [205, 206]. In Figure 2.37 we show the fabrication procedure of textured glass by using polystyrene nano spheres on glass and then etching it using reactive ion etching to form structures of different aspect ratios

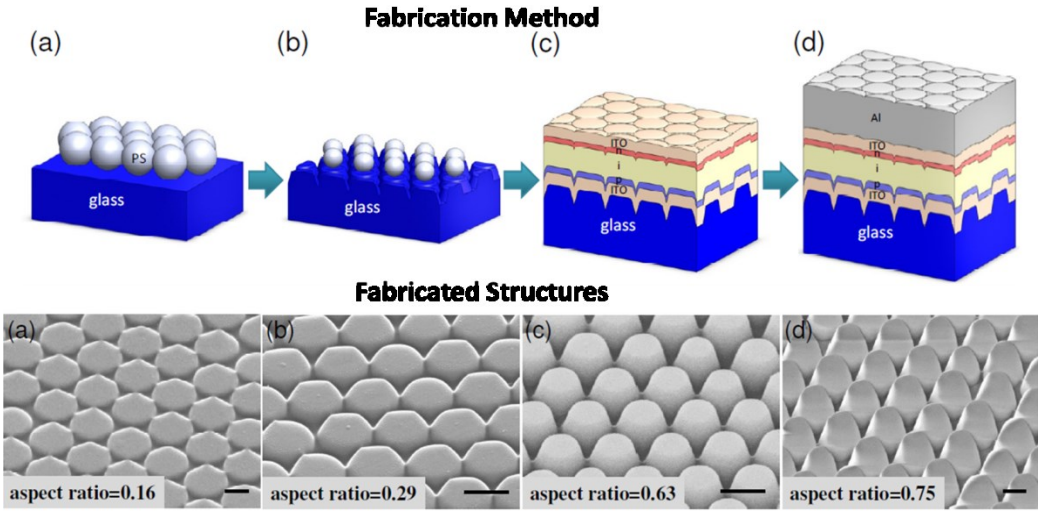

Figure 2.37: (Top) Fabrication process of textured glass (bottom) Various fabricated structures of different aspect ratios

2.4.5 New developments

2.4.5.1 Intermediate reflectors (IR)

In recent years there has been research to develop intermediate reflector at the junction layer in a micromorph tandem cell which can help in reducing any type of optical losses i.e. light can be reflected back to top cell and transmitted to bottom cell efficiently without hampering carrier collection between nc-Si:H and a-Si:H i.e. high conductivity in the direction of current flow with minimal loss of voltage due to recombination [21, 22, 207-216]. There have been many approaches for studying this starting with the incorporation of silicon oxide layer [21, 22, 215] or silicon nitride and Zinc oxide layer[23, 207, 212-214] which can be textured in various ways to adding metal nano particles for plasmonic light trapping[216].

Silicon oxide is essentially an insulator, that can be modified by addition of dopants like phosphine and diborane during growth to modify not only the bandgap but also to make it conductive enough for use as an intermediate reflector. The main idea is to replace the junction (n+) with n-type doped SiOx layer. As the bandgap of SiOx is higher it would not absorb the longer wavelengths and if designed properly it can also help in providing scattering effect to enhance light absorption in the top cell as shown in Figure 2.38(c). It has been shown by various

groups that it can lead to better current densities for both top and bottom cell with use of intermediate reflectors.

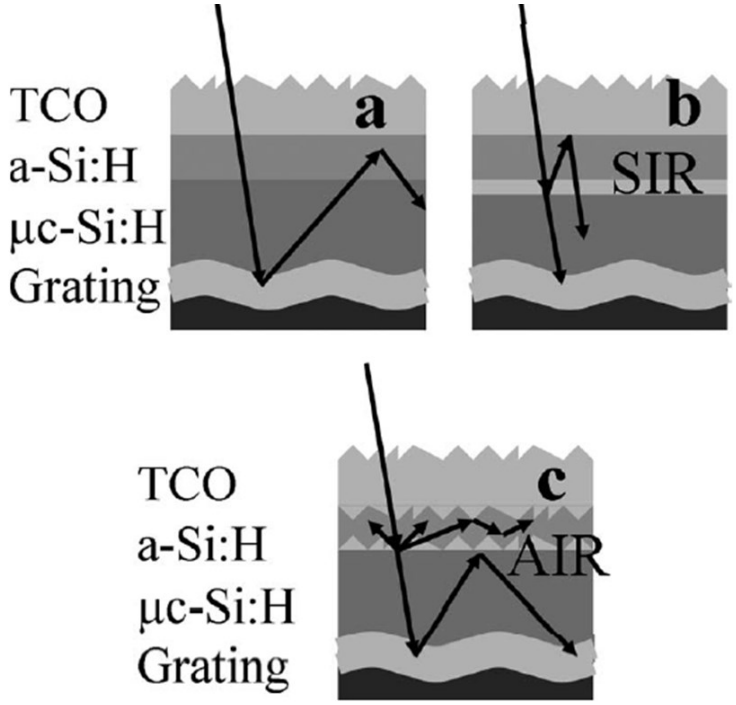

Figure 2.38: Schematic diagram of micromorph cell with (a) no IR (b) flat IR (c) IR for light trapping[21]

ZnO is widely used as an Anti-Reflective Coating (ARC) for solar cells and it can also be incorporated as an IR in the cells since it can be grown through CVD methods as well as sputtering depending on the desired requirement. The use of ZnO provides additional current in both top and bottom cells. It can also be optimized to produce various structures according to requirement including random orientation [213] and periodic arrangement including 3-D photonic crystal [171, 207, 217]. It has been shown that ZnO is a little more problematic to deal with than SiOx, as it leads to shunting and lower yield [213]. Another method that can be employed and was talked about in the Plasmonics section is the inclusion of metal nano particles as an intermediate reflector.

2.4.5.2 Doped Silicon Oxide

In the past few years the use of doped silicon oxide has been on the rise. The interest has widely risen due to the development of the ability to get conductive silicon oxide and it multifaceted usability; some have been listed below

- It can be grown by PECVD methods in the same chamber which allows for similar processing techniques used for other layers in the micromorph cell making it more compatible[20].
- There has been research into replacing ZnO layer with SiOx to make process ability easier as SiOx is more compatible with growth of the next silicon layers when compared to ZnO [20, 218].
- Higher bandgap implies it does not absorb in the same region as the micromorph cells [21, 215, 218].
- Ability to dope it with phosphine makes it conductive, although it does have an effect on the bandgap and refractive index which are higher than silicon bandgap. This property allows it to replace the conducting n+ layer. Previously n+ layers absorbed photons that were lost due to recombination, therefore decreasing recombination losses with SiOx (See Figure 2.39) [20, 218].
- It can also be doped p-type by changing the dopant during processing to boron to be used as the wide bandgap window layer[19].
- It can be used as an Intermediate reflectors (IR)[21, 215].

Most groups use a mixture of Silane and carbon dioxide in a PECVD reactor to grow SiOx where they can be doped either n-type or p-type with the use of phosphine or diborane. The change in the material properties can be controlled by various deposition parameters such as CO_2/SiH_4 ratios the discharge power, substrate temperature and the doping amount. Figure 2.40 shows the change in refractive index and conductivity with changing different process parameters

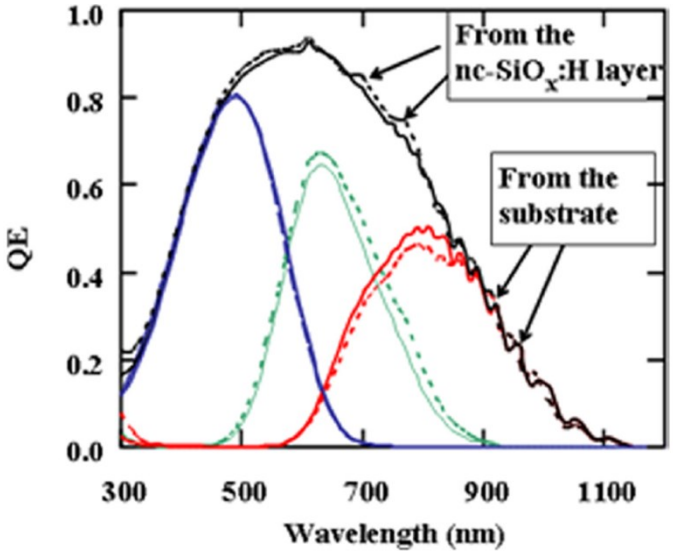

Figure 2.39: QE curves of two a-Si:H/a-SiGe:H/nc-Si:H triple junction solar cells: baseline cell (solid lines) without nc-SiOx:H and (dashed lines) improved cell with an n-type nc-SiOx:H [20].

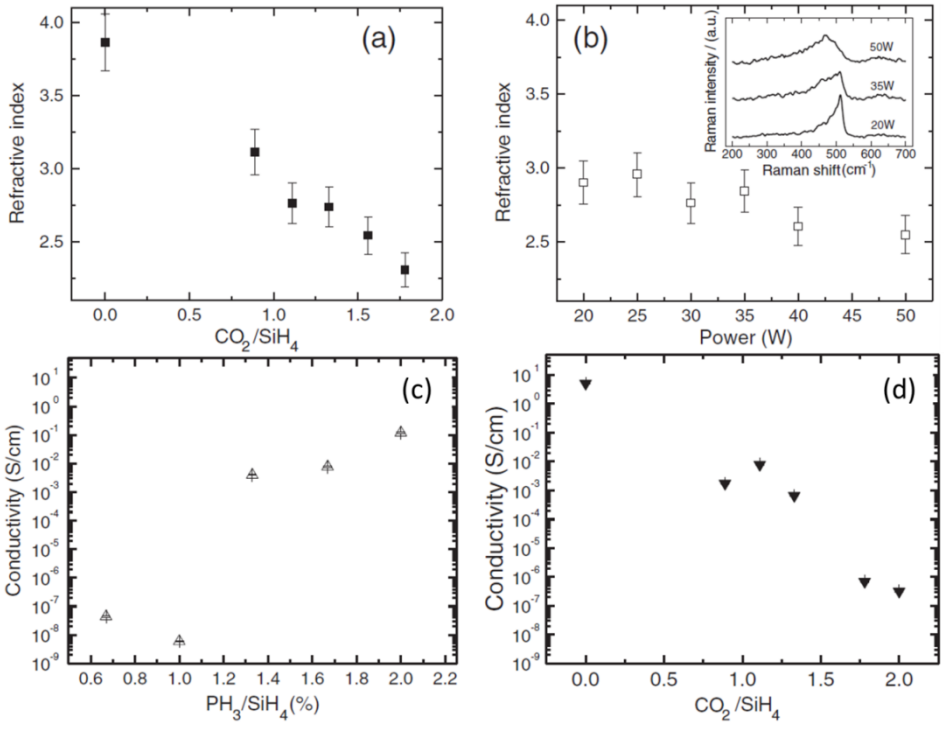

Figure 2.40: Properties (a),(b) Refractive index (c),(d) conductivity of SiOx layer with (a),(d) Carbon dioxide flow (b) discharge power (c) phosphine flow during deposition[218]

2.5 Cost reduction methods

It is imperative that for thin film solar cells to keep production costs as low as possible for competing with other solar cell technologies. In the previous sections we discussed how this can be done by Light Management which in turn would increase the efficiency. The cost of fabricating the solar cell plays a very important role; as thin films major selling point is the low cost and many factors play a role in the total cost of the cell and each of them have to be taken account of keeping in mind the cost to benefit.

In commercial application, time plays a very important role and a high throughput process is very important. The advantage that the thin film process carries is that it employs easy processing techniques which have been transferred for roll to roll processing. Most groups in research scale use processes which have a growth rate 1-5Å/s for a-Si:H deposition and 5-10Å/s for nc-Si:H deposition. But these processes need to be ramped up to industry scale and therefore also growth rate has to be increased to advance faster growth. There has been work by various groups to increase deposition rates for both a-Si:H and nc-Si:H to higher growth rates, while producing good quality material .

The use of flexible substrates in solar cell application opens up many applications. The growth processes used for thin film silicon solar cell can use temperatures from 150^{o}C - 500^{o}C and if we can keep the processing to low temperatures; i.e. we maintain a low thermal budget then we can gain in total production costs as high temperature maintenance require more energy and hence higher costs. This becomes more important when we want to do a roll to roll process; a low thermal budget can also lead to less maintenance on the line and hence low down time costs which again can lead to higher throughput.

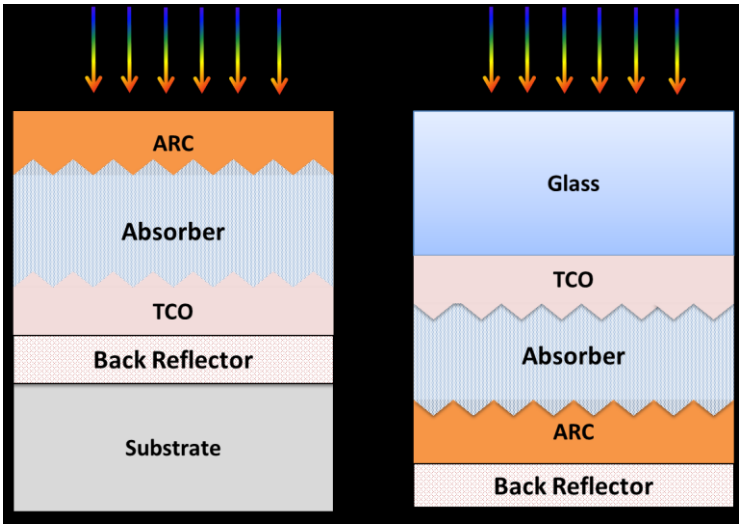

Figure 2.41: Solar cell configuration (a) Substrate and (b) Superstrate

The most common substrate used in the solar cell application is glass which is used for superstrate type configuration (Figure 2.41(a)). The general method is to first deposit the higher bandgap material (a-Si:H) as the light would get in from the glass side and then the lower bandgap material (nc-Si:H) deposited as the bottom cell. But, it has been observed that growth of nc-Si:H requires higher temperature since it involves nucleation of crystalline phase (see section 2.2) and therefore for commercial purpose it is easier to work with a substrate type configuration. There has been also thrust to move away from glass towards using flexible substrates for which opens a new arena to explore new applications [91, 92, 137, 219-230]. Flexible substrates mostly consists of film deposition on thin stainless steel[219] or plastic substrates such as polyimide, PEN and many more [137, 223, 225, 227, 229-231]. This thesis deals with the use of flexible substrates and further details are provided in later sections.

Materials and Methods

3.1 Deposition methods

The deposition methods used in this work have been dependent on the devices fabricated. We show a schematic diagram of a standard device used in the thesis in Figure 3.1. We will describe the fabrication method for each of the layers and the standard properties required for a good layer. We start with the active layers of the device which the silicon based layers which have been fabricated with plasma enhanced chemical vapor deposition (PECVD). We have also used evaporation to deposit metallic layers for back reflectors as well as for better contacts. Finally a brief description of the sputtering technique which is used for depositing the transparent conducting oxides (TCO) namely indium tin oxide (ITO) used in this work zinc oxide (ZnO) can serve as a good TCO, but we have mainly used for light trapping related purpose.

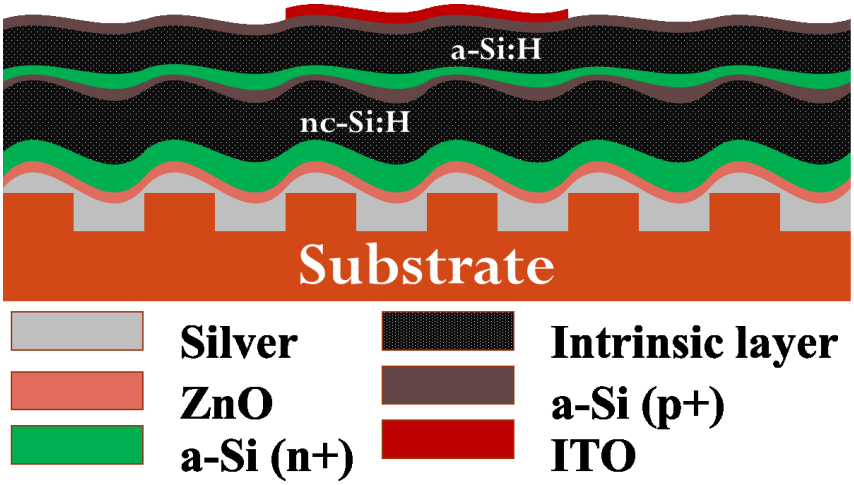

Figure 3.1: Schematic diagram of a micromorph device used in this work

3.1.1 Plasma enhanced Chemical Vapor Deposition (PECVD)

Thin film silicon solar cells predominantly use PECVD systems for the device fabrication [232]. In a typical CVD process the precursors are broken down and then can react in the chamber to finally yield a deposited film. We use two different PECVD reactors for deposition purposes namely Reactor 1 (R1) and Reactor 2 (R2). R1 is primarily used to deposit the intrinsic nc-Si:H layer to avoid contamination from dopant gases, whereas all the doping layers are done in R2. We also deposit a-Si:H intrinsic layers in R2. While R2 is being used for the doped layers

we take extreme care to purge our the dopants from the chamber before depositing the intrinsic a-Si:H layer. Since our deposition involves toxic gases, special care has been taken to set-up toxic gas detectors and also feedback controls to avoid any accidents. We also have controlled exhaust system and also perform regular monitoring of all the gas cylinders.

A schematic diagram of the PECVD reactor (R1) is shown in Figure 3.2 which consists of the main reactor chamber which is being fed by the controlled flow of different precursor gases through calibrated mass flow controllers. The reactor chamber pressure is maintained through a set of turbo-molecular and mechanical pumps. The gases are then ionized in the chamber by a capacitively coupled RF plasma source which is generated by 8116A HP function generator to a RF power amplifier. The output from the amplifier is coupled to a bird wattmeter through which it is provided to the chamber through an electrode. We use a L-shaped tuner consisting of an inductor and set of capacitors to ensure maximum power transfer into the system. Impedance matching is done manually to ensure highest net power transfer (forward –reflected power) into the system. Plasma is initiated by creating a high electric field across the electrode with the substrate/chamber grounded, the precursor gases are ionized and then stable plasma can be maintained at lower electric field.

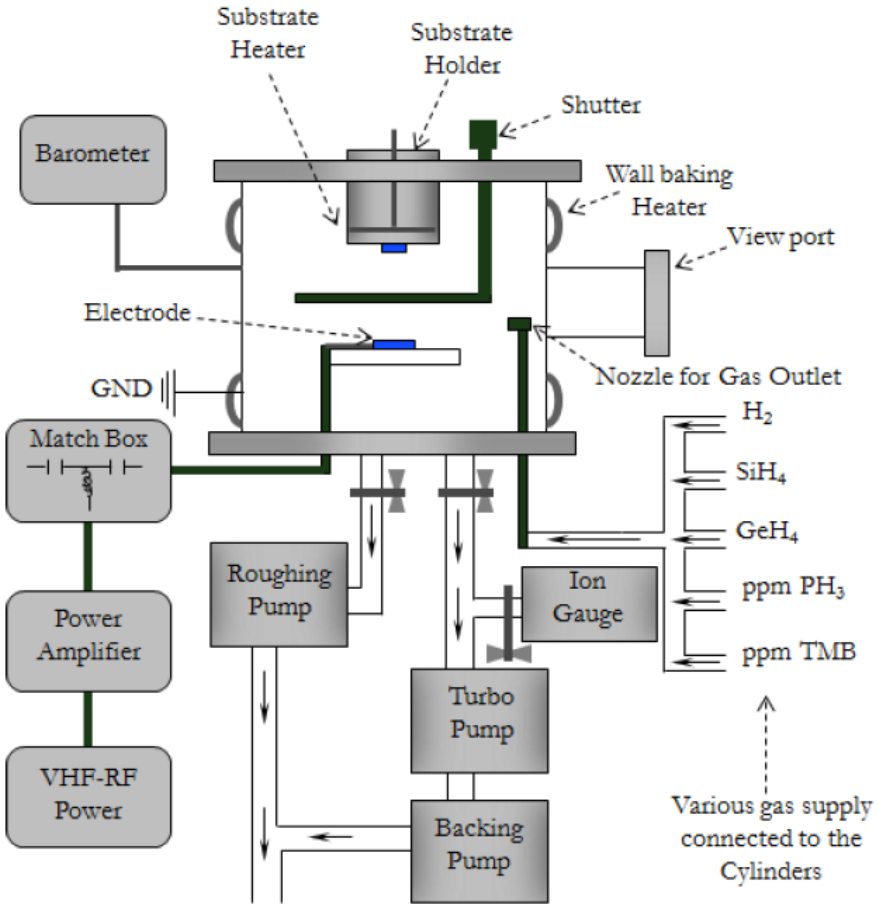

Figure 3.2: Schematic diagram for our in-house PECVD chamber [61]

The deposition occurs everywhere i.e. the cold walls and the substrates. A shutter is in place very close to the substrate so that no deposition takes place until the plasma is stabilized and film growth is controlled. Due to the deposition on the walls and regular buildup of film on the electrode, regular cleaning is done for maintenance of the reactors. After every cleaning process the reactors are then qualified again for proper film growth before making devices on them again. For consistency, we maintain a detailed log of device processing methods with various input/output parameters that are supplied/measured on the reactor during the growth of the film. We also maintained a clean room free from dust as they lead to unwanted problems in devices such as shunting or poor performance.

The growth of films is a complex process and involves many variables; we will talk about procedure followed for depositing a film (more relevant to R2 with both dopant and intrinsic

deposition. R1 conditions are similar with slight modifications mentioned below and also some of the procedures used are different.

1. *History of the chamber:* here we are talking about what type of depositions was previously done in the chamber that could also affect your layer since the chamber may have some contaminant which could stick around. To avoid this we try to do oxygen plasma clean of the chamber to avoid cross contamination. This is especially important when deposition has to be done after deposition of another dopant type.
2. *Substrate Loading:* Substrates were loaded on a solid stainless steel (SS) block which was inserted with a thermocouple to get a better temperature reading and a heater coil to deposit films at desired temperature. Substrates were clamped manually with a set of holders and screws with holes able to sustain higher temperature; special care was taken when glass or plastic substrates were used to avoid breaking or sticking of substrate on holder respectively. The whole substrate holder was then loaded into the reactor and essential electrical and mechanical parts fitted properly.
3. *Reactor Chamber conditioning:* The chamber was not a load lock system, therefore more care had to be taken to purge out all the atmospheric gases that may have gone in during the short time of transfer of the substrate holder; when idle the reactor chamber was maintained in vacuum with a blank plate on top. Appropriate purges were done using clean nitrogen gas to remove the remaining contaminants in the chamber following which the gas lines were cleaned by purging the intrinsic and dopant lines which are separate flow tubes to the chamber to avoid cross contamination (intrinsic layer). The plasma is then ignited and stabilized and we coated the walls with fresh film to avoid any old contaminant from the wall; this time is also used to heat the substrate to appropriate temperature.
    a. *Substrate Temperature:* The substrate temperature determines the quality of film growing on it. In case of a-Si:H lower temperatures lead to void formation during growth which leads to cracking and shunted devices, that can be mitigated a little by using higher hydrogen dilution but we still get poor quality films at room temperature. For nc-Si:H temperature plays a bigger role as crystallinity is effected to a great extent by the growth temperature. It has been shown by various groups that as temperature increases so does crystallinity[64].

There have also been reports that the grain size also increases when we increase the growth temperature and the ratio of <220>/<111> orientation of grain also increase which is favorable for transport [61, 64]. Additionally, we also mention for the ease of writing all temperatures mentioned are the set temperatures, whereas the actual temperature on the substrate may be a little lower (SS may be close but plastic substrates may be at ~20^{o}C than set temperature).

4. *Film growth:* The shutter was closed during all the above processes and after the condition for growth is set the shutter is opened for film growth which has been calibrated previously. The parameters that have to be set here are
    a. *Flow rate of different precursor gases:* The ratio of gases determine the film properties along with other factors listed here. For example for an n+ layer the PH_3/SiH_4 ratio is the main variable to change the conductivity of the film in R2. An important example for R1 is the dilution ratio or H_2/SiH_4 ratio which determines the crystallinity of the growing nc-Si:H film as discussed in last chapter.
    b. *Input power:* Power determines not only the growth rate, but also affects the crystallinity of the growing film especially while growing nc-Si:H films. The idea is to grow the films at a higher growth rate to get higher throughput, but it has to be done in a controlled manner such that the film quality does not suffer due to high ion energy density. Therefore one of the methods used is to use high power with high chamber pressure so that ion energy density is lower. We use a power between 5-8 watts for growth of a-Si:H and nc-Si:H is grown at 30-40 watts depending on other conditions used during growth.
    c. *Chamber Pressure:* The chamber pressure determines the amount of gas present in the chamber at the time of deposition and in our case most of our deposition is done between 50-500mTorr, while etching is done at low chamber pressure (5-20mTorr) so as to maintain high ion energy and minimize the collisions have to be minimized. The deposition is preferred to be done at higher chamber pressure as that means there would be more collisions of ions and hence the ion energy would decrease before it reaches the substrate leading to lower damage on the films. It has also been shown that higher chamber

pressure may lead to higher deposition rates due to higher ion flux next to the substrate.

d. *Plasma source:* As discussed above we have RF plasma source which is capacitively coupled to the chamber. We deposit at frequency range of 44-48MHz, which is higher than the standard method of using 13.56MHz. There are various advantages of using VHF-PECVD which is discussed in more detail in section 3.1.1.1.

e. *Growth conditions:* All the films grown are previously grown and measured during calibration runs. The growth rate is determined by growing thick films and then interpolating or extrapolating for desired thickness. During change from the doped layer to the intrinsic layer we take care to purge the chamber properly and since oxygen plasma cannot be used we also etch the walls with hydrogen to clean any dopant remaining on the walls along with purging lines and chamber. In case of nc-Si:H we transferred sample from R2 to R1 after cooling it down to decrease reactivity from exposure during transfer and also minimum time is maintained during transfer.

f. *Completion:* The device is cooled to temperature below 150^{o}C before removing from the chamber. We also take care during cooling from higher temperature >250^{o}C to make sure that we cool it in chamber which has high hydrogen content to prevent effusion from the films. The film/device is removed marked then taken for the next step or measurements.

3.1.1.1 Advantages of VHF-PECVD

The use of higher frequencies is basically to increase the growth rate while not having deteriorating growing film (Figure 3.3(a)). While different groups have different ranges for the maximum deposition rate the trend towards higher growth rate with increasing frequency is noticeable. It can also be seen that different power densities also increase in the frequency , leads to increasing the growth rate as shown in Figure 3.3(b). Let us look at the effect more closely starting with the plasma conditions. In each cycle the electrons can easily move compared to the ions basically due to their mass and can get collected easily so it leads to a small depletion of electrons leading to an increased potential difference between the glow discharge and electrons. In time however with multiple cycles the positive ions do reach the

other end. Now if we decrease the sheath thickness as shown in Figure 3.4(b) then it would be favorable as the ion bombardment would be much lower and also the power is coupled better [233]. It should be mentioned that ultra-high frequency may not be also good as it would not affect heavy ions which would then be immobile.

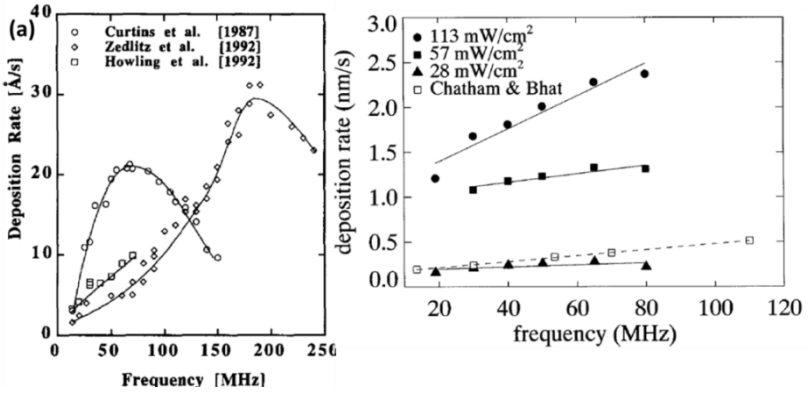

Figure 3.3: (a) Deposition rate versus frequency data for various groups [233, 234] (b) Deposition rate versus frequency for various power densities [235]

It has also been seen that when the frequency is increased the ion energy of the ions impinging on the surface decreases and this has been attributed to both the bulk plasma and reduced plasma sheath potential [236]. There have been reports suggesting that there is an enhanced ion flux on the growth surface at higher frequencies, which lead to high surface reactivity of the film precursor. Therefore, the higher frequency has higher ion flux at lower bombardment energy making it favorable for growth of silicon films especially nc-Si:H [236].

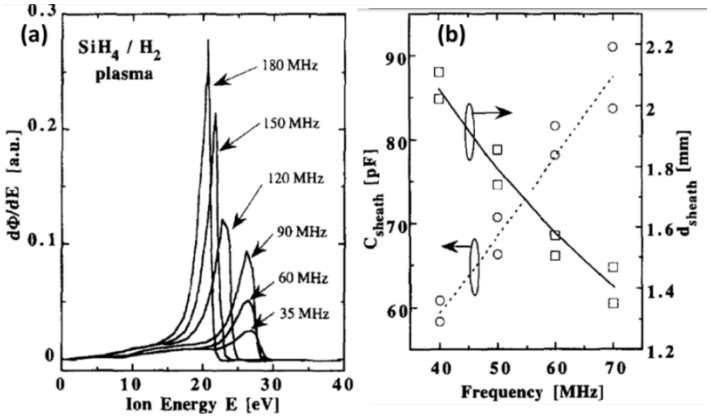

Figure 3.4: (a) Energy distribution of ions impinging on surface from H_2/SiH_4 plasma and (b) Measured sheath capacitance and correspondingly calculated sheath distance [233, 236]

3.1.1.2 Design of cells

In this section we mention the basic features of the standard cells we fabricate, the conditions change with different substrates

3.1.1.2.1 Amorphous silicon

a-Si:H layers are grown on SS substrate first have a n+ layer which is doped heavily using phosphine (5% PH_3 tank)mostly fabricated at temperature above 250^{o}C. The reactor is then purged and then conditioned before deposition of the intrinsic layer which is fabricated with dilution ratio between 7-10:1 depending on the temperature of deposition, lower temperature layers are grown with higher dilution ratio. The intrinsic layer is also doped with incremental amount of doping as the film gets doped un-intentionally by oxygen in the chamber; the strategy used here is that we give the push to holes which have travel a longer distance by doping with increasing amounts of boron with the help of trimethyl boron (TMB). This boron content is increased towards the middle part of the device and then kept constant as the carriers may have had gained enough kinetic energy to reach the p+ where they would be conducted away.

Before the p+ we have a window layer of wider bandgap layer by doping with methane to add carbon in the layer while making conducting with help of a little phosphine. This window layer has a dual function as it blocks the boron from p+ to diffuse into the intrinsic layer while it also helps in increasing the open circuit voltage. The window layer has to be kept in check as it adds to the series resistance if too thick or heavily doped with carbon. Another method of decreasing series resistance is to start grading with ppm amounts of phosphine before starting to grade with TMB at the start of the intrinsic layer. The p+ is designed such that the first layer provides a step from the wide bandgap window layer and then we have a very thin 15-18nm layer microcrystalline p+ followed up by amorphous p+. The p+ thickness was limited to 20nm such that it did not absorb much as photons absorbed in the layer would be lost to recombination.

3.1.1.2.2 Nano crystalline silicon

We use two methods to grow nc-Si:H cells and will discuss both methods here. Hydrogen profile cells are grown on amorphous n+ by first starting with an incubation layer of a-Si:H which is used to nucleate nc-Si:H crystallites. The seed layer played an important role in determining

the V_{oc} of the cell as dilution ratio decreased so did the V_{oc} if other condition were kept constant. We started with a high dilution ratio >20 to start the nucleation process once nucleated the dilution ratio was gradually reduced as the deposition continued mostly ending up below 15. The dilution ratio was continuously decreased and faster if a higher dilution ratio was used to start with, another factor kept in mind was the temperature and power as with higher temperature lower dilution ratio can be used and the same is true for power. Although changing temperature has a more pronounced effect.

The intrinsic layer also needs to be doped similarly to counteract the unintentionally doped oxygen by using TMB, but at a much lower level than in case of a-Si:H. Here also we can start with phosphine and gradually move to boron grading which helps in decreasing series resistance. But the doping has to be kept to minimum to keep recombination down.

After the nc-Si: layer was fabricated an amorphous cap layer was deposited to protect the nc-Si: layer and moreover to passivate the intrinsic layer which had to be transferred to R2 for the deposition of p+. The cap layer thickness was ~5nm, whereas we have seen that if thicker amorphous layer acts as a barrier which may lead to drop in FF. We again use a three layer process to deposit p+ starting with an amorphous layer followed by highly conducting nano crystalline p+ and then finally an amorphous p+ layer.

The other method of depositing nc-Si: layers is the super lattice method of depositing alternating layers of a-Si:H and nc-S:H layers. Here the dilution ratio can be kept constant for the whole layer the determining factors here are the times for each layer which is generally kept 10/1 i.e. for nc-Si:H/a-Si:H growth thickness in nanometers. The dilution can be changes according to the temperature of deposition. The other steps are similar as it required an incubation seed layer and doping for better carrier collection against un-intentional oxygen doping and finally we always end with an amorphous layer which works as passivating cap layer. The p+ remains same as in hydrogen profile cells.

3.1.2 Thermal Evaporation

Thermal Evaporation is a widely used technique by the thin film industry to deposit good quality material. The basic idea is to create a vacuum where the mean free path of the particle is high enough that when they are sublimate using a source they can deposit at the colder surface

in front moving from a source towards the substrate. We use a thermal heat source in an in-house built thermal evaporator as shown in Figure 3.5. For thickness measurement and growth we use a quartz crystal whose vibration frequency is known and the changes are recorded using a digital thickness monitor calibrated for each type of metal. We have assumed tooling factor=100% due to large distance between source, substrate and the quartz crystal. All depositions were done with substrate at room temperature.

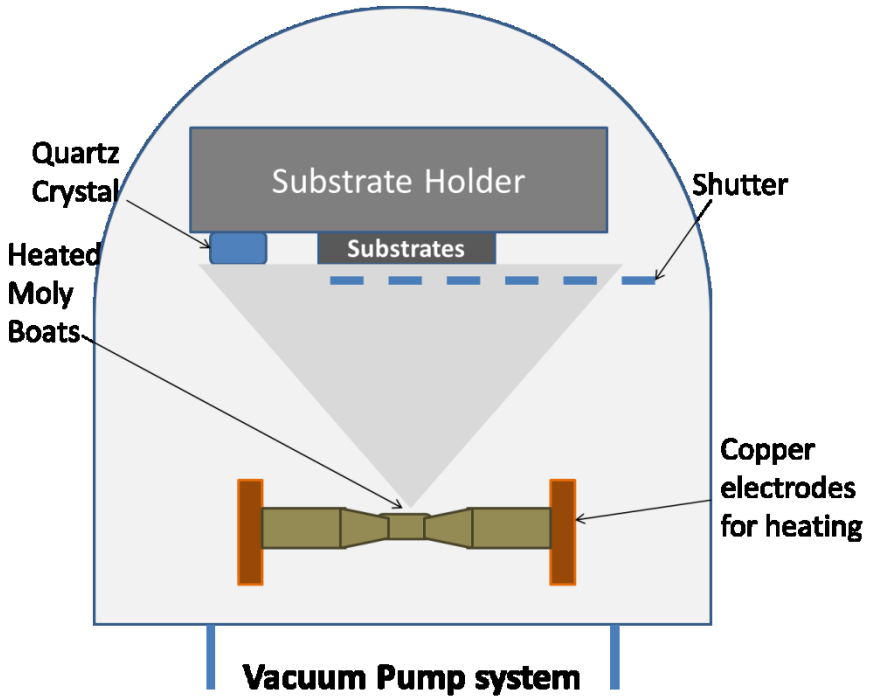

Figure 3.5: Schematic Diagram for Thermal Evaporation

The substrates are loaded facing down and the source material is loaded on a molybdenum boat for silver or aluminum and for chromium evaporation commercially available chromium source rods are used. After loading the substrate the system is pumped down using a set of mechanical pumps and turbo molecular pumps. The evaporation is done at pressures below $2x10^{-6}$mTorr to avoid any oxidation. The evaporation rates were kept constant 5-7Å/s for Ag, 20-25Å/s for Al and 1-1.5Å/s for Cr. Before actual deposition took place on the substrate care was taken to qualify the rate of deposition by depositing on the shutter first. The substrates were allowed to cool down before they can be removed for vacuum. Chromium was added on the substrates for back reflector as an adhesion layer for silver which is used as the back reflector.

The use of aluminum is mainly as the bus bars on top of the device for improving current collection and decreasing series resistance.

3.1.3 Sputtering

Sputtering is a faster deposition process than evaporation, although widely used for metal deposition on the semiconductor industry we use it mainly to deposit two types of Transparent conducting oxides (TCOs) namely Zinc oxide (ZnO) and Indium tin oxide (ITO). The basic idea of sputtering revolves around using excited argon ions to bombard the targets of the TCOs which would bombard the target to release ions from the target to get deposited on the substrate loaded. Even though DC plasma is a possibility here as the films are conducting, we mostly used RF plasma as it gave better quality films at higher growth rate. We used an in-house built sputter system for the depositions and have capability to both DC and RF sputtering. A schematic diagram of the system used is shown in Figure 3.6.

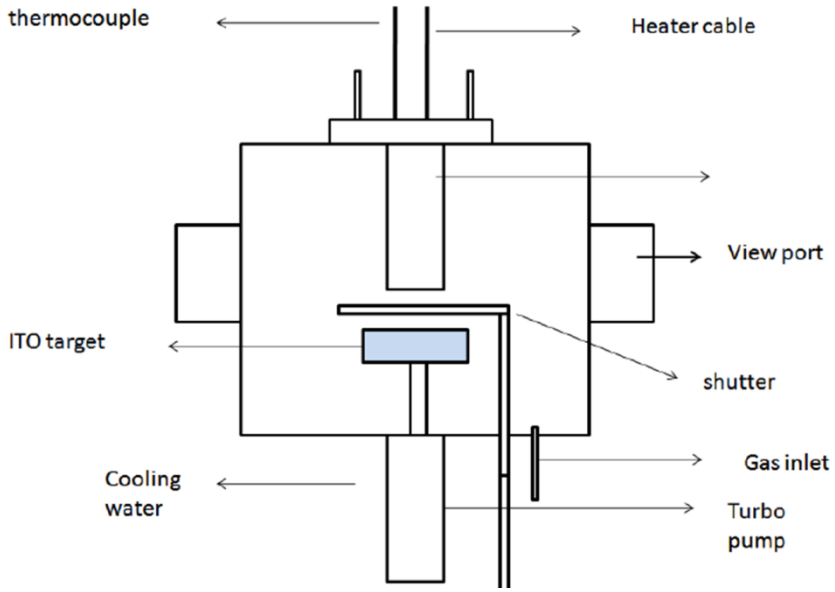

Figure 3.6: Schematic diagram for in-house Sputtering system [64]

A very important part of the solar cell is the TCO and we will discuss the TCO's used in this thesis below;

a) *Indium Tin Oxide (ITO):* ITO is widely used as a TCO by the solar industry although recent trends have been to move towards cheaper material as in ZnO due to the

increasing costs and the lack of Indium in the world reserves. It has also been affected by the heavy use of ITO by the display technologies. We deposit ITO at higher temperatures ranging from 200^{o}C-300^{o}C depending on the substrate capabilities. Our ITO has a sheet resistivity of 2 x 10^{-4} ohm-cm. The ITO deposition is calibrated regularly by using a microscopic glass to deposit thick films through which growth rate is calculated and resistivity measurements are made by four point probe. The transmission properties suggest that we have more than 80% transmission (Figure 3.7) in the absorption range of the solar cell. In most cases we use a 70nm layer of ITO which is the calculated quarter wavelength anti-reflection coating.

b) *Zinc Oxide:* ZnO is a wide band semiconductor which can be doped to make it conducting. The widely used dopant is Al while other dopants have also been tried such as Gallium, boron, indium etc. We use aluminum doped ZnO in particular our target is doped with 2 atomic % Al. Although ZnO can also be used as a front contact TCO, for this thesis we have used ITO as our front contact anti-reflection coating, while ZnO:Al is used for the back reflection in substrates prepared for light management, it is a common material for most of the light management schemes as it is used as the spacer separating the metal layer of the back reflector and the semiconductor mainly done to decrease recombination due to metal-semiconductors, it also helps in coupling light into the semiconductor having a refractive index of ~1.9-2.1. An additional use is the back reflector namely etched ZnO discussed in last chapter and in further chapters. The sheet resistivity of ZnO:Al film is ~5 x 10^{-4} ohm-cm and the transmission is shown in Figure 3.7

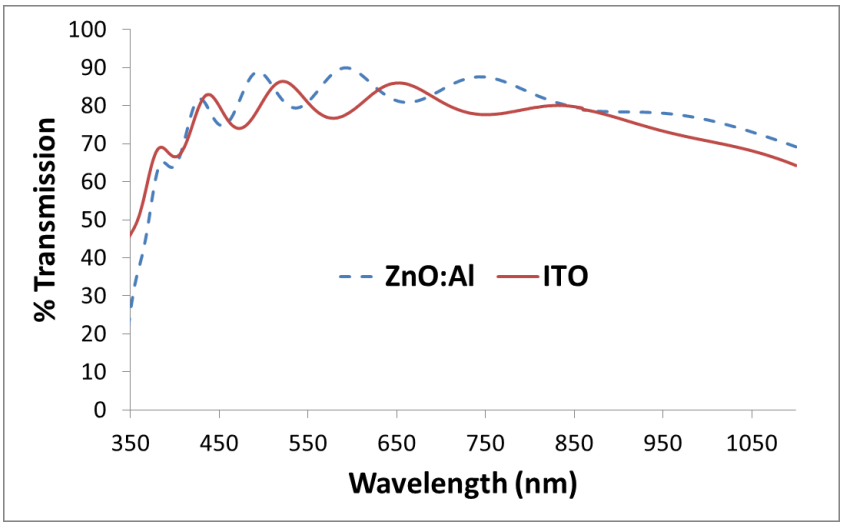

Figure 3.7: Transmission of ITO and ZnO:Al

3.2 Substrate Preparation Methodology

We have used a variety of substrates in this thesis as it includes deposition on plastic substrates. The substrates used are given below

- Glass
- Stainless steel (SS)
- Poly ethyl naphthalate (PEN)
- Polyimide (Kapton)
- Polymer on stainless steel (POS)

Each of these substrates varied in characteristics and their main change was due to the change in fabrication process due to the additional boundary of process temperature limitation for each substrate. A more descriptive method of the choice of substrate is given in the later chapters. While here we would go through the procedure of preparation of each substrate.

3.2.1 Glass

We used standard microscopic glass or corning 7059 glass when required for deposition of films for different film measurements. It could also be used in case we needed to make superstrate type solar cells where light comes in through the glass in which case we used SnO_2 or ZnO:Al coated glass. A standard procedure was used for cleaning where we boil the glass

substrates of 2”x2” size in acetone and further clean by ultra-sonication in methanol, after this the glass was stored in fresh methanol until used.

3.2.2 Stainless steel (SS)

SS was used for all calibration devices and in general to qualify all devices before they can be fabricated on plastics or otherwise any special structure. In addition it also formed the base substrate for randomly textured substrates as in annealed silver and etched ZnO in our case. The SS we used flexible as it was 5 mils thick and pre-polished on one side which came from United solar group. The cleaning consisted of similar methods with an additional step of boiling in mixture of ammonium hydroxide, hydrogen peroxide and deionized water before the ultra-sonication step and then storing in methanol until used.

3.2.3 Poly ethyl naphthalate (PEN)

We collaborated with Light wave power for substrates and their nano imprinting of structures on this substrate. Although PEN has a known process able temperature up to 200^{o}C, we found that at those temperatures it would not be possible to fabricate them on PEN itself when an imprinted structure is on it. The PEN substrate was therefore qualified before fabrication at each time by annealing it in an oven set at 200^{o}C to check if there is considerable bending or formation of cracks or other defects. Due to the presence of the chemical surfactant allowing higher processing temperature care was taken to bow of any particles that may have been lodged on it by blowing nitrogen at high pressure and then heating in an oven for qualification. This was followed up with thermal evaporation of Cr/Ag at room temperature as the back reflector and then sputtering ZnO:Al at 150^{o}C.

3.2.4 Polyimide (Kapton)

Kapton is also a plastic substrate which can handle higher temperatures and was prepared in a method very similar to PEN substrates with a variation in the qualification process where the oven temperature was set to 250^{o}C, basically saying that the qualification consisted of the annealing at the highest processing temperature that the substrate would undergo during the complete fabrication process.

3.2.5 Polymer on stainless steel (POS)

POS is used to fabricate devices at higher temperature by giving the plastic a backing structure for mechanical support. It could withstand higher processing temperatures and this was useful especially for fabricating nc-Si:H. The method of substrate preparation was kept similar to that used for plastic substrates discussed before.

3.2.6 Scanning Electron Microscope (SEM)

A very important part of the substrate preparation method consisted of looking at what the fabricated structure looks like and how they behave even after they have been annealed and if there are structural changes that are deteriorating to the devices. A SEM is a widely technique for looking at the topographical image which is our main use, but today is used for a wide variety of applications. A simple explanation for the process is that electrons are generated from a gun which is focused on the sample and these electron interact with the sample and after their interaction they are collected by different detectors collecting back scattered electrons (used in our case), secondary electron, x-ray detector and many more depending on the required use. We used a Raith system capable of e-beam lithography to look at our structures at various stages of the fabrication not only during substrate preparation but also after the device fabrication.

3.2.7 Atomic Force Microscopy (AFM)

We have used AFM to measure 3-D topography especially important for light trapping structures as a height plays an important role. We used an AFM system supplied from Veeco Instruments. The AFM is a very sensitive system unlike SEM it can give us idea in the z- direction also. It works on the principle that a small cantilever with a very sharp tip on 2-5nm when very close to the surface of the film feels forces acting on it and if we can follow this path we can measure features on it. It houses a piezoelectric base on which the sample is loaded and the cantilever scans on it. There is a laser which is pointed to the head of the cantilever with a photo detector detecting each movement of the cantilever as a feedback control processing how much the cantilever needs to move in the z-direction. The complete image is formed by making multiple line scans which are completed by moving automatically to predefined size of the sample. This method is tedious and a little slow also the size of sample to be scanned is a maximum of 32µm x32µm.

The cantilever can be either in contact mode or non-contact mode, for all our measurements we were using taping mode since we had structural changes which had large continuously changing height through the surface.

3.3 Characterization Techniques

There is a variety of characterization methods that were used during the development of the work carried out in this thesis. It is very important to measure the amount of change that each variable in the process causes not only that many of the measurement have been quantified which have given to rise to a clear path of direction to move for a better quality material or essentially better properties as such. Some of the methods of characterization have been introduce in this chapter.

3.3.1 Current Voltage measurement (IV)

The power conversion efficiency of a solar cell is dependent on the V_{oc} , I_{sc} and the FF of the solar cell and is quantitatively related as shown below

$$\boldsymbol{PCE} = \frac{\boldsymbol{V_{oc}} * \boldsymbol{I_{sc}} * \boldsymbol{FF}}{\boldsymbol{Incident\ Power}}$$

Where Voc denotes the open circuit voltage or the voltage across the load when the current is zero, Isc is the short-circuit current or the current flowing on shorted circuit and FF is the fill factor which is defined by the square-ness of the curve, it can also be called the ratio of the areas of the smaller rectangle (Vmp,Imp) to Larger rectangle(Voc,Isc) where Vmp and Imp are the maximum voltage and maximum current respectively (Figure 3.8). The solar cell is also affected by two more major resistances called the shunt resistance (Rsh) and the series resistance (Rser) calculated using the equivalent circuit of a solar cell as shown in **Equivalent circuit diagram for a solar cell**Figure 3.9

$$I = I_L - I_d - I_{sh}$$

$$= I_L - I_0 \left\{ exp\left[\frac{q(V + IR_{ser})}{nKT} \right] - 1 \right\} - \frac{V + IR_{ser}}{R_{sh}}$$

In general, R_{ser} is calculated by taking the slope of the IV plot where the current is zero and R_{sh} is slope where voltage is zero. An ideal solar cell would have $R_{ser} = 0$ and $R_{sh} = \infty$.

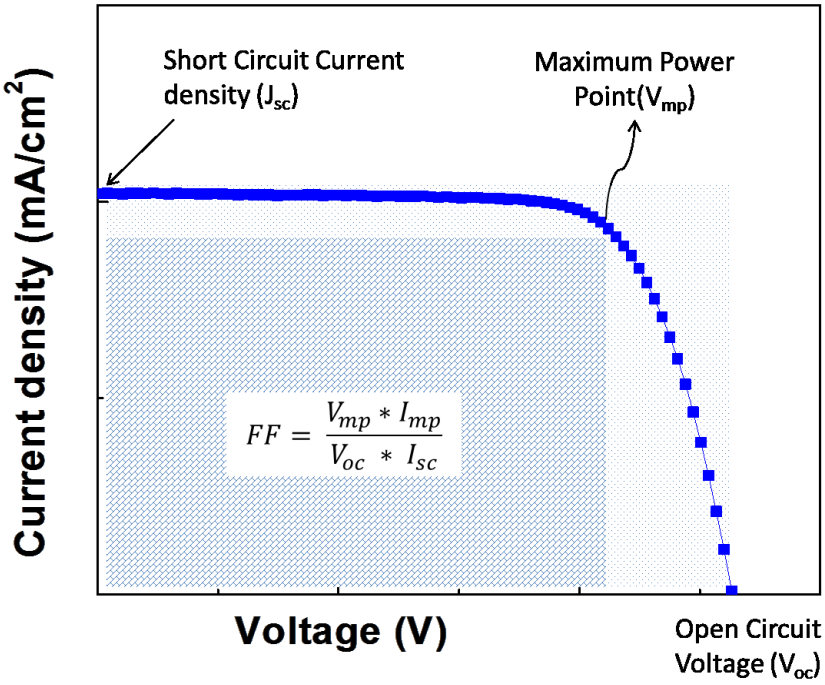

Figure 3.8: IV curve for a Solar cell

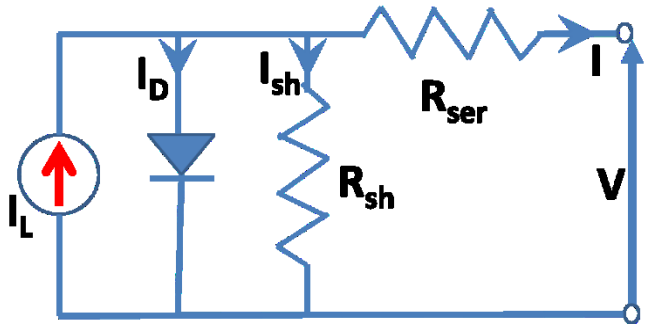

Figure 3.9: Equivalent circuit diagram for a solar cell

3.3.2 Quantum Efficiency

A solar cell converts light from the sun to energy, the sun has a large spectrum range and only a part of it is used by the solar cell to convert into energy. Therefore, quantum efficiency is needed to know the performance of the cell at different wavelengths/energy. The measurement definition is divided into two parts external or internal. External quantum efficiency (EQE) is ratio of number of collected carriers to the number of incident photons at a particular energy

whereas internal quantum efficiency (IQE) does not take into account the reflection losses. IQE is defines as the number of collected carriers to the number of photons absorbed by the solar cell. Figure 3.10 shows the EQE curve for a a-Si:H device where the total current density can also be calculated using the area under the curve.

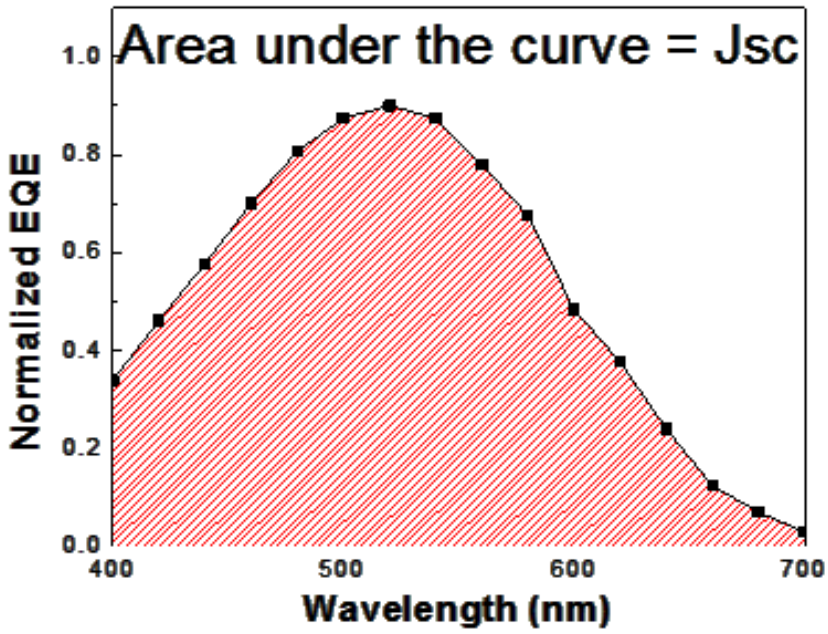

Figure 3.10: External Quantum Efficiency of a solar cell

We also use the same setup to find carrier collectability of our devices i.e. by applying a forward bias (decreasing electric field) or reverse bias (increasing electric field) we can determine how carrier collection is affected by the lack or improved electric field. This also helps in determining the quality of the devices or which carrier may be affecting the device a better discussion has been provided in further chapters. For thin film Silicon samples, which in our case is mainly limited by hole collection capabilities, an important characterization method is the QE v/s bias measurement where we change the electric field applied on the device and measure the change in QE at a particular wavelength. The wavelength chosen is generally longer wavelengths which get absorbed at the lower part of the device close to n+ and so holes need to travel the longest distance to reach the p+.

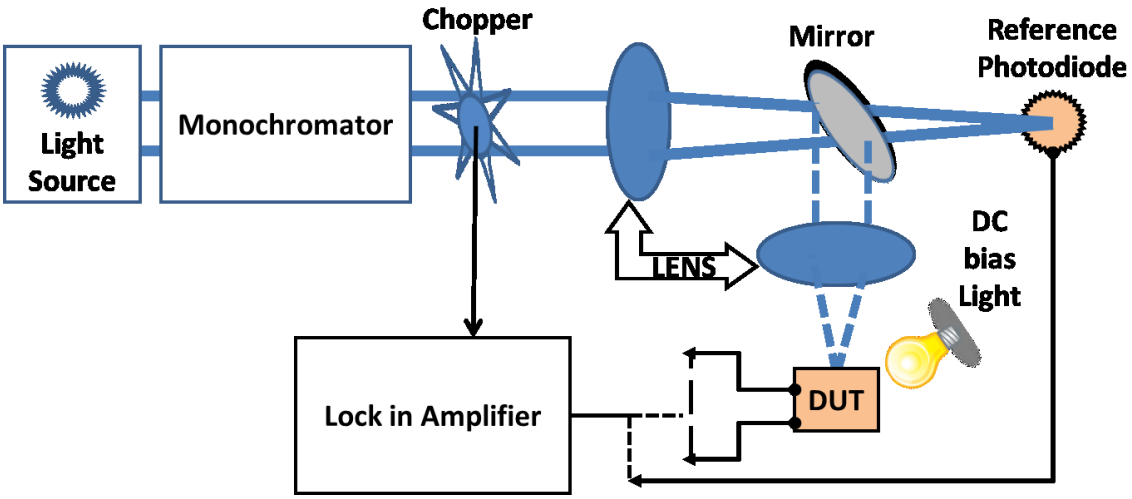

Figure 3.11: Schematic diagram of quantum efficiency setup

The system set-up is built in house consisting of monochromatic wavelength generation from a monochromator which uses a grating structure to emit a light of particular wavelength which is then passed through slits and then focused using a lens and mirror set-up to fall on either the sample or the reference photodiode. The reference photodiode is a standard silicon photodiode whose response is known. The sample is probed to pick up signal after being activated by light from the monochromator which is chopped using a chopper at 13.56Hz to separate the noise from outside light and monochromator a lock-in amplifier is used with the probing system to pick up only signal change due to light coming from the monochromator. The reference photodiode is used a reference for day to day changes or light intensity variation from the monochromator. A schematic diagram for the setup is also shown in Figure 3.11 for better understanding. There is also a DC bias light which is used to create photo generated carriers to fill midgap states and fix the quasi Fermi levels. We also use additional filters for cutting second or higher order light coming from the monochromator.

In case of tandems when the cells are connected together in series we need to also determine how each cell is performing to make adjustments to the process for improving the device further. We use light bias method where we saturate one of the cells by applying for top cell a blue light source so that it when it is saturated with carriers any carrier generated at the bottom cell can be collected easily, by this we can determined performance of the bottom cell.

Similar method is used to measure the top cell only this time we use red light to saturate the bottom cell.

3.3.3 Capacitance Measurements

The method of using capacitance to determine properties of semiconductors has been used for several years. We use multiple impedance spectrometers to find two important factors in the device. Firstly the determination of thickness electrically is a standard method. In this method the device is considered to be assumed to function like a parallel plate capacitor and the thickness of the capacitor is found by the relationship $C = \varepsilon * A/d$, where ε is the dielectric constant, A is the area and d is the thickness. In case of device, the depletion width is measured under high reverse bias which is approximately the thickness of the intrinsic layer. The measurement frequency also plays an important role and the previously mentioned measurement is made at high frequency to avoid the influence of trap levels in the semiconductor.

The influence of frequency is utilized for the measurement of defect densities and the doping densities in the device. This method was first proposed the Kimerling et. al.[237] where they showed that if voltage is applied at low frequency then at very low voltages only shallow traps would respond and at higher reverse bias voltages both shallow and deep defects would respond. Also, at very high frequencies the curve would saturate and would yield the depletion width of the device as shown in Figure 3.12. Further analysis into the plot in Figure 3.12 shows two sets of slopes where each one can be used to estimate defect density at particular region by using equation

$$\frac{1}{C^2} = \frac{2}{q\,\varepsilon_s} * \frac{V_a}{N_A}$$

Where, ε_s is dielectric constant of semiconductor V_a is the applied voltage and N_A is the defect density.

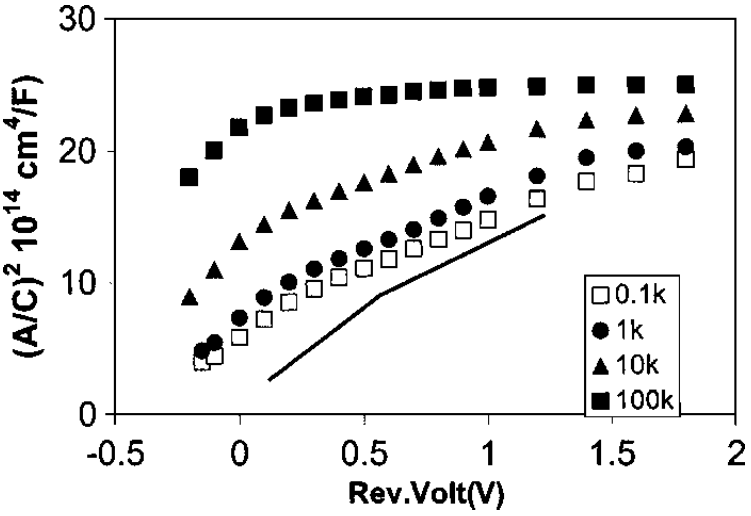

Figure 3.12: Capacitance versus voltage at different frequencies [238]

Further influence of frequency can be used to predict the level of defect at different energy levels using the relationship as below

$$\vartheta = \vartheta_0 * exp[-(E_C - E_T)/K_B T]$$

Where, E_T is the trap energy level and $\vartheta_0 = N_C * \sigma * v$, and N_C is the effective density of state, σ is the capture cross-section and v is the thermal velocity. The method and calculation is explained in more details elsewhere [239, 240]. This method is used to then predict the number of traps at each energy level.

3.3.4 Raman spectroscopy

Raman spectroscopy is an important tool for quick determination of the crystallinity of the film/device in comparison to the most general method of using X-ray diffraction method. It is based on the principle of an incident photon interaction causing an inelastic collision (Raman scattering). The change in energy of the incident photon due to interaction with the sample is called as Raman shift. This depends on the vibrational frequency of the bond, and in case of crystalline material which has the same bond length throughout resulting in a sharp peak at a value, for Silicon a phonon of 64meV or a peak at 520cm^{-1}. But, in case of amorphous samples the bond lengths are distributed resulting in a distribution centered on the main bond. This method is then used predict the crystallinity by integrating the area under the curve for the crystalline and the amorphous part, for silicon 520cm^{-1} and 480 cm^{-1} respectively. Other

approaches are also used to quantify the crystallinity, where a third peak is used to predict the crystallinity of the sample.

The important factors in the measurement are the wavelength of the laser used which determines at what depth is the film is being measured. Short wavelength only provides near surface analysis and to go deeper a long wavelength is necessary. It is also important to use low power/intensity to avoid unintentional crystallization due to the laser. Furthermore, exposure times and number of repetition to get an average value and also to decrease noise can be used to further improve the signal response

3.3.5 Optical spectroscopy

The optical properties are very important for the solar cell characterization and there are many important things to determine for a good solar cell. We use two optical spectrophotometers for our measurements namely the Cary 5000 supplied by Varian and another spectrophotometer from ocean optics.

Absorption coefficient determines the ability of the material to absorb photons and is very important factor in determining the quality of grown films. We can also determine the bandgap of the grown material using this data. The absorption of a-Si:H and nc-Si:H depends on the growth process parameters like growth temperature, dilution ratio, dopants used etc.

Transmission is another measurement that is regularly done. It is especially important for the TCO's used since there primary function is to not absorb in the absorption region of the absorber as well as perform as a antireflective coating (ARC). When we deposit ARC, the thickness plays a major role. We deposit ~70nm (quarter wavelength ARC) for which we need to determine the growth rate properly to have precise control over the thickness of ARC deposited. For which we need to measure thickness which can be estimated by the following equation

$$T = \frac{\lambda_1 * \lambda_2}{2\,(n_1\lambda_2 - n_2\lambda_1)}$$

where λ_1 and λ_2 are consecutive peaks or troughs and n_1 and n_2 is their corresponding refractive indices as shown in Figure 3.13. This method of calculating thickness is also valid for opaque films such as silicon thin films -the only change is we need to measure reflection as in Figure 3.13.

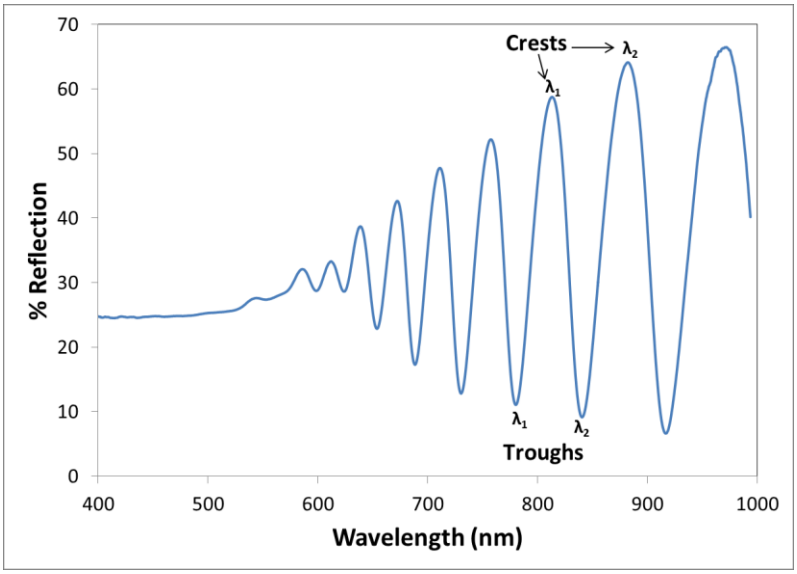

Figure 3.13: Reflection measured on a film to measure thickness

In case of back reflectors which are textured light is not only reflected in the normal angle but in multiple angles. Therefore, we pay more attention to diffused reflection where in the last case we looked at only specular reflection. We can measure total reflection for final determination of reflective quality of the back reflector as well as diffused reflection for making comparison of our back reflectors to improve their functionality.

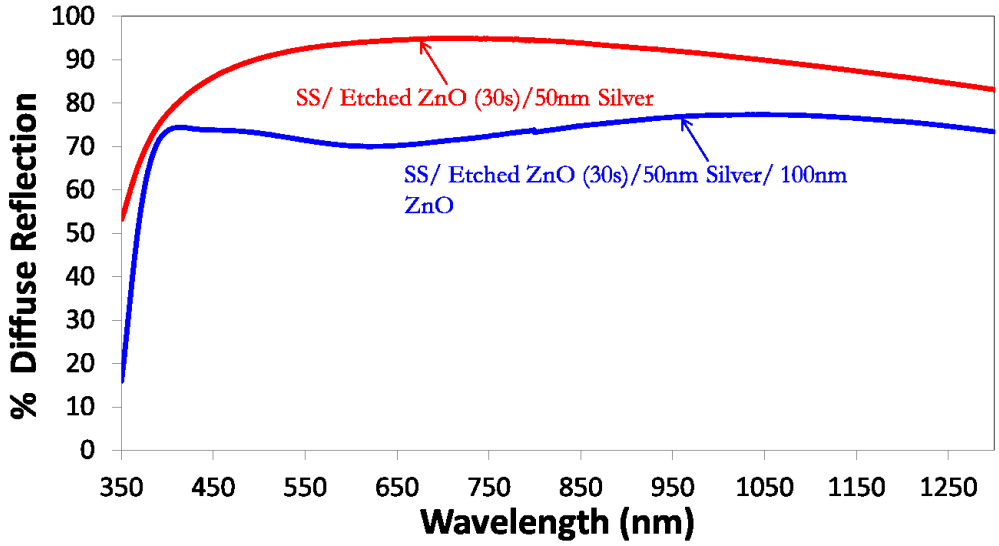

Figure 3.14: Diffused reflection for etched ZnO:Al substrates

Results and Discussion

In this chapter we will look at all the work carried out during this thesis for light management and economic fabrication methods. We will also look at the new structures that have been used for this method, their working mechanisms and their performance in real scale devices.

4.1 Random or Lambertian methods

We had discussed in earlier sections the randomly oriented disordered structures. We also fabricated our own randomly oriented structures mainly to see and learn about their effectiveness in light trapping. We used two methods namely the annealed silver and etched zinc oxide, although more methods exists too. We have discussed the major methods of fabrication for the structures and shown approaches of other groups are working on in the Literature review

4.1.1 Etched Zinc Oxide

Aluminum doped Zinc oxide (ZnO:Al) was deposited on pre-cleaned SS substrates using magnetron sputtering. He thickness of ZnO:Al was about 1-2µm, to get randomly oriented crater like structures they had to be etched using dilute HCl. It was then covered with a layer of silver for the back reflection and finally a spacer layer of 100nm ZnO:Al was deposited. A schematic diagram of the structure is shown in Figure 4.1.

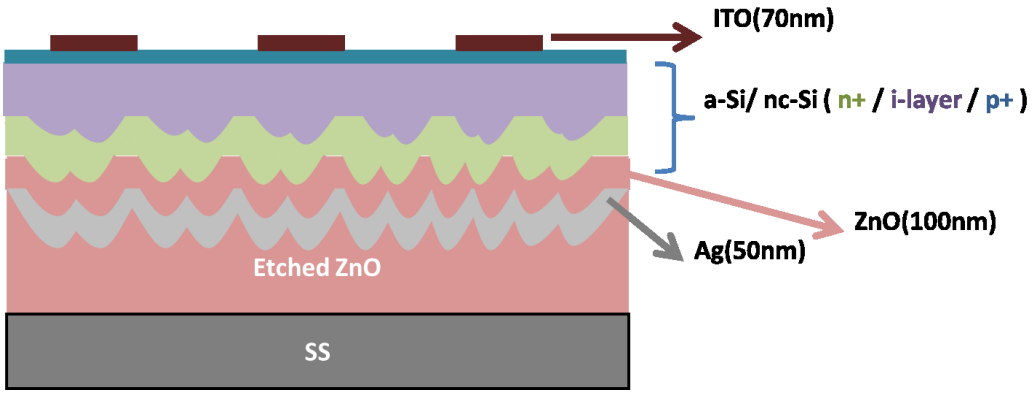

Figure 4.1: Schematic Diagram of a device on etched ZnO:Al

To etch the substrate we prepared fresh solutions of dilute hydrochloric acid (HCl). The initial optimization took some time for us to see what etch rate would be easy for us to control as too high concentration etched away ZnO:Al too fast. Therefore a very dilute solution of HCl of 0.185% has been chosen for this study. The etch rate was slow and also uneven when we just allowed to etch inside the solution and therefore we went for agitation of solution such that continuously new solvent is available for etching which lead to a uniform etching pattern also.

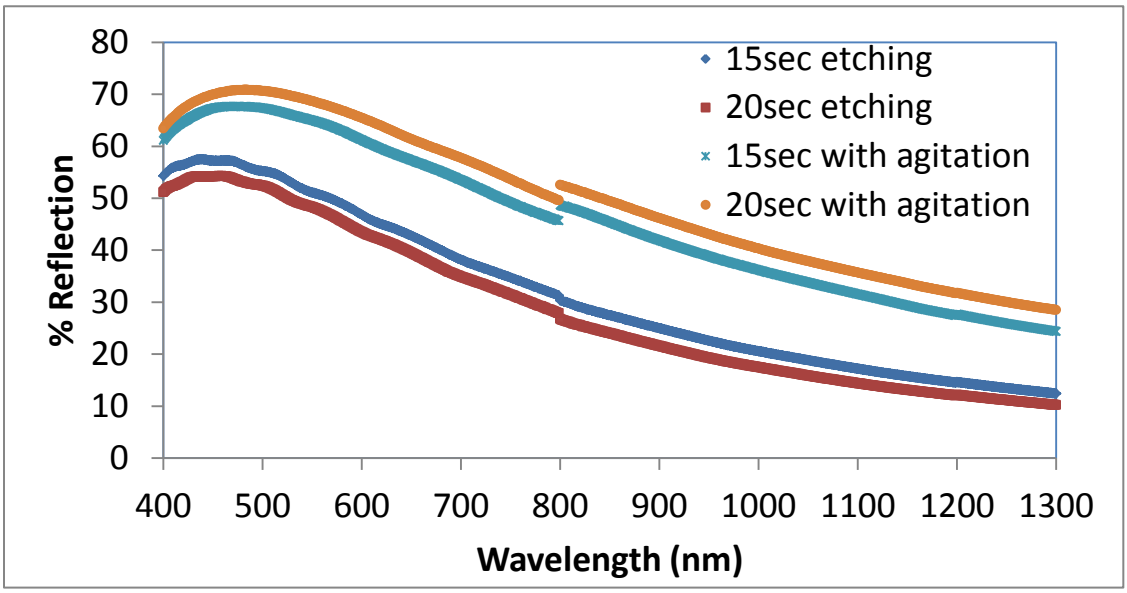

Figure 4.2: Effect of Agitation during etching of ZnO:Al by dilute HCl

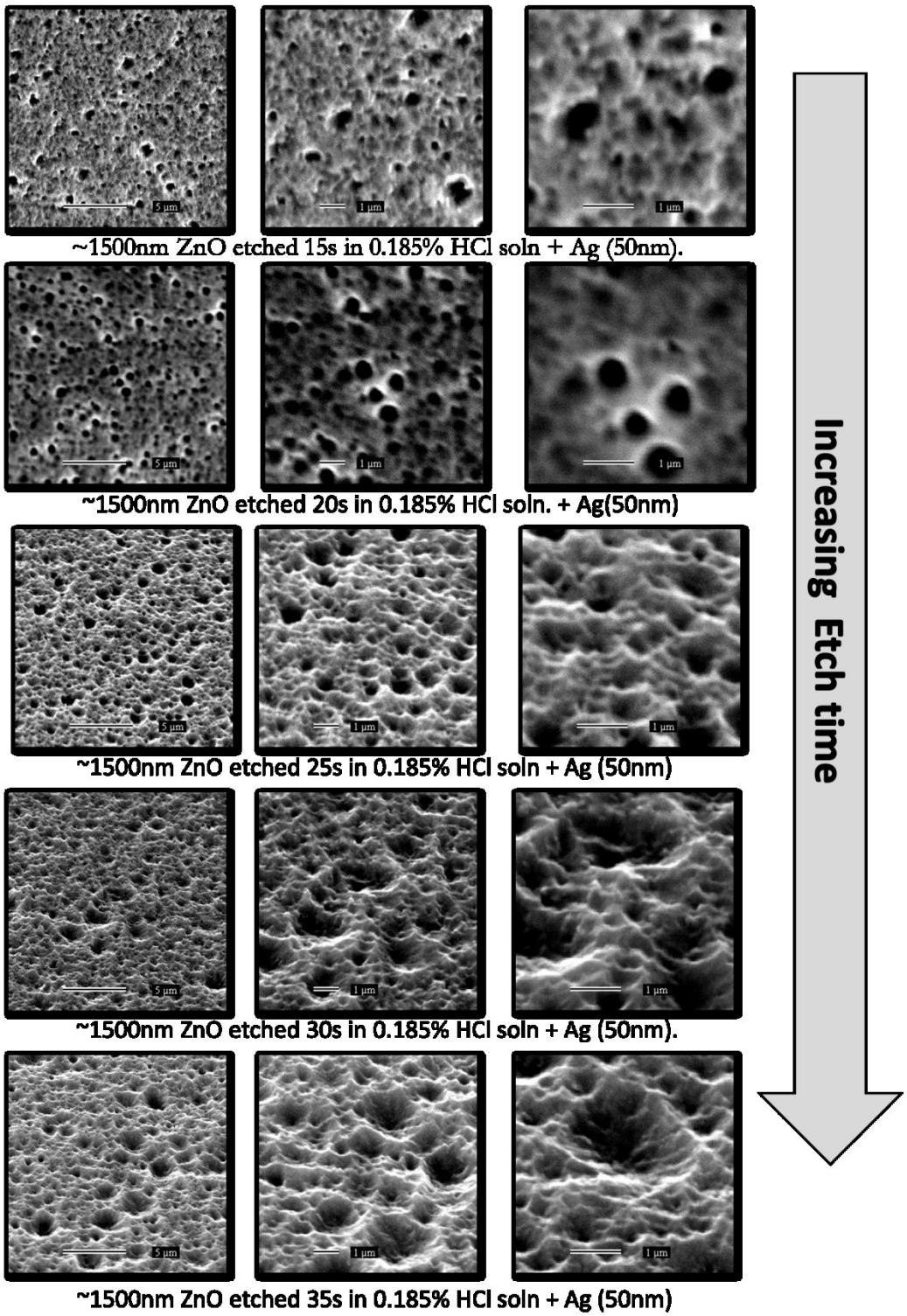

Figure 4.3: SEM images of ZnO:Al with increasing etching time in dilute HCl

We varied the etching time and took various SEM images to see the effect of etching. In Figure 4.3 we show how the etching time affects the change in features formed on the ZnO:Al after deposition of 50nm of Ag. The obvious result that emerges out here is that increase in the size of the feature sizes when etch time is increased and also the surface roughness (σ_{rms}) increases from 73.5 nm to 111nm when etch time is increased for 25 second to 35 seconds pictorially represented in Figure 4.4. Here I must mention that horizontally the images are in different scales and we are trying to show that there is a uniform change in features not only in the feature size but also all over the substrate.

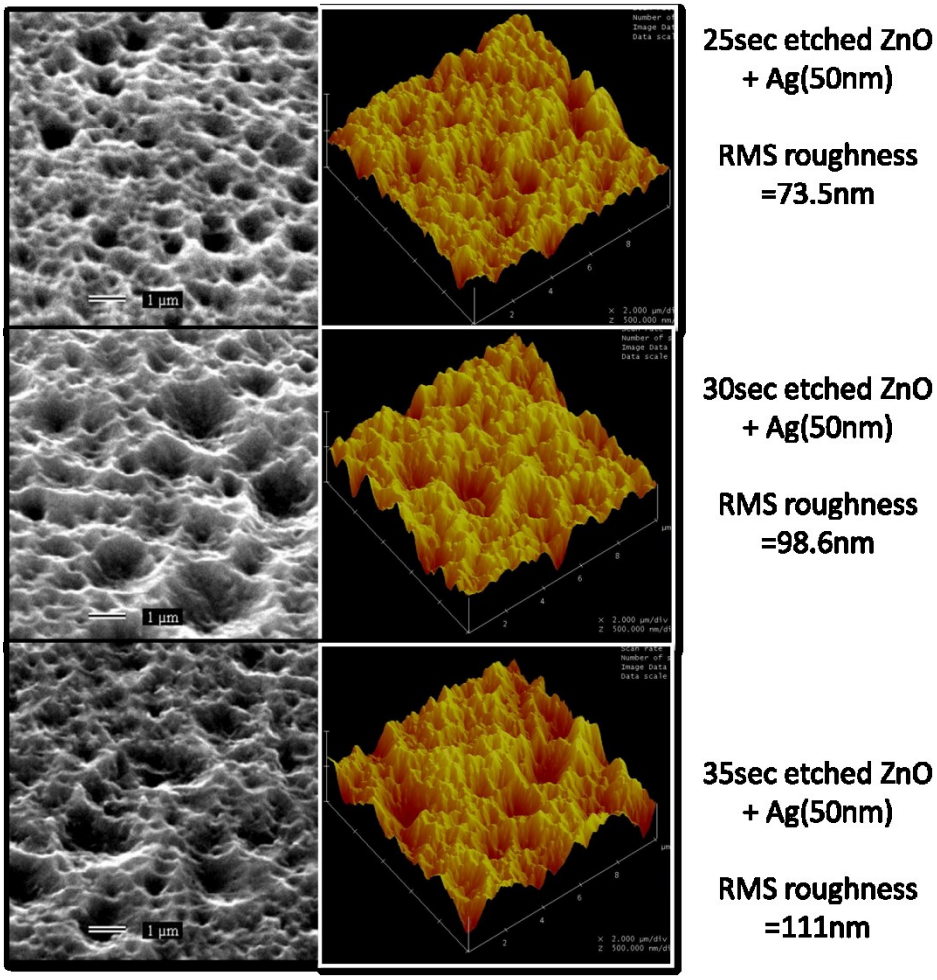

Figure 4.4: SEM and AFM images of Etched ZnO:Al

In addition the SEM images showing structures formed that diffusely reflect light in multiple directions when it hits the silver surface, we also measured the reflective properties to see how well the substrate performs in scattering light in different directions. We measure the specular

and diffuse components of reflectance using an integrating sphere. We see that when we increase the etch time we also have better total reflection (specular + diffused) from the surface. But it has noticed by various groups if the surface roughness is too high it would lead to defects [94, 95, 119]. In our case the surface roughness increases to 73-111nm for 25 second to 35 second etching time, and high surface roughness leads to lower V_{oc} and drop in FF. We made a choice to stay at maximum of 30second etching since at higher roughness device quality deteriorated [94, 97].

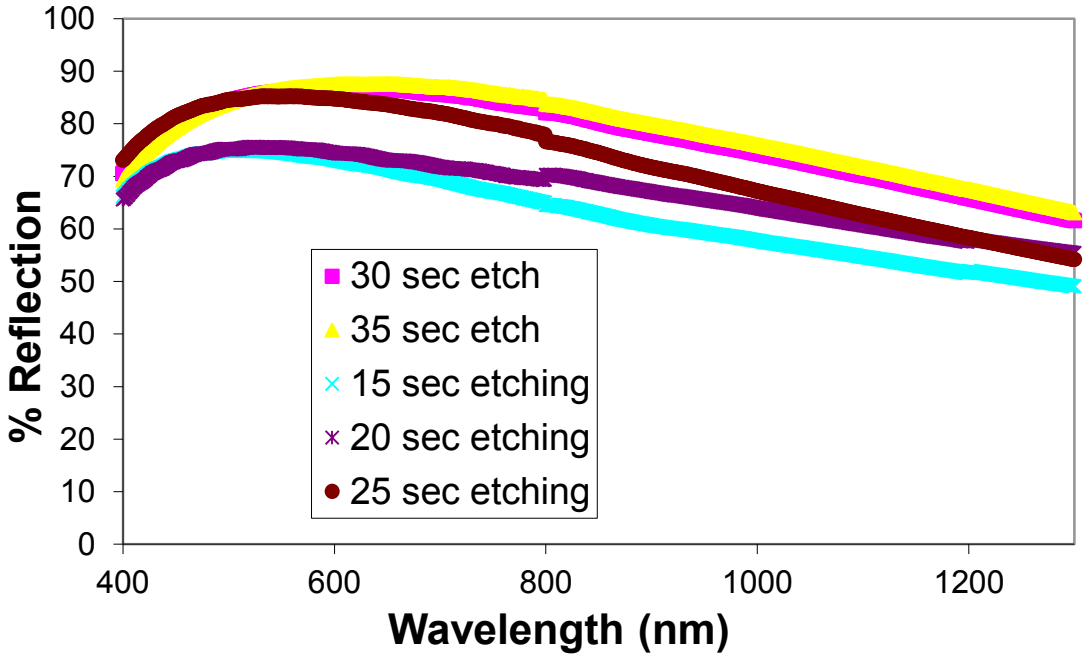

Figure 4.5: Total Reflection from varying time of etching for etched ZnO:Al substrates

4.1.2 Annealed Silver

We used SS substrates for depositing a thin layer of silver (~200nm) where we also had a thin layer of chromium (~50nm) as an adhesive layer. The chromium was used as we found that without it the silver would eventually peel off from the SS which may be immediately after the layer deposition or even be a month later. But, with chromium as an adhesion layer there was no peeling unless the SS substrate was not properly cleaned.

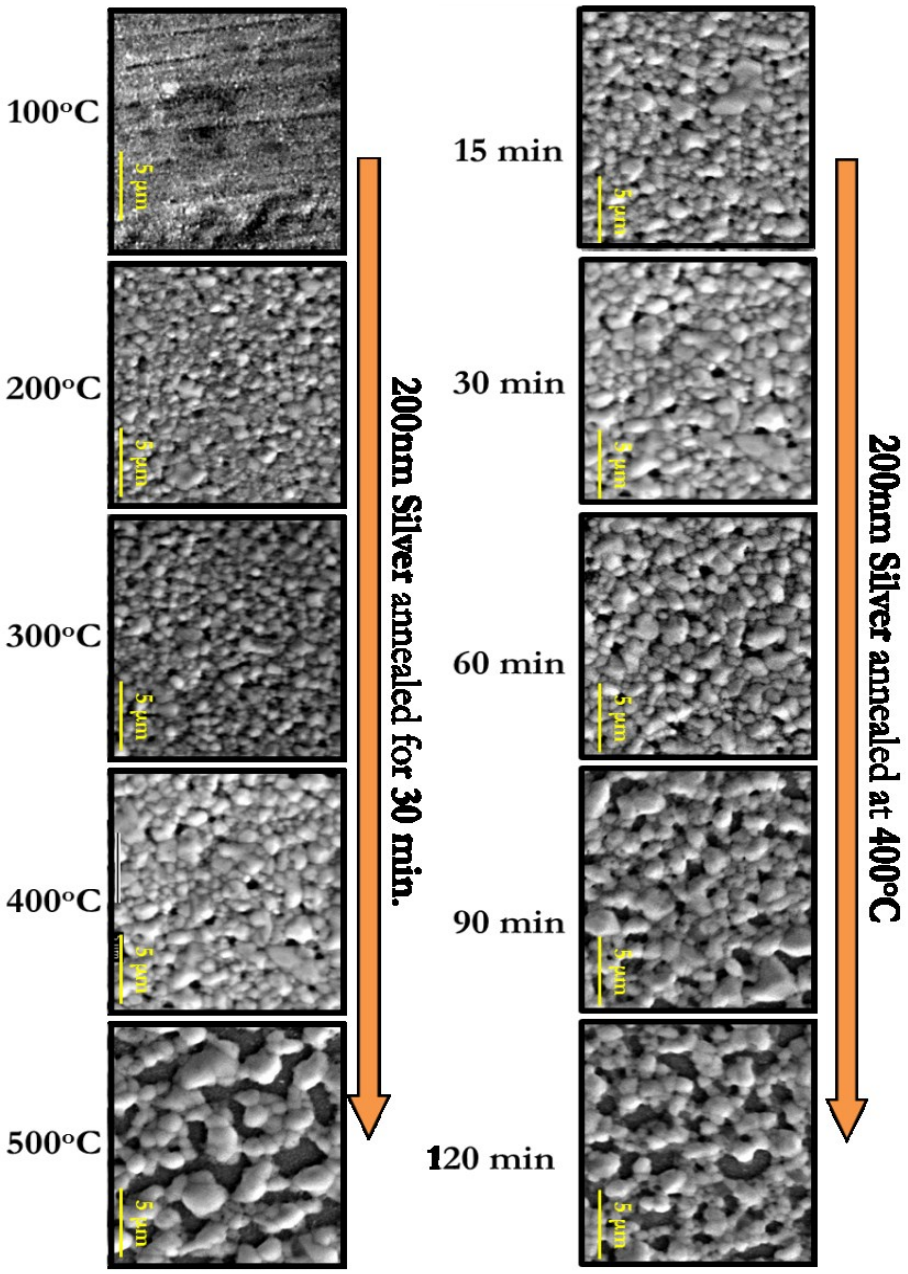

Figure 4.6: Effect of temperature and time on annealing of silver[61]

We deposited ~200nm of silver by thermal evaporation and then annealed the substrates in an oven at higher temperatures in air to agglomerate the deposited silver. In Figure 4.6 we show map of how the silver agglomerates at different conditions; on the left the change in temperature at constant time where at low temperatures, the agglomeration process is very slow it picks up pace at high temperatures and then at higher temperatures (see 500^{o}C) the agglomeration is rapid such that the surface is depleted of silver itself. On the right in Figure 4.6

we show how the same effect is also valid as the time passes the agglomerates keep growing at one particular temperature here 400^{o}C, again for 120 min of annealing the film is again depleted of silver. We mention that we do need a continuous film not only to support reflection also to keep the resistance low which would increase if there is a discontinuous film. We have made devices and chose for our case we get better devices for annealing at 400^{o}C for 30 minutes for which we get a surface roughness of ~50.7nm as shown in Figure 4.7.

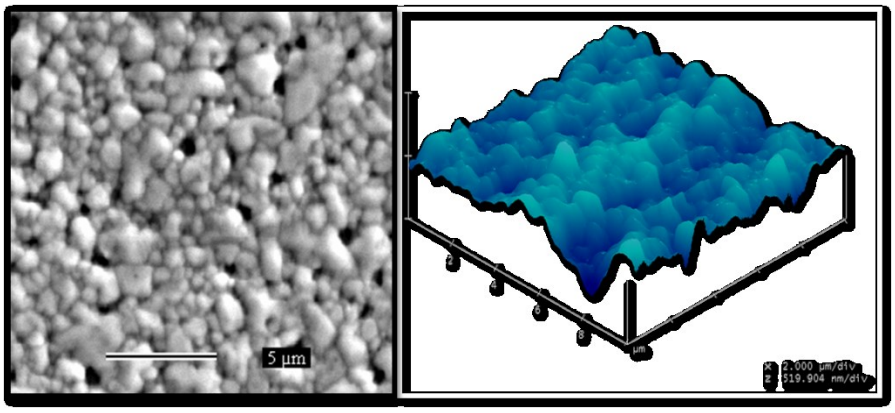

Figure 4.7: SEM and AFM image of silver on SS annealed for 30min at 400^{o}C

4.1.3 Device Comparison

We also fabricated devices on the prepared randomly oriented structures and compared them to devices prepared on SS/Ag which is a similar planar substrate as it has the silver layer at the bottom but instead of scattering light in multiple directions it would behave like planar mirror. The comparisons have been shown for etched ZnO:Al in Figure 4.8 and for annealed silver in Figure 4.9 with a summary shown in Table 4.1

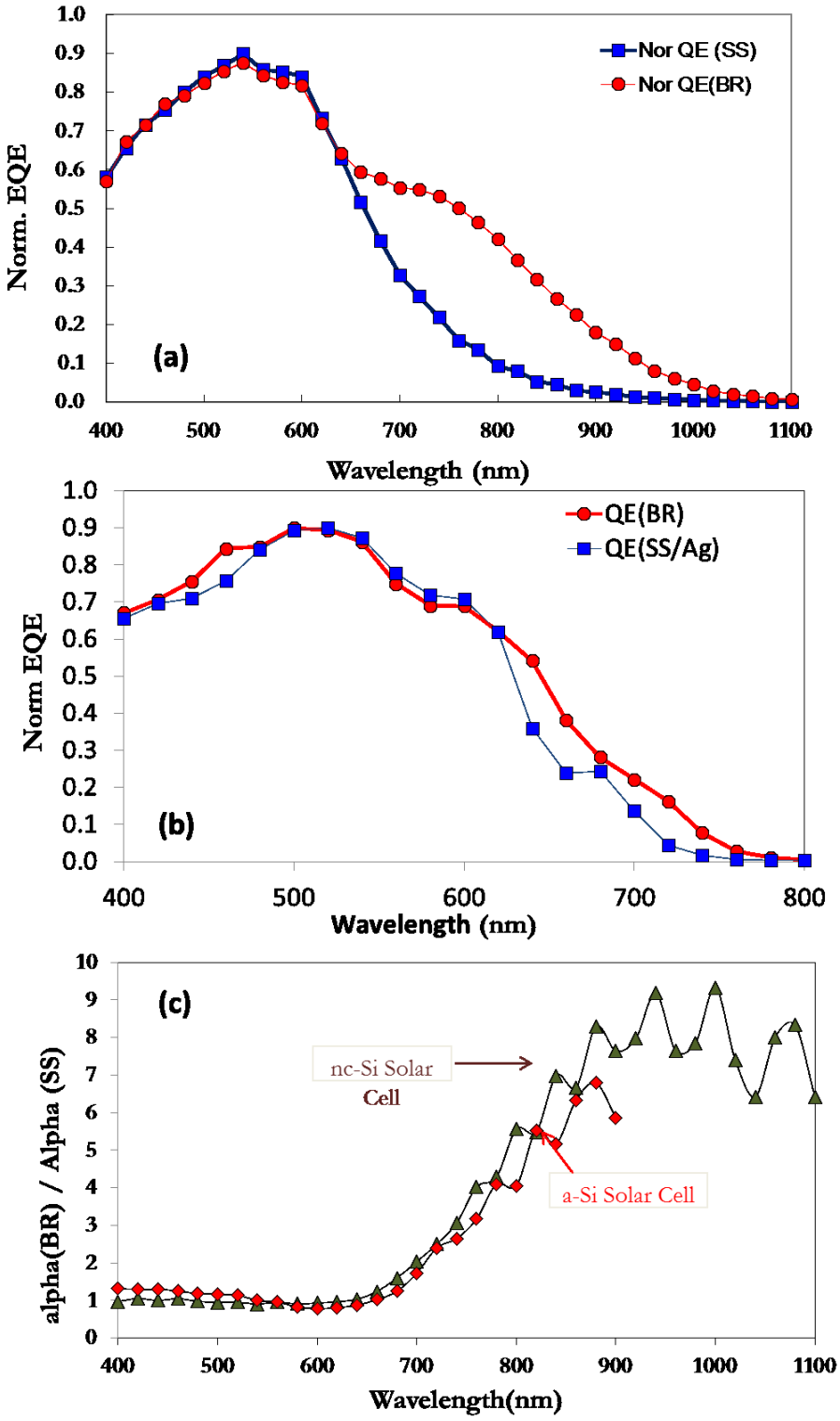

Figure 4.8: Comparison of etched ZnO to SS/Ag substrate (a)nc-Si:H device (b) a-Si:H cell (c) enhancement factor

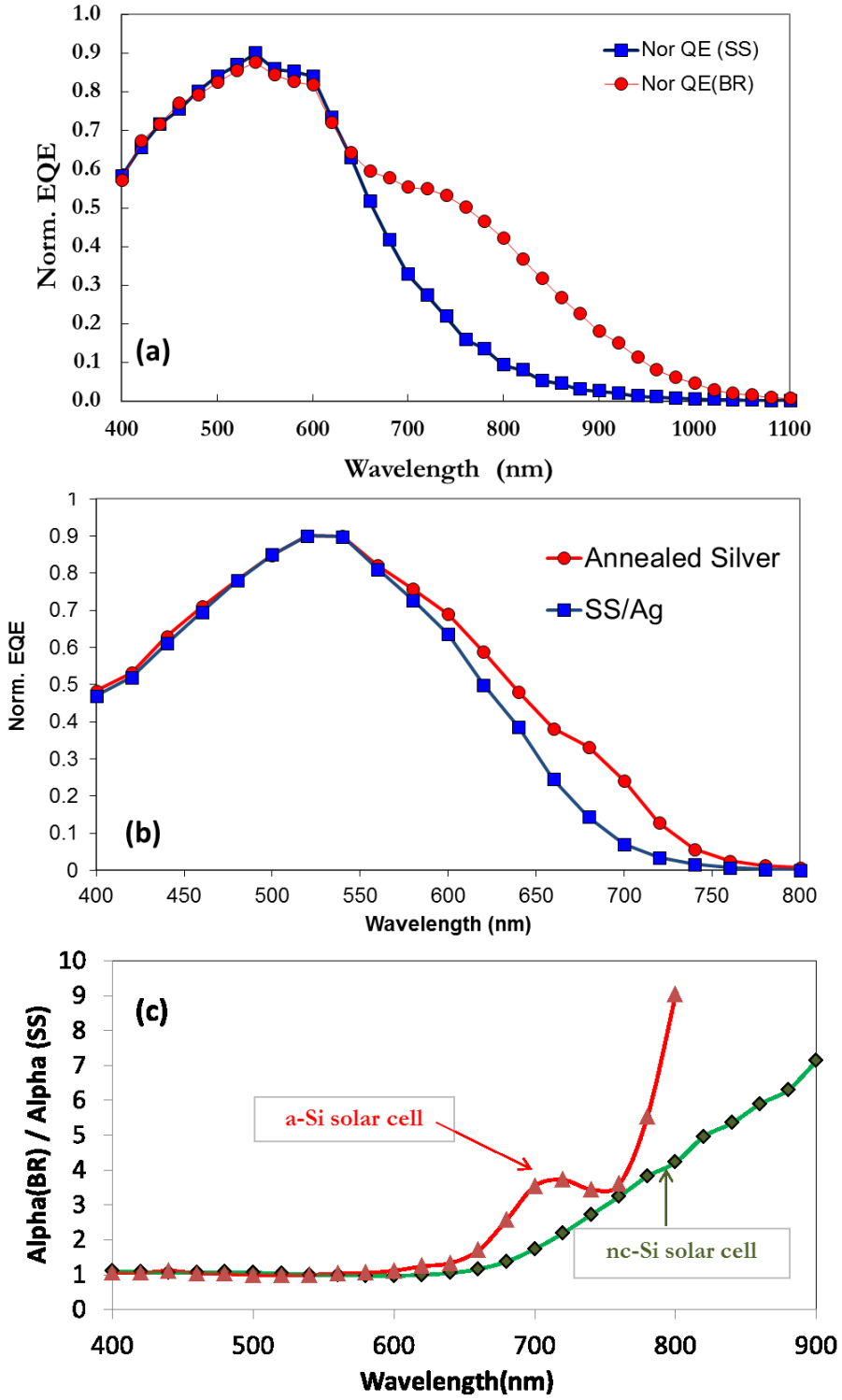

Figure 4.9: Comparison of annealed silver to SS/Ag substrate (a)nc-Si:H device (b) a-Si:H cell (c) enhancement factor

Table 4.1: Comparison of device made on random back reflectors

	SS/Ag		Etched ZnO:Al		Annealed Silver	
	nc-Si :H	a-Si:H	nc-Si :H	a-Si:H	nc-Si :H	a-Si:H
Jsc (mA/cm^2)	15.44	10.34	18.57	12.69	17.93	11.38
Voc (Voltage)	0.5	0.849	0.5	0.841	0.47	0.87
FF	53.79	57	57.2	58.4	53.5	63.3
Rseries (Ω)	74	119	51	75	60	115
Rshunt (kΩ)	3593	10172	2.70	7.73	2.1	10.69
Efficiency	4.22%	5.00%	5.57%	6.23%	4.51%	6.26%
QE (800nm/700nm)	0.098	0.071	0.34	0.242	0.31	0.22
Jsc from QE (mA/cm^2)	15.69	11.48	19.47	12.89	17.20	13.43
i-Layer thickness (µm)	1.72	0.251	1.72	0.251	1.40	0.233

The above table shows that there is significant increment in the current density which in turn leads to higher efficiency both in case of etched ZnO:Al and in the case of annealed silver. The change in efficiency is 30+% in case of nc-Si:H and ~25% for a-Si:H for the etched ZnO:Al substrates whereas the annealed silver samples had little lower thickness but here also we do see significant improvement. In Figure 4.8(c) and Figure 4.9(c) we specify a term enhancement factor which compares the increase in absorption due to the back reflector the calculation is based on a simple back calculation of the effective absorption coefficient ta each wavelength in the two samples using the formula

$$\frac{EQE(\lambda)}{1-R(\lambda)} = 1 - e^{-\alpha(\lambda)t}$$

Where, EQE(λ) , R(λ) and α(λ) are the external quantum efficiency , total reflection from the device and absorption coefficient at particular wavelength, t is for thickness of the absorber layer. Using this calculation we estimate the change of effective absorption coefficient and in plotted showing and enhancement factor greater than seven times that of SS/Ag substrates.

4.2 Periodic structures

Biswas & Zhou had developed the work for using a photonic crystal structure for use as a light trapping structure for thin film solar cells [140, 142]. The design consisted of a 2-D photonic crystal, and simulations were done to predict their effectiveness. The whole structure was simulated using the parameters such as pitch of the structures, and the geometry of the structure were optimized using scattering matrix method where Maxwell's equation were solved in fourier domain such that maximum absorption can be achieved. The photonic structure has its advantages since it diffract lights which reach it in different wave guided modes that travel nearly parallel to the surface while randomly oriented structures scatter light in multiple directions. It has been shown by Springer et. al. that there may be losses during reflection from the textured silver surface, they measured at each reflection the loss could be 3-8% which they attributed to excitation of surface plasmon modes and with multiple reflections the loss would add up rapidly at IR wavelengths [117]. The enhancement ratio predicted theoretically is close to 50 but including losses with a roughened reflector the enhancement has been estimated closer to 10 rather [241] . The absorption enhancement due to the photonic crystal has been shown in Figure 4.10 where at long wavelengths it performs even better than the lambertian limit of $4n^2$.

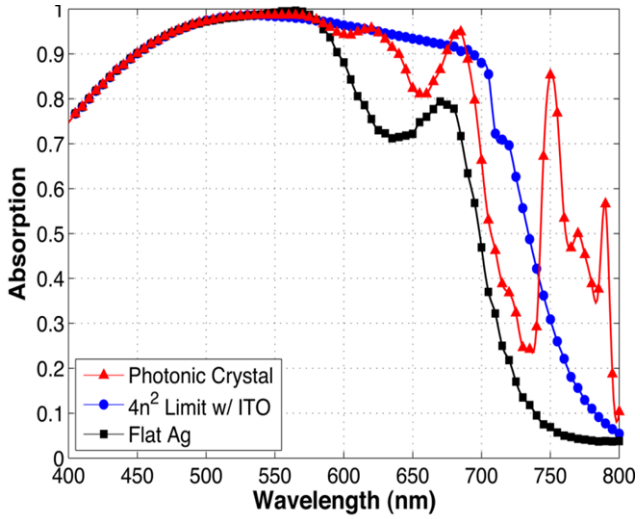

Figure 4.10: Absorption enhancement comparison for a photonic crystal and Lambertian limit[142]

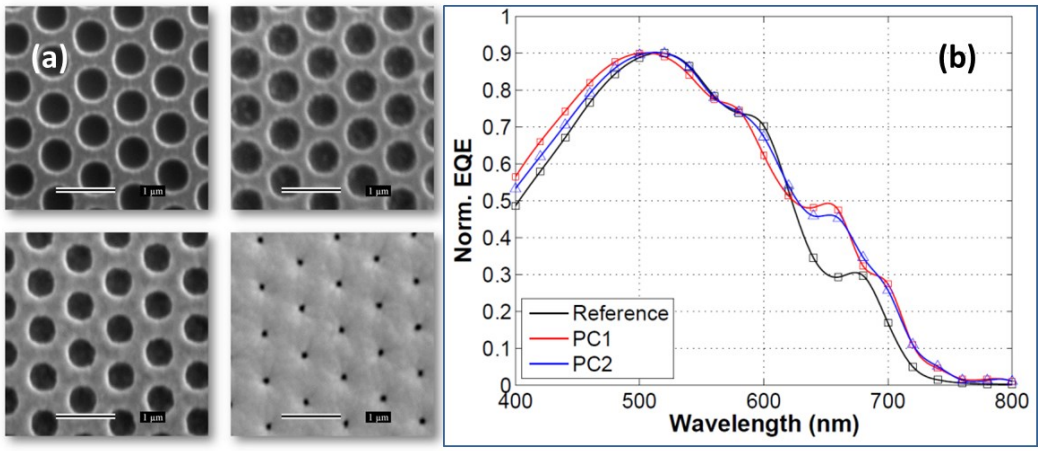

Figure 4.11: (a) SEM images of the photonic crystal structure at different steps of processing (b) EQE curve comparison between photonic crystal and planar SS/Ag [139]

The above results (Figure 4.10) were from simulation, we also showed it experimentally on the photonic crystal structure fabricated on c-Si wafer by formed by reactive ion etching by the work done by B. Curtin for his master's thesis where in Figure 4.11(b) the enhancement in the EQE curve due to the use of photonic crystal showing higher current than the reference which is a planar SS/Ag substrate. In Figure 4.11(a) SEM images are shown of the photonic crystal structure prepared on c-Si starting from top left is the photonic crystal only and then on right is the after silver deposition and then followed up by ZnO:Al in the bottom left and finally is after the final device fabrication. In each step we notice that the depositions are conformal to the structure also.

Table 4.2: Properties of various substrates

Max. Use Temp.	**Material**	**Characteristics (good, OK, bad)**
700^0C	Glass	Clear, brittle, good chemical resistance, cheap
900^0C	Steel	Opaque, moderate CTE, moderate chemical resistance, poor surface finish
300^0C	*Polyimide (Kapton)*	*high CTE, good chemical resistance, medium cost, high moisture absorption*
250^0C	Polyetheretherketone (PEEK)	Amber color, good chemical resistance, expensive, low moisture absorption
230^0C	Polyethersulfone (PES)	Clear, good dimensional stability, poor solvent, resistance, expensive, moderate moisture absorption
200^0C	Polyetherimide (PEI)	Strong, brittle, hazy/colored, expensive
200^0C	*Polyethylenenapthalate (PEN)*	*Clear, moderate CTE, good chemical resistance, inexpensive, moderate moisture absorption*
120^0C	Polyester (PET)	Clear, moderate CTE, good chemical resistance, inexpensive, moderate moisture absorption

But using c-Si wafer as the base substrate is not a feasible economical way to move forward, we had to look for different substrates to replace the wafer used in the above case. We looked at various possibilities of substrates listed in Table 4.2 where we have also listed the properties of each of the possible substrates starting with the temperature it can be used, followed by important characteristic properties which are important for solar cell fabrication (color coded for usability). The first three on the list have all been industrially applied - namely glass is widely used as a substrate for superstrate type devices, SS was used by the largest manufacturer of thin film silicon solar cells in 2000's i.e. Uni-Solar and Kapton is used by Power film -a plant close to us in Boone. But, as you go down the list we have more plastic based substrates and the last two in the list are inexpensive with other good and moderate properties which make them a

substrate to consider. PEN is our choice of material due to this beating PET due to its limits in processing temperature.

4.2.1 PEN substrates

PEN stands for polyethylnaphthalate and is going to be one of the major substrates used in this thesis. There were many challenges we had to face trying to adopt a new flexible plastic substrate for deposition rather than the old substrates like glass and SS that we used. We had to change our processing techniques and went through a qualification process before we could make devices on PEN substrates.

4.2.1.1 Problems faced

The first major hurdle was learning about how the polymer would behave when treated with heat. We worked with different variations of PEN which was treated chemically to stabilize it for higher temperature usage by Light Wave Power who we collaborate with for this project. The qualification process consisted of first testing the substrate in a conventional oven to see if there is very large bending or cracking. Once we were through this process, films were deposited on it to see if they peel off or crack. Our initial films did peel off or used to crack after removing from the reactor as shown in Figure 4.12. However, we realized very soon that if there was any moisture or oxygen in the substrates which degassed would lead to these problems. We took two steps that is a thin layer of metal was coated during the initial processing by Light Wave Power during their high temperature step that PEN did not absorb any moisture also we made it a practice to heat substrate in conventional oven at their deposition temperature so there is no degassing in the reactor. After that we were able to deposit films which were of better quality.

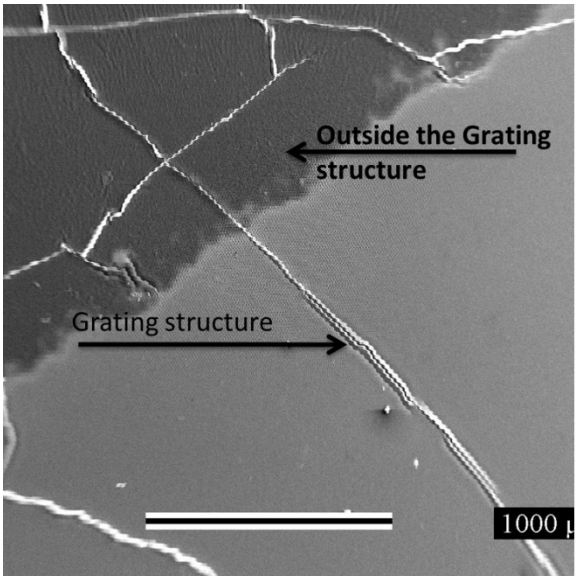

Figure 4.12: SEM image of PEN structure showing cracks on the film

Finally we also did make devices on PEN as shown in Figure 4.15 (planar), for fabricating devices we had to change the method of fabrication as most devices were fabricated at high temperature (mostly 300^{o}C). The device fabrication process had to be modified to get acceptable devices, the changes made consisted of increasing the hydrogen flow and depositing at a higher dilution ratio for a-Si:H cells such that we did not result in void formation due to lack of lateral movement due to lower temperature on the substrate. As deposition temperature was lower we also got a material with a higher band gap which resulted in giving a higher V_{oc} of 0.95-1V compared to devices at higher temperature which had V_{oc} of 0.85-0.9V.

The next step was to go for making the 2-D photonic crystal structures on these plastic structures, for which we got help from our collaborators light wave power for fabricating the patterns on the devices through nano-imprinting technology. The working principle (as shown in Figure 4.13) here is that a negative stamp is fabricated and is used to stamp the polymer when heated and then is removed while cooling to make sure that the structure is maintained on the polymer and the stamp can be re-used a chemical treatment is applied which also keeps the PEN substrate be able to handle higher temperature as mentioned before. The stamp can be re-used to make many substrates in the same way. It is important to mention here this process is also applicable for roll to roll processing where the roll would contain the inverse stamp and the structures can be fabricated as the polymer moves through.

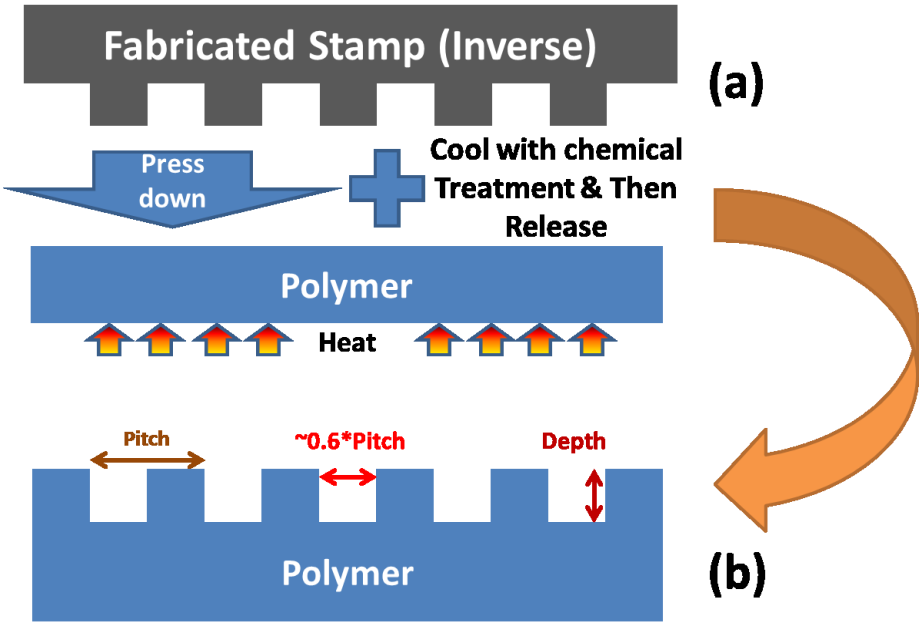

Figure 4.13: Schematic diagram for nano imprinting the polymer with desired structure

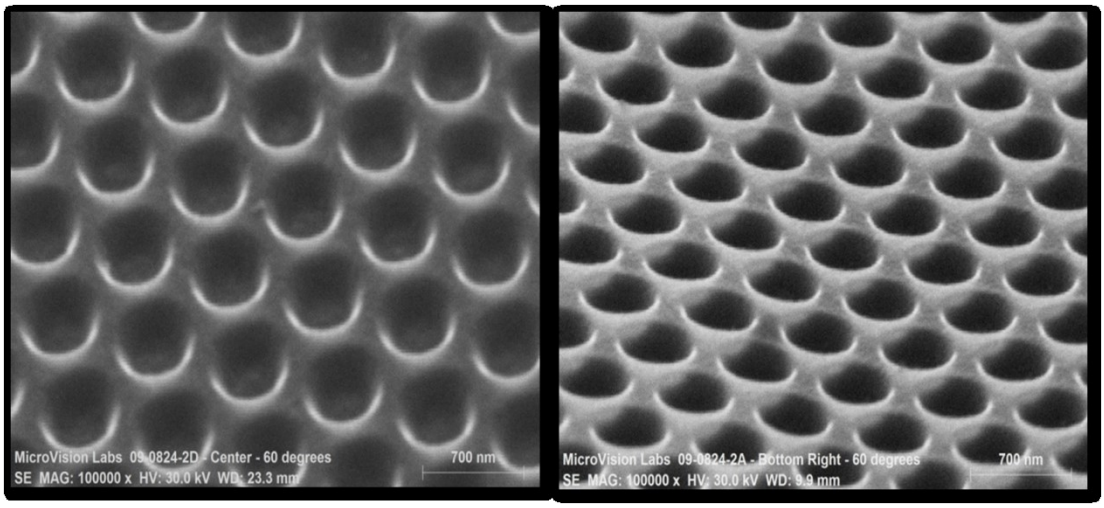

Figure 4.14: SEM image of 2-D photonic structure on PEN substrates

In Figure 4.14 we show the SEM image of the 2-D photonic structure which has cylindrical holes arranged in a triangular lattice which imitates the theoretical design. The cylinders have a diameter of ~450nm and the pitch is ~760nm and a depth of 250nm.

The next step was to prepare these fabricated structures by Light Wave Power for fabrication of solar cells and we followed the same procedure as mentioned for the planar PEN substrates. Here we faced more obstacles as the devices fabricated initially were having a lot of

shunting problems (drop in voltage mainly due to high recombination current which may be due to formation micro cracks at the sharp features) in contrast to planar PEN devices that did not have shunting problems. Due to shunting we had a lot of devices failing and even devices which were working had large variations of V_{oc} and FF. To resolve this uncertainty, we changed our fabrication technique and increased the n+ thickness on which we got better devices in terms of only shunting though as shown in Figure 4.15. We suspect that it may be due to the sharp edges formed in the new structure as shown in Figure 4.16.

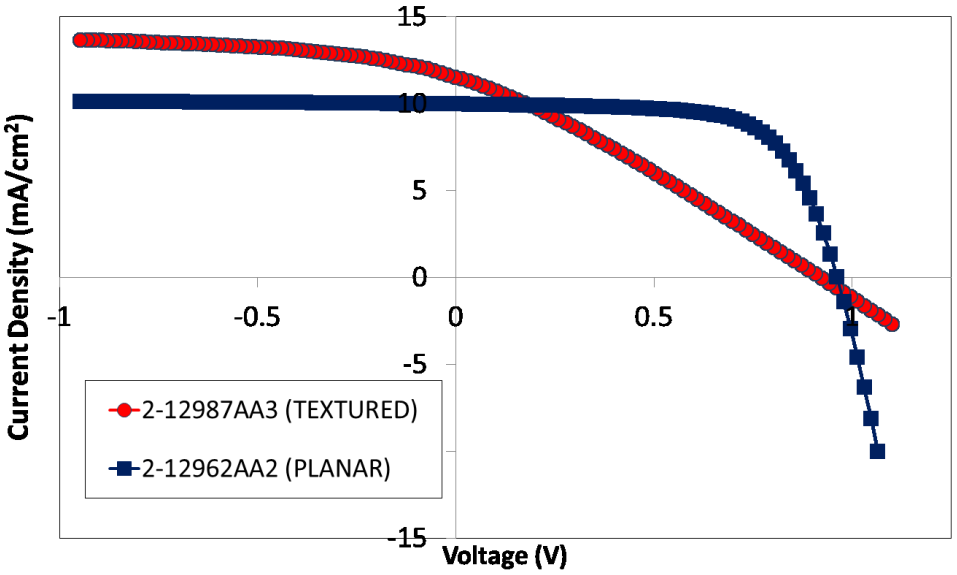

Figure 4.15: High resistance problem in textured PEN substrates

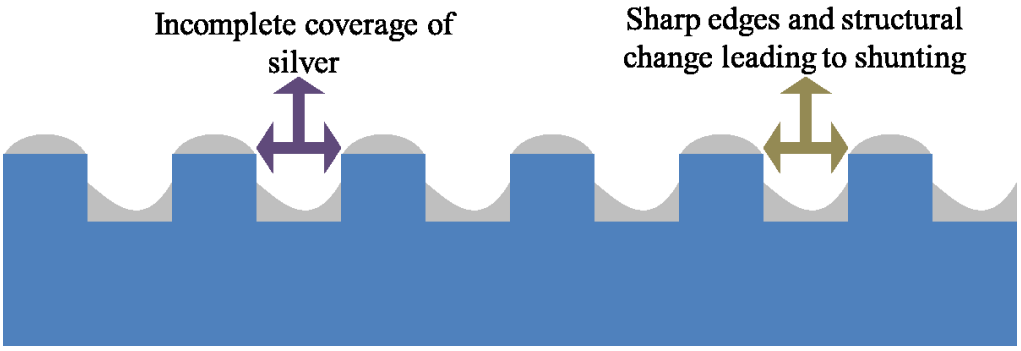

Figure 4.16: Problems faced with textured PEN substrates

But even with thicker n+ layer we did not have good results initially, but we did have control over V_{oc} but had very high series resistance and as shown in Figure 4.15, we suspected this

problem to be coming from incomplete coverage of silver which additionally may not have been thin but may be due to the fact we are doing thermal evaporation where keep the substrate fixed may provide shadowing to some inner areas. Although it can be argued that if we rotated the substrate in the x-y plane we may have been able to deposit all areas. But due to limitation with our equipment, we adopted a thicker layer of silver (~200nm) to get complete coverage. In case of commercialization we can also do sputtering which has better coverage than evaporation. A new improved structure was prepared as shown in Figure 4.17.

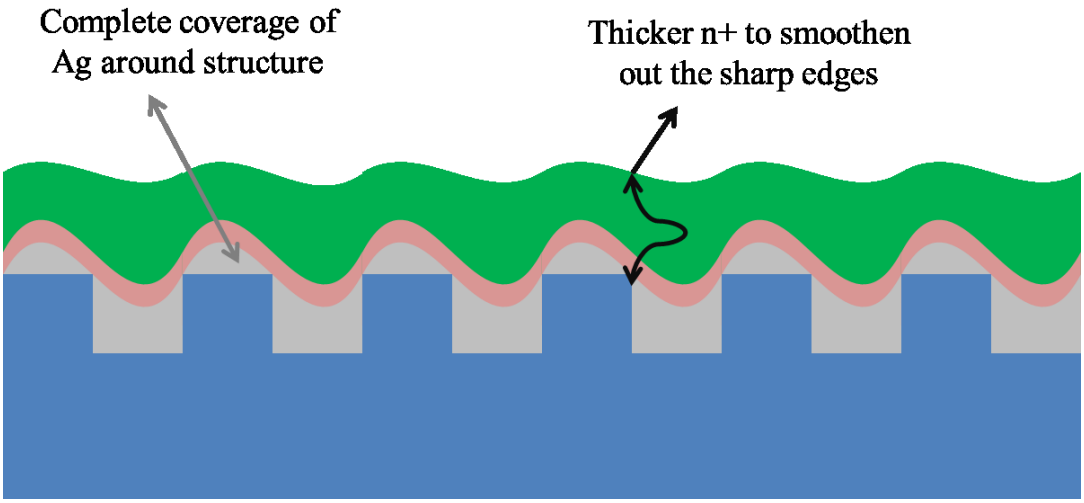

Figure 4.17: Improved structure for deposition on textured PEN substrate

The device structure has an n+ layer at the bottom of the cell as shown in Figure 4.1 where the n+ is between the i-layer and the back reflector. Photons going through the highly doped p+ and n+ are absorbed but effectively lost as the carriers generated due to photons here would recombine inside the doped layers and be lost. We tried to design the n+ to have a higher bandgap such that it does not absorb in the same wavelength region as that of the i- layer. The p+ is less effective in absorption since the thickness is usually less than ~20nm. The improved design for textured PEN substrate (Figure 4.17), however has a thicker n+ which makes it even more important to make a higher bandgap n+ layer.

The bandgap can be increased by doping with carbon, however as the bandgap increases so does the electron affinity and there has to be careful design such that the resistance and bandgap can be kept in check. We performed a number of experiments trying to control the bandgap while not increasing the series resistance. The major challenges here were that we had

to decrease the silane/methane flow rate to increase the bandgap while the phosphine was kept high to keep the film conducting. We also noticed that if we changed the power we had different amounts of carbon in the film which changed the properties of n+. After the optimization of a-(Si,C):H n+ we started making devices on the PEN substrates.

4.2.1.2 a-Si:H cells on PEN

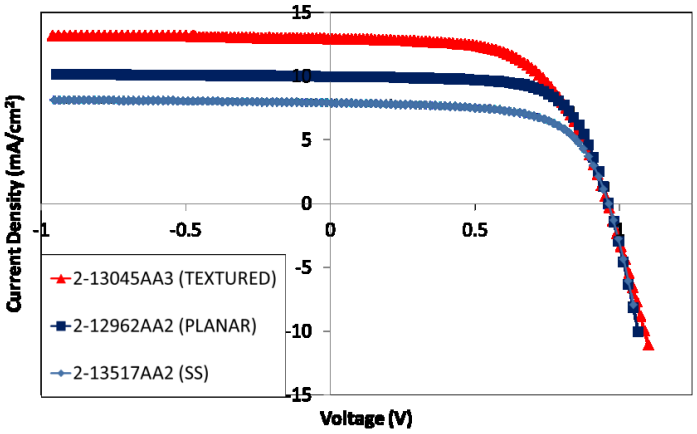

Figure 4.18: Current-Voltage measurement of a-Si:H device on PEN substrates

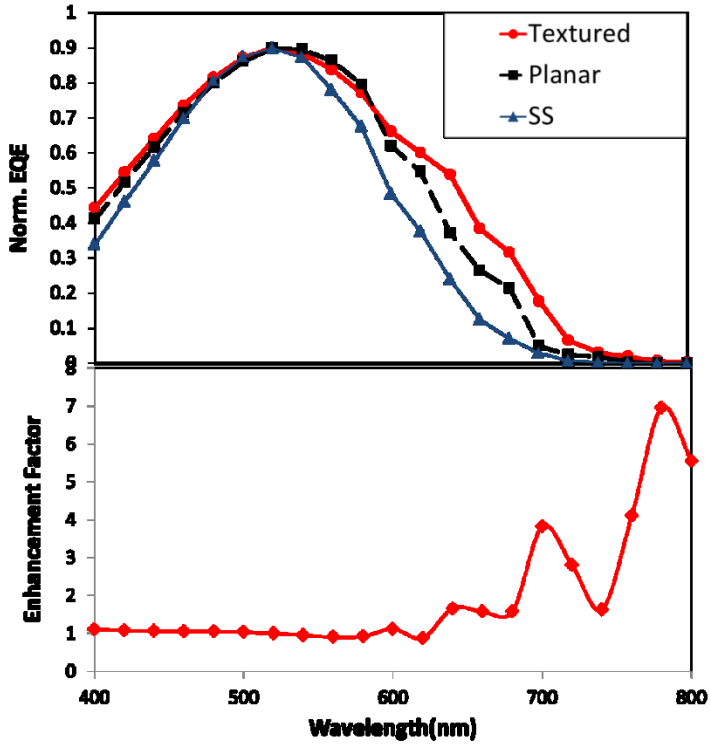

Figure 4.19: EQE and enhancement factor of a-Si:H device on PEN substrates

We show the IV characteristics of a-Si:H device fabricated on nano hole PEN substrates both textured and on planar PEN and as a baseline device on SS is also shown. All the devices are fabricated with a similar fabrication method, keeping all the parameters and conditions similar, except for the different substrates. In Figure 4.18 we see that there is a current enhancement of ~28% from SS to planar PEN with a silver mirror like structure at back. While a change of more than 60% in current density can be observed when we have a textured 2-D photonic structure on PEN substrate. When we compare the 2-D photonic structure to the planar structure to see the effective light trapping from the photonic structure, we obtain approximately 30% increase in current density. The overall efficiency was ~7.5% for the cells deposited on the 2-D photonic structures on PEN.

In Figure 4.19, we show the external quantum efficiency for the cells whose IV curve is shown in Figure 4.18, and we observe that the current enhancement is due to increased absorption at longer wavelengths in the red and infra-red region. The enhancement factor has been calculated by comparing the effective absorption coefficients of the photonic structure and the planar PEN devices. The enhancement factor when using SS is as the baseline is much higher. The photo of the final device on each substrate is shown in Figure 4.20. It should also be mentioned here that the planar PEN structure is not a completely flat silver substrate due to some agglomeration taking place on plastic substrates and also for plastic substrates lower temperature annealing can lead to agglomeration unlike the case for SS shown in section 4.1.2.

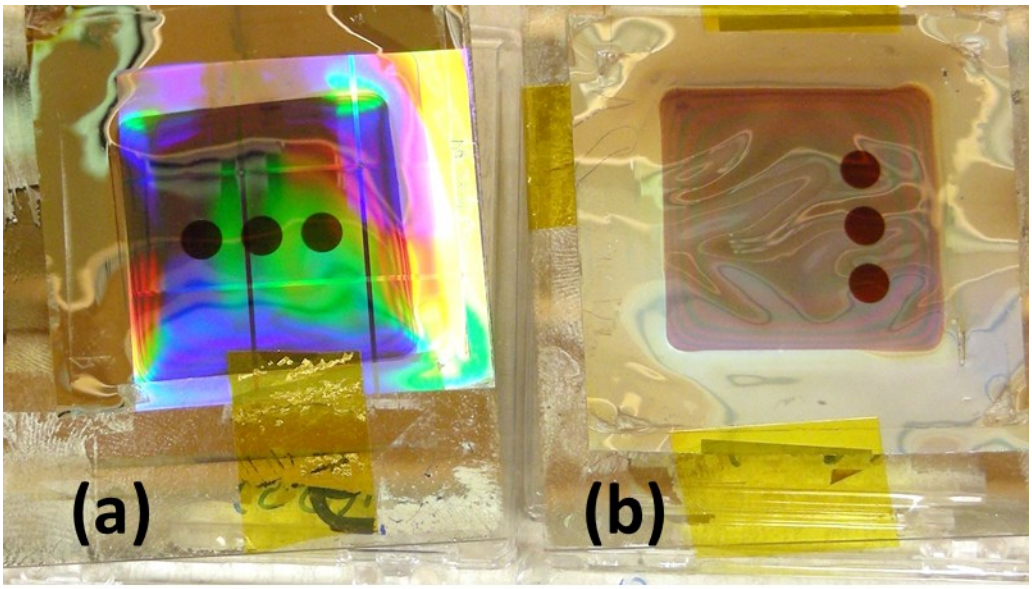

Figure 4.20: Photographs of PEN substrates (a) photonic hole structure and (b) Planar PEN

4.2.1.3 a-Si:H/a-Si:H tandem solar cells

Tandem cells can be fabricated using a-Si:H where we make two junction tandems connected in series where the voltages add up but the cells have lower currents as the cells have to share the photons in their absorption wavelength range. We prepared a-Si:H/a-Si:H tandem solar cell with a thinner bottom cell as the photonic structure. To increase the effective current in the bottom cell, the top cell is made thinner about quarter thickness of the bottom cell. The junction between the cells in a tandem cell is made with a thin p+ and n+ layer, but at low temperature it is more difficult to fabricate the junction layer. We can make either a-Si or nc-Si 'n+' at the junction layer when nc-Si n+ can give better conductivity; it also lowers the V_{oc} as shown in Figure 4.21. Therefore, we have continued with a-Si n+ with more phosphine.

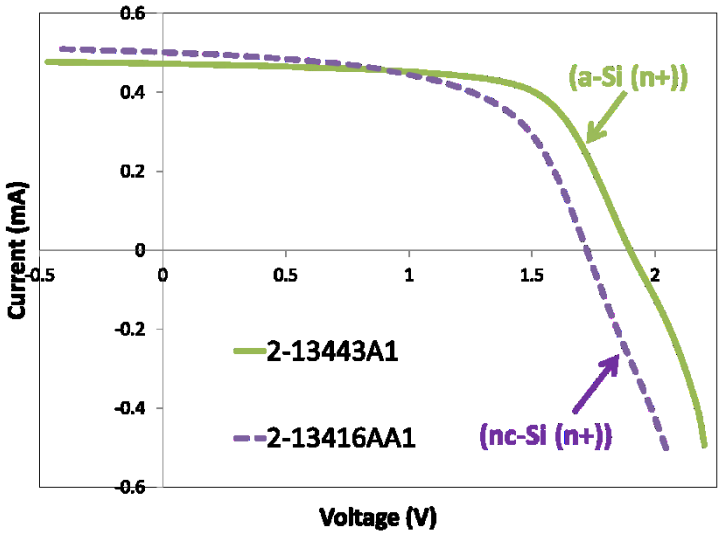

Figure 4.21: Comparison of a-Si and nc-Si n+ as junction layer in a tandem cell

We made two identical tandem cells on planar and textured PEN substrates after optimizing a working a-Si n+ layer in the junction layer with additional phosphine to increase conductivity. The tandem cells were made at the same temperature of 200^{o}C for both the top and bottom cells. The results are shown in Figure 4.22(a) where we get ~25% improvement in the current density in a tandem cell on a 2-D photonic structure compared to a planar PEN substrate, similar to the improvement show in single cells in last section. We also show the EQE curve for the tandem cell on the photonic structure on PEN substrate showing a current density of 6.23mA/cm^2 on the top cell which would limit the current density of the tandem cell. The overall efficiency is ~7.4% for the tandem cell. The Voc is 1.74V which is lower than the addition of two single junction cells which may be due to the junction layer moreover the FF also suffers due to the junction layer which is ~67%. There are inherent advantages to this tandem cell in comparison to the single cell as the top cell which would absorb most of the high energy photons would be very thin and hence would have a high electric field. Moreover, the bottom cell is also now protected due to the top cell absorbing the high energy photons. This helps reduce the effect of light induced degradation on a tandem cell compared to a single cell [24].

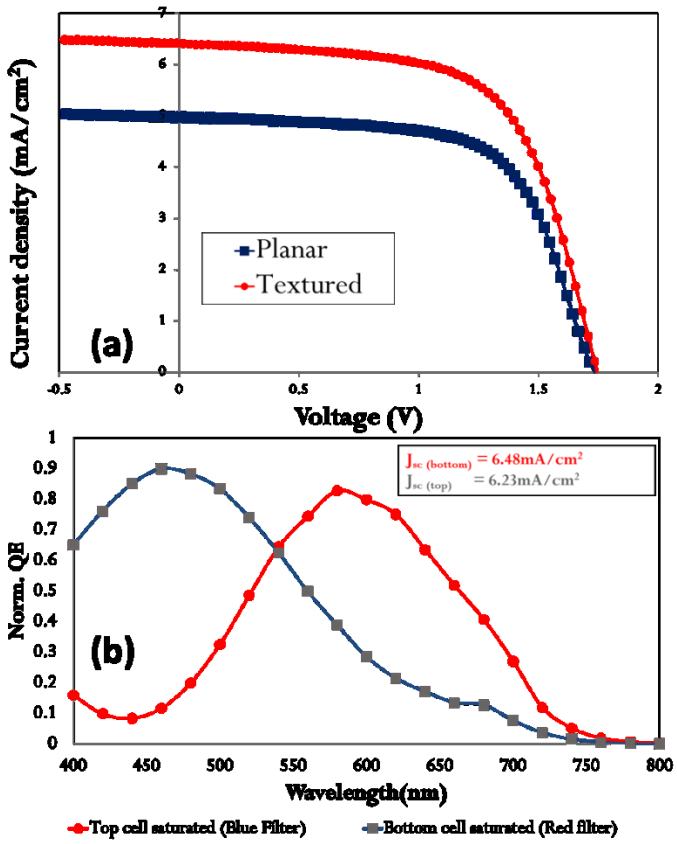

Figure 4.22: IV and EQE of a-Si:H/a-Si:H tandem solar cell on PEN substrates

Although we were able to show enhancement in current with an a-Si:H/a-Si:H tandem cell, it should have materials of complimentary band gaps to be really effective. Various groups have establishes that a combination of nc-Si:H and a-Si:H prove to be very close to the best choice of material for a two junction tandem cell [66].

4.2.1.4 nc-Si:H on PEN substrate

The fabrication of nc-Si:H on a PEN substrate was difficult due to lower deposition temperature. Nc-Si:H requires higher deposition temperature for nucleation of crystallites, or much higher hydrogen dilution ratios to crystallize. We used hydrogen profiling here to fabricate the devices whereas most devices are fabricated in the superlattice method in our group. A single nc-Si:H cell grown at temperatures below 200^{o}C is shown in Figure 4.23 where we can extract nearly an extra third of the current density of the planar PEN by employing a photonic structure. The effect of the photonic structure is exemplified by the increased absorption in the red and the infra-red region shown in Figure 4.23(b), proving that in both a-Si:H and nc-Si:H we

can get a about 30% improvement in current density by employing 2-D photonic structure on plastic substrates with fabrication temperature below 200°C.

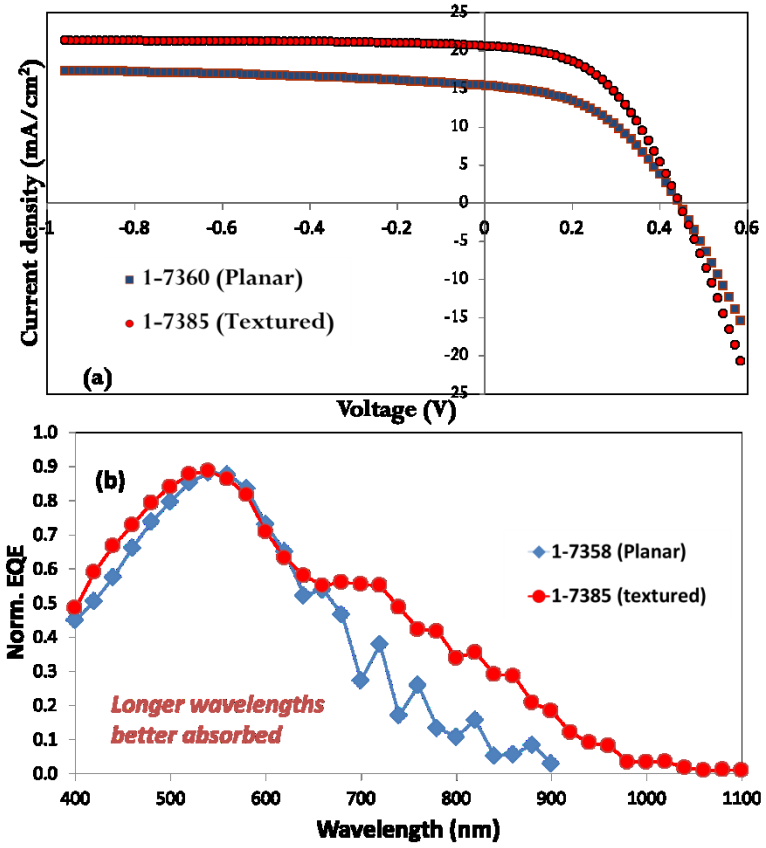

Figure 4.23: IV and EQE of nc-Si:H single cell on PEN substrates

Furthermore, we fabricated micromorph cells with both nano crystalline and amorphous layer grown at ~200°C as shown in Figure 4.24. The micromorph cell gives an efficiency of ~8% with a current density of 9.8mA/cm^2 which is limited by the top a-Si:H layer. The V_{oc} have added up from both the cells to result in a V_{oc} ~1.4V which means that there is low loss from the junction layer. Although in this cell we have deliberately made the top cell limiting because the bottom cell performance is limited with a low FF which can be observed in Figure 4.23(a). The nc-Si:H cell is limited in efficiency due to carrier collection problems which is mainly due to the low quality of the intrinsic layer from the low growth temperature we are forced to employ due to the limitations from the PEN substrate.

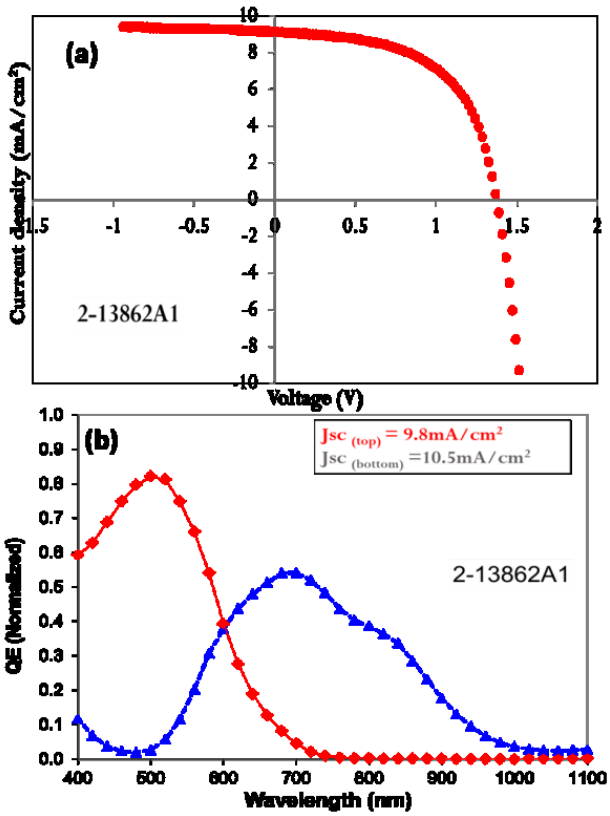

Figure 4.24: IV and EQE curve for micromorph cell on textured PEN substrate

4.2.2 Kapton Substrate

Due to the lower quality of nc-Si:H at low temperature deposition, we looked at substrates that can handle higher temperature. The choice of substrate was Kapton, also called polyimide, which can handle deposition temperatures of 300^{o}C. The same 2-D photonic structures were fabricated on Kapton substrates with the help of Light Wave Power. The nano imprinted structures were then examined under SEM and AFM as shown in Figure 4.25 which show that the embossed 2-D photonic hole structures can be successfully imprinted on Kapton also. The SEM image is taken at an edge of the patterning showing the continuous array of holes arranged in triangular lattice.

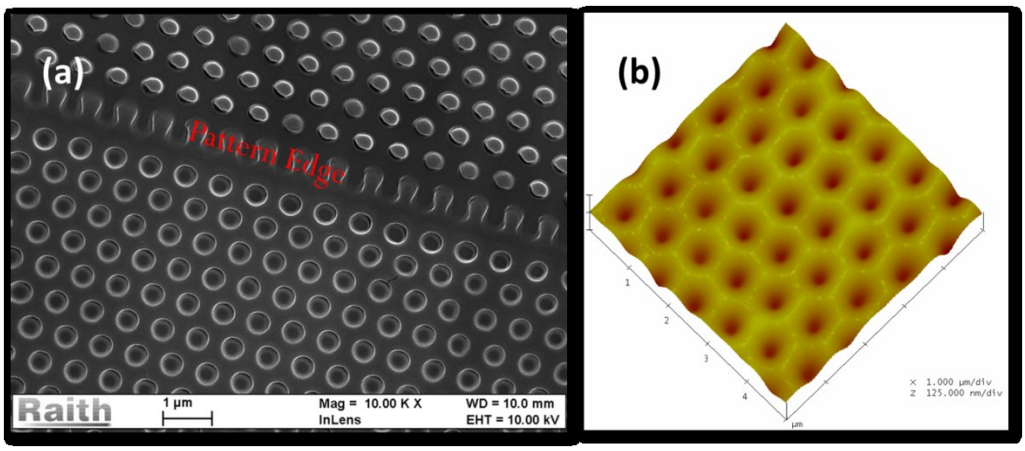

Figure 4.25: 2-D photonic structures on Kapton substrate (a) SEM image and (b) AFM image

4.2.2.1 nc-Si:H cell on Kapton

The next step was the fabrication of nc-Si:H on the nano imprinted Kapton substrates which can handle higher temperatures. Here we have used a superlattice design[64, 242] to deposit nc-Si:H, with alternating layers of nc-Si:H/a-Si:H allowing independent control of crystallinity [243, 244]. The solar cell with a thin ~816 nm nc-Si:H/a-Si:H absorber layer , having a 12 period structure. The superlattice was formed by alternately cycling the RF power for 180 s at high power (30W) for nc-Si and 90 s at low power (3W) for a-Si:H respectively. Stopping the nc-Si:H growth by reducing the RF power prevents the nano-crystallites from growing and coalescing, and prevents the large angle grain boundaries that are detrimental for electronic transport [242]. Growth of the a-Si:H layer generates a new seed layer on which the next layer of nc-Si:H nucleates. The parameter space for layer thicknesses has been studied in detail by Kocka et al [243], and it was found that 3-5 nm thick a-Si:H layers can interrupt growth of nc-Si:H. Having such thin a-Si:H layers is advantageous for reducing light-induced degradation effects, and increasing light absorption. Using such thin a-Si:H layers permits photo-excited carriers to transport through such a-Si:H layers without losses in the presence of the external field. Photo-excited carriers generated in a-Si:H layers can easily diffuse to the neighboring nc-Si:H layers and transport through thin a-Si:H layers to the respective electrode. The constraints of achieving high electronic transport, rather than enhancing optical absorption, dictate the individual layer thicknesses. Growth conditions were optimized for growth temperatures ~225°C, to prevent thermal expansion and degradation of the kapton substrate. Raman measurements indicate a

crystalline volume fraction of ~45% and amorphous fraction of 55%, consistent with these values.

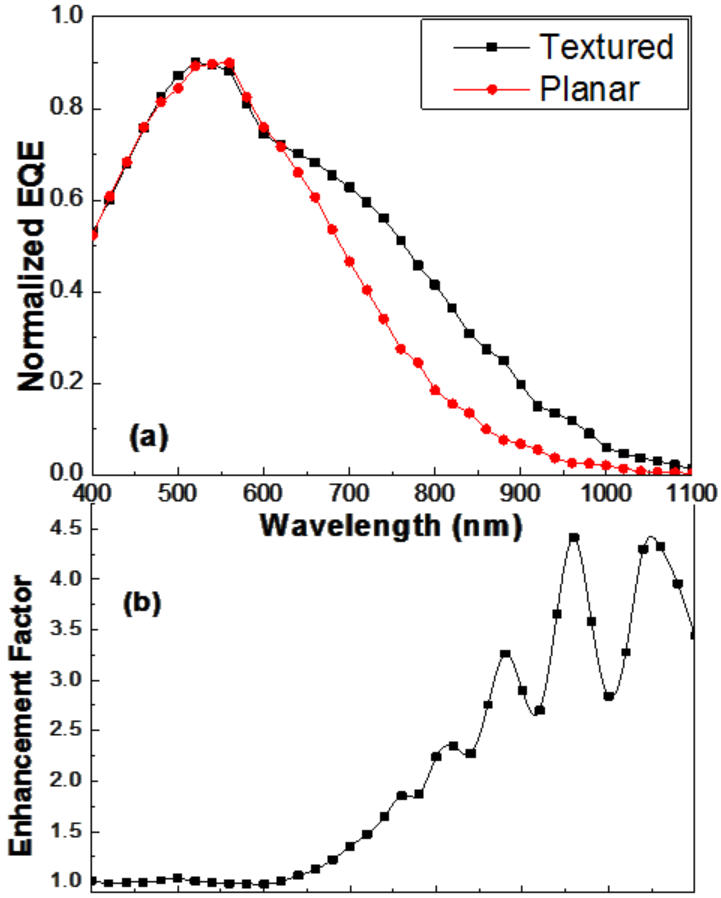

Figure 4.26: (a) Norm. EQE and (b) enhancement factor of supperlattice nc-Si:H device fabricated on embossed Kapton

The external quantum efficiency (EQE) was measured as a function of the wavelength shown in Figure 4.26(a). There is a highly enhanced collection of long-wavelength photons from 600 nm to the band edge of 1100 nm. The QE-derived short circuit current (J_{sc}), is enhanced from 17.3 mA/cm^2 to 20.9 mA/cm^2, for a total enhancement of 21%. The current on similar thickness cells made on stainless steel is 14 mA/cm^2, yielding a PC-based enhancement of ~50% over the stainless steel substrate. The enhancement factor is shown in Figure 4.26(b), or the ratio of the QE between textured and flat substrates, exceeds 2 for wavelengths above 800nm, and approaches 4.5 at the band edge. We expect that considerably higher currents (>28

mA/cm^2) could be obtained with thicker super-lattice i-layers, thereby making such super-lattice devices competitive with the state-of-the-art nc-Si devices.

The current-voltage (I-V) characteristic in Figure 4.27 demonstrates low series resistance and excellent collection of carriers at reverse bias. The open circuit voltage (V_{oc}) and fill factors (FF) are is 0.45 V and 62% for the planar and 0.42 V and 60% for the textured cell, typical of nc-Si devices. Maintaining high quality n and p-layers is essential for good device results. We find a power conversion efficiency (PCE) of 6% for the textured vs. 5% for the planar solar cell. Higher cell efficiencies are expected for thicker cells.

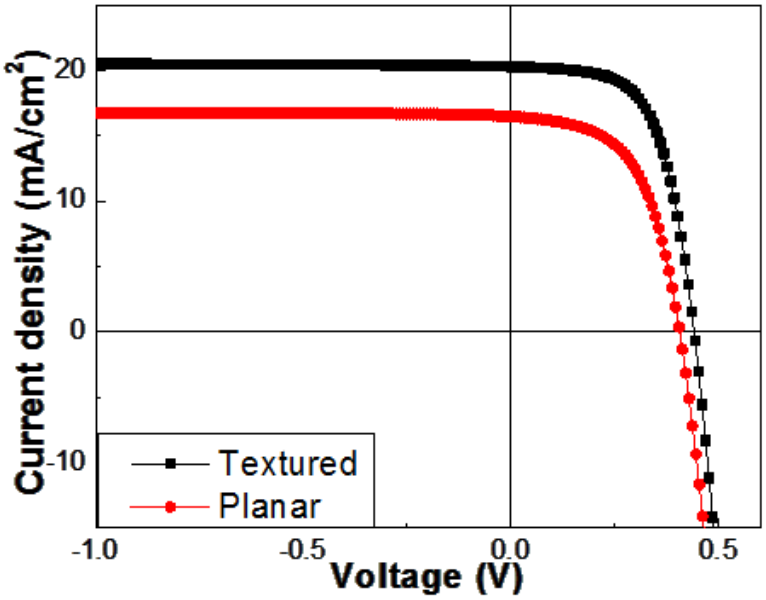

Figure 4.27: Current-Voltage for nc-Si:H cell on Kapton substrate

4.2.2.2 Micromorph cell on Kapton

The aim of getting a good nc-Si:H single cell was to apply it to get higher efficiency by fabricating a tandem micromorph device. We fabricate the bottom nc-Si:H cell at higher temperature (250^{o}C) as mentioned in last section while the a-Si:H cell is fabricated similar to conditions that were used before during fabricating on PEN substrates (200^{o}C).

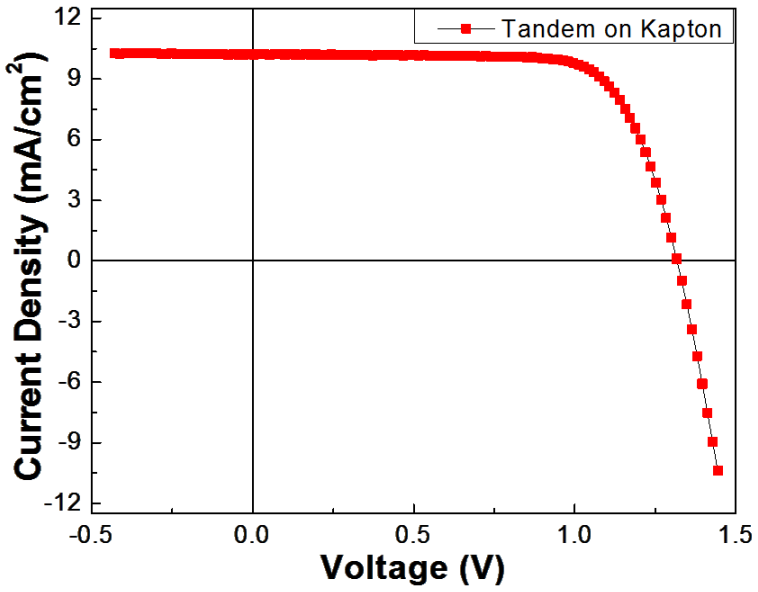

Figure 4.28: IV curve of tandem cell on textured Kapton substrate

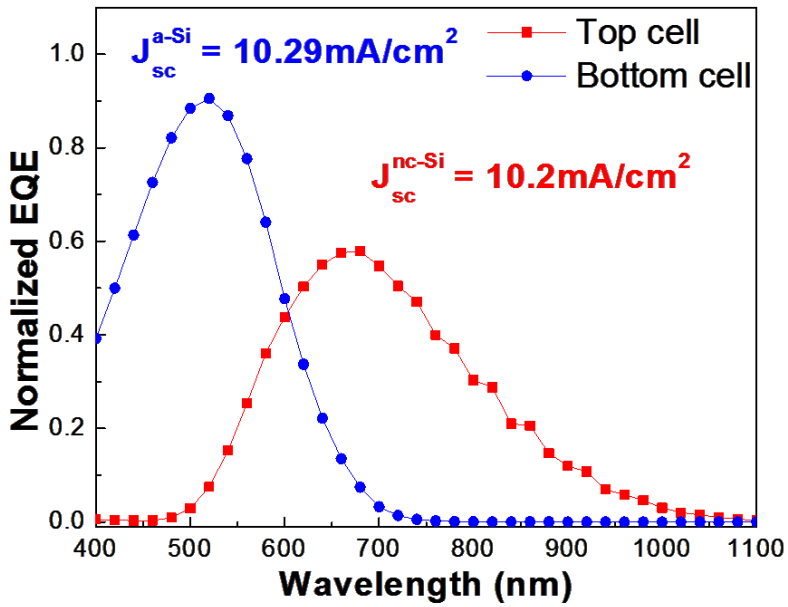

Figure 4.29: Normalized EQE curve for a tandem cell on textured kapton substrate

The micromorph cell fabricated on the kapton substrate with 2-D photonic structure resulted in a cell which gave ~9.9% efficiency (Figure 4.28). We optimized the both the bottom and top cell to get very good current matching in the cells to get a current density of 10.2mA/cm^2 shown in Figure 4.29 while the top cell give 10.29mA/cm^2. During the optimization

we were able to fabricate devices with high FF (>70%). The open circuit voltages also added up to give cells with (Voc>1.32V).

4.2.2.3 Problems faced with Kapton

During fabrication of devices on kapton substrate we were mostly affected by the difference in coefficient of thermal expansion which led the substrate to bend or curl up after the film/device was grown on kapton. This made device characterization and deposition of ITO very difficult on it. We had to be very careful not to put extra stress on the film which may lead to formation of cracks.

To avoid this problem we started to load kapton on a SS substrate, i.e. before depositing any layer on the kapton substrate it was stuck to a SS plate that we used for our standard deposition with a polyimide tape to hold it. The substrate was kept on all the steps from then on to the final characterization of the device.

4.2.3 Polymer on SS (POS)

SS is a widely used substrate which is cheap and readily available. For application as a substrate SS has to be polished smooth on at least one side (for planar) such that it does not lead to defects in the films growing on it. Surface finishing the steel for thin film deposition adds to cost, whereas SS can be rolled thin to be used as a flexible substrate. We can also try adding controlled modified structure on the steel itself but it still remains difficult due to intrinsic nano meter sized structures on steel. If we consider polymers then they have lower working temperature which limits their usage. Now, if we consider the pros of SS being both cheap and widely available, we can fabricate structures on PEN by nano imprinting easily. Therefore, we used polymer coated on SS that would give the polymer mechanical support such that they can be used at higher temperatures.

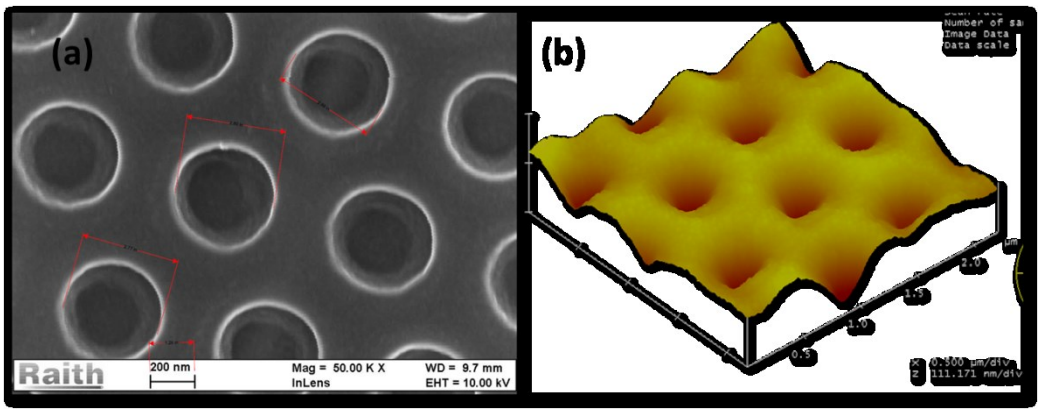

Figure 4.30: (a) SEM and (b) AFM images of POS for testing effect of annealing

The structures were prepared on POS with either PEN or kapton coating on SS and then tested if the structures hold at higher temperatures or the features formed from imprinting were lost or deformed. The methodology consisted of heating in oven or even in the reactor and then observing SEM and AFM images and measuring different characteristic features to see if there was any change in the structure due to the annealing at higher temperature as shown in Figure 4.30. The images showed that the structures formed remain intact at high temperature annealing of 300^{o}C. This result gave us more room to fabricate devices while we still had flexible and cheap substrates which could be nano-imprinted to form structures with the help of Light Wave Power.

We then fabricated nc-Si:H devices on the POS substrates, the IV curve and EQE have been shown in Figure 4.31 and Figure 4.32 respectively. The devices here are also fabricated at 250^{o}C whereas it can also be fabricated at higher temperatures if required. The enhancement is similar to the devices fabricated in kapton without having to deal with the bending of it. Additionally kapton is also not that cheap a substrate which has been noted from Table 4.2

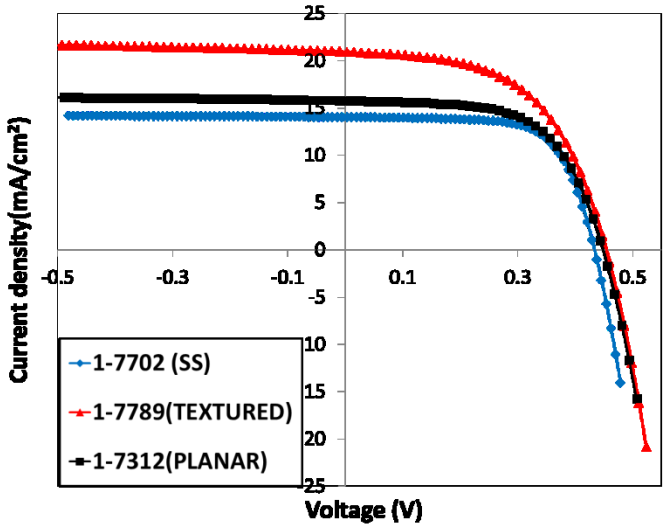

Figure 4.31: IV curve of nc-Si:H device on POS

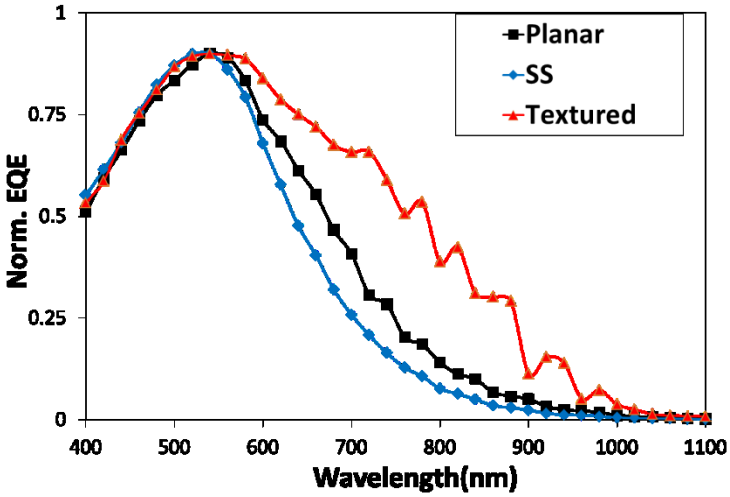

Figure 4.32: EQE curve of nc-Si:H on POS

4.2.4 Photonic-Plasmonic Structures

Plasmons are created due to the interaction of metal syrfaces with electro-magnetic waves and it is widely used for solar cell applications for current enhancement as discussed in the literature review. We are going to specifically consider the surface plasmon modes that form at the interface of metal and semiconductor layer. These surface plasmons propagate parallel to the metal semiconductor interface as they are longitudinal. The surface plasmon modes have large field intensity in the absorber layer, where it decays exponentially into the semiconductor as shown in Figure 4.33 [85, 176]. This method has been used by various groups to make

plasmonic solar cells using periodic structures to couple the modes for to increase absorption in solar cell [85, 129, 131, 133, 245]. In case of silver at the back, the plasmon mode is shifted to near infra-red by using ($\varepsilon_s + 2\varepsilon_m = 1$) where ε_s and ε_m stand for the dielectric functions of semiconductor or the metal respectively.

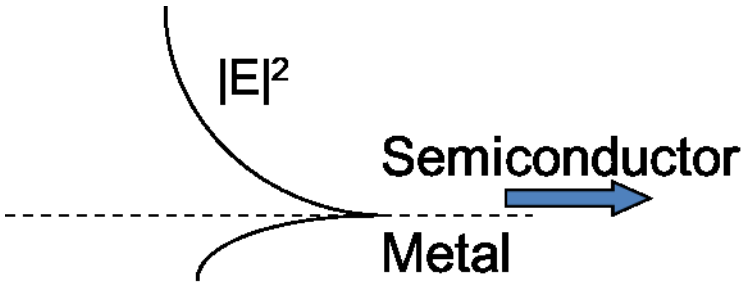

Figure 4.33: Schematic showing Surface plasmon mode

4.2.4.1 Concept of periodic photonic-plasmonic structures

When we use roughened silver at the back reflector, there is a creation of localized surface plasmons in the Ag nano structures but they may not lead to increase in absorption which has been note by other groups for randomly textured surfaces which may lead to losses. However it is possible to use these structures also effectively re-radiate under appropriate conditions [176, 182]. Thus appropriate design can lead to increased absorption with the help of a periodic structure with a geometry that is favorable for plasmonic enhancement.

There are two modes of enhancement in a periodically structured back reflector. Firstly, the photonic enhancement is due to incident light being diffracted into wave guided modes travelling parallel to the layers, where at long wavelengths we have many available wave guiding modes. Another enhancement is due to plasmonic in nature where if the shape and size of metal particle is favorable then it leads to formation surface plasmon polaritons which propagate parallel to metal surface and also provide a field decaying into the semiconductor which leads to increased light intensity in the region close to metal and therefore enhanced absorption . These two mechanisms together can couple to each other to give higher enhanced absorption than when they act separately. This method is shown figuratively in Figure 4.34 where we can combine both the methods to get a periodic structure with nano pillars.

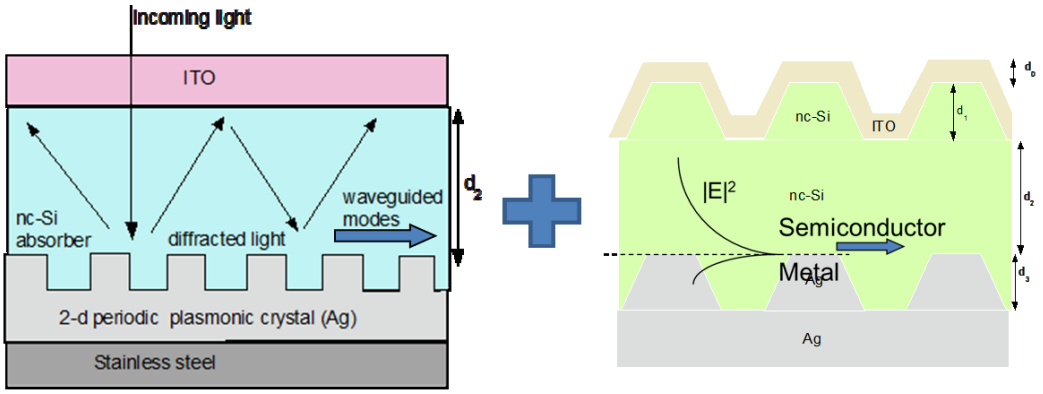

Figure 4.34: Concept of photonic-plasmonic structures

The simulation of the devices showed that the Lambertian limit of $4n^2$ enhancement can be exceeded by employing a photonic plasmonic structure. A comparison is shown in Figure 4.35 with different structures i.e. the Yablanovitch limit [71] (which is the same as $4n^2$ limit,) then the additional curve is $4n^2$ limit with the additional reflection loss from the top therefore it takes into consideration the light that enter the cell only, the third one is a flat silver substrate and is compared to photonic-plasmonic structure. The simulation predicts that the designed structure is significantly better than the flat silver and it also exceeds the classical 4n2 limit when reflection losses are added and is comparable to the Yablanovitch limit and can do even better at some wavelengths above 900nm. Further details about it can be found on the simulation details in a paper by Biswas et. al. [75].

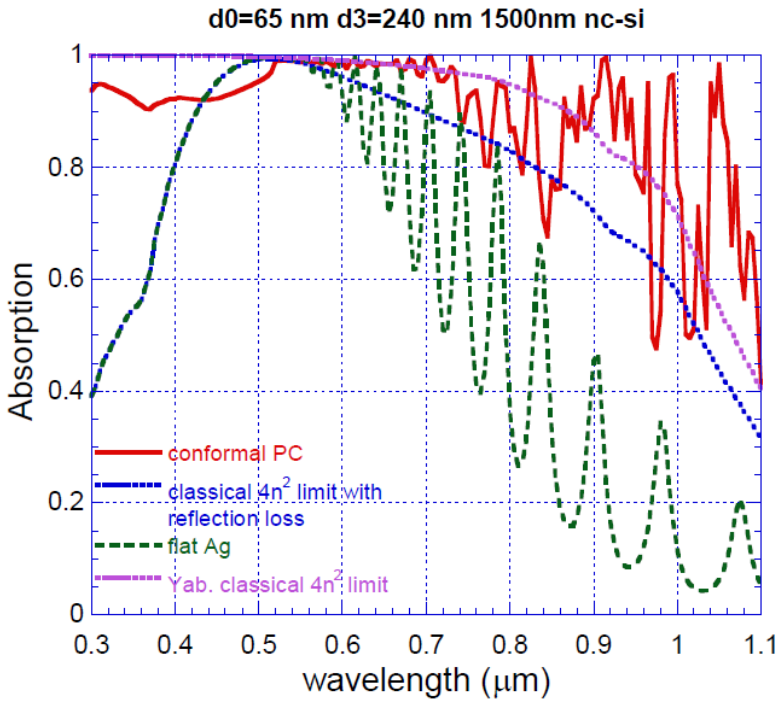

Figure 4.35: Comparison of absorption for different methods of light trapping through simulations [75]

4.2.4.2 Devices on Photonic-Plasmonic structures

We then tried to fabricate the photonic plasmonic structures on flexible substrates by nano imprinting technology. We have named the photonic-plasmonic structures as nano-bump and the photonic structures as nano hole due to their shape and for ease of communication. The fabricated structures were characterized under SEM which showed that the pitch is ~750nm as shown in Figure 4.36(a). We also show an SEM image of the nano-bump structure after the deposition of silver and ZnO:Al. The AFM image reveals that the fabricated structure has features (nano pillars with smoothened top) of height ~180nm shown in Figure 4.37. The structure was then pretested as we had done for other substrates mentioned before, and then nc-Si:H devices were fabricated on them.

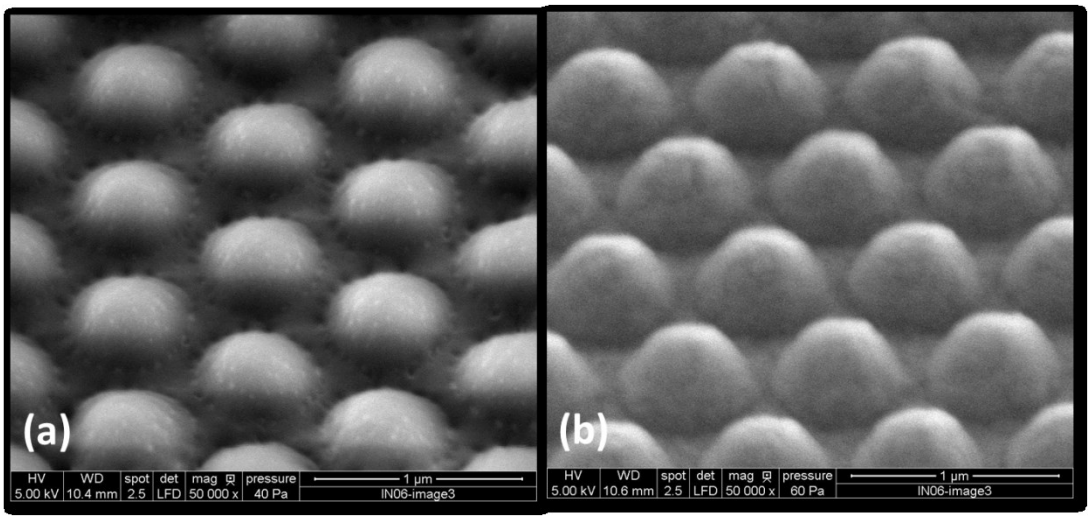

Figure 4.36: SEM Images of nano-bump structures on Polymer on SS. (a) As received (b) with Ag/ZnO:Al

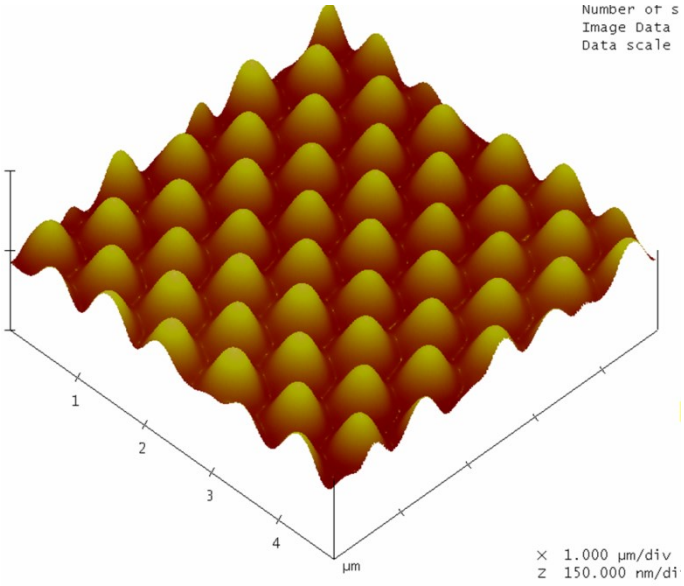

Figure 4.37: AFM image of nano-bump structure

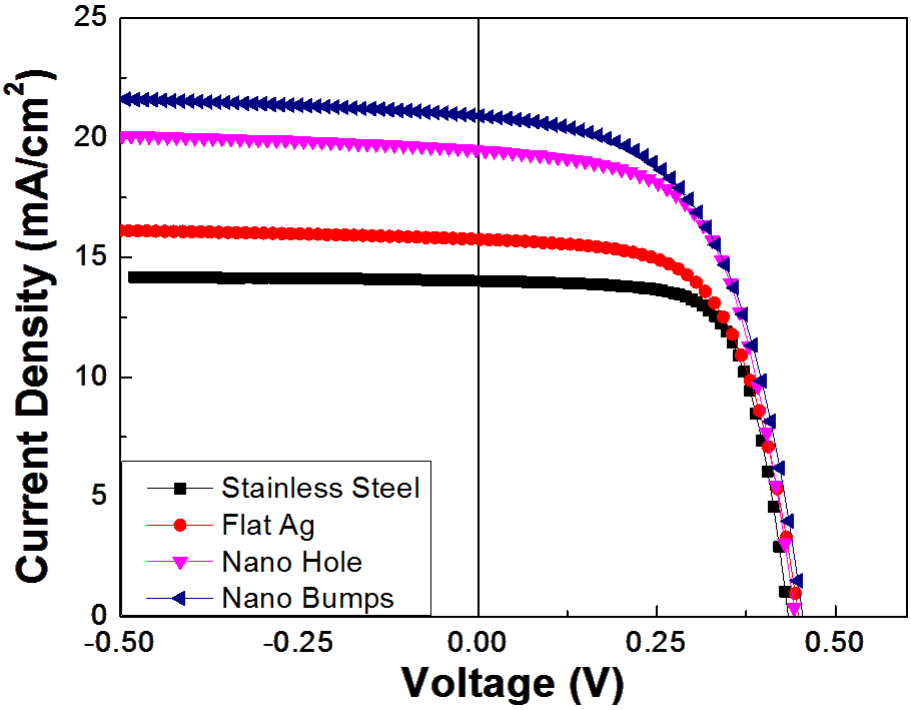

Figure 4.38: IV curve for nano-bump structure in comparison to other structures

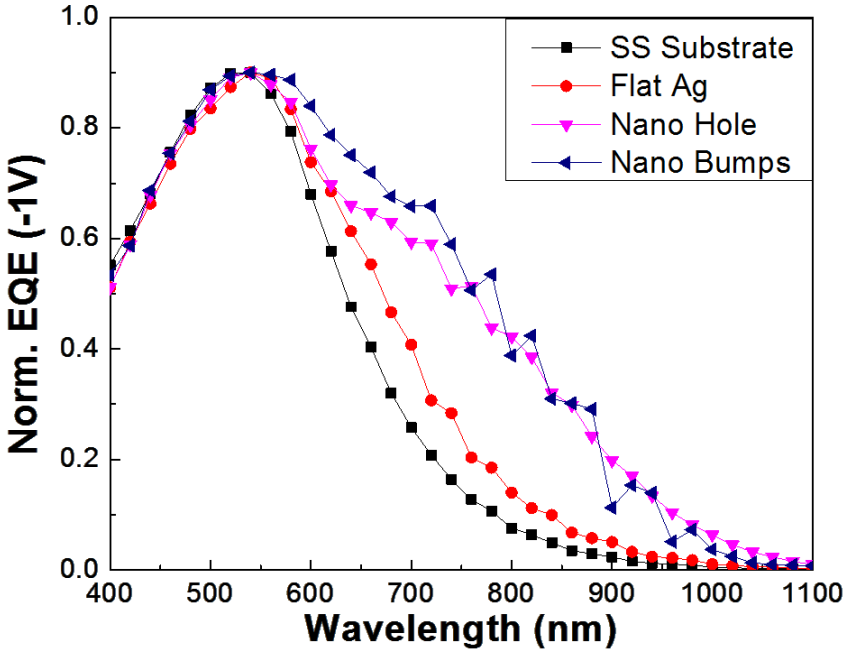

Figure 4.39: EQE curve for nano-bump structure in comparison to other structures

The next step in improving the current density was using the nano-bump structure (photonic- plasmonic), which further improves the current in the cell. In Figure 4.38 and Figure

4.39 the IV curve and EQE curve for nc-Si:H device of thickness ~1µm is shown prepared on different substrates while we had already seen improvement due to nano-hole (photonic) structure there is further increase in current density with nano-bump. The increase in current is mostly between the 600-800nm for nano-bump compared to nano-hole, while the rest of the wavelength are comparable.

Superlattice cells: An additional simulation is also shown in Figure 4.40(a) for a nc-Si:H/a-Si:H superlattice absorber we find an optimum structure with tapered nano pillars of height 180 nm, a base radius of R/a=0.4 (where a is the pitch), and the height of the front texture d1=105 nm, demonstrating conformality between the front and bottom texture. We have adopted the absorber layer thickness of the experiment of 816 nm, comprising of alternate layers of nc-Si:H (60 nm) and a-Si:H (8 nm) and 12 periods. By simulating the wavelength dependent absorption in Figure 4.40(a) and calculate the weighted absorption <Aw> weighted by the solar spectrum, over the entire wavelength range of interest (400-1100nm). This yields an absorption enhancement of more than 25%. At wavelengths (λ>600nm), the photon absorption is substantially enhanced over a flat Ag-back reflector shown in Figure 4.40(a) generating a predicted overall enhancement of 25% of the weighted absorption or the short circuit current. We show for comparison the expected absorption for a loss-less Lambertian back-reflector, in a nc-Si:H absorber layer of the same thickness, where the path length is enhanced by $4n(\lambda)^2$ at each wavelength λ [246], where n is the wavelength dependent refractive index. This enhancement factor can approach ~50 in silicon. The plasmonic back-reflector can exceed the Lambertian back-reflector near the band edge (>800nm). At shorter wavelengths the absorption maxima of the plasmonic back-reflector lie above the $4n^2$ limit of nc-Si:H, although the overall absorption is lower. However there are significant losses [117, 247], from excitation of surface plasmon modes in the random textured back reflector, and it has been predicted [241] that experimental enhancements are considerably less than the $4n^2$ factor.

Angular measurements of nc-Si:H cells: We also measured angular dependence of the cells with varying incident angle of illumination. The simulations suggest that periodic back reflectors perform better when the light is incident 15^o-40^o from normal incidence i.e. the nano-bump structure is more effective in channeling light when incident at an angle. In case of experimental work on fabricated devices we see that absorption is less affected by the angle of incidence for textured substrates with a maximum at 19^o in case of this measurement. Whereas, we see that

for planar structures the absorption decreases mostly monotonically after 10° from normal. This is important as the sun also shines at different angles through the day.

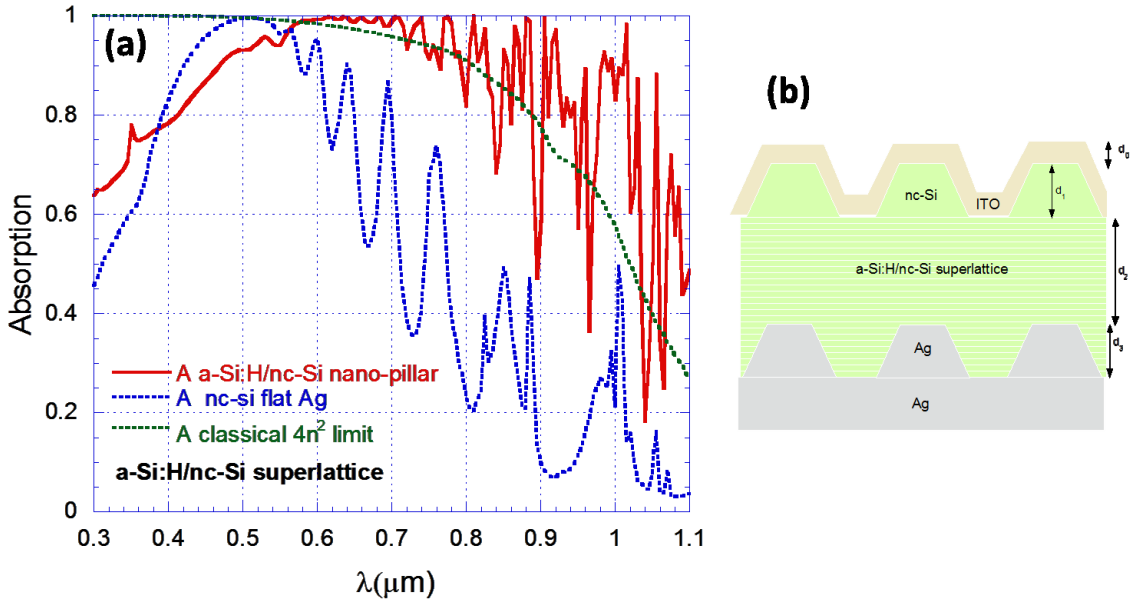

Figure 4.40: (a) Simulation result for superlattice structure on photonic-plasmonic structure and (b) schematic diagram of a superlattice cell on photonic-plasmonic structure

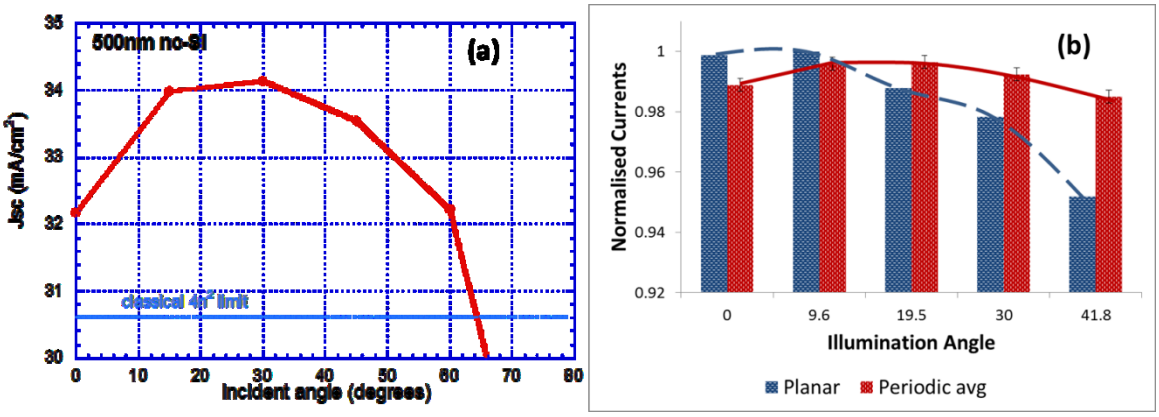

Figure 4.41: Angular dependence of photocurrent of solar cell (a) simulated result on photonic plasmonic structure and (b) Experimental comparison between planar and periodic structure.

4.3 Comparison with randomly roughened structures

We have discussed various photon management strategies that maximize the photo-current. Though we showed that simulation shows that nano-bump or photonic-plasmonic

substrate would outperform others there is need for a systematic comparison experimentally on devices to show which structure performs the best. We do this by systematically comparing nc-Si:H solar cells grown on a series of randomly roughened and periodically textured back-reflectors (BRs). To make meaningful comparisons, the nc-Si absorber layer thicknesses were kept the same and the solar cell device architecture were identical in the entire series of solar cells on both families of substrates.

For experimental comparison, we used six distinct types of back reflectors. The first was a planar SS substrate with no metallic coating. The next type was a SS substrate with a Cr (5 nm)/Ag (200nm) layer deposited on it, followed by 80 nm of ZnO. The third type of back reflectors were made from annealed Ag/ZnO deposited on SS as discussed in section 4.1.2. The fourth textured reflector was fabricated from etched ZnO back reflectors prepared by the methods described in section 4.1.1. A distribution of feature sizes between 400 -1500 nm was observed in both types of roughened substrates (third and fourth families). The thin ZnO layer on top of Ag prevents the interaction of Ag with Si during and after the device deposition.

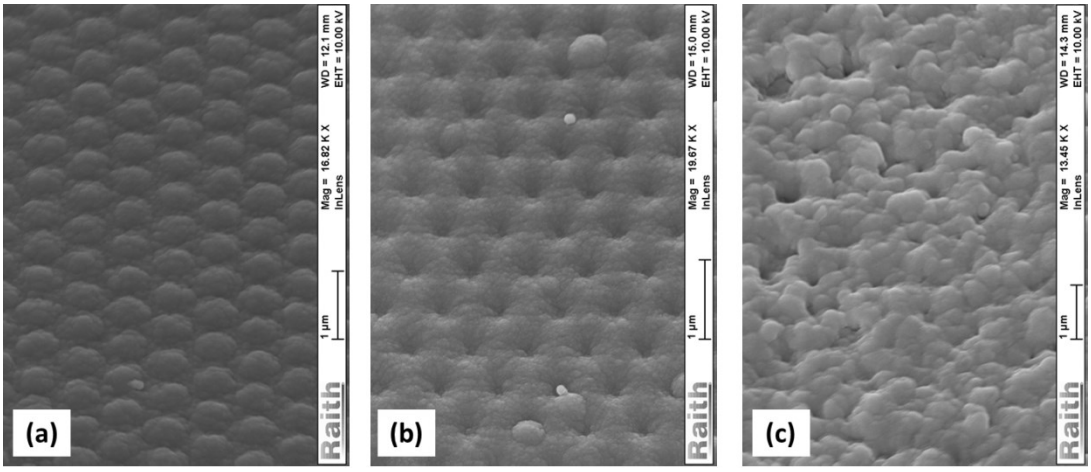

Figure 4.42: SEM images from the top of ITO showing the conformal growth of the solar cell on (a) nano-bump, (b) nano-hole and (c) etched ZnO/Ag

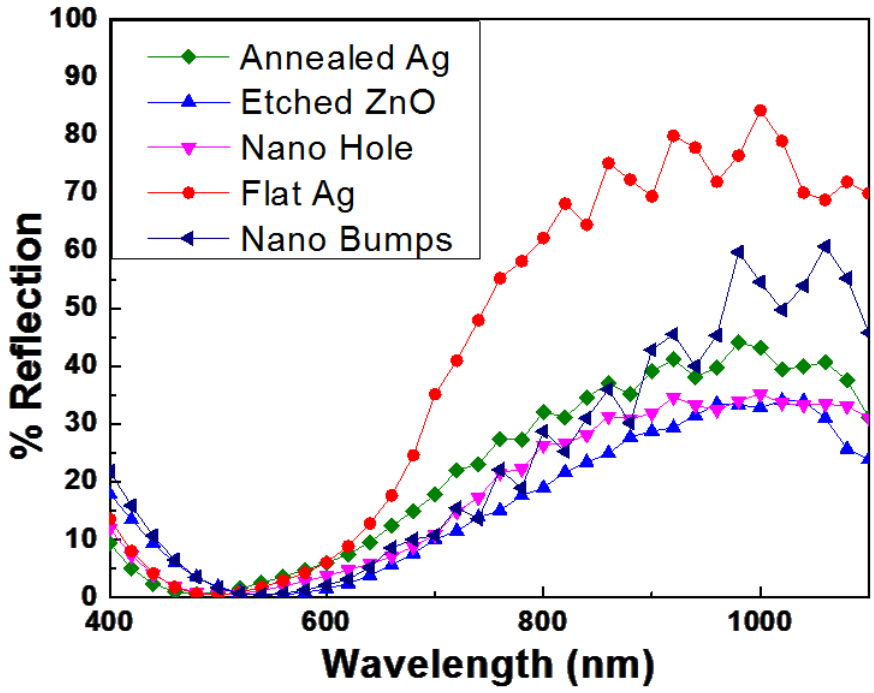

Figure 4.43: Reflection from top of the ITO after device fabrication on each substrate

To compare randomly roughened BRs with periodically textured substrates, we utilized the SS substrates with periodic nano-structures prepared using nano-imprint lithography at Light Wave Power. The pitch of the periodic pattern was ~750 nm, determined to be an optimum following extensive rigorous scattering matrix simulations [75, 136, 142]. The nano-bump (Figure 4.36), a feature found in simulations to enhance light absorption with a height of ~180 nm, near the optimum. The nano-hole arrays(Figure 4.30) had depths of 200 nm as optimized previously[135]. The above sequence of Ag/ZnO deposition, followed by the deposition of n-i-p layers at temperatures below 250^{o}C, was performed on these periodically textured BRs. The cells grow conformally as shown in Figure 4.42, with the substrate pattern observed at the top of the cell. The reflectance also varies with the structure as the incoming light is also affected by the texture on top of the surface as we see from Figure 4.43 the reflectance from textured substrate are much lower due scattering on ITO leading to less light getting reflected back compared to flat Ag on SS.

Before device fabrication, we performed optical measurements to characterize the randomly roughened BRs used for comparison substrates by measuring reflectance which is similar to the data shown in Figure 4.5 for etched ZnO:Al. These comparison reflectors had 5nm

Cr and, 200nm Ag, 80nm ZnO:Al on them. We selected annealed Ag and etched ZnO:Al reflectors as benchmark “best” reflectors, because they had a structure similar to that shown in Figure 4.4 for etched ZnO:Al and Figure 4.7 for annealed silver that leads to very high diffuse reflectance, exceeding 70% over the entire spectral range (400-1100 nm), comparable to the state-of-the-art [103, 248-250]

To enable meaningful characterization of randomly roughened BRs with periodically textured BRs, nearly the same thickness of intrinsic layers (0.9µm) and exactly identical solar cell architecture was followed on both substrates. The intrinsic layer crystallinity was kept at ~55% which was verified by Raman spectroscopy. We performed both optical and electrical characterization to compare nc-Si:H solar cells made on the six families of substrates. We measured both device I-V curves shown in Figure 4.44 and the EQE to obtain the wavelength dependent photo-current between 400 -1100 nm (Figure 4.45) for all devices to confirm the I-V curves. We observe the EQE to have a maximum of ~90% near 530 nm. We used a -1.0 volt bias measurement in EQE to ensure complete collection of photo-generated carriers. In general, there was only ~2-3% difference between EQE at 0V and at -1 V. Similarly, the discrepancy between actual currents observed in I-V testing under the simulator and calculated from QE was also within 2-3%.

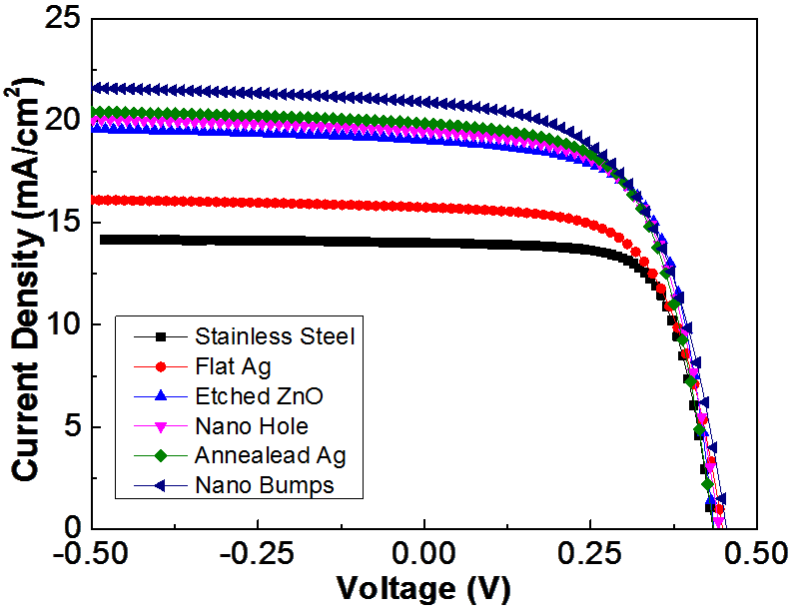

Figure 4.44: IV characteristics for nc-Si:H solar cells on various substrates namely SS, flat Ag, random textured annealed Ag/ZnO, random textured etched ZnO/Ag, periodic nano-hole and periodic nano-bump substrates.

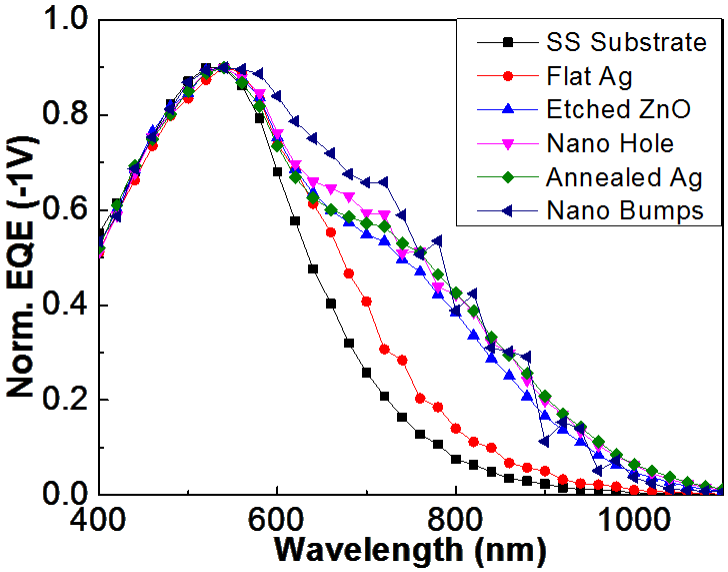

Figure 4.45: EQE in reverse bias for nc-Si:H solar cells on various substrates namely SS, flat Ag, random textured annealed Ag/ZnO, random textured etched ZnO/Ag, periodic nano-hole and periodic nano-bump substrates.

The progression of the results for the currents estimated from EQE is given in Table 4.3 and has been extracted from Figure 4.45. The reason for calculating currents from EQE is because this calculation is independent of the state of the solar simulator, i.e. the simulators always vary

a few % over time, and measuring EQE and then multiplying by the standard photon spectrum eliminates the errors due to this simulator creep. We found that the actual currents from measured I-V curves were within a 2-3 % of the calculated currents.

Table 4.3: Summary of devices fabricated on different substrates

Type of Back Reflector		**J_{sc}**	**% Enhancement over**	
		(mA/cm^2)	SS+Ag	Bare SS
References	Bare SS	14.2	--	
	SS + Ag	16.1	--	13
Random texturing	Annealed Ag/ZnO	20.4	27	43
	Etched ZnO	19.9	18	39
Periodic Texturing	Nano Hole/Ag/ZnO	20.4	27	43
	Nano pillar/Ag/ZnO	21.5	34	51

The data in Table 4.3 show that the lowest current is obtained for cells deposited on bare SS. Putting Ag on SS improves the current by 13%. Using either etched ZnO + silver gives a higher current. Using either annealed Ag or nano-holes imprinted substrates improves results and shows a 27% improvement over flat silver and finally, the nano-bump (photonic-plasmonic) structure gives the best results, an increase of 34% over flat silver.

The EQE show that cells on the Ag coated nano-hole, nano-bump, and randomly roughened substrates are considerably enhanced over the flat Ag/ZnO and SS substrates at long wavelengths (>580 nm) up to the band edge (1100 nm).The EQE oscillations for the periodic substrates are due to the diffraction of light from the periodic BR. The EQE for the photonic plasmonic back reflector exceeds that of the etched ZnO and annealed Ag BRs over a wide wavelength (λ=580-800 nm). It is very significant that the photo-current Jsc for the periodic

nano-bump substrate is the highest (21.5 mA/cm^2), exceeding that of the randomly roughened annealed Ag BR. the etched ZnO/Ag and a simple nano-photonics structure by comfortable margins-margins much greater than the experimental uncertainties.

Note that for maximum plasmonic enhancement the back n+ layer should be very thin so that the reradiated photons from the plasmonic effect are not absorbed directly into it. Our devices had relatively thick back n+ layers, ~0.25 μm. This was done to avoid shorts. Calculations show that the best effects are obtained when the back n+ layer thickness is <100nm.

We chose absorber layer thickness of ~0.9μm, typical for micro-morph cells, and our expectation is that these conclusions will be observed for other cell thicknesses. Although surface plasmons can cause losses in random back reflectors, it has been proposed that a substantial fraction of light coupled into localized plasmonic modes at the Ag/ZnO interface can be re-radiated as scattered light in optimized textured back reflectors[251], and dynamical effects need further understanding.

The external quantum efficiency (EQE) for the various solar cells as a ratio of to that of the flat silver substrate as a function of wavelength is shown in Figure 4.46. The highest EQE is for the periodic back reflector of nano-bumps over the entire spectral range. We further validated these conclusions by calculating the apparent optical absorption coefficient $\alpha(\lambda)$ for the solar cells (Figure 4.47) on the different substrates, factoring out slight variations in the thickness(t) of the absorber layers and the reflectance for various substrates which is shown in Figure 4.43. This yields highest optical absorption for the periodic back-reflector of nano-bumps. The corresponding current-voltage measurements show the highest current (20.5 mA/cm^2) for the nano-bump back reflector which is significantly higher than the next value of 20 mA/cm^2 for the annealed Ag/ZnO back reflector, with values at a reverse bias of -1V.

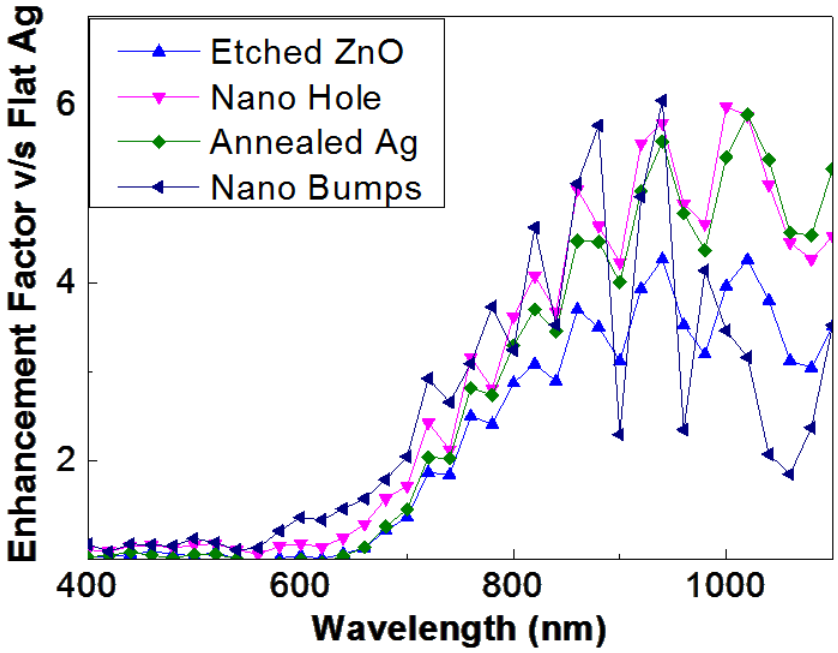

Figure 4.46: Enhancement factor of various substrates relative to flat silver substrate

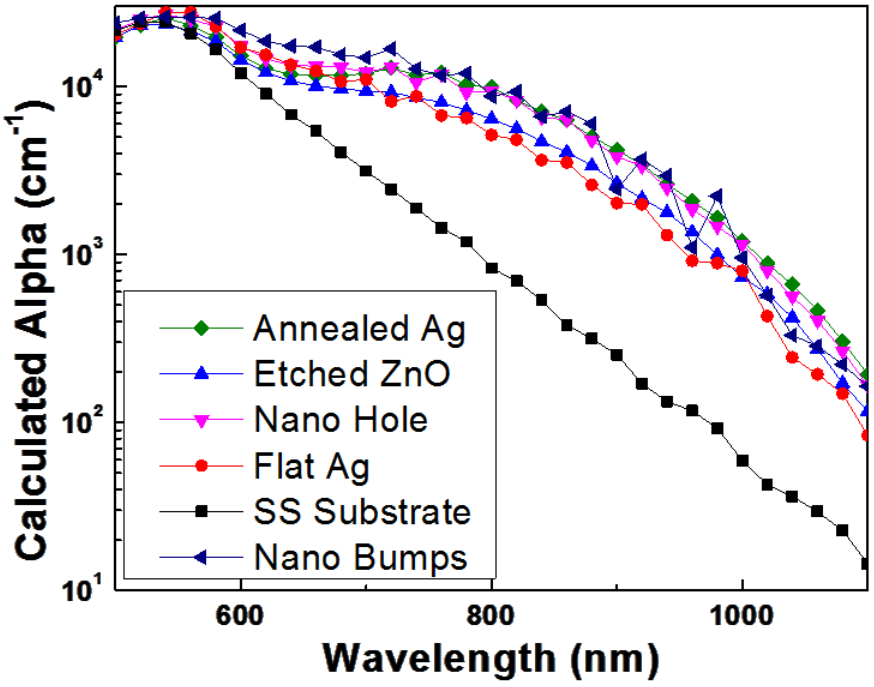

Figure 4.47: Calculated effective absorption coefficient of nc-Si:H cell of 0.9µm in different substrates

The highest external quantum efficiency and absorption coefficient was found for the periodically textured nano-bump back reflector. This photonic-plasmonic back reflector also exhibited the highest current density. This indicates that the periodic photonic-plasmonic back-reflectors have a device performance that may exceed the commonly used randomly textured back reflectors. The reasons underlying these results are the highly beneficial diffraction from the periodic texture, resulting in densely spaced waveguide modes, where light propagates parallel to the interface. Such modes cannot be realized with randomly textured back reflectors. Furthermore the propagating surface plasmons in the periodic photonic-plasmonic back reflectors are highly beneficial in enhancing absorption, with large light concentration near the back reflector.

4.4 Modified structures

Both randomly textured and periodic back-reflector arrays increase the photon path length by different mechanisms. It is an open question which mechanism is more effective, although we showed in section 4.3 that photonic-plasmonic back reflectors have slightly higher current than randomly textured substrates. An interesting direction is to combine the properties of randomly textured and periodically textured photonic-plasmonic back-reflectors into a single structure, thereby utilizing the advantages of both types of structures. The basic idea is illustrated schematically in Figure 4.48(a) where the device utilizes a 2-d photonic-plasmonic structure based on simulation. In Figure 4.48(b) we show a device on a modified photonic-plasmonic substrate where random smaller-scale structures have been incorporated into periodic structure. This is analogous to having small scale random scattering features superimposed on larger scale features [252].

Figure 4.48: Schematic diagram of device structures on (a) photo-plasmonic substrate (b) modified photo-plasmonic substrate

We developed modified photonic-plasmonic substrates based on the tendency of silver to agglomerate on heating in air, to form silver islands. We post-annealed silver after evaporating

~200 nm of Ag on the photo-plasmonic substrates at room temperature in a vacuum chamber at pressures <$2x10^{-6}$ Torr. The photonic-plasmonic substrates were annealed in air at various temperatures and the substrates were then observed under a scanning electron microscope. It was found that low temperatures and short times were enough to initiate the agglomeration as shown in Figure 4.49(a), in contrast to the higher temperature or longer times used in the random annealed silver back reflector. We observed that at temperatures close to 250 °C we lost the regular periodicity of the underlying photonic-plasmonic substrates as the Ag agglomeration was very rapid and could overwhelm the underlying structure as shown in Figure 4.49(b). A second proof of the effective change due to high temperature annealing is shown in Figure 4.50 where we see that after annealing at high temperature the diffused reflection has lost the effect from the periodic structure (the characteristic crest and troughs), while annealing at 150^{o}C still follows similar trend as that of the un-annealed structure. Therefore, a lower temperature of 150°C was chosen and anneal times were varied to obtain different degrees of roughness.

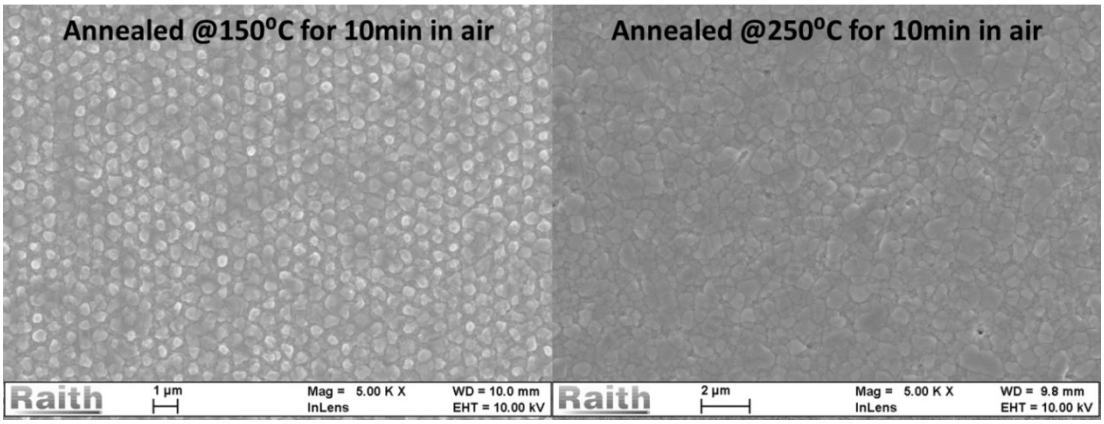

Figure 4.49: Effect of annealing at (a) 150^{o}C and (b) 250^{o}C for 10 minutes in air

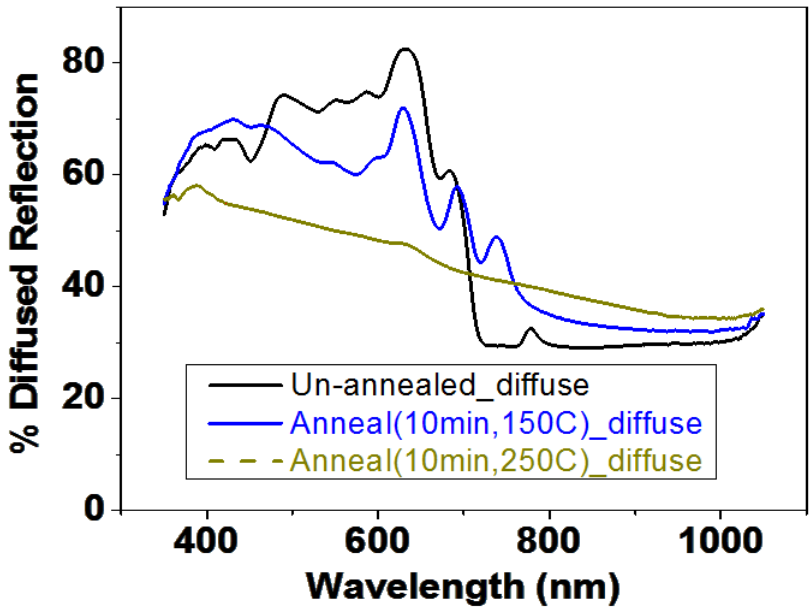

Figure 4.50: Diffused Reflection of nano-bump structure after annealing in air for 10min at different temperatures

Figure 4.51 shows the development of modified photonic-plasmonic substrates by the annealing process. Figure 4.51(a) shows the substrate at very short anneal time of 1 minute, in which most of the structure confirms with the pristine sample. At higher magnification we observe small grains of silver with sizes of ~20-70 nm spread uniformly in the sample. As we go to longer annealing times we see that the silver grains start growing and the conical structure on the photo-plasmonic substrate loses some of its features due to agglomeration of silver. At the region between the cones there is development of more complex disordered structures due to Ag agglomeration. As the annealing time increases from 1 to 15 minutes, the cones acquire more random shapes and the silver agglomeration increases as is evident from Figure 4.51(b) to Figure 4.51(d). A similar change can be observed from the AFM images also shown in Figure 4.52 moving from left to right the silver grains start to look like they are forming on top by 5min anneal and then in 15min anneal time we see the development of lot of small grains of silver.

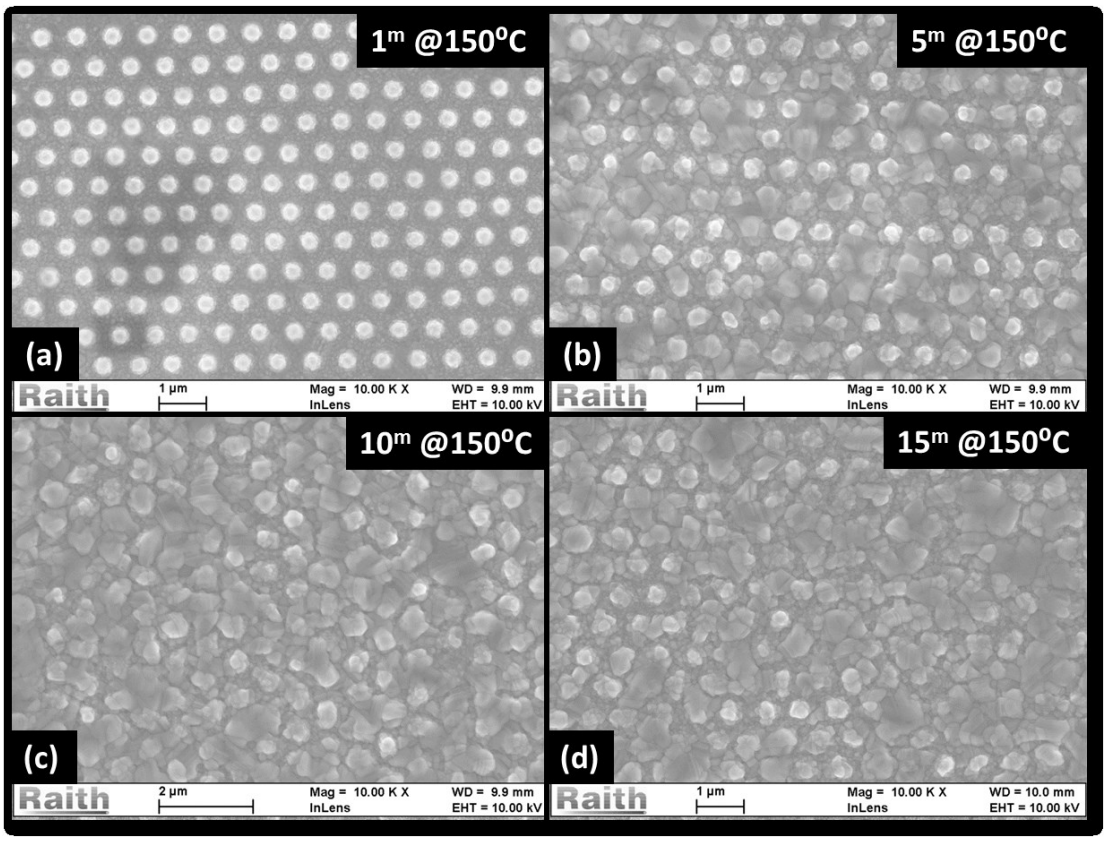

Figure 4.51: SEM images of modified photonic-plasmonic structures by annealing silver in air at 150°C for (a)1 minute (b) 5 minutes (c)10 minutes (d) 15minutes

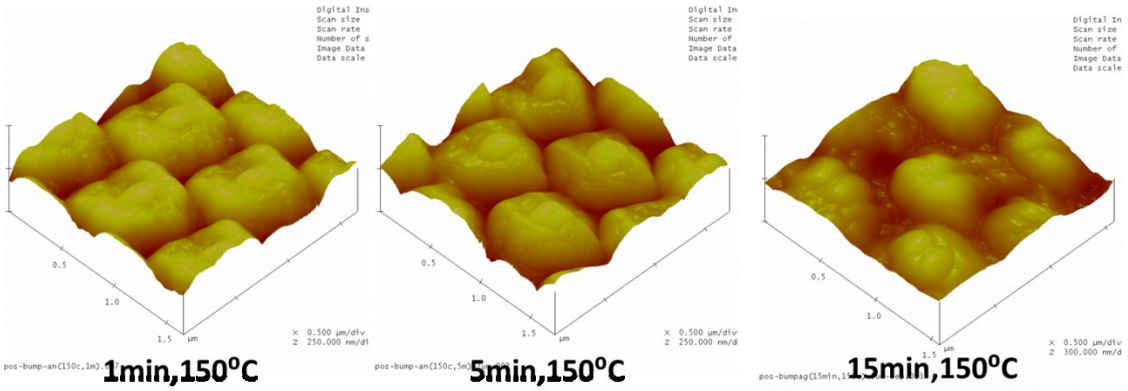

Figure 4.52: AFM images of modified photonic-plasmonic structures

Even though random nano-structures start nucleating, the structural periodicity is still maintained, as seen in the AFM topography image (Figure 4.52) of the modified photo-

plasmonic substrate even after 15 minutes anneal at 150°C. To further characterize these structures we measured the reflectance from three substrates- namely the reference un-annealed (pristine) array, 1 minute annealed array and 10 minute annealed array at 150°C (Figure 4.53). Since the final devices have a ZnO layer the reflection measurements (Figure 4.53) were done after depositing the ZnO layer. The total reflectance for the 10 min anneal substrate is slightly broadened, lower in magnitude, and is shifted to longer wavelengths, in comparison to the reference un-annealed substrate. A similar trend is observed for the 1minute annealed substrate but the effect it is much less pronounced, with the reflectance following the pristine sample more closely. The diffuse reflectance has changed considerably for the 10 minute anneal. The diffuse reflectance decreases at short wavelengths (<600 nm), but increases at long wavelengths between 800-1000 nm. We attribute this to the formation of small Ag particles which tend to scatter light at longer wavelengths. However these small Ag particles also absorb strongly at shorter wavelengths, and likely decrease the diffuse reflectance.

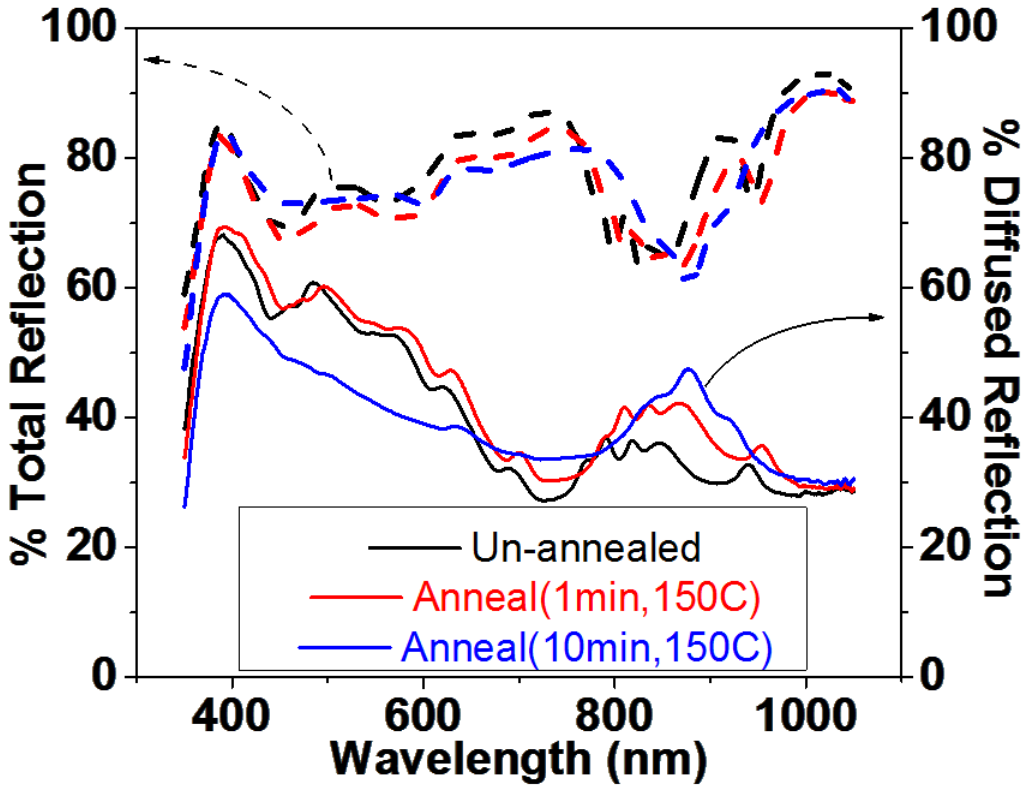

Figure 4.53: Total reflection of modified photonic-plasmonic structure

Identical nc-Si:H devices with 0.9 µm thickness were fabricated on the reference substrates and the two modified photonic-plasmonic substrates after 1 and 10 minute annealing. The external quantum efficiency (EQE) was measured for these three samples (Figure 4.54), at -1V to ensure complete collection. Also shown for comparison is a solar cell grown on a flat Ag ZnO substrate. There is a large improvement (~28%) of the EQE derived J_{sc} between the flat and the periodically textured substrate. The EQE derived J_{sc} is 16 mA/cm^2 for the flat device, compared with 20.5 ±0.5 mA/cm^2 for the un-annealed device, indicating a 28% enhancement. The EQE J_{sc} is 20.4 ±0.5 mA/cm^2 and 20.0 ±0.5 mA/cm^2 for the 1 minute and 10 minute annealed devices, indicating no significant improvement in the current after adding the additional random texture

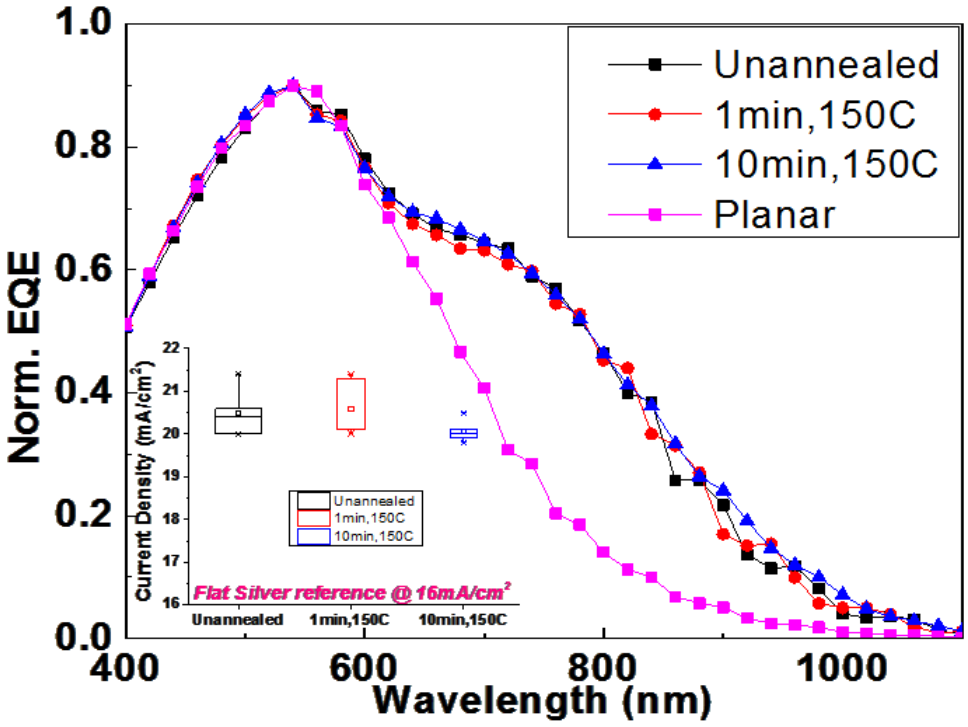

Figure 4.54: EQE on 0.9µm thick nc-Si device fabricated on different types of photo-plasmonic substrates

The EQE of all three photonic-plasmonic devices are very similar. Only small changes are observed between the annealed and un-annealed devices. For an even closer comparison we measured the EQE enhancement ratio from the photonic-plasmonic substrate (Figure 4.55). There is little difference between 1 minute anneal and the pristine sample, as expected from the very similar measured total reflectance. For the 10 minute anneal substrate there is a slight increase in absorbance at longer wavelengths, but this change is similar to the standard

deviation or variation from sample to sample. Furthermore, the devices had a V_{oc} ~0.45V and fill factor FF ~0.55 that did not vary significantly with annealing. Hence there is no statistically significant increase in the EQE or cell performance on incorporating random features with the photonic plasmonic substrates.

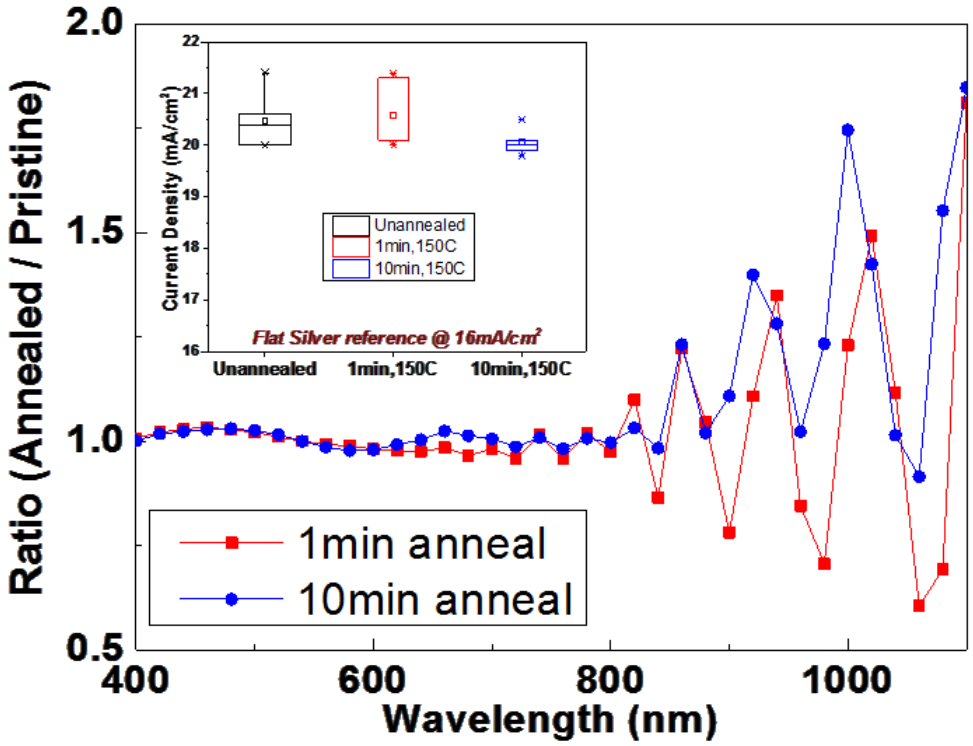

Figure 4.55: Enhancement in the absorption in modified photo-plasmonic substrates to pristine

4.5 Additional methods

Germanium has a better absorption coefficient than silicon, and if we can incorporate Ge in our cells we can increase the effective absorption in the cell. A superlattice (SL) cell consists of alternate layer of a-Si:H and nc-Si:H and a method to increase absorption is to incorporate germanium in the amorphous layer of the superlattice is studied by Nayan et. al. [61]. The purpose of the thin a-(Si,Ge) layer is to increase absorption in the solar cell, since a-(Si,Ge) has a higher absorption coefficient than nano Si at wavelength of ~600-700 nm. The amorphous layer is deposited using the same discharge as for the nano crystalline phase, but at a much lower power level. In case of the amorphous layer a mixture of silane germane and hydrogen is used whereas germane is turned off during the nano crystalline growth phase. Multiple cycles of

growth are used to build up the total thickness of the cell. The bandgap of the amorphous layer is controlled by changing the silane/germane ratio during growth. A schematic of the device structure with a superlattice is shown in Figure 4.56(a).

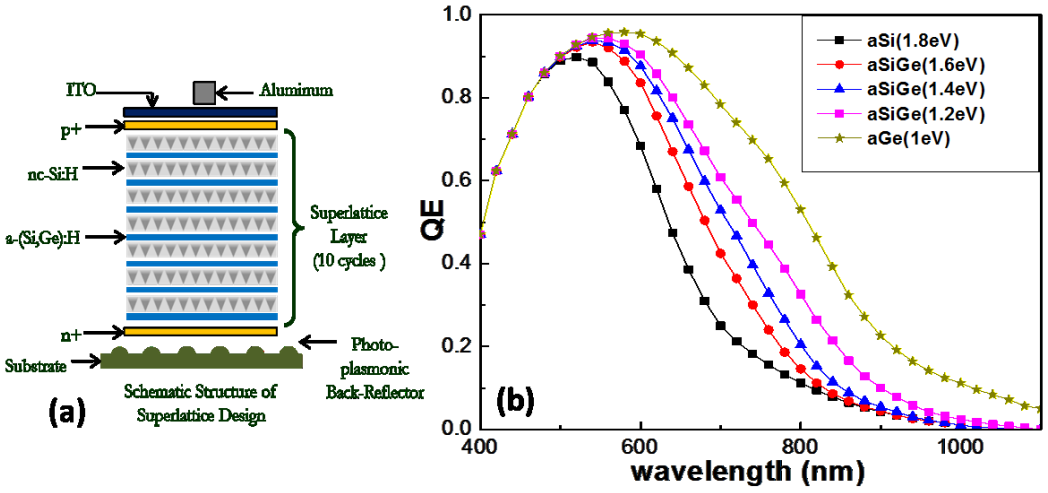

Figure 4.56: (a)Schematic diagram of a superlattice device with a-Si,Ge/nc-Si on a photo-plasmonic substrate and (b) simulation result for 10 layers of nc-Si:H and a-(Si,Ge):H SL [61]

Furthermore, we also show the use of Ge in the super lattice structure to improve the current density. The addition of Ge in the amorphous layer of the super lattice helps to enhance the absorption especially for λ>600nm as shown by simulation for 10 alternating layers of a-(Si,Ge):H and nc-Si:H is plotted in Figure 4.56(b). To exemplify the statement we made device with different flows of Ge in the superlattice by varying the flow of GeH_4. The EQE curves are plotted in Figure 4.57(a), showing the increase in EQE with increase in the ratio of $GeH_4/(SiH_4+GeH_4)$ flows. The absorption coefficient also improves when we make the a-(Si,Ge):H layer thicker in each of the cycle, which leads to increase in the EQE at longer wavelengths (600-800nm) shown in Figure 4.57(b).

In Figure 4.58, we show the un-optimized EQE of SL devices fabricated on nano-bump substrate and a similar device on SS, in which we can clearly see the strong absorption in longer wavelengths. The fabrication of superlattice devices with a-(Si,Ge):H fabrication is not simple, as including a thin a-(Si,Ge) layer in the superlattice does improve the absorption there is bandgap mismatch between the layers which leads to poor quality devices due to lack of collection of carriers with the in-built field. To tackle this issue we dope the a-(Si,Ge) layers with ppm amount of Phosphine gas during deposition which improves the devices quality/carrier collection. Also,

the nc-Si layer is doped small amount of TMB to avoid cross contamination from residual phosphine

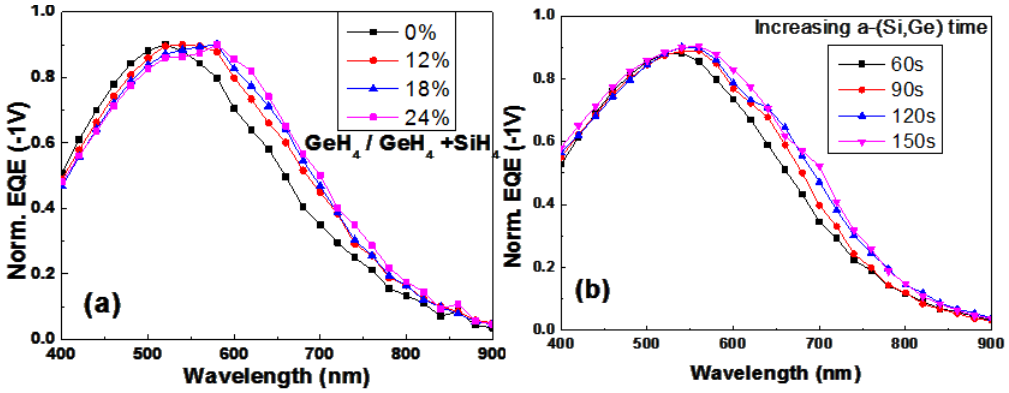

Figure 4.57: Absorption enhancement in SL device with (a) increasing Ge content in a-(Si,Ge) layer (b) increasing thickness of a-(Si,Ge) layer in the SL [61]

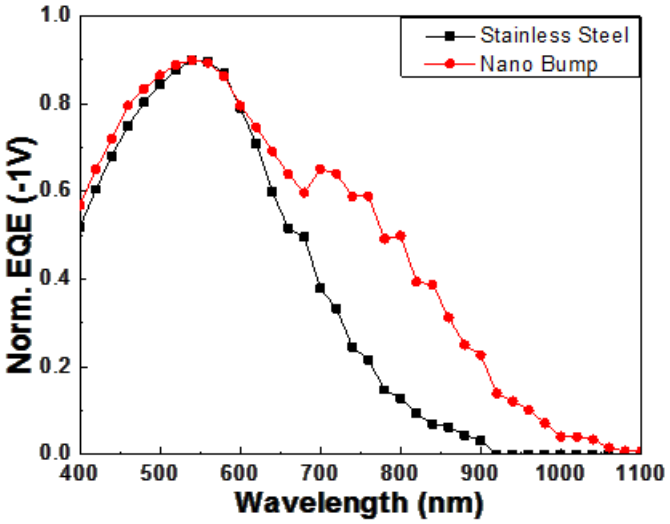

Figure 4.58: EQE plot for SL device with a-(Si,Ge):H fabricated on nano-bump structures

Summary

This chapter summarizes the work done with important results and provides directions for future work

5.1 Conclusions

The main objective of the thesis was to look at the feasibility of periodic texturing to enhance the absorption in thin film silicon solar cells while making it industrially feasible to apply in a cost effective manner. The work done to achieve these goals is summarized as follows.

- We show the methodology for producing randomly roughened structure namely etched ZnO:Al and annealed silver, and the procedures to optimize them for thin film silicon solar devices. Both a-Si:H and nc-Si:H devices were fabricated on the randomly textured substrates and we showed 25-30% improvement of the current density relative to planar cells.
- Design of a new photonic structure is shown which predicted higher absorption in the solar cells by coupling photons into wave guiding modes such that they stay in absorber layer. We showed experimentally that these structures can be fabricated by inexpensive nano-imprinting technology which can be ramped up to roll to roll processing for commercial purposes having high throughput in manufacturing solar cells.
- The use of plastic substrates is feasible for production of thin film silicon solar cells which would reduce the cost and help in developing flexible PV modules that are well suited for building-integrated applications and for portable, foldable, PV power products.
- The plastic substrates with photonic structure show a current enhancement of over 30% over planar plastic substrates. We have also discussed various challenges that we faced during their fabrication and discussed our methodology for solving the problems.
- We also show the fabrication of a-Si:H and nc-Si:H cells on different plastic substrates namely PEN which has maximum working temperature of 200^{o}C and kapton substrates which could handle up to 275^{o}C. The introduction of a polymer

coated SS substrate has also been discussed which is flexible and can handle higher temperatures of 300^{o}C.

- The use of plasmonics has been also incorporated along with the photonic characteristics of the structure to form a photonic–plasmonic structure. By using periodic structures we have the photonic effect and by using favorable geometry i.e. nano cones we can couple the surface plasmons polaritons to wave guiding modes to get increased absorption. The differences in randomly textured method and the new method of increasing absorption with periodic structures have been also discussed. These structures perform better than a structure with only a photonic structure.
- Micromorph tandem cells have been shown with thin nc-Si:H layers (<1µm) to give an efficiency just below 10% (9.9%).
- A comparison of all the above structures have been studied experimentally showing that the best cell is found to be on the photonic-plasmonic structure. The experiment is done by fabricating all the devices at similar conditions.
- A modified structure is also studied where intentional controlled randomness is built-up in a controlled manner on the photonic-plasmonic structures. The device performance is not statistically different from the photonic-plasmonic structures although trend is towards decreasing the absorption in cells.
- A method of using Ge in the amorphous cycle of amorphous silicon growth has been suggested which can lead to increased absorption in the Ge devices.

5.2 Future Directions

- Cross-sectional imaging of the structures would give us an idea of the structure conformity after the device has been fabricated.
- Transmission electron microscopy images can be done to look at the formation of the superlattice structure. In the designed structures one direction is to look at the regions with sharp edges in textured substrates, especially for initiation of cracks or defects.
- Doping germanium in the devices leads to very good current enhancement, but can be done to optimize the cell to make thin cells for tandem solar cells. The cell

optimization is required to get high efficiency especially in terms of carrier collection and increasing open circuit voltage.

- Ultra-thin silicon solar cells has been studied by various groups especially for a-Si:H cells to reduce light induced degradation. The same concepts can also be applied to the periodic structures.
- Employing silicon oxide SiO_x layers as the doped layer can help the light management for the cells as it has a higher bandgap than silicon and can be employed also as intermediate reflector which can decrease the thickness of top a-Si:H layer. In addition SiO_x can also be the junction layer in tandem cells leading to reduced loss in photons. It can act as the dielectric layer between metal and the semiconductor hence replace ZnO:Al from our present structure, allowing all fabrication steps in a single chamber. The use of SiO_x has spurred much worldwide work and has led to high efficiency a-Si:H and nc-Si:H cells.

Bibliography

[1] W. Shockley, and H. J. Queisser, “Detailed balance limit of efficiency of p-n junction solar cells,” *Journal of Applied Physics,* vol. 32, no. 3, 1961, 1961.

[2] R. C. Chittick, Alexande.Jh, and H. F. Sterling, “Preparation and properties of amorphous silicon,” *Journal of the Electrochemical Society,* vol. 116, no. 1, 1969, 1969.

[3] A. Shah *et al.*, “Intrinsic microcrystalline silicon (mu c-Si : H) deposited by VHF-GD (very high frequency-glow discharge): a new material for photovoltaics and optoelectronics,” *Materials Science and Engineering B-Solid State Materials for Advanced Technology,* vol. 69, Jan 19, 2000.

[4] A. Shah *et al.*, “Towards very low-cost mass production of thin-film silicon photovoltaic (PV) solar modules on glass,” *Thin Solid Films,* vol. 502, no. 1-2, Apr 28, 2006.

[5] S. Liu *et al.*, "Approaching single-junction theoretical limit using ultra-thin GaAs solar cells with optimal optical designs." pp. 002082-002087.

[6] X. Wang *et al.*, "Approaching the Shockley-Queisser limit in GaAs solar cells." pp. 002117-002121.

[7] M. A. Green *et al.*, “Solar cell efficiency tables (version 40),” *Progress in Photovoltaics,* vol. 20, no. 5, Aug, 2012.

[8] C. J. Brabec, N. S. Sariciftci, and J. C. Hummelen, “Plastic solar cells,” *Advanced Functional Materials,* vol. 11, no. 1, Feb, 2001.

[9] M. Gratzel, “Dye-sensitized solar cells,” *Journal of Photochemistry and Photobiology C-Photochemistry Reviews,* vol. 4, no. 2, Oct 31, 2003.

[10] M. Gratzel, “Photoelectrochemical cells,” *Nature,* vol. 414, no. 6861, Nov 15, 2001.

[11] A. Ennaoui *et al.*, “Iron disulfide for solar-energy conversion,” *Solar Energy Materials and Solar Cells,* vol. 29, no. 4, May, 1993.

[12] C. Wadia, A. P. Alivisatos, and D. M. Kammen, “Materials Availability Expands the Opportunity for Large-Scale Photovoltaics Deployment,” *Environmental Science & Technology,* vol. 43, no. 6, Mar 15, 2009.

[13] Y. Wu *et al.*, “Synthesis and photovoltaic application of copper(I) sulfide nanocrystals,” *Nano Letters,* vol. 8, no. 8, Aug, 2008.

[14] W. E. Spear, and P. G. Lecomber, “Substitutional doping of amorphous silicon,” *Solid State Communications,* vol. 17, no. 9, 1975, 1975.

[15] http://www.energyresearch.nl/2/energy-options/solar-cells/background/types/thin-layers/.

[16] **M. Mikolasek**. "Current status and progress in the new generation’s silicon based solar cells," http://www.posterus.sk/?p=1247#respond.

[17] O. Vetterl *et al.*, “Intrinsic microcrystalline silicon: A new material for photovoltaics,” *Solar Energy Materials and Solar Cells,* vol. 62, no. 1-2, Apr 15, 2000.

[18] R. A. Street, “Doping and the Fermi energy in amorphous-silicon,” *Physical Review Letters,* vol. 49, no. 16, 1982, 1982.

[19] R. Biron *et al.*, “Window layer with p doped silicon oxide for high V-oc thin-film silicon n-i-p solar cells,” *Journal of Applied Physics,* vol. 110, no. 12, Dec 15, 2011.

[20] B. Yan *et al.*, “Innovative dual function nc-SiOx:H layer leading to a > 16% efficient multi-junction thin-film silicon solar cell,” *Applied Physics Letters,* vol. 99, no. 11, Sep 12, 2011.

[21] T. Soederstroem *et al.*, “Asymmetric intermediate reflector for tandem micromorph thin film silicon solar cells,” *Applied Physics Letters,* vol. 94, no. 6, Feb 9, 2009.

[22] A. Lambertz, T. Grundler, and F. Finger, “Hydrogenated amorphous silicon oxide containing a microcrystalline silicon phase and usage as an intermediate reflector in thin-film silicon solar cells,” *Journal of Applied Physics,* vol. 109, no. 11, Jun 1, 2011.

[23] S. Fahr, C. Rockstuhl, and F. Lederer, "Intermediate reflectors in thin film solar cells comprising randomly textured surfaces," *Photonics for Solar Energy Systems Iii*, Proceedings of SPIE-The International Society for Optical Engineering R. B. Wehrspohn and A. Gombert, eds., 2010.

[24] D. L. Staebler, and C. R. Wronski, “Reversible conductivity changes in discharge-produced amorphous Si,” *Applied Physics Letters,* vol. 31, no. 4, 1977, 1977.

[25] A. H. M. Smets, W. M. M. Kessels, and M. C. M. van de Sanden, “Vacancies and voids in hydrogenated amorphous silicon,” *Applied Physics Letters,* vol. 82, no. 10, Mar, 2003.

[26] H. Fritzsche, “Development in understanding and controlling the Staebler-Wronski effect in a-Si : H,” *Annual Review of Materials Research,* vol. 31, 2001, 2001.

[27] A. H. Mahan *et al.*, “Structural changes in a-Si : H film crystallinity with high H dilution,” *Physical Review B,* vol. 61, no. 3, Jan 15, 2000.

[28] P. A. Fedders, Y. Fu, and D. A. Drabold, “Atomistic origins of light-induced defects in a-Si,” *Physical Review Letters,* vol. 68, no. 12, Mar 23, 1992.

[29] R. Biswas, B. C. Pan, and Y. Y. Ye, “Metastability of amorphous silicon from silicon network rebonding,” *Physical Review Letters,* vol. 88, no. 20, May 20, 2002.

[30] R. Biswas, and B. C. Pan, “Microscopic nature of Staebler-Wronski defect formation in amorphous silicon,” *Applied Physics Letters,* vol. 72, no. 3, Jan 19, 1998.

[31] N. Wang, and V. L. Dalal, “Improving stability of amorphous silicon using chemical annealing with helium,” *Journal of Non-Crystalline Solids,* vol. 352, no. 9-20, Jun 15, 2006.

[32] I. Shimizu, “Formation of stable Si network at low T-s by controlling chemical reaction at growing surface,” *Solar Energy Materials and Solar Cells,* vol. 66, no. 1-4, Feb, 2001.

[33] A. Shyam, “Fabrication of high quality, low bandgap amorphous Silicon & amorphous Silicon Germanium alloy solar cell by Chemical Annealing,” Electrical and Computer Engineering, Iowa State University, 2011.

[34] C. Haegglund, and S. P. Apell, “Plasmonic Near-Field Absorbers for Ultrathin Solar Cells,” *Journal of Physical Chemistry Letters,* vol. 3, no. 10, May 17, 2012.

[35] N. N. Lal *et al.*, “Using spacer layers to control metal and semiconductor absorption in ultrathin solar cells with plasmonic substrates,” *Physical Review B,* vol. 85, no. 24, Jun 25, 2012.

[36] J. Trevino *et al.*, “Plasmonic-photonic arrays with aperiodic spiral order for ultra-thin film solar cells,” *Optics Express,* vol. 20, no. 10, May 7, 2012.

[37] Y. Kuang *et al.*, “Nanorod solar cell with an ultrathin a-Si:H absorber layer,” *Applied Physics Letters,* vol. 98, no. 11, Mar 14, 2011.

[38] V. E. Ferry *et al.*, “Light trapping in ultrathin plasmonic solar cells,” *Optics Express,* vol. 18, no. 13, Jun 21, 2010.

[39] S. Komuro *et al.*, “The dynamics of photoexcited carriers in microcrystalline silicon,” *Journal of Applied Physics,* vol. 56, no. 6, 1984, 1984.

[40] S. Veprek *et al.*, “Parameters controlling the deposition of amorphous and microcrystalline silicon in si-h discharge plasmas,” *Journal De Physique,* vol. 42, no. NC4, 1981, 1981.

[41] Z. Iqbal, F. A. Sarott, and S. Veprek, “Optical-absorption in hydrogenated microcrystalline silicon,” *Journal of Physics C-Solid State Physics,* vol. 16, no. 10, 1983, 1983.

[42] W. E. Spear, G. Willeke, and P. G. Lecomber, “Electronic-properties of microcrystalline silicon prepared in the glow-discharge plasma,” *Physica B & C,* vol. 117, no. MAR, 1983, 1983.

[43] J. Meier *et al.*, “Complete microcrystalline p-i-n solar-cell - crystalline or amorphous cell behavior,” *Applied Physics Letters,* vol. 65, no. 7, Aug 15, 1994.

[44] P. Torres *et al.*, “Device grade microcrystalline silicon owing to reduced oxygen contamination,” *Applied Physics Letters,* vol. 69, no. 10, Sep 2, 1996.

[45] J. Meier *et al.*, "On the way towards high efficiency thin film silicon solar cells by the ''micromorph'' concept."

[46] R. W. Collins *et al.*, “Evolution of microstructure and phase in amorphous, protocrystalline, and micro crystalline silicon studied by real time spectroscopic ellipsometry,” *Solar Energy Materials and Solar Cells,* vol. 78, no. 1-4, Jul, 2003.

[47] J. Bailat *et al.*, “Microstructure and open-circuit voltage of n-i-p microcrystalline silicon solar cells,” *Journal of Applied Physics,* vol. 93, no. 9, May 1, 2003.

[48] E. Vallat-Sauvain *et al.*, “Influence of the substrate's surface morphology and chemical nature on the nucleation and growth of microcrystalline silicon,” *Thin Solid Films,* vol. 485, no. 1-2, Aug 1, 2005.

[49] J. Kocka *et al.*, “Basic features of transport in microcrystalline silicon,” *Solar Energy Materials and Solar Cells,* vol. 78, no. 1-4, Jul, 2003.

[50] A. Matsuda, “Formation kinetics and control of microcrystallite in mu-c-Si-H from glow-discharge plasma,” *Journal of Non-Crystalline Solids,* vol. 59-6, no. DEC, 1983, 1983.

[51] V. L. Dalal, “Fundamental considerations regarding the growth of amorphous and microcrystalline silicon and alloy films,” *Thin Solid Films,* vol. 395, no. 1-2, Sep 3, 2001.

[52] C. C. Tsai *et al.*, “Film formation mechanisms in the plasma deposition of hydrogenated amorphous-silicon,” *Journal of Applied Physics,* vol. 59, no. 8, Apr 15, 1986.

[53] K. Ohkawa *et al.*, “Stability of a-Si : H solar cells deposited by Ar-treatment or by ECR techniques,” *Solar Energy Materials and Solar Cells,* vol. 66, no. 1-4, Feb, 2001.

[54] S. Lebib, and P. R. I. Cabarrocas, “Effects of ion energy on the crystal size and hydrogen bonding in plasma-deposited nanocrystalline silicon thin films,” *Journal of Applied Physics,* vol. 97, no. 10, May 15, 2005.

[55] P. R. I. Cabarrocas, “Plasma enhanced chemical vapor deposition of silicon thin films for large area electronics,” *Current Opinion in Solid State & Materials Science,* vol. 6, no. 5, Oct, 2002.

[56] J. R. Abelson, “Plasma deposition of hydrogenated amorphous-silicon - studies of the growth surface,” *Applied Physics a-Materials Science & Processing,* vol. 56, no. 6, Jun, 1993.

[57] B. C. Pan, and R. Biswas, “Structure and simulation of hydrogenated nanocrystalline silicon,” *Journal of Applied Physics,* vol. 96, no. 11, Dec 1, 2004.

[58] B. J. Yan *et al.*, "Microstructure evolution with thickness and hydrogen dilution profile in microcrystalline silicon solar cells," *Amorphous and Nanocrystalline Silicon Science and Technology- 2004*, Materials Research Society Symposium Proceedings G. Ganguly *et al.*, eds., 2004.

[59] H. Li *et al.*, “Controlling the quality of nanocrystalline silicon made by hot-wire chemical vapor deposition by using a reverse H-2 profiling technique,” *Journal of Non-Crystalline Solids,* vol. 354, no. 19-25, May 1, 2008.

[60] J. Gu *et al.*, “High quality microcrystalline Si films by hydrogen dilution profile,” *Thin Solid Films,* vol. 515, no. 2, Oct 25, 2006.

[61] N. Chakravarty, "(aSiGe/ncSi) Superlattice thin film silicon solar cell," Electrical and Computer Engineering, Iowa State University, 2011.

[62] J. Yang, and S. Guha, "Status and future perspective of a-Si:H, a-SiGe:H, and nc-Si:H thin film photovoltaic technology," pp. 74090C-74090C, 2009.

[63] X. Han *et al.*, "Improvement of hydrogenated microcrystalline silicon solar cell performance by VHF power profiling technique," *Solar Energy Materials and Solar Cells,* vol. 94, no. 2, Feb, 2010.

[64] A. Madhavan, "Alternative designs for nanocrystalline silicon solar cells," Electrical and Computer Engineering, Iowa State University, 2009.

[65] A. S. Brown, and M. A. Green, "Limiting efficiency for current-constrained two-terminal tandem cell stacks," *Progress in Photovoltaics,* vol. 10, no. 5, Aug, 2002.

[66] F. Meillaud *et al.*, "Efficiency limits for single junction and tandem solar cells," *Solar Energy Materials and Solar Cells,* vol. 90, no. 18-19, Nov 23, 2006.

[67] M. A. Green, and M. J. Keevers, "Optical-properties of intrinsic silicon at 300 k," *Progress in Photovoltaics,* vol. 3, no. 3, May-Jun, 1995.

[68] A. Goetzberger , J. Knobloch, and B. Voss, *Crystalline Silicon Solar Cells*: John Wiley & sons, 1998.

[69] A. R. Burgers, "How to design optimal metallization patterns for solar cells," *Progress in Photovoltaics,* vol. 7, no. 6, Nov-Dec, 1999.

[70] E. Yablonovitch, and G. D. Cody, "Intensity enhancement in textured optical sheets for solar-cells," *Ieee Transactions on Electron Devices,* vol. 29, no. 2, 1982, 1982.

[71] T. Tiedje *et al.*, "Limiting efficiency of silicon solar-cells," *Ieee Transactions on Electron Devices,* vol. 31, no. 5, 1984, 1984.

[72] H. W. Deckman *et al.*, "Optically enhanced amorphous-silicon solar-cells," *Applied Physics Letters,* vol. 42, no. 11, 1983, 1983.

[73] E. A. Schiff, "Thermodynamic limit to photonic-plasmonic light-trapping in thin films on metals," *Journal of Applied Physics,* vol. 110, no. 10, Nov 15, 2011.

[74] H. R. Stuart, and D. G. Hall, "Thermodynamic limit to light trapping in thin planar structures," *Journal of the Optical Society of America a-Optics Image Science and Vision,* vol. 14, no. 11, Nov, 1997.

[75] R. Biswas, and C. Xu, "Nano-crystalline silicon solar cell architecture with absorption at the classical 4n(2) limit," *Optics Express,* vol. 19, no. 14, Jul 4, 2011.

[76] C. Battaglia *et al.*, "Light Trapping in Solar Cells: Can Periodic Beat Random?," *Acs Nano,* vol. 6, no. 3, Mar, 2012.

[77] X. Sheng *et al.*, "Light trapping limits in plasmonic solar cells: an analytical investigation," *Optics Express,* vol. 20, no. 14, Jul 2, 2012.

[78] H. Zhao *et al.*, "Light Trapping in Thin Film Silicon Solar Cells: An Assessment," *Thin Film Solar Technology Iii*, Proceedings of SPIE L. A. Eldada, ed., 2011.

[79] E. D. Kosten, E. L. Warren, and H. A. Atwater, "Ray optical light trapping in silicon microwires: exceeding the 2n(2) intensity limit," *Optics Express,* vol. 19, no. 4, Feb 14, 2011.

[80] E. Garnett, and P. Yang, "Light Trapping in Silicon Nanowire Solar Cells," *Nano Letters,* vol. 10, no. 3, Mar, 2010.

[81] D. M. Callahan, J. N. Munday, and H. A. Atwater, "Solar Cell Light Trapping beyond the Ray Optic Limit," *Nano Letters,* vol. 12, no. 1, Jan, 2012.

[82] J. N. Munday, D. M. Callahan, and H. A. Atwater, "Light trapping beyond the 4n(2) limit in thin waveguides," *Applied Physics Letters,* vol. 100, no. 12, Mar 19, 2012.

[83] J. Bhattacharya *et al.*, “A photonic-plasmonic structure for enhancing light absorption in thin film solar cells,” *Applied Physics Letters,* vol. 99, no. 13, Sep 26, 2011.

[84] K. R. Catchpole, and A. Polman, “Design principles for particle plasmon enhanced solar cells,” *Applied Physics Letters,* vol. 93, no. 19, Nov 10, 2008.

[85] H. A. Atwater, and A. Polman, “Plasmonics for improved photovoltaic devices,” *Nature Materials,* vol. 9, no. 3, Mar, 2010.

[86] F. J. Haug *et al.*, “Resonances and absorption enhancement in thin film silicon solar cells with periodic interface texture,” *Journal of Applied Physics,* vol. 109, no. 8, Apr 15, 2011.

[87] Z. Yu, A. Raman, and S. Fan, “Fundamental limit of light trapping in grating structures,” *Optics Express,* vol. 18, no. 19, Sep 13, 2010.

[88] Z. Yu, A. Raman, and S. Fan, “Fundamental limit of nanophotonic light trapping in solar cells,” *Proceedings of the National Academy of Sciences of the United States of America,* vol. 107, no. 41, Oct 12, 2010.

[89] G. Yue *et al.*, “Optimization of back reflector for high efficiency hydrogenated nanocrystalline silicon solar cells,” *Applied Physics Letters,* vol. 95, no. 26, Dec 28, 2009.

[90] J. Bhattacharya *et al.*, “Comparison of optical properties of periodic photonic–plasmonic and randomly textured back reflectors for nc-Si solar cells,” *Journal of Non-Crystalline Solids,* vol. 358, no. 17, pp. 2313-2318, 9/1/, 2012.

[91] J.-S. Cho *et al.*, “Effect of nanotextured back reflectors on light trapping in flexible silicon thin-film solar cells,” *Solar Energy Materials and Solar Cells,* vol. 102, Jul, 2012.

[92] J.-S. Cho, S. Baek, and J. C. Lee, “Surface texturing of sputtered ZnO:Al/Ag back reflectors for flexible silicon thin-film solar cells,” *Solar Energy Materials and Solar Cells,* vol. 95, no. 7, Jul, 2011.

[93] A. Banerjee, and S. Guha, “Study of back reflectors for amorphous-silicon alloy solar-cell application,” *Journal of Applied Physics,* vol. 69, no. 2, Jan 15, 1991.

[94] M. Python *et al.*, “Microcrystalline silicon solar cells: effect of substrate temperature on cracks and their role in post-oxidation,” *Progress in Photovoltaics,* vol. 18, no. 7, Nov, 2010.

[95] M. Python *et al.*, “Relation between substrate surface morphology and microcrystalline silicon solar cell performance,” *Journal of Non-Crystalline Solids,* vol. 354, no. 19-25, May 1, 2008.

[96] J. Yang *et al.*, "Light trapping in hydrogenated amorphous and nano-crystalline silicon thin film solar cells."

[97] B. Yan *et al.*, “Correlation of texture of Ag/ZnO back reflector and photocurrent in hydrogenated nanocrystalline silicon solar cells,” *Solar Energy Materials and Solar Cells,* vol. 104, Sep, 2012.

[98] M. Boccard *et al.*, “Multiscale Transparent Electrode Architecture for Efficient Light Management and Carrier Collection in Solar Cells,” *Nano Letters,* vol. 12, no. 3, Mar, 2012.

[99] M. Berginski *et al.*, “The effect of front ZnO : Al surface texture and optical transparency on efficient light trapping in silicon thin-film solar cells,” *Journal of Applied Physics,* vol. 101, no. 7, Apr 1, 2007.

[100] S. Fay *et al.*, “Rough ZnO layers by LP-CVD process and their effect in improving performances of amorphous and microcrystalline silicon solar cells,” *Solar Energy Materials and Solar Cells,* vol. 90, no. 18-19, Nov 23, 2006.

[101] P. Nunes *et al.*, “Effect of different dopant elements on the properties of ZnO thin films,” *Vacuum,* vol. 64, no. 3-4, Jan, 2002.

[102] H. Zhu *et al.*, “Study of thermal stability of ZnO:B films grown by LPCVD technique,” *Applied Surface Science,* vol. 258, no. 16, Jun 1, 2012.

[103] M. Berginski *et al.*, “Recent development on surface-textured ZnO : Al films prepared by sputtering for thin-film solar cell application,” *Thin Solid Films,* vol. 516, no. 17, Jul 1, 2008.

[104] A. M. K. Dagamseh *et al.*, “ZnO : Al films prepared by rf magnetron sputtering applied as back reflectors in thin-film silicon solar cells,” *Thin Solid Films,* vol. 516, no. 21, Sep 1, 2008.

[105] C. Agashe *et al.*, “Efforts to improve carrier mobility in radio frequency sputtered aluminum doped zinc oxide films,” *Journal of Applied Physics,* vol. 95, no. 4, Feb 15, 2004.

[106] S. Fernandez *et al.*, “Development of two-step etching approach for aluminium doped zinc oxide using a combination of standard HCl and NH4Cl etch steps,” *Thin Solid Films,* vol. 520, no. 14, May 1, 2012.

[107] Y. Wang *et al.*, “Effective light trapping in thin film silicon solar cells from textured Al doped ZnO substrates with broad surface feature distributions,” *Applied Physics Letters,* vol. 100, no. 26, Jun 25, 2012.

[108] B. Rech *et al.*, “New materials and deposition techniques for highly efficient silicon thin film solar cells,” *Solar Energy Materials and Solar Cells,* vol. 74, no. 1-4, Oct, 2002.

[109] J. Krc *et al.*, “Effect of surface roughness of ZnO : Al films on light scattering in hydrogenated amorphous silicon solar cells,” *Thin Solid Films,* vol. 426, no. 1-2, Feb 24, 2003.

[110] O. Kluth *et al.*, “Texture etched ZnO : Al coated glass substrates for silicon based thin film solar cells,” *Thin Solid Films,* vol. 351, no. 1-2, Aug 30, 1999.

[111] J. Muller *et al.*, “TCO and light trapping in silicon thin film solar cells,” *Solar Energy,* vol. 77, no. 6, 2004, 2004.

[112] J. Muller *et al.*, “Development of highly efficient thin film silicon solar cells on texture-etched zinc oxide-coated glass substrates,” *Solar Energy Materials and Solar Cells,* vol. 66, no. 1-4, Feb, 2001.

[113] J. Springer *et al.*, “Light trapping and optical losses in microcrystalline silicon pin solar cells deposited on surface-textured glass/ZnO substrates,” *Solar Energy Materials and Solar Cells,* vol. 85, no. 1, Jan 1, 2005.

[114] A. Illiberi *et al.*, “Growth of ZnOx:Al by high-throughput CVD at atmospheric pressure,” *Journal of Crystal Growth,* vol. 347, no. 1, May 15, 2012.

[115] T. Soederstroem *et al.*, "ZnO Transparent conductive oxide for thin film silicon solar cells," *Oxide-Based Materials and Devices*, Proceedings of SPIE F. H. Teherani *et al.*, eds., 2010.

[116] T. Soederstroem *et al.*, “TCOs for Nip Thin Film Silicon Solar Cells,” *Progress in Photovoltaics,* vol. 17, no. 3, May, 2009.

[117] J. Springer *et al.*, “Absorption loss at nanorough silver back reflector of thin-film silicon solar cells,” *Journal of Applied Physics,* vol. 95, no. 3, Feb 1, 2004.

[118] S. Nicolay *et al.*, “Control of LPCVD ZnO growth modes for improved light trapping in thin film silicon solar cells,” *Solar Energy Materials and Solar Cells,* vol. 95, no. 3, Mar, 2011.

[119] H. B. T. Li *et al.*, “Structural defects caused by a rough substrate and their influence on the performance of hydrogenated nano-crystalline silicon n-i-p solar cells,” *Solar Energy Materials and Solar Cells,* vol. 93, no. 3, Mar, 2009.

[120] C. Battaglia *et al.*, “Micromorph thin-film silicon solar cells with transparent high-mobility hydrogenated indium oxide front electrodes,” *Journal of Applied Physics,* vol. 109, no. 11, Jun 1, 2011.
[121] C. Battaglia *et al.*, “Nanoimprint Lithography for High-Efficiency Thin-Film Silicon Solar Cells,” *Nano Letters,* vol. 11, no. 2, Feb, 2011.
[122] C. Battaglia *et al.*, “Nanomoulding of transparent zinc oxide electrodes for efficient light trapping in solar cells,” *Nature Photonics,* vol. 5, no. 9, Sep, 2011.
[123] C. Battaglia *et al.*, “Efficient light management scheme for thin film silicon solar cells via transparent random nanostructures fabricated by nanoimprinting,” *Applied Physics Letters,* vol. 96, no. 21, May 24, 2010.
[124] B. W. Lewis, “Silica Nanosphere Textured Back Reflectors for Increased Absorption in Thin Film Amorphous Silicon Solar Cells,” Electrical and Computer Engineering, Iowa State University, 2010.
[125] X. Chen *et al.*, “Broadband Enhancement in Thin-Film Amorphous Silicon Solar Cells Enabled by Nucleated Silver Nanoparticles,” *Nano Letters,* vol. 12, no. 5, May, 2012.
[126] H. R. Tan *et al.*, “Plasmonic Light Trapping in Thin-film Silicon Solar Cells with Improved Self-Assembled Silver Nanoparticles,” *Nano Letters,* vol. 12, no. 8, pp. 4070-4076, Aug, 2012.
[127] M. G. Deceglie *et al.*, “Design of Nanostructured Solar Cells Using Coupled Optical and Electrical Modeling,” *Nano Letters,* vol. 12, no. 6, Jun, 2012.
[128] V. E. Ferry, A. Polman, and H. A. Atwater, “Modeling Light Trapping in Nanostructured Solar Cells,” *Acs Nano,* vol. 5, no. 12, Dec, 2011.
[129] V. E. Ferry *et al.*, “Plasmonic nanostructures for enhanced absorption in ultrathin film solar cells,” *Abstracts of Papers of the American Chemical Society,* vol. 241, Mar 27, 2011.
[130] V. E. Ferry *et al.*, “Optimized Spatial Correlations for Broadband Light Trapping Nanopatterns in High Efficiency Ultrathin Film a-Si:H Solar Cells,” *Nano Letters,* vol. 11, no. 10, Oct, 2011.
[131] V. E. Ferry, J. N. Munday, and H. A. Atwater, “Design Considerations for Plasmonic Photovoltaics,” *Advanced Materials,* vol. 22, no. 43, Nov 16, 2010.
[132] V. E. Ferry *et al.*, "Plasmonic light trapping for thin film a-si:h solar cells," *35th Ieee Photovoltaic Specialists Conference*, IEEE Photovoltaic Specialists Conference, 2010.
[133] V. E. Ferry *et al.*, “Improved red-response in thin film a-Si:H solar cells with soft-imprinted plasmonic back reflectors,” *Applied Physics Letters,* vol. 95, no. 18, Nov 2, 2009.
[134] V. E. Ferry *et al.*, “Plasmonic Nanostructure Design for Efficient Light Coupling into Solar Cells,” *Nano Letters,* vol. 8, no. 12, Dec, 2008.
[135] R. Biswas *et al.*, “Enhanced nanocrystalline silicon solar cell with a photonic crystal back-reflector,” *Solar Energy Materials and Solar Cells,* vol. 94, no. 12, Dec, 2010.
[136] R. Biswas, and D. Zhou, “Simulation and modelling of photonic and plasmonic crystal back reflectors for efficient light trapping,” *Physica Status Solidi a-Applications and Materials Science,* vol. 207, no. 3, Mar, 2010.
[137] S. Pattnaik *et al.*, "Amorphous silicon solar cells on plastic based photonic structures."
[138] R. Biswas *et al.*, "Surface plasmon enhancement of optical absorption of thin film a-si:h solar cells," *2009 34th Ieee Photovoltaic Specialists Conference, Vols 1-3*, IEEE Photovoltaic Specialists Conference, 2009.

[139] B. Curtin, R. Biswas, and V. Dalal, “Photonic crystal based back reflectors for light management and enhanced absorption in amorphous silicon solar cells,” *Applied Physics Letters,* vol. 95, no. 23, Dec 7, 2009.

[140] R. Biswas, and D. Zhou, "Improved Photon Absorption in a-Si:H Solar Cells using Photonic Crystal Architectures," *Amorphous and Polycrystalline Thin-Film Silicon Science and Technology-2008*, Materials Research Society Symposium Proceedings A. Nathan *et al.*, eds., 2008.

[141] D. Zhou, and R. Biswas, "Enhanced photon harvesting in a-si:h solar cells with photonic crystals," *Pvsc: 2008 33rd Ieee Photovoltaic Specialists Conference, Vols 1-4*, IEEE Photovoltaic Specialists Conference, 2008.

[142] D. Zhou, and R. Biswas, “Photonic crystal enhanced light-trapping in thin film solar cells,” *Journal of Applied Physics,* vol. 103, no. 9, May 1, 2008.

[143] R. Biswas, and D. Zhou, "Enhancing light-trapping and efficiency of solar cells with photonic crystals," *Amorphous and Polycrystalline Thin-Film Silicon Science and Technology 2007*, Materials Research Society Symposium Proceedings V. Chu *et al.*, eds., 2007.

[144] A. Bozzola, M. Liscidini, and L. C. Andreani, “Photonic light-trapping versus Lambertian limits in thin film silicon solar cells with 1D and 2D periodic patterns,” *Optics Express,* vol. 20, no. 6, Mar 12, 2012.

[145] S. Juechter *et al.*, "Preparation of periodically arranged metallic nanostructures using nanoimprint lithography," *Photonics for Solar Energy Systems Iv*, Proceedings of SPIE R. Wehrspohn and A. Gombert, eds., 2012.

[146] J. Li, H. Yu, and Y. Li, “Solar energy harnessing in hexagonally arranged Si nanowire arrays and effects of array symmetry on optical characteristics,” *Nanotechnology,* vol. 23, no. 19, May 17, 2012.

[147] E. R. Martins *et al.*, “Engineering gratings for light trapping in photovoltaics: The supercell concept,” *Physical Review B,* vol. 86, no. 4, Jul 9, 2012.

[148] A. Oskooi *et al.*, “Partially disordered photonic-crystal thin films for enhanced and robust photovoltaics,” *Applied Physics Letters,* vol. 100, no. 18, Apr 30, 2012.

[149] G. Zheng *et al.*, “Enhancement of optical absorption in amorphous silicon thin film solar cells with periodical nanorods to increase optical path length,” *Optics Communications,* vol. 285, no. 10-11, May 15, 2012.

[150] S. Solntsev, and M. Zeman, "Optical modeling of thin-film silicon solar cells with submicron periodic gratings and nonconformal layers," *European Materials Research Society Conference Symposium: Advanced Inorganic Materials and Concepts for Photovoltaics*, Energy Procedia G. Conibeer *et al.*, eds., 2011.

[151] A. Campa *et al.*, “Optimal design of periodic surface texture for thin-film a-Si:H solar cells,” *Progress in Photovoltaics,* vol. 18, no. 3, May, 2010.

[152] C.-C. Chin, Y.-H. Ye, and D.-W. Huang, "Efficiency improvement in nanorod amorphous silicon thin film with ultrathin metal electrode for photovoltaic application," *Holography, Diffractive Optics, and Applications Iv*, Proceedings of SPIE-The International Society for Optical Engineering Y. Sheng, C. Yu and L. Chen, eds., 2010.

[153] S. B. Mallick, M. Agrawal, and P. Peumans, “Optimal light trapping in ultra-thin photonic crystal crystalline silicon solar cells,” *Optics Express,* vol. 18, no. 6, Mar 15, 2010.

[154] M. Agrawal, and M. Frei, “Rigorous optical modeling and optimization of thin-film photovoltaic cells with textured transparent conductive oxides,” *Progress in Photovoltaics,* vol. 20, no. 4, Jun, 2012.

[155] M. Agrawal, P. Peumans, and Ieee, "The physical limits of light trapping in thin-films and photonic structures that operate at the limit," *2009 34th Ieee Photovoltaic Specialists Conference, Vols 1-3*, IEEE Photovoltaic Specialists Conference, 2009.

[156] M. Agrawal, and P. Peumans, "Broadband optical absorption enhancement through coherent light trapping in thin-film photovoltaic cells," *Optics Express,* vol. 16, no. 8, Apr 14, 2008.

[157] J. Zhu *et al.*, "Nanodome Solar Cells with Efficient Light Management and Self-Cleaning," *Nano Letters,* vol. 10, no. 6, pp. 1979-1984, Jun, 2010.

[158] J. Zhu *et al.*, "Nanostructured photon management for high performance solar cells," *Materials Science & Engineering R-Reports,* vol. 70, no. 3-6, Nov 22, 2010.

[159] J. Zhu *et al.*, "Optical Absorption Enhancement in Amorphous Silicon Nanowire and Nanocone Arrays," *Nano Letters,* vol. 9, no. 1, Jan, 2009.

[160] K. X. Wang *et al.*, "Absorption Enhancement in Ultrathin Crystalline Silicon Solar Cells with Antireflection and Light-Trapping Nanocone Gratings," *Nano Letters,* vol. 12, no. 3, Mar, 2012.

[161] S. John, "Strong localization of photons in certain disordered dielectric superlattices," *Physical Review Letters,* vol. 58, no. 23, pp. 2486-2489, 06/08/, 1987.

[162] K. M. Ho, C. T. Chan, and C. M. Soukoulis, "Existence of a photonic gap in periodic dielectric structures," *Physical Review Letters,* vol. 65, no. 25, Dec 17, 1990.

[163] J. D. J. Joannopoulos, Steven G. Winn, Joshua N.Meade, Robert D., *Photonic Crystals:Molding the Flow of Light (Second Edition)*, Princeton, NY: Princeton University Press, 2008.

[164] J. Buencuerpo *et al.*, "Optical absorption enhancement in a hybrid system photonic crystal - thin substrate for photovoltaic applications," *Optics Express,* vol. 20, no. 14, Jul 2, 2012.

[165] K. Q. Le *et al.*, "Comparing plasmonic and dielectric gratings for absorption enhancement in thin-film organic solar cells," *Optics Express,* vol. 20, no. 1, Jan 2, 2012.

[166] P. Bermel *et al.*, "Improving thin-film crystalline silicon solar cell efficiencies with photonic crystals," *Optics Express,* vol. 15, no. 25, Dec 10, 2007.

[167] L. Zeng *et al.*, "Demonstration of enhanced absorption in thin film Si solar cells with textured photonic crystal back reflector," *Applied Physics Letters,* vol. 93, no. 22, Dec 1, 2008.

[168] L. Zeng *et al.*, "Efficiency enhancement in Si solar cells by textured photonic crystal back reflector," *Applied Physics Letters,* vol. 89, no. 11, Sep 11, 2006.

[169] E. Yablonovitch, T. J. Gmitter, and K. M. Leung, "Photonic band-structure - the face-centered-cubic case employing nonspherical atoms," *Physical Review Letters,* vol. 67, no. 17, Oct 21, 1991.

[170] S. Y. Lin *et al.*, "A three-dimensional photonic crystal operating at infrared wavelengths," *Nature,* vol. 394, no. 6690, Jul 16, 1998.

[171] R. B. Wehrspohn, and J. Uepping, "3D photonic crystals for photon management in solar cells," *Journal of Optics,* vol. 14, no. 2, Feb, 2012.

[172] R. Biswas *et al.*, "Theory of subwavelength hole arrays coupled with photonic crystals for extraordinary thermal emission," *Physical Review B,* vol. 74, no. 4, Jul, 2006.

[173] Z.-Y. Li, and L.-L. Lin, "Photonic band structures solved by a plane-wave-based transfer-matrix method," *Physical Review E,* vol. 67, no. 4, pp. 046607, 04/15/, 2003.

[174] G. Gomard *et al.*, "Two-dimensional photonic crystal for absorption enhancement in hydrogenated amorphous silicon thin film solar cells," *Journal of Applied Physics,* vol. 108, no. 12, Dec 15, 2010.

[175] G. Gomard *et al.*, "Light harvesting by planar photonic crystals in solar cells: the case of amorphous silicon," *Journal of Optics,* vol. 14, no. 2, Feb, 2012.

[176] S. Pillai *et al.*, "Surface plasmon enhanced silicon solar cells," *Journal of Applied Physics,* vol. 101, no. 9, May 1, 2007.

[177] D. Derkacs *et al.*, "Improved performance of amorphous silicon solar cells via scattering from surface plasmon polaritons in nearby metallic nanoparticles," *Applied Physics Letters,* vol. 89, no. 9, Aug 28, 2006.

[178] S. H. Lim *et al.*, "Photocurrent spectroscopy of optical absorption enhancement in silicon photodiodes via scattering from surface plasmon polaritons in gold nanoparticles," *Journal of Applied Physics,* vol. 101, no. 10, May 15, 2007.

[179] R. A. Pala *et al.*, "Design of Plasmonic Thin-Film Solar Cells with Broadband Absorption Enhancements," *Advanced Materials,* vol. 21, no. 34, Sep 11, 2009.

[180] P. Matheu *et al.*, "Metal and dielectric nanoparticle scattering for improved optical absorption in photovoltaic devices," *Applied Physics Letters,* vol. 93, no. 11, Sep 15, 2008.

[181] F. J. Haug *et al.*, "Influence of the ZnO buffer on the guided mode structure in Si/ZnO/Ag multilayers," *Journal of Applied Physics,* vol. 106, no. 4, Aug 15, 2009.

[182] F. J. Haug *et al.*, "Plasmonic absorption in textured silver back reflectors of thin film solar cells," *Journal of Applied Physics,* vol. 104, no. 6, Sep 15, 2008.

[183] R. E. I. Schropp *et al.*, "Nanostructured thin films for multibandgap silicon triple junction solar cells," *Solar Energy Materials and Solar Cells,* vol. 93, no. 6-7, Jun, 2009.

[184] R. H. Franken *et al.*, "Understanding light trapping by light scattering textured back electrodes in thin film n-i-p-type silicon solar cells," *Journal of Applied Physics,* vol. 102, no. 1, Jul 1, 2007.

[185] R. B. Dunbar, T. Pfadler, and L. Schmidt-Mende, "Highly absorbing solar cells-a survey of plasmonic nanostructures," *Optics Express,* vol. 20, no. 6, Mar 12, 2012.

[186] M. D. Brown *et al.*, "Plasmonic Dye-Sensitized Solar Cells Using Core-Shell Metal-Insulator Nanoparticles," *Nano Letters,* vol. 11, no. 2, Feb, 2011.

[187] I. K. Ding *et al.*, "Plasmonic Dye-Sensitized Solar Cells," *Advanced Energy Materials,* vol. 1, no. 1, Jan 1, 2011.

[188] S. D. Standridge, G. C. Schatz, and J. T. Hupp, "Distance Dependence of Plasmon-Enhanced Photocurrent in Dye-Sensitized Solar Cells," *Journal of the American Chemical Society,* vol. 131, no. 24, Jun 24, 2009.

[189] A. E. Ostfeld, and D. Pacifici, "Plasmonic concentrators for enhanced light absorption in ultrathin film organic photovoltaics," *Applied Physics Letters,* vol. 98, no. 11, Mar 14, 2011.

[190] J.-L. Wu *et al.*, "Surface Plasmonic Effects of Metallic Nanoparticles on the Performance of Polymer Bulk Heterojunction Solar Cells," *Acs Nano,* vol. 5, no. 2, Feb, 2011.

[191] R. Xu *et al.*, "Influence of the light trapping induced by surface plasmons and antireflection film in crystalline silicon solar cells," *Optics Express,* vol. 20, no. 5, Feb 27, 2012.

[192] K. R. Catchpole, and A. Polman, "Plasmonic solar cells," *Optics Express,* vol. 16, no. 26, Dec 22, 2008.

[193] R. Biswas *et al.*, "Photonic and plasmonic crystal based enhancement of solar cells-overcoming the Lambertian classical 4n2 limit," *Journal of Material Research,* vol. (unpublished), 2012.

[194] L. Yu *et al.*, "Radial junction amorphous silicon solar cells on PECVD-grown silicon nanowires," *Nanotechnology,* vol. 23, no. 19, 2012-May-17, 2012.

[195] Y. Zhan *et al.*, "Enhanced photon absorption of single nanowire alpha-Si solar cells modulated by silver core," *Optics Express,* vol. 20, no. 10, May 7, 2012.

[196] S. Brittman *et al.*, "Absorption of Light in a Single-Nanowire Silicon Solar Cell Decorated with an Octahedral Silver Nanocrystal," *Nano Letters,* vol. 11, no. 12, Dec, 2011.

[197] E. C. Garnett *et al.*, "Nanowire Solar Cells," *Annual Review of Materials Research, Vol 41,* vol. 41, 2011, 2011.

[198] M. D. Kelzenberg *et al.*, "Photovoltaic measurements in single-nanowire silicon solar cells," *Nano Letters,* vol. 8, no. 2, Feb, 2008.

[199] M. J. Naughton *et al.*, "Efficient nanocoax-based solar cells," *Physica Status Solidi-Rapid Research Letters,* vol. 4, no. 7, Jul, 2010.

[200] M. Vanecek *et al.*, "Nanostructured three-dimensional thin film silicon solar cells with very high efficiency potential," *Applied Physics Letters,* vol. 98, no. 16, Apr 18, 2011.

[201] M. D. Kelzenberg *et al.*, "Enhanced absorption and carrier collection in Si wire arrays for photovoltaic applications," *Nature Materials,* vol. 9, no. 3, Mar, 2010.

[202] M. D. Kelzenberg *et al.*, "High-performance Si microwire photovoltaics," *Energy & Environmental Science,* vol. 4, no. 3, Mar, 2011.

[203] H. M. Branz *et al.*, "Nanostructured black silicon and the optical reflectance of graded-density surfaces," *Applied Physics Letters,* vol. 94, no. 23, Jun 8, 2009.

[204] Z. N. Yu *et al.*, "Fabrication of large area subwavelength antireflection structures on Si using trilayer resist nanoimprint lithography and liftoff," *Journal of Vacuum Science & Technology B,* vol. 21, no. 6, Nov-Dec, 2003.

[205] T.-G. Chen *et al.*, "Nano-patterned glass superstrates with different aspect ratios for enhanced light harvesting in a-Si:H thin film solar cells," *Optics Express,* vol. 20, no. 10, May 7, 2012.

[206] W. Zhang *et al.*, "Rough glass by 3d texture transfer for silicon thin film solar cells," *Physica Status Solidi C - Current Topics in Solid State Physics, Vol 7 No 3-4,* vol. 7, no. 3-4, 2010, 2010.

[207] S. Fahr *et al.*, *Photonic Crystal Intermediate Reflector in Micromorph Tandem Solar Cells*, 2011.

[208] S. Fahr, C. Rockstuhl, and F. Lederer, "Improving the efficiency of thin film tandem solar cells by plasmonic intermediate reflectors," *Photonics and Nanostructures-Fundamentals and Applications,* vol. 8, no. 4, Sep, 2010.

[209] S. Fahr, C. Rockstuhl, and F. Lederer, "The interplay of intermediate reflectors and randomly textured surfaces in tandem solar cells," *Applied Physics Letters,* vol. 97, no. 17, Oct 25, 2010.

[210] C. Rockstuhl *et al.*, "The impact of intermediate reflectors on light absorption in tandem solar cells with randomly textured surfaces," *Applied Physics Letters,* vol. 94, no. 21, May 25, 2009.

[211] A. Bielawny *et al.*, "3D photonic crystal intermediate reflector for micromorph thin-film tandem solar cell," *Physica Status Solidi a-Applications and Materials Science,* vol. 205, no. 12, Dec, 2008.

[212] P. G. O'Brien *et al.*, "Photonic crystal intermediate reflectors for micromorph solar cells: a comparative study," *Optics Express,* vol. 18, no. 5, Mar 1, 2010.

[213] G. Bugnon *et al.*, "LPCVD ZnO-based intermediate reflector for micromorph tandem solar cells," *Solar Energy Materials and Solar Cells,* vol. 95, no. 8, Aug, 2011.

[214] C. Rockstuhl *et al.*, "Photon Management in Thin-Film Solar Cells," *Fourth International Workshop on Theoretical and Computational Nanophotonics*, AIP Conference Proceedings D. N. Chigrin, ed., 2011.

[215] P. Buehlmann *et al.*, "In situ silicon oxide based intermediate reflector for thin-film silicon micromorph solar cells," *Applied Physics Letters,* vol. 91, no. 14, Oct 1, 2007.

[216] S. Fahr, C. Rockstuhl, and F. Lederer, "Metallic nanoparticles as intermediate reflectors in tandem solar cells," *Applied Physics Letters,* vol. 95, no. 12, Sep 21, 2009.

[217] J. Uepping *et al.*, "Three-Dimensional Photonic Crystal Intermediate Reflectors for Enhanced Light-Trapping in Tandem Solar Cells," *Advanced Materials,* vol. 23, no. 34, Sep 8, 2011.

[218] X. D. Zhang *et al.*, "Plasma deposition of n-SiOx nanocrystalline thin film for enhancing the performance of silicon thin film solar cells," *Thin Solid Films,* vol. 520, no. 2, Nov 1, 2011.

[219] B. Yan, J. Yang, and S. Guha, "Amorphous and nanocrystalline silicon thin film photovoltaic technology on flexible substrates," *Journal of Vacuum Science & Technology A,* vol. 30, no. 4, Jul, 2012.

[220] J.-S. Cho, S. Baek, and K. H. Yoon, "Enhancement of light trapping by textured back electrodes in tandem micromorph n-i-p silicon thin film solar cells," *Current Applied Physics,* vol. 11, no. 1, Jan, 2011.

[221] J. Escarre *et al.*, "High fidelity transfer of nanometric random textures by UV embossing for thin film solar cells applications," *Solar Energy Materials and Solar Cells,* vol. 95, no. 3, Mar, 2011.

[222] F. Meillaud *et al.*, "Realization of high efficiency micromorph tandem silicon solar cells on glass and plastic substrates: Issues and potential," *Solar Energy Materials and Solar Cells,* vol. 95, no. 1, Jan, 2011.

[223] J. K. Rath *et al.*, "Fabrication of thin film silicon solar cells on plastic substrate by very high frequency PECVD," *Solar Energy Materials and Solar Cells,* vol. 94, no. 9, Sep, 2010.

[224] T. Soederstroem *et al.*, "Flexible micromorph tandem a-Si/mu c-Si solar cells," *Journal of Applied Physics,* vol. 107, no. 1, Jan 1, 2010.

[225] F. J. Haug *et al.*, "Development of micromorph tandem solar cells on flexible low-cost plastic substrates," *Solar Energy Materials and Solar Cells,* vol. 93, no. 6-7, Jun, 2009.

[226] J. K. Rath *et al.*, "Thin film silicon modules on plastic superstrates," *Journal of Non-Crystalline Solids,* vol. 354, no. 19-25, May 1, 2008.

[227] T. Soderstrom *et al.*, "Optimization of amorphous silicon thin film solar cells for flexible photovoltaics," *Journal of Applied Physics,* vol. 103, no. 11, Jun 1, 2008.

[228] K. Soederstroem *et al.*, "Highly reflective nanotextured sputtered silver back reflector for flexible high-efficiency n-i-p thin-film silicon solar cells," *Solar Energy Materials and Solar Cells,* vol. 95, no. 12, Dec, 2011.

[229] K. Soederstroem *et al.*, "UV-nano-imprint lithography technique for the replication of back reflectors for n-i-p thin film silicon solar cells," *Progress in Photovoltaics,* vol. 19, no. 2, Mar, 2011.

[230] V. L. Dalal, K. Erickson, and I. Ieee, "Microcrystalline Si and (Si,Ge) solar cells on plastic substrates," *Conference Record of the Twenty-Eighth Ieee Photovoltaic Specialists Conference - 2000*, Ieee Photovoltaic Specialists Conference, 2000.

[231] K. Tao *et al.*, "Low-temperature preparation of flexible a-Si:H solar cells with hydrogenated nanocrystalline silicon p layer," *Vacuum,* vol. 86, no. 10, Apr 27, 2012.

[232] R. E. I. Schropp, and M. Zeman, *Amorphous and Microcrystalline Silicon Solar Cells: Modeling, Materials, and Device Technology*: Kluwer Academic, 1998.

[233] U. Kroll *et al.*, "Potential of VHF-plasmas for low-cost production of a-Si:H solar cells," *Solar Energy Materials and Solar Cells,* vol. 48, no. 1-4, Nov, 1997.

[234] J. Meier *et al.*, "Amorphous solar cells, the micromorph concept and the role of VHF-GD deposition technique," *Solar Energy,* vol. 77, no. 6, 2004, 2004.

[235] W. van Sark, J. Bezemer, and W. F. van der Weg, "VHF a-Si : H solar cells: A systematic material and cell study," *Journal of Materials Research,* vol. 13, no. 1, Jan, 1998.

[236] M. Heintze, and R. Zedlitz, "New diagnostic aspects of high rate a-Si:H deposition in a VHF plasma," *Journal of Non-Crystalline Solids,* vol. 198, May, 1996.

[237] Kimerlin.Lc, "Influence of deep traps on measurement of free-carrier distributions in semiconductors by junction capacitance techniques," *Journal of Applied Physics,* vol. 45, no. 4, 1974, 1974.

[238] V. L. Dalal, and P. Sharma, "Defect density and diffusion length of holes in nanocrystalline silicon devices," *Applied Physics Letters,* vol. 86, no. 10, Mar 7, 2005.

[239] T. Walter *et al.*, "Determination of defect distributions from admittance measurements and application to Cu(In,Ga)Se-2 based heterojunctions," *Journal of Applied Physics,* vol. 80, no. 8, Oct 15, 1996.

[240] D. Congreve, "*Calculation of defect densities in nano-crystalline and amorphous silicon devices using differential capacitance measurements.*," Electrical and Computer Engineering, Iowa State University, 2011.

[241] J. Nelson, *The Physics Of Solar Cells*: Imperial College Press, 2003.

[242] V. L. Dalal, and A. Madhavan, "Alternative designs for nanocrystalline silicon solar cells," *Journal of Non-Crystalline Solids,* vol. 354, no. 19-25, May 1, 2008.

[243] J. Kocka *et al.*, "Amorphous/microcrystalline silicon superlattices - the chance to control isotropy and other transport properties," *Applied Physics Letters,* vol. 79, no. 16, Oct 15, 2001.

[244] K. H. Jun *et al.*, "Low degradation and fast annealing effects of amorphous silicon multilayer processed through alternate hydrogen dilution," *Journal of Applied Physics,* vol. 88, no. 8, Oct 15, 2000.

[245] K. R. Catchpole *et al.*, "Plasmonics and nanophotonics for photovoltaics," *Mrs Bulletin,* vol. 36, no. 6, Jun, 2011.

[246] E. Yablonovitch, "Statistical ray optics," *Journal of the Optical Society of America,* vol. 72, no. 7, 1982, 1982.

[247] L. R. Dahal *et al.*, "Plasmonic characteristics of ag/zno back-reflectors for thin film si photovoltaics." *33rd IEEE Photovoltaic Specialists Conference,* 2008.

[248] A. Poruba *et al.*, "Optical absorption and light scattering in microcrystalline silicon thin films and solar cells," *Journal of Applied Physics,* vol. 88, no. 1, Jul 1, 2000.

[249] C. Rockstuhl *et al.*, "Comparison and optimization of randomly textured surfaces in thin-film solar cells," *Optics Express,* vol. 18, no. 19, Sep 13, 2010.

[250] H. Sai *et al.*, "Enhancement of light trapping in thin-film hydrogenated microcrystalline Si solar cells using back reflectors with self-ordered dimple pattern," *Applied Physics Letters,* vol. 93, no. 14, Oct 6, 2008.

[251] A. V. Shah *et al.*, "Basic efficiency limits, recent experimental results and novel light-trapping schemes in a-Si : H, mu c-Si : H and 'micromorph tandem' solar cells," *Journal of Non-Crystalline Solids,* vol. 338, Jun 15, 2004.

[252] O. Isabella, J. Krc, and M. Zeman, "Modulated surface textures for enhanced light trapping in thin-film silicon solar cells," *Applied Physics Letters,* vol. 97, no. 10, Sep 6, 2010.

Appendix: Novel hybrid amorphous/organic tandem junction solar cell

Modified from a paper submitted to Journal of Photovoltaics

Sambit Pattnaik, Teng Xiao, R Shinar, J Shinar and V. L. Dalal

Due to their potential ultralow-cost, organic solar cells (OSCs) are a promising technology. Bulk heterojunction OSCs have achieved power conversion efficiency (PCE) of ~10%, yet even this is far below that of inorganic cells. Typical OSCs suffer from a narrow range of photon absorption. Previous efforts addressed this problem by fabricating tandem OSCs, with cells absorbing in complementary bands. However, their efficiency remains far below that of inorganic tandem cells, and importantly, they do not address the problem of OSC degradation. This paper describes radically new designs of tandem junction cells based on a combination of an amorphous (Si,C):H cell and a P3HT:PCBM cell. The individual cells can be connected electrically in series or in parallel, with the band gaps of the inorganic materials adjusted to match the currents in the tandem units. The un-optimized series-connected PCE obtained was increased by 25% by using a tandem cell arrangement. The tandem designs also address the critical problem of light-induced degradation, significantly reducing it.

6.1 Introduction

OSCs are an important photovoltaic technology for solar energy conversion due to their potential ultralow cost and promise as easy to fabricate, flexible and high-performance energy sources [1]. Recent bulk heterojunction OSCs, where a polymeric donor is coupled to an electron acceptor molecule, have achieved solar PCEs of ~ 10% [1-6]. However, as is well known, un-encapsulated OSCs typically suffer from severe degradation upon exposure to light, moisture, and oxygen, with the decrease in the short circuit current I_{SC} in some cases amounting to almost 45% over ~200 hours of illumination [5, 7-14]. One of the reasons for the limits on the efficiency of the current generation of OSCs is the relatively poor absorption of organic cells. For example, the commonly used P3HT:PCBM (where P3HT is poly(3-hexylthiophene) and PCBM is 1-(3-methoxycarbonyl)-propyl-1-phenyl-(6,6)C_{61}) system has a strong absorption in the ~450-625 nm range, but poorer absorption below ~450 nm or beyond ~625 nm as shown in Figure 6.1.1. The narrow absorption range is typical of most organic PV materials and leads to a considerable loss

in solar conversion efficiency for organic solar cells. The obvious way to overcome such efficiency loss is to use a tandem solar cell structure, where one can use organic materials with complementary absorption spectra [15-23]. However, such systems are not optimal from a design viewpoint, in that they do not approach the ~42% efficiency of inorganic crystalline tandem junction cells [4], or the ~20% efficiency of inorganic thin film cells[4]; A less obvious way is to use a combination of an inorganic material and an organic material with complementary absorption spectra in a tandem arrangement. In this paper, we pursue this less obvious combination with the a-(Si,C):H cell as the first cell and the organic P3HT cell as the second cell.

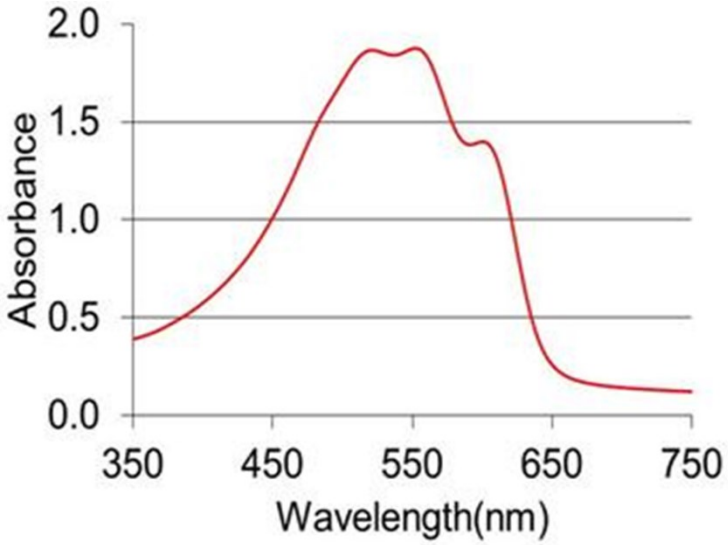

Figure 6.1.1: Absorption of P3HT film

In this paper, we show that radically new design of tandem cells, which includes a combination of an inorganic thin-film cell, an intermediate transparent conductor, and an organic cell, can approach the high efficiency expected from a tandem cell arrangement. This design also addresses the critical problem of degradation due to light exposure. The design is such that one can electrically connect the cells either in series or in parallel (i.e., with separate electrical connections), as the need may be, and thus potentially avoid the difficult problem of current matching between the two cells. The experiments prove the concept and demonstrate the expected high V_{OC} ~ 1.5 V in the series-connected tandem combination of amorphous a-(Si,C):H and P3HT:PCBM-based cells. The overall PCE increased by ~25% when the cells were

connected in series compared to the efficiency of the organic cell by itself. The external quantum efficiency (EQE) data measured on the individual cells confirm that both cells contribute to the power. We note that for improved solar cell stability, a-(Si,C):H, rather than a-Si:H, is the appropriate combination for the P3HT:PCBM-based cell. For other organic units, we have the flexibility of using other a-Si:H alloys, either with varied levels of incorporated C or with Ge.

6.2 Experimental Details

The two fundamental designs tested are shown in Figure 6.2.1. In Figure 6.2.1(a) the organic cell is fabricated on indium tin oxide (ITO) that covers the inorganic cell with both units on the same side of the substrate (Design A); that is, the units are connected optically and electrically in series. In the design shown in Figure 6.2.1(b) the inorganic cell is fabricated on one side of the glass substrate (coated with ZnO), and the organic cell is fabricated on ITO on the opposite side of the same glass substrate (Design B), i.e., the units can be connected independently, or by shorting the ZnO and the ITO, in series.

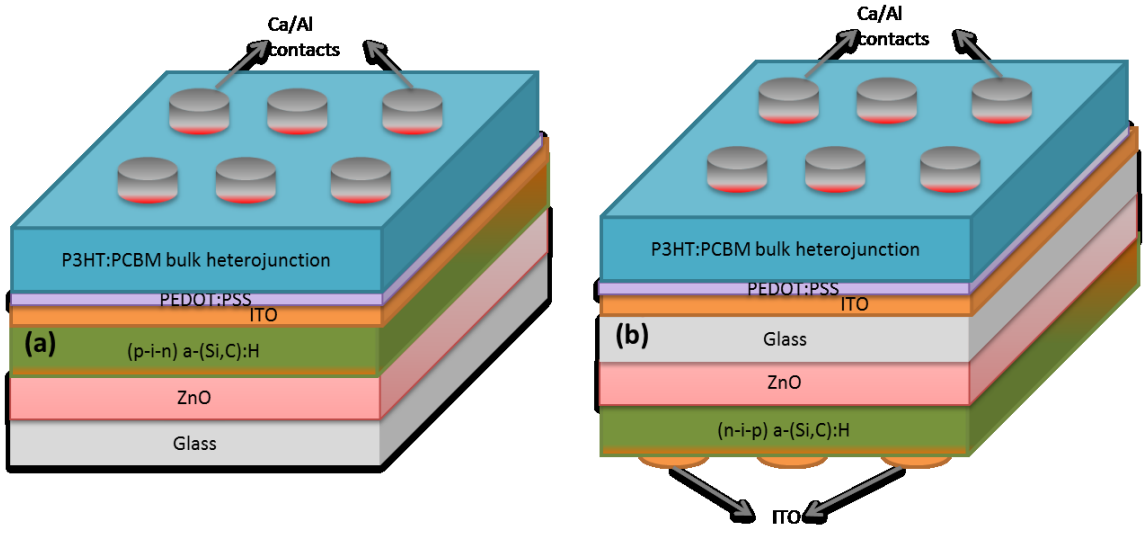

Figure 6.2.1: Schematic Diagram of cells (a) Design A and (b) Design B

The inorganic cell is of the standard p-i-n or n-i-p type [24-26], with all three layers, p, i, and n containing Si, C, H and appropriate dopants. The organic cell consists of the usual PEDOT:PSS/P3HT:PCBM/metal configuration [27]. The Tauc bandgap of the a-(Si,C):H intrinsic layer (~ 2 eV) and its thickness (~80nm) are selected so as to match the current produced in the

organic cell if a series electrical connection is to be used. The p+ and n+ layers are also fabricated from a-(Si,C):H so that light can be transmitted through them without significant absorption. This cell was deposited using standard PECVD techniques for depositing amorphous solar cells. Next, an ITO layer of ~280 nm is sputtered at 250ºC using a DC-magnetron sputtering at 5 mTorr onto the n+ a-(Si,C):H layer so as to provide an ohmic contact to the n+ layer. The next layer is a PEDOT:PSS layer spin-coated on the ITO layer as a hole extraction layer [1], which also reduces the RMS surface roughness of ITO from ~4.5 nm to ~2.7 nm. The second cell deposited onto this layer is an organic P3HT:PCBM bulk-heterojunction cell deposited using a spin-coating, the fabrication of the organic cell is detailed in a previous manuscript [18]. A Ca/Al metallic contact provides the electron extracting contact for the organic cell. The fabrication procedure for Design A has been shown diagrammatically in Figure 6.2.3, similar methods are followed for design B also. The intermediate ITO layer can also be contacted independently to study the characteristics of each of the individual cells. As shown later, a major advantage of these designs is in filtering of high-energy photons that may otherwise damage the organic cell. The a-(Si,C):H cell is provided with a transparent conducting oxide (TCO) contact to let in light. Current matching is not necessary if the two cells are not electrically in series, but are connected to their respective loads in independent circuits (Design B). In that case, both cells can be used separately, though they are optically in series, with the light passing first through the top inorganic cell.

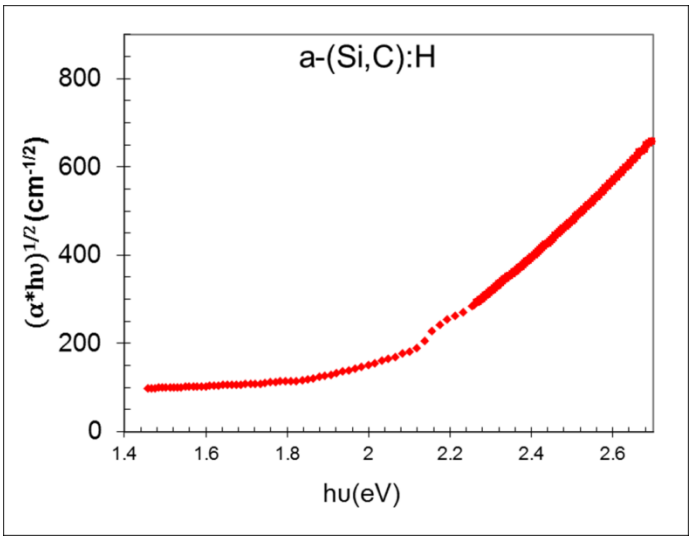

Figure 6.2.2: Tauc plot for the i-layer of the a-(Si,C):H cell

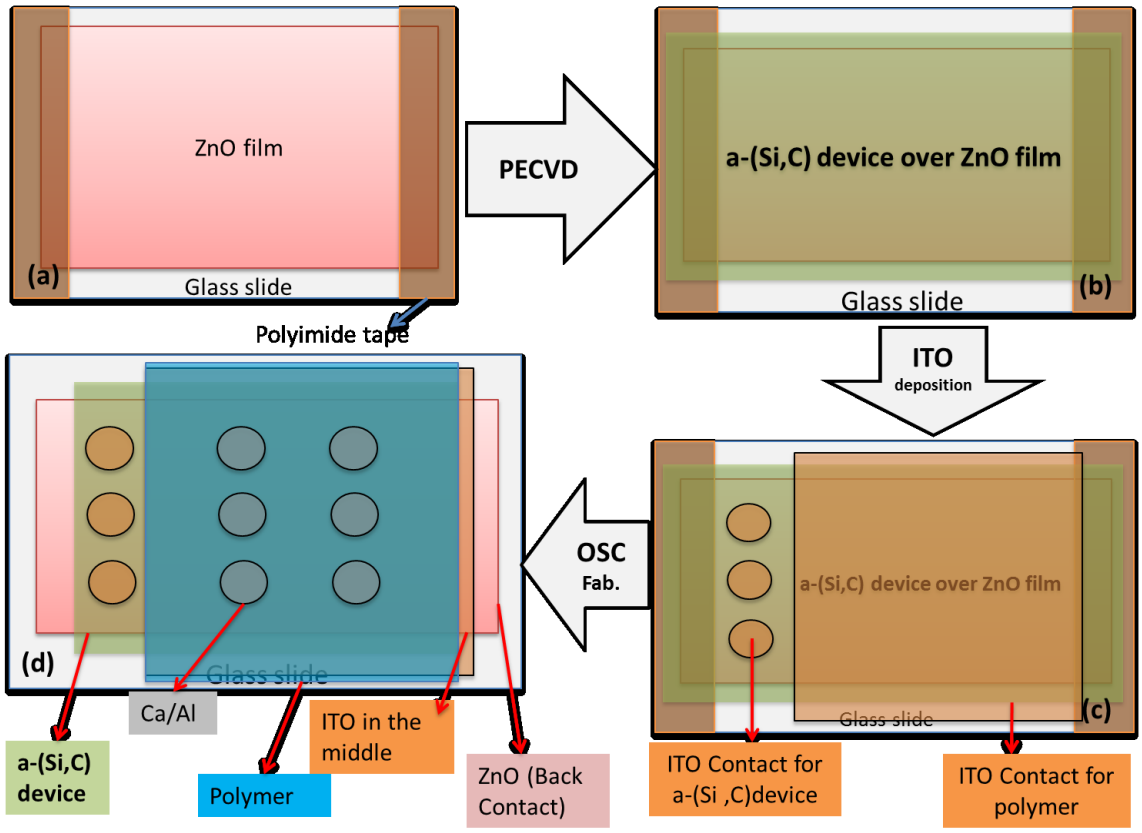

Figure 6.2.3: Fabrication procedure for cell in Design A

6.3 Results and Discussion

6.3.1 Device Results

The illuminated *I-V* curves for the tandem cells of designs A and B are shown in Figure 6.3.1Figure 6.2.1. Figure 6.3.1(a) shows also the I-V curve of the reference single organic cell and that of the inorganic unit of the tandem as in design A. Figure 6.3.1(b) shows also the I-V curves of the single units that comprise the tandem cell of design B. The single thin inorganic unit of design A showed a PCE of 3.9% and V_{OC} ~ 0.95 V. The organic cell when illuminated directly is typically capable of ~4.5% efficiency with V_{OC} ~ 0.61 V, as seen in the illuminated *I-V* curve of Figure 6.3.1(a). Figure 6.3.1(c) shows the normalized EQE of the inorganic unit of design A tandem and that of the organic reference cell. Similar EQE data were obtained for the design B tandem as shown in Figure 6.3.1(d). As seen, the inorganic units were successfully designed to match the current of the organic cell. The tandem *I-V* curves clearly show V_{OC} ~ 1.5 V, the

approximate sum of the voltages of each cell, proving that both cells are contributing to the V_{OC}. The PCE of the un-optimized design A tandem junction cell is ~5.6% (an increase of ~24% compared to the single unit OSC), and though this structure was not yet optimized, it shows a promising new concept with the flexibility to change the inorganic materials so as to match organic cells based on other materials.

The interesting thing to observe is that the fill factor of the tandem cell is exceptionally good, 77%, thus proving that the intermediate contacting layer, ITO, is an excellent tunnel-recombination junction for both electrons and holes. The use of ITO with a very low sheet resistivity of ~2-3x10^{-4} ohm-cm, which is transparent in absorption region of the organic-inorganic cells, is a major achievement. To show how important this intermediate ITO layer is for the high performance of the cell, we contrast our results for the fill factor with the results of a previous work from Kim et al. on a-Si/P3HT:PCBM tandem cell [28]. shows the IV curve obtained for their cells, showing significant collection problems in the tandem cell. In Fig. 8, we show the external quantum efficiency (EQE) data for our tandem cell, showing an excellent match in current generated by the first and the second cells. To measure the EQE on tandem devices a secondary light source was used to saturate the top and bottom cells by external blue and red bias light illumination, respectively. That is, saturation with blue light yields the EQE for the organic cell, and with red light, for the inorganic cell.

Further proof that both cells are contributing to the current comes from measuring the EQE curve for each cell. Very clearly, from the QE data, the a-(Si,C):H-based cell primarily absorbs blue photons, and the organic cell primarily absorbs the green-yellow-red photons, as illustrated in Figure 6.3.3. We note that the absorbance of the inorganic cell in the ~400 - 475 nm range is stronger than that of the OSC and while this strong absorbance by the inorganic cell reduces the absorption by the organic cell in that wavelength range, the overall performance of the tandem structure improved relative to the performance of the OSC alone.

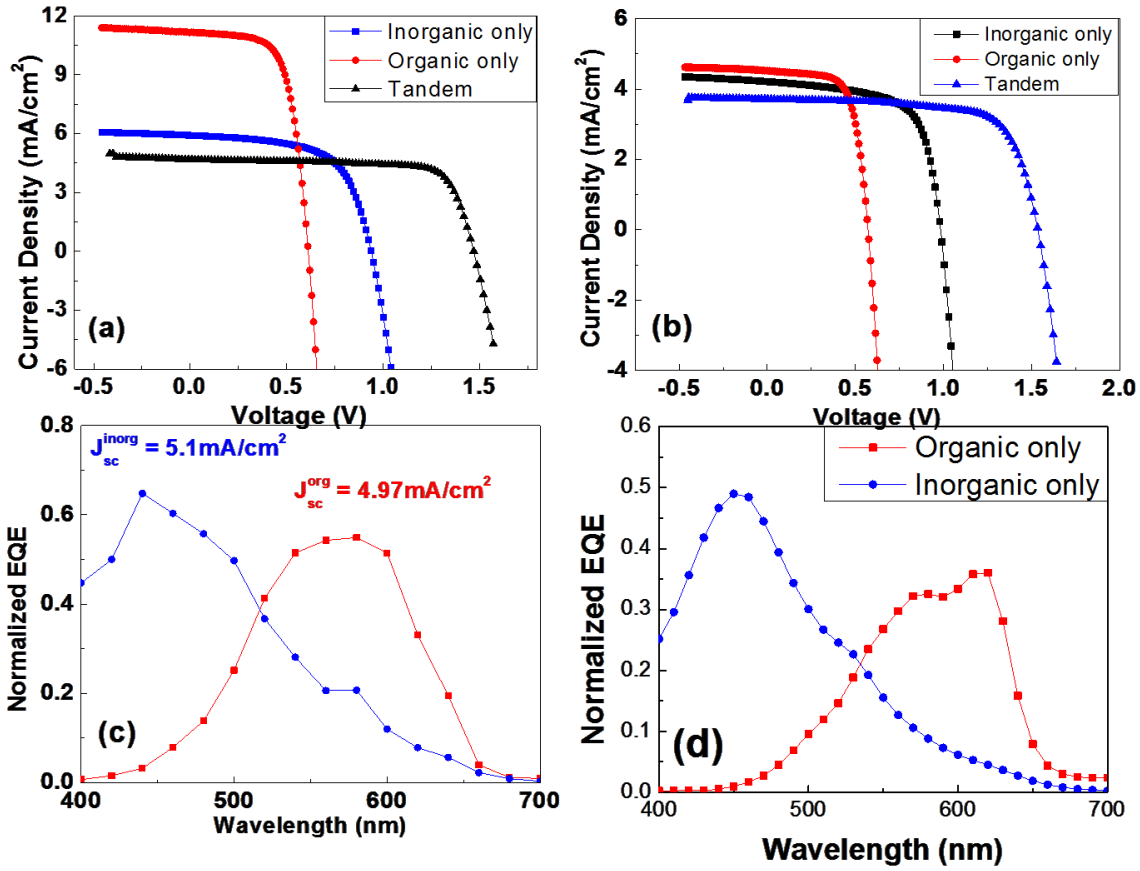

Figure 6.3.1: Illuminated I-V curves of (a) (Design A)-Tandem cell with that of its thin a-(Si,C):H-based cell, and that of the reference organic cell (b) (Design B) tandem cell and those of its thin inorganic and organic units. Normalized EQE of the inorganic unit (blue circles and line) of design A and that of the standard organic unit (red squares and line) of cells in (c) Design A and (d) Design B

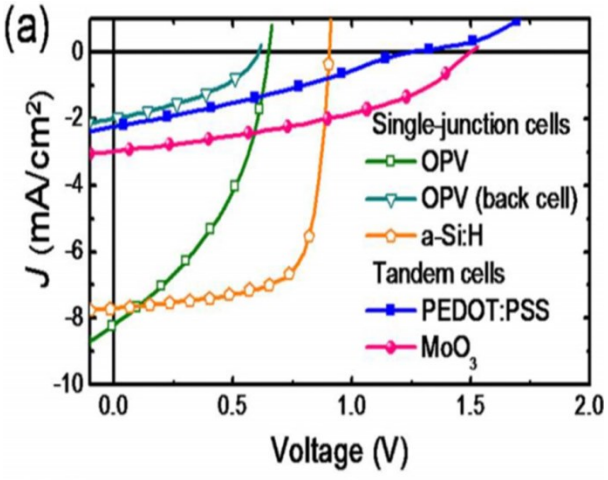

Figure 6.3.2: I-V curve of a tandem cell (blue and red) prepared by Kim et al without using an intermediate ITO layer [28].

6.3.2 Stability of Organic Solar cells

Another major advantage of these new tandem structures is that the high-energy photons are absorbed by the top inorganic cell as shown in Figure 6.3.3. Therefore, they are not available to contribute to the degradation of the OSC. One expects that high energy photons would do more damage to the organic cell than lower energy photons. Thus, the intrinsic stability of the tandem structure should be better than that of an organic cell by itself.

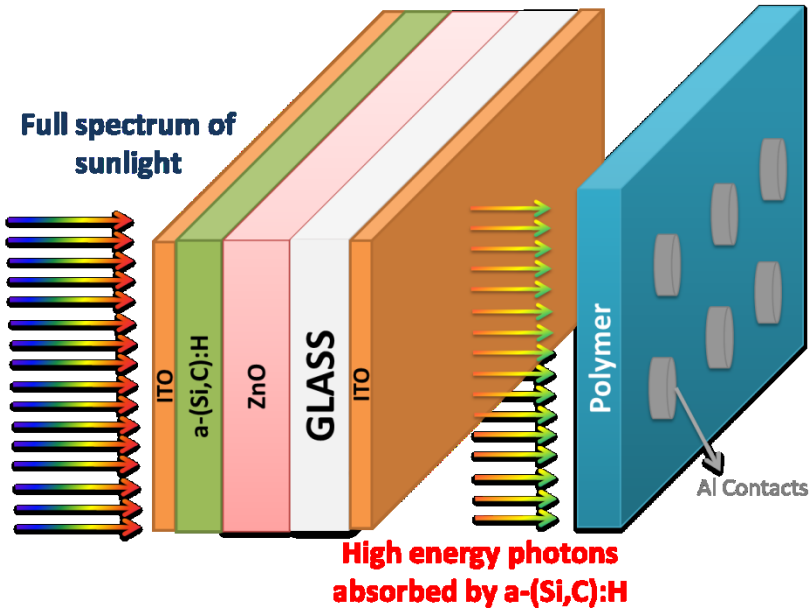

Figure 6.3.3: Demonstration of the light absorption by the tandem inorganic-organic cell with the high-energy photons absorbed by the inorganic cell

This expected behavior was confirmed by doing a careful experiment in which the organic cell was exposed to the full spectrum of sunlight at 2X sun intensity (200 mW/cm^2 form an Oriel xenon simulator) for 100 hours in a nitrogen atmosphere and its performance measured continuously during that period. Then, an identical companion cell was shielded with a filter made from the a-(Si,C):H cell similar to that of Figure 6.2.1, and the cell was exposed again to illumination from the xenon source. Care was taken to increase the illumination intensity falling on the organic cell (by using a lens) so that it produced exactly the same current as with full solar spectrum exposure, ~ 20 mA/cm^2, so that meaningful comparisons of stability could be made for the two types of exposure. The results are shown in Figure 6.3.4(b). As seen from that figure, while a reduction of ~9% in I_{SC} and ~4% in the V_{OC} were observed for the organic cell in ~100 hours of 2-suns irradiation (initial I_{SC} ~20 mA/cm^2) with a full solar spectrum irradiation,

those values were reduced to ~4% and <2%, respectively, due to the presence of the a-(Si,C):H. We note that the initial I_{SC} and PCEs (~4.5%) of both organic cells tested were similar prior to the degradation measurements and the two cells were made in the same run.

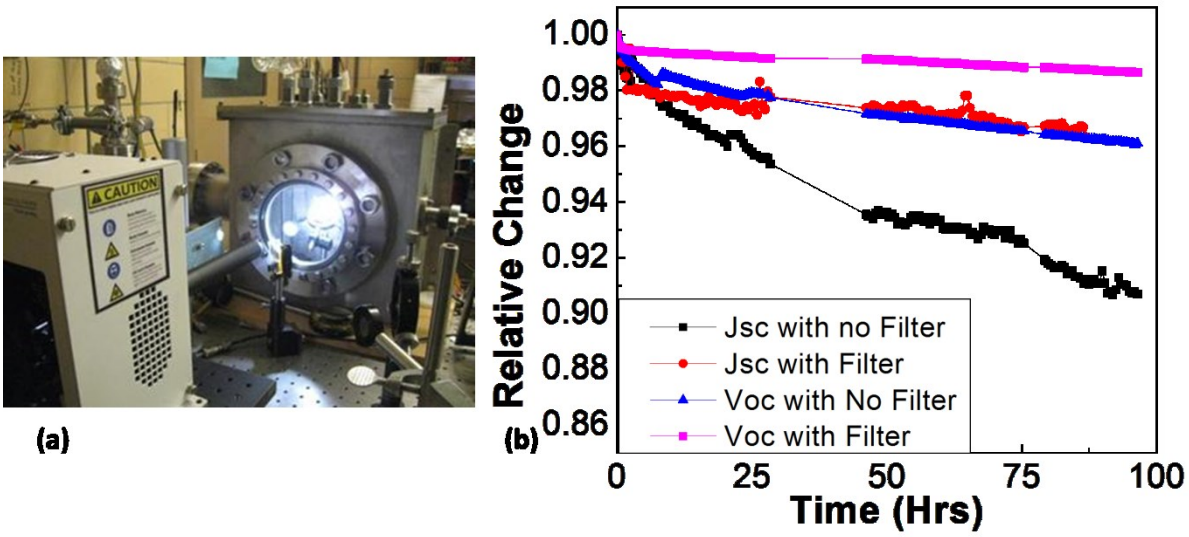

Figure 6.3.4: (a) Photograph of the stability measurement system and (b) Relative change in Voc and Jsc of OSC on exposure for 100hrs

To confirm that there were significant differences occurring in the fundamental material properties when the organic cell was exposed to different spectral content of radiation, we measured EQE of the device under short circuit conditions. These results are shown in Figure 6.3.5(a). It distinctly shows that there is a reduction in the EQE, corresponding to the reduction in currents, and that the reduction is less when the organic cell is shielded from high energy photons. To further confirm that the changes in the QE, currents and voltages are due to fundamental changes in the properties of P3HT/PCBM when it is subjected to different spectra of light, we measured defect densities using the capacitance-frequency technique [29]. These results are shown in Figure 6.3.5(b), which clearly shows a large increase, in defect density when the cell is subjected to the full spectrum of simulated sunlight as opposed to a filtered spectrum. These results are different from previous work [30] on small changes in photo-conductivity of P3HT/PCBM when subjected to light alone, since a photovoltaic device is a *minority* carrier device whose lifetime, and therefore the QE is extremely sensitive to changes in mid-gap states, whereas the photo-conductivity device is a *majority* carrier device, which could be quite insensitive to changes in mid-gap densities if the majority carrier mobility is much larger than

the minority carrier mobility, as is the case for P3HT, and the recombination statistics favor changes in minority carrier lifetime but not of majority carriers [31].

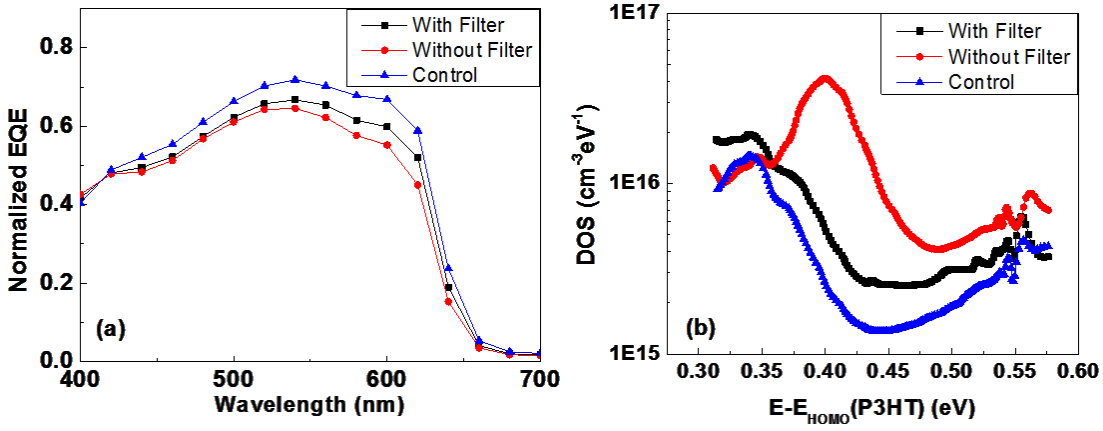

Figure 6.3.5: (a) EQE curves for organic only samples measured pristine(control), after degradation for ~100hrs in N2 where simulated sunlight shines on the organic sample through an a-(Si,C):H filter (with filter) and (without filter) (b) Defect density of the organic only device in above mentioned conditions

Note that a tandem arrangement automatically reduces the degradation in the fill factor, since the top cell, being relatively stable, anchors the fill factor of the tandem arrangement even in the presence of degradation of the bottom (organic) cell. Note also that while we have used an a-(Si,C):H-based cell for demonstrating the concept, other materials, such as (Zn,Cd)Te [32] with appropriate band gaps, can also be used for the inorganic cell. Since this cell is deposited first, the deposition can be done at elevated temperatures, followed by lower-temperature deposition of the organic cell on the other side of the substrate or on a transparent conducting electrode on the inorganic cell.

6.4 Potential of higher efficiency hybrid tandem cells

While this paper has shown a first demonstration of the success of the hybrid tandem cell approach, albeit at a relatively low efficiency (5.7%), it is useful to discuss how one can increase the conversion efficiency significantly. Obviously, one needs an organic material with more complementarity in absorption than can be provided by P3HT. An a-Si:H cell can easily produce a current of 10-12 mA/cm2. The quantum efficiency of an a-Si:H cell will begin to decrease rapidly beyond ~650 nm. Therefore, the organic material must be such that it strongly absorbs in a complementary region, i.e., from~600-650 nm to ~900 nm. Such materials do exist, for example Furan-based polymers and benzotrithiophene-based polymers being developed

respectively by the Frechete group [33] and the McCulloch group [34]. Other polymers that have a low bandgap and a broader absorption range are also being developed [35]. When combined with the increase in current that can be offered by using photonic and plasmonic enhancements, it is reasonable to expect a J_{sc} of ~12 mA/cm^2, a V_{oc} of ~1.8-1.9 V, and a FF of 80%, for a total conversion efficiency of ~17-18%. A triple junction cell is expected to exceed 20%. All these cells can be fabricated using technology that is being developed currently. Such efficiencies would be revolutionary. For increasing the efficiency further, one can use a photonic or plasmonic approach to enhance infrared light absorption in the organic cell [21, 36-40] thereby increasing its current significantly.

6.5 Conclusions

In summary, we have shown how a novel tandem cell arrangement in an electrically series design, comprising a thin a-(Si,C):H based inorganic top cell, and an organic bottom cell, results in an improved PCE of 5.6% in an un-optimized series design, which is a ~24% increase relative to that of the OSC alone. The V_{OC} of the tandem junction cells, ~1.5 V, is the sum of the values of the separate cells, as expected. Optimization of such tandem cells, deposited on a transparent, insulating substrate, can lead to significantly higher efficiencies. One can optimize the structures by manipulating the thickness of the cell and changing the C content so that the bandgap varies and the absorption in a-(Si,C):H precisely complements that of the organic cell. The new device materials and architecture allow for either series connection or electrically independent tandem arrangements, thereby eliminating the current matching problem. The new structure also reduces the degradation of the organic device by filtering the high-energy photons.

References

[1] F. Krebs, *Polymeric Solar Cells Materials, Design, Manufacture*, Lancaster, PA: DES*tech* publication, Inc., 2010.

[2] Y. Y. Liang *et al.*, "For the Bright Future-Bulk Heterojunction Polymer Solar Cells with Power Conversion Efficiency of 7.4%," *Advanced Materials,* vol. 22, no. 20, pp. E135-+, 2010.

[3] S. Sista *et al.*, "Highly Efficient Tandem Polymer Photovoltaic Cells," *Advanced Materials,* vol. 22, no. 3, pp. 380-+, 2010.

[4] M. A. Green *et al.*, "Solar cell efficiency tables (version 37)," *Progress in Photovoltaics,* vol. 19, no. 1, pp. 84-92, 2011.

[5] C. J. Brabec *et al.*, "Polymer-Fullerene Bulk-Heterojunction Solar Cells," *Advanced Materials,* vol. 22, no. 34, pp. 3839-3856, Sep, 2010.

[6] R. F. Service, “Outlook Brightens for Plastic Solar Cells,” *Science,* vol. 332, no. 6027, Apr 15, 2011.

[7] M. Jorgensen, K. Norrman, and F. C. Krebs, “Stability/degradation of polymer solar cells,” *Solar Energy Materials and Solar Cells,* vol. 92, no. 7, pp. 686-714, 2008.

[8] M. O. Reese *et al.*, “Pathways for the degradation of organic photovoltaic P3HT : PCBM based devices,” *Solar Energy Materials and Solar Cells,* vol. 92, no. 7, pp. 746-752, Jul, 2008.

[9] K. Kawano *et al.*, “Degradation of organic solar cells due to air exposure,” *Solar Energy Materials and Solar Cells,* vol. 90, no. 20, pp. 3520-3530, 2006.

[10] B. Zimmermann, U. Wurfel, and M. Niggemann, “Longterm stability of efficient inverted P3HT:PCBM solar cells,” *Solar Energy Materials and Solar Cells,* vol. 93, no. 4, pp. 491-496, 2009.

[11] H. Neugebauer *et al.*, “Stability and photodegradation mechanisms of conjugated polymer/fullerene plastic solar cells,” *Solar Energy Materials and Solar Cells,* vol. 61, no. 1, pp. 35-42, Feb, 2000.

[12] E. A. Katz *et al.*, “Out-door testing and long-term stability of plastic solar cells,” *European Physical Journal-Applied Physics,* vol. 36, no. 3, pp. 307-311, Dec, 2006.

[13] F. C. Krebs, and K. Norrman, “Analysis of the failure mechanism for a stable organic photovoltaic during 10000 h of testing,” *Progress in Photovoltaics,* vol. 15, no. 8, pp. 697-712, 2007.

[14] B. Paci *et al.*, “Photo-degradation and stabilization effects in operating organic photovoltaic devices by joint photo-current and morphological monitoring,” *Solar Energy Materials and Solar Cells,* vol. 92, no. 7, pp. 799-804, Jul, 2008.

[15] J. Y. Kim *et al.*, “Efficient tandem polymer solar cells fabricated by all-solution processing,” *Science,* vol. 317, no. 5835, pp. 222-225, 2007.

[16] A. Hadipour *et al.*, “Solution-processed organic tandem solar cells,” *Advanced Functional Materials,* vol. 16, no. 14, pp. 1897-1903, 2006.

[17] T. Ameri *et al.*, “Organic tandem solar cells: A review,” *Energy & Environmental Science,* vol. 2, no. 4, pp. 347-363, 2009.

[18] C. F. Zhang *et al.*, “Simple tandem organic photovoltaic cells for improved energy conversion efficiency,” *Applied Physics Letters,* vol. 92, no. 8, Feb, 2008.

[19] O. Hagemann *et al.*, “All solution processed tandem polymer solar cells based on thermocleavable materials,” *Solar Energy Materials and Solar Cells,* vol. 92, no. 11, pp. 1327-1335, Nov, 2008.

[20] R. Schueppel *et al.*, “Controlled current matching in small molecule organic tandem solar cells using doped spacer layers,” *Journal of Applied Physics,* vol. 107, no. 4, Feb, 2010.

[21] K. Tvingstedt *et al.*, “Folded reflective tandem polymer solar cell doubles efficiency,” *Applied Physics Letters,* vol. 91, no. 12, Sep, 2007.

[22] F. C. Chen, and C. H. Lin, “Construction and characteristics of tandem organic solar cells featuring small molecule-based films on polymer-based subcells,” *Journal of Physics D-Applied Physics,* vol. 43, no. 2, Jan, 2010.

[23] A. Colsmann *et al.*, “Organic tandem solar cells comprising polymer and small-molecule subcells,” *Applied Physics Letters,* vol. 89, no. 20, 2006.

[24] I. A. Yunaz *et al.*, “Wide-gap a-Si1-xCx:H solar cells with high light-induced stability for multijunction structure applications,” *Solar Energy Materials and Solar Cells,* vol. 95, no. 1, pp. 107-110, 2011.

[25] J. Shinar *et al.*, "Microstructure and hydrogen dynamics in hydrogenated amorphous silicon carbides," *Physical Review B,* vol. 60, no. 23, pp. 15875-15889, Dec, 1999.

[26] A. Catalano, J. Newton, and A. Rothwarf, "a-$Si_{1-x}C_x$-H alloys for multijunction solar cells," *IEEE Transactions on Electron Devices,* vol. 37, no. 2, pp. 391-396, 1990.

[27] T. Xiao *et al.*, "Simple routes for improving polythiophene: fullerene-based organic solar cells," *Organic Electronics,* vol. 12, no. 2, pp. 257-262, 2011.

[28] T. Kim *et al.*, "Organic-inorganic hybrid tandem multijunction photovoltaics with extended spectral response," *Applied Physics Letters,* vol. 98, no. 18, May 2, 2011.

[29] J. Bhattacharya *et al.*, "Photo-induced changes in fundamental properties of organic solar cells," *Applied Physics Letters,* vol. 100, no. 19, May 7, 2012.

[30] M. O. Reese *et al.*, "Photoinduced Degradation of Polymer and Polymer-Fullerene Active Layers: Experiment and Theory," *Advanced Functional Materials,* vol. 20, no. 20, Oct 22, 2010.

[31] J. G. Simmons, and G. W. Taylor, "Nonequilibrium steady-state statistics and associated effects for insulators and semiconductors containing an arbitraty distribution of traps," *Physical Review B-Solid State,* vol. 4, no. 2, 1971, 1971.

[32] T. L. Chu *et al.*, "Films and junctions of Cadmium Zinc Telluride," *Journal of Applied Physics,* vol. 71, no. 11, pp. 5635-5640, Jun, 1992.

[33] C. H. Woo *et al.*, "Incorporation of Furan into Low Band-Gap Polymers for Efficient Solar Cells," *Journal of the American Chemical Society,* vol. 132, no. 44, Nov 10, 2010.

[34] C. B. Nielsen *et al.*, "A benzotrithiophene-based low band gap polymer for polymer solar cells with high open-circuit voltage," *Journal of Materials Chemistry,* vol. 21, no. 44, pp. 17642-17645, 2011.

[35] L. Dou *et al.*, "Tandem polymer solar cells featuring a spectrally matched low-bandgap polymer," *Nature Photonics,* vol. 6, no. 3, Mar, 2012.

[36] S. S. Kim *et al.*, "Plasmon enhanced performance of organic solar cells using electrodeposited Ag nanoparticles," *Applied Physics Letters,* vol. 93, no. 7, 2008.

[37] K. Tvingstedt *et al.*, "Surface plasmon increase absorption in polymer photovoltaic cells," *Applied Physics Letters,* vol. 91, 2007.

[38] B. P. Rand, P. Peumans, and S. R. Forrest, "Long-range absorption enhancement in organic tandem thin-film solar cells containing silver nanoclusters," *Journal of Applied Physics,* vol. 96, no. 12, pp. 7519-7526, Dec, 2004.

[39] S. B. Rim *et al.*, "An effective light trapping configuration for thin-film solar cells," *Applied Physics Letters,* vol. 91, no. 24, Dec, 2007.

[40] D. Duche *et al.*, "Improving light absorption in organic solar cells by plasmonic contribution," *Solar Energy Materials and Solar Cells,* vol. 93, no. 8, pp. 1377-1382, Aug, 2009.